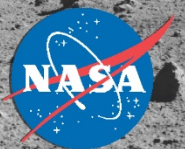
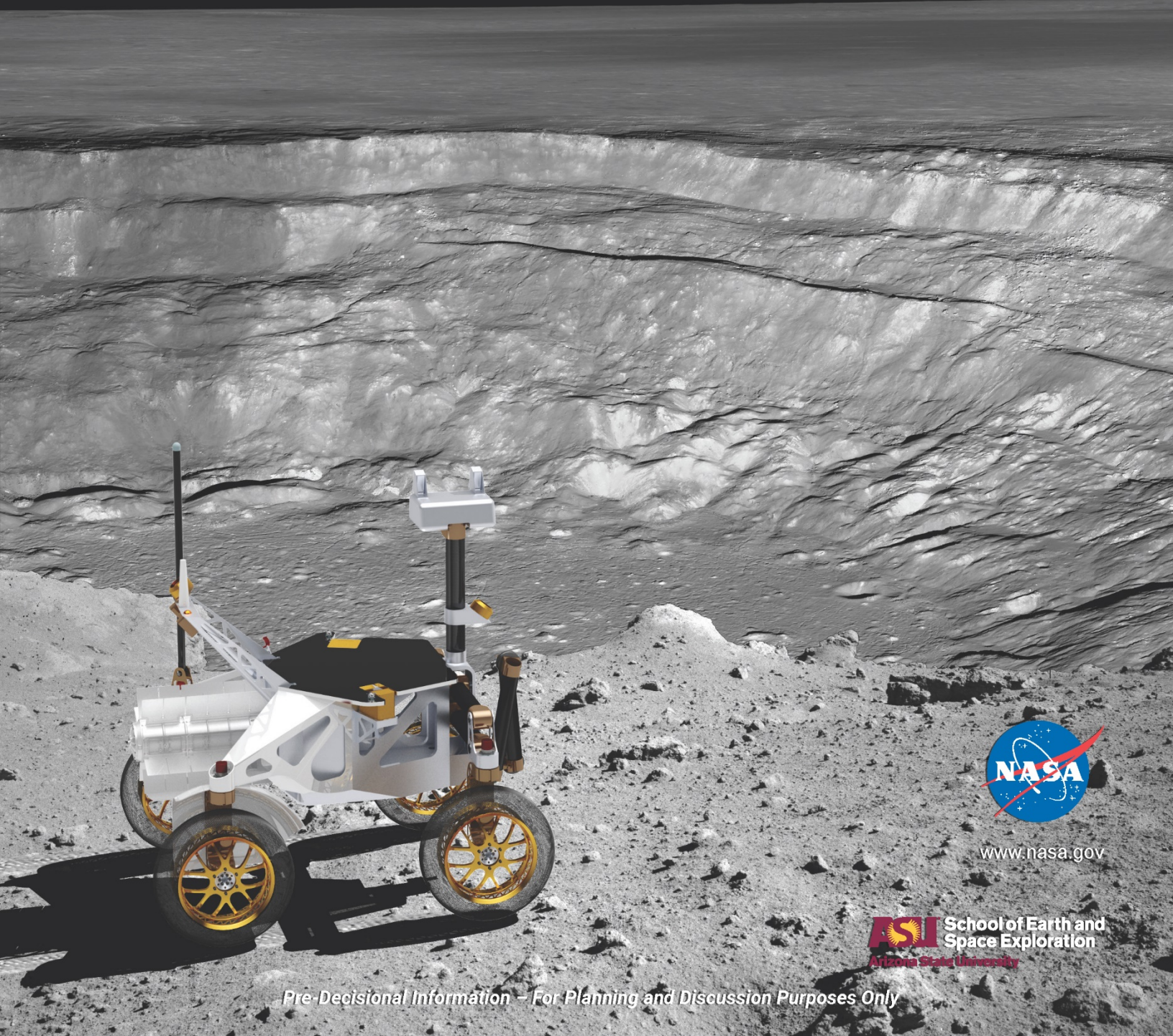


National Aeronautics and Space Administration

Intrepid Planetary Mission Concept Study Report

PI: Mark Robinson, Arizona State University
robinson@ser.asu.edu

Study Lead: John Elliott, Jet Propulsion Laboratory
john.o.elliott@jpl.nasa.gov



www.nasa.gov



Pre-Decisional Information – For Planning and Discussion Purposes Only

Disclaimers/Acknowledgements

Pre-Decisional Information – For Planning and Discussion Purposes Only

The research was carried out at the Jet Propulsion Laboratory, California Institute of Technology, under a contract with the National Aeronautics and Space Administration (80NM0018D0004).

The cost information contained in this document is of a budgetary and planning nature and is intended for informational purposes only. It does not constitute a commitment on the part of JPL and/or Caltech.

© 2020. All rights reserved.

INTREPID

TRAVERSING FOUR BILLION YEARS OF LUNAR HISTORY

Intrepid's investigation across six diverse geologic regions would reveal undiscovered aspects of lunar evolution, paving the way for the next decade of planetary exploration.

SCIENCE THEMES AND OBJECTIVES:

THEME 1 Evolution of the lunar interior and nature of the Procellarum KREEP Terrane

- 1.1 Determine the cause of extended volcanism in the Procellarum region
- 1.2 Determine the cause of the lunar crustal asymmetry
- 1.3 Test hypotheses for the origin of non-basaltic volcanism
- 1.4 Determine composition of deep mantle from pyroclastic deposits
- 1.5 Determine decline of core dynamo and magnetic field over time

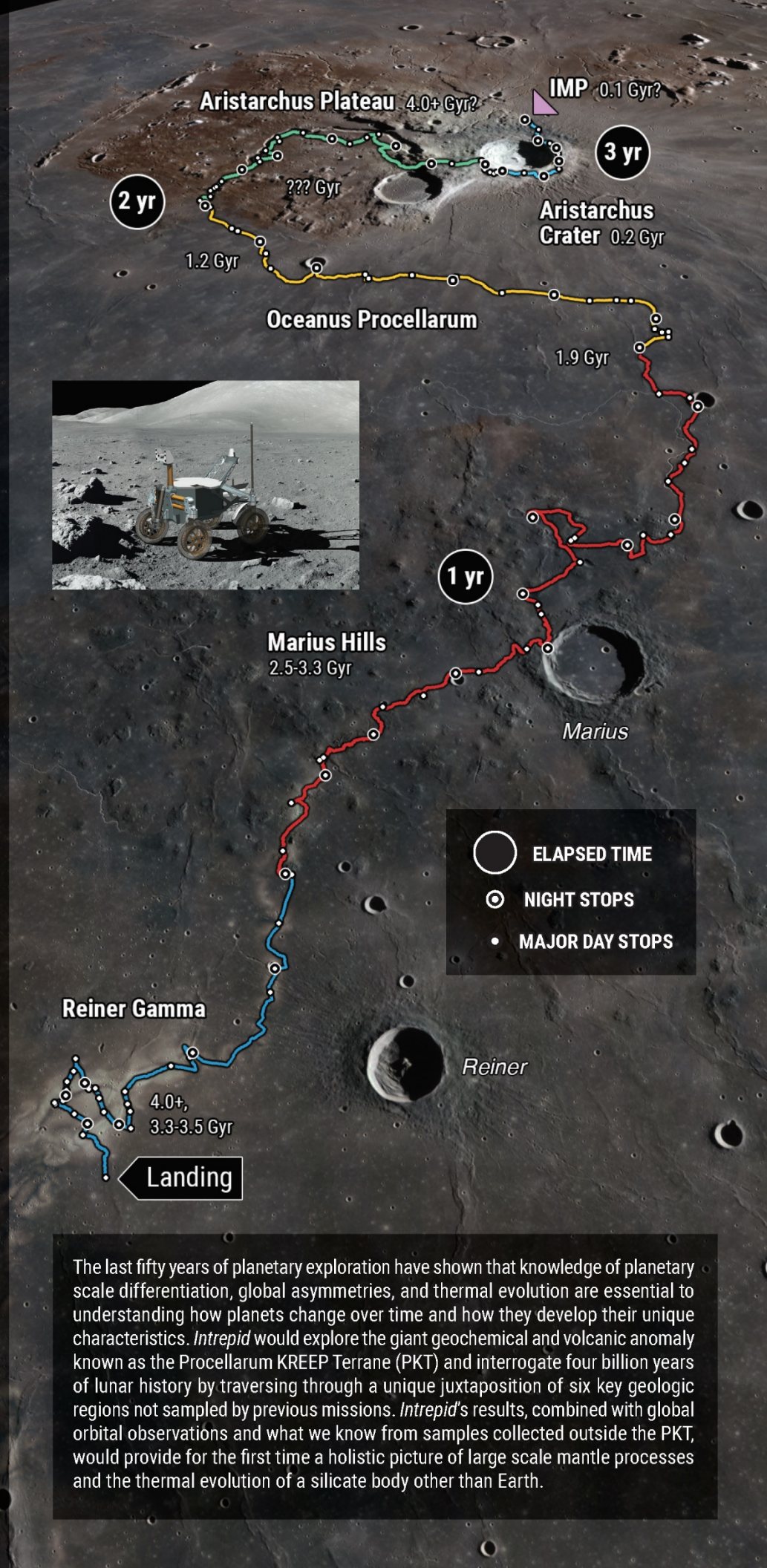
THEME 2 Diversity of styles of magmatism

- 2.1 Characterize flood basalt emplacement, rilles, flows, vents
- 2.2 Determine origin(s) and composition(s) of cones, domes and shields
- 2.3 Characterize pyroclastic volcanism processes: composition and physical state
- 2.4 Determine the relationship between intrusive (plutonic) and effusive (volcanic) materials

THEME 3 Post-emplacment modification of magmatic materials

- 3.1 Test hypotheses of impact crater formation, ballistic sedimentation, ray formation
- 3.2 Determine target material influence on impact crater formation
- 3.3 Determine the causes of magnetic anomalies, swirls and space weathering

Pre-Decisional Information – For Planning and Discussion Purposes Only



The last fifty years of planetary exploration have shown that knowledge of planetary scale differentiation, global asymmetries, and thermal evolution are essential to understanding how planets change over time and how they develop their unique characteristics. *Intrepid* would explore the giant geochemical and volcanic anomaly known as the Procellarum KREEP Terrane (PKT) and interrogate four billion years of lunar history by traversing through a unique juxtaposition of six key geologic regions not sampled by previous missions. *Intrepid's* results, combined with global orbital observations and what we know from samples collected outside the PKT, would provide for the first time a holistic picture of large scale mantle processes and the thermal evolution of a silicate body other than Earth.

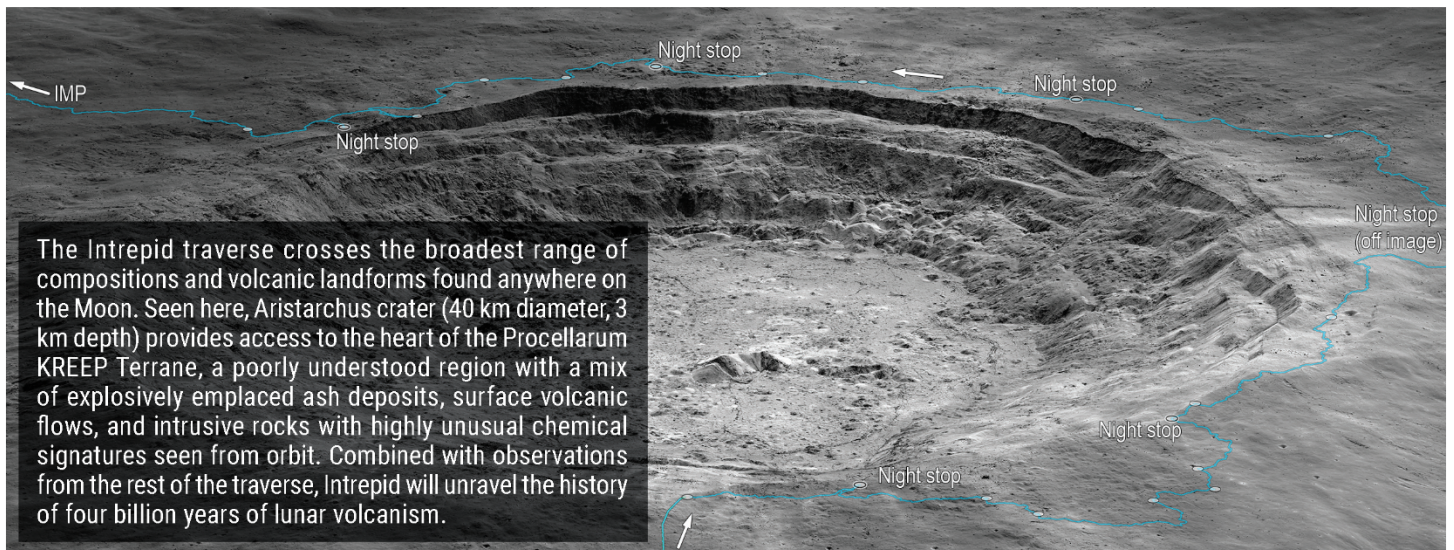
MISSION CONCEPT

The *Intrepid* mission concept relies on high-TRL hardware, advanced autonomy, detailed traverse pre-planning, night operations, and a disciplined concept of operations that enable the investigation of 133 major and 981 minor scientific sites along an ~1800 km traverse over 4 Earth years (3-years nominal, plus 1-year margin).

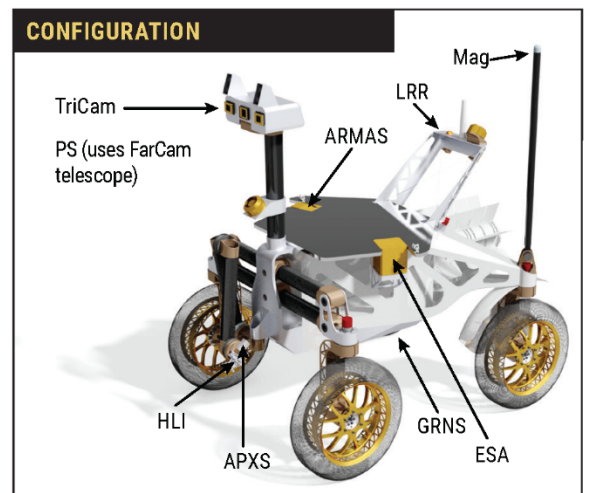
- *Intrepid* would touch down just south of the **Reiner Gamma** magnetic anomaly and traverse across and along the “swirl” to definitively test hypotheses for the origin of the anomaly and swirl (intrusive rock >4 Gyr, basalts 3.3 to 3.5 Gyr in age).
- *Intrepid* would then traverse the **Marius Hills** volcanic complex (2.5 Gyr) to investigate cones, flows, vents, and putative volcanic ash deposits.
- Next, *Intrepid* would rove northward across **Oceanus Procellarum**, some of the youngest (1.2 Gyr to 1.9 Gyr) lunar mare deposits, making a suite of compositional observations of the mare and rays from Aristarchus crater to test hypotheses concerning the existence of KREEP-rich basalts and ray mixing systematics.
- Once on the **Aristarchus plateau**, *Intrepid* would characterize the largest pyroclastic deposit on the Moon (perhaps 2.5 Gyr), unlocking the deep mantle and prospecting for potential H deposits.
- *Intrepid* would then traverse the rim of the impressive **Aristarchus crater** (~0.2 Gyr), assessing ejected crustal material within the PKT (3.5 Gyr to >4.0 Gyr).
- Finally, *Intrepid* would investigate a newly discovered type of volcanic landform, **Irregular Mare Patches** (IMP), which are proposed to represent the youngest (<100 Myr) volcanism on the Moon.

IMPLEMENTATION HIGHLIGHTS

- Rover mass 371 kg (MEV), 2.5 m by 2.0 m footprint
- Power supplied by Next-Gen RTG (274 W EOM) for day/night rover activities
- Four-wheeled design with all-wheel drive and steering for efficient mobility
- Large (80-cm diameter) compliant wheels for improved mobility and longevity
- Robotic arm (5 degree-of-freedom) for autonomous instrument placement
- Mast (2 degree-of-freedom) for science instrument pointing and navigation
- Omni antenna provides Earth communication while in motion; two high-gain fixed antennas provide high-bandwidth downlink when stopped
- Autonomous driving leverages Mars rover capabilities and state-of-the-art terrestrial technology
- Autonomous instrument placement leverages decades of technology development and demonstrations on terrestrial prototypes
- Total cost within New Frontiers budget



INSTRUMENT	DERIVED SCIENCE PRODUCT
ARMAS	Galactic cosmic ray flux
Gamma Ray Neutron Spectrometer (GRNS)	Elemental abundance
Alpha Particle X-ray Spectrometer (APXS)	Elemental abundance
Magnetometer (Mag)	Magnetic field strength, depth, orientation, polarity
Electrostatic Analyzer (ESA)	Solar wind flux to surface
TriCam: Stereo RGB Imager, BW FarCam	Landform morphology, albedo, visible color
Point Spectrometer (PS) uses FarCam telescope	Mineral abundance from spectral reflectance
Hand Lens Imager (HLI)	Micro-texture, color, rover inspection, Earth imaging
Inertial Measurement Unit (IMU)	Subsurface density
Laser Retroreflector (LRR)	Location of rover



Mark Robinson, PI
robinson@ser.asu.edu

ASU School of Earth and Space Exploration
Arizona State University

JPL
Jet Propulsion Laboratory
California Institute of Technology

Carnegie Mellon University, First Mode, Honeybee Robotics, Johns Hopkins University, Johns Hopkins University Applied Physics Laboratory, Johnson Space Center, Lunar and Planetary Institute, Malin Space Science Systems, Stanford University, University of New Hampshire, Washington University in St. Louis

Pre-Decisional Information – For Planning and Discussion Purposes Only

Study Participants

Intrepid Science Team

David Blewett	Johns Hopkins University Applied Physics Laboratory
Brett Denevi	Johns Hopkins University Applied Physics Laboratory
Michael Fitzgerald	Arizona State University
Terrence Fong	Ames Research Center
Elizabeth Frank	First Mode
Lee Graham	Johnson Space Center
Peter Illsley	First Mode
Brad Jolliff	Washington University
David Lawrence	Johns Hopkins University Applied Physics Laboratory
Samuel Lawrence	Johnson Space Center
Kevin Lewis	Johns Hopkins University
Prasun Mahanti	Arizona State University
Heather Meyer	Lunar and Planetary Institute
Elizabeth Rampe	Johnson Space Center
Kevin Reinhart	Arizona State University
Mark Robinson	Arizona State University
Harlan Spence	University New Hampshire
Emerson Speyerer	Arizona State University
Julie Stopar	Lunar and Planetary Institute
Sonia Tikoo	Stanford University
Chris Vorhees	First Mode
Robert Wagner	Arizona State University
David Wettergreen	Carnegie Mellon University

Several ASU School of Earth and Exploration classes explored the Intrepid concept over the years and made positive contributions to the effort.

- 2013 SES 405
- 2013 GLG 494/598
- 2020 SES 405

JPL Study Team

Mission Study Team	Additional Mobility Team	Additional Autonomy Team
Mineh Badalians-Vanigh	Fred Calef	Martin Feather
Paul Briggs	Scott Howe	Lorraine Fesq
Catherine Elder	Brett Kennedy	Michael McHenry
John Elliott	Andrew Kennett	Hiro Ono
Kurt Gonter	Mark Maimone	Michael Paton
Ron Hall	Patrick McGarey	Joseph Rossino
Jim Jackson	Scott Moreland	Olivier Toupet
Io Kleiser	Austin Nicholas	Bill Whitaker
Larry Matthies	Brian Wilcox	
Rudra Mukherjee		
Kristine McGowan	With significant additional participation from the members of JPL's	
Issa Nesnas	A-Team and Team X	
Raul Polit-Casillas		
Miles Smith		
Eric Sunada		
Thaddaeus Voss		

**PLANETARY SCIENCE DECADAL SURVEY****Table of Contents**

Disclaimers/Acknowledgements.....	i
Fact Sheet.....	ii
Study Participants.....	iv
Executive Summary.....	viii
1 SCIENTIFIC OBJECTIVE	1
Introduction.....	1
Science Themes and Objectives	1
Traverse: Six Key Lunar Geologic Regions	2
Science Overview.....	5
Regolith vs. Outcrop	5
The Third Dimension	5
Expected Significance and Traceability to NASA Goals and Objectives	6
Instrument Suite and Measurements	6
Outreach Opportunities.....	10
2 HIGH-LEVEL MISSION CONCEPT.....	11
Concept Maturity Level	11
Technology Maturity	11
Key Trades.....	13
3 TECHNICAL OVERVIEW.....	14
Instrument Payload Description.....	14
Flight System	14
Concept of Operations	20
Risk List.....	25
4 DEVELOPMENT SCHEDULE AND SCHEDULE CONSTRAINTS.....	26
High-Level Mission Schedule	26
Technology Development Plan	26
Development Schedule and Constraints.....	28
5 MISSION LIFE-CYCLE COST.....	28
Costing Methodology and Basis of Estimate.....	28
Cost Estimate(s).....	29
Potential Cost Savings.....	29

Appendices

A ACRONYMS	A-1
B DESIGN TEAM STUDY REPORT.....	B-1
B.1 Intrepid Mission Concept: Frequently Asked Questions.....	B-1
B.2 Tracking the Traverse: Intrepid ConOps Planning Detail.....	B-17
B.3 JPL Team X Report.....	B-39
C SPECIAL TECHNICAL ANALYSES.....	C-1
C.1 Mobility.....	C-1
C.2 Autonomy.....	C-7
C.3 Thermal Control.....	C-12



C.4 Architecture..... C-19

D ADDITIONAL INFORMATION ON TECHNOLOGIES AND TECHNIQUES D-1

D.1 Additional Cost Modeling Information D-1

D.2 Wrap factors..... D-1

D.3 SEER..... D-3

D.4 TruePlanning..... D-5

D.5 SOCM..... D-10

E REFERENCES E-1

Figures

Figure 1-1. Intrepid traverse map (Appendix B.1.5)..... 2

Figure 1-2. Rover schematic showing instrument accommodation..... 8

Figure 1-3. Spectra of lunar mineral separates from Apollo samples 15555 and 70035 (crushed and sieved to <45 μm size fraction; Isaacson et al., 2011), and lunar orange and green volcanic glass from the RELAB library, shocked plagioclase from Pieters (1996). Solid lines indicate lab spectra and diamonds show PS bandpass centers. Solid RGB color indicate sensitivity of HLI and SCI. Vertical line separates CCD (left) and InGaAs (right) detectors..... 9

Figure 1-4. Weight percent oxides for Apollo and Luna basalt groups measured in the laboratory compared to the expected analytical uncertainty (precision) for the APXS. TiO₂ and FeO are two of the main parameters, along with K₂O and MgO, to discriminate lunar mare basalt groups. 9

Figure 2-1. Thermal switch design..... 12

Figure 3-1. The Intrepid Rover study developed complete designs for options utilizing radioisotope power (right) and solar/batteries (left). 15

Figure 3-2. Intrepid C&DH Block Diagram..... 18

Figure 3-3. Rover WEB layout for RTG version (top) and Solar (bottom)..... 19

Figure 3-4. Data volume generation for the mission has 66.5% margin against the total mission downlink capacity. 23

Figure 3-5. A day in the life of Intrepid..... 24

Figure 4-1. Notional High-Level Schedule Assuming a 2030 Launch. 26

Tables

Table 1-1. Science Traceability Matrix. Note that the Laser Retro-Reflector is not required to meet or address any Intrepid science objectives. 7

Table 1-2. Intrepid relevance to key NASA exploration documents (Region Abbreviations: RG – Reiner Gamma; MH – Marius Hills; OP – Oceanus Procellarum; AP – Aristarchus Plateau; AC – Aristarchus Crater; IMP – Irregular Mare Patch). The “(all)” notation under region indicates that all the regions would contribute some understanding to the particular question while the called out region(s) are the most significant contributors..... 8

Table 1-3. Intrepid instrument suite. Power and mass estimates from high TRL instruments, except Point Spectrometer. Note: TriCam, PS and HLI share same electronics box inside rover – only one rover interface for power and data for these three instruments (instrument capabilities, not requirements)..... 10

Table 2-1. Instrument Heritage Table. 11



Table 2-2. Key Mobility Requirements and Constraints.	13
Table 2-3. Mobility Trades, Selection, and Rationale.....	13
Table 2-4. Autonomy-related Trades, Selection, and Rationale.	14
Table 3-1. Intrepid Rover Mass Table.....	15
Table 3-2. Intrepid Power Modes.....	16
Table 3-3. Flight System Element Characteristics Table.....	16
Table 3-4. Onboard and ground activities.....	17
Table 3-5. Why Intrepid ops is more efficient than Mars ops.....	21
Table 3-6. Definitions of terms used in this section.....	21
Table 3-7. Mission Operations and Ground Data Systems Table (DSN and NEN).....	23
Table 3-8. Intrepid’s adoption of existing technologies and proven instrument designs facilitates a high-performance mission with manageable risks.....	25
Table 4-1. Key Phase Duration Table.....	26
Table 4-2. Technology Development Plan.....	27
Table 5-1. JPL Team X and cost model estimates for Intrepid (FY25\$M).....	29
Table 5-2. Total Mission Cost Funding Profile for the RTG Option. (FY costs ¹ in Real Year Dollars, Totals in Real Year and FY25 Dollars.).....	30
Table 5-3. Total Mission Cost Funding Profile for the Solar Option. (FY costs ¹ in Real Year Dollars, Totals in Real Year and FY25 Dollars.).....	30



Executive Summary

The last fifty years of planetary exploration have shown that knowledge of planetary scale differentiation, global asymmetries, and thermal evolution are key to understanding how planets change over time and how they develop their unique characteristics. Intrepid will traverse the giant geochemical and volcanic anomaly known as the Procellarum KREEP Terrane (PKT) and interrogate four billion years of lunar history by traversing through a unique juxtaposition of six key geologic regions not sampled by previous missions. Intrepid's instruments will provide high precision geochemistry from the surface and subsurface as well as characterizing regolith properties and interactions with the space environment, all at the meter to centimeter scale. This robust suite of measurements is required to meet our objectives, and such measurements cannot be acquired from orbit.

The Intrepid mission concept is based on a traverse of 1800 km; no other planetary rover has come close to that distance. *Why* is the long traverse needed and *how* will we succeed?

Why... A traverse across the heart of the PKT enables a journey through *four billion years* of lunar volcanic history. Key regions include the Reiner-Gamma formation, Marius Hills volcanic complex, Oceanus Procellarum basalts, Aristarchus crater ray material, Aristarchus Plateau volcanic materials (including the largest pyroclastic deposit on the Moon), Aristarchus crater and its near-rim deep ejecta, and the Aristarchus Irregular Mare Patch (proposed age <100 million years). The varied geologic landforms found only along this traverse allow Intrepid to address three key planetary science themes: 1) Evolution of the lunar interior (including the nature of the PKT). 2) Diversity of styles of magmatism on a differentiated silicate planetary body. 3) Post emplacement modification of volcanic materials, including space weathering, cratering, and regolith development. These themes are divided into twelve scientific objectives addressable with straightforward measurements (elemental, spectral reflectance, imaging, space environment, magnetic) and will provide a scientific return that will redefine our understanding of fundamental planetary processes (including thermal evolution, formation of crust, volcanology, impact cratering, and regolith processes) while making existing (and future) orbital remote sensing measurements more valuable (of the Moon and other terrestrial bodies).

How... Covering 1800 km in 4 years (3 years nominal, plus 1 year margin) requires a high degree of pre-planning and automation. The Intrepid science themes and objectives are tied to pivotal planetary science questions that grew out of decades of planetary science and exploration. We know what we do not know, and we now know where to go to obtain the required observations to fill in the blanks. The Intrepid team has mapped out (down to the meter scale) the locations of 133 focused investigation sites and over 900 minor sites ("interval stops") that cover with redundancy all of our measurement objectives. Additionally, most of the instruments acquire observations while traversing (some continuously, others intermittently) resulting in an 1800 km trail of data linking each site.

In terms of the Intrepid science strategy one must think differently. The pre-planned route enables the acquisition of observations required to retire our objectives; certainly Intrepid will make unforeseen discoveries but these cannot derail the mission. Intrepid will document these discoveries and move on – the discovery may be the impetus for another mission – but Intrepid will stay on course and retire its objectives in the given time frame.

Intrepid's scientific objectives require exploration through the full preserved record (*four billion years*) of volcanic materials in the PKT, and the pre-planned traverse represents the shortest route possible. Although 1800 km would be by far the longest planetary traverse ever undertaken, there are no technological barriers in the way of accomplishing this ambitious mission. The biggest development task is refinement and testing of existing autonomy systems (software) to meet the rigorously defined mission requirements. Intrepid's journey through four billion years of volcanic history, combined with global orbital observations and what we know from samples collected outside the PKT, will provide for the first time a holistic picture of large-scale mantle processes and the thermal evolution of a silicate body other than Earth.

Finally, Intrepid's relatively rapid pace, utilization of state-of-the-art autonomy, varied lunar landscape, and variety of science questions present a unique education and outreach opportunity. Near real time communication will allow the public to ride along with Intrepid, inspiring the next generation of engineers, scientists, teachers, and artists.



1 SCIENTIFIC OBJECTIVE

Introduction

Recent and ongoing lunar missions provide the planetary science community with a wealth of measurements enabling critical new insights into lunar geosciences. Observations from Kaguya, Chang'e, Chandrayaan, and the Lunar Reconnaissance Orbiter missions have increased our understanding of the lithologies present in the lunar crust [Matsunaga *et al.*, 2008; Nakamura *et al.*, 2009; Obtake *et al.*, 2009], regolith properties [Hapke and Sato, 2016], the distribution and timing of volcanic features [Braden *et al.*, 2014; Elder *et al.*, 2017; Haruyama *et al.*, 2009; Staid *et al.*, 2011], crater formation [Ghent *et al.*, 2016; Povilaitis *et al.*, 2018; Speyerer *et al.*, 2016], tectonism [Banks *et al.*, 2012; Watters *et al.*, 2012; Watters *et al.*, 2019], and the nature and distribution of lunar swirls [Deneri *et al.*, 2016; Hendrix *et al.*, 2016; Neish *et al.*, 2011]. These new results, along with the previous sixty years of lunar investigations, establish the Moon as the cornerstone of our understanding of many planetary processes, including crust-mantle differentiation, impact processes, volcanism, and space weathering on airless bodies (Appendix B.1.1).

While these new orbital observations have contributed significantly to our understanding of the evolution of the Moon, new surface measurements are needed to facilitate detailed investigations of key sites, answer outstanding science questions, and provide ground truth for orbital remote sensing observations. We propose a highly mobile rover, Intrepid, to investigate six key lunar geologic regions: (1) Reiner Gamma magnetic anomaly, (2) Marius Hills volcanic complex, (3) Oceanus Procellarum basalts, (4) Aristarchus Plateau, (5) Aristarchus crater and its ejecta, and (6) an Irregular Mare Patch north of Aristarchus crater. Intrepid would explore these features over the course of a 4-year mission (3-year primary; 1-year margin). The Intrepid mission concept and proposed traverse are specifically designed to address key outstanding science questions related to Decadal Survey goals and NASA lunar exploration objectives while strengthening interpretations of remotely sensed datasets collected over the past 25 years.

The Intrepid configuration includes three body mounted instruments (gamma ray and neutron spectrometer, linear energy transfer detector, electrostatic analyzer); three science cameras (wide angle 3-color stereo camera pair, and monochrome

telephoto camera) and an ultraviolet to near-infrared point spectrometer all mounted on a two degree-of-freedom mast; a magnetometer on a boom; and a hand lens camera and X-ray spectrometer deployed from a five degree-of-freedom arm. A deck mounted passive laser retroreflector rounds out the instrument complement. Intrepid would be powered by a Next-Gen RTG (12-GPHS) that allows night operations, a critical aspect of the mission ConOps.

Science Themes and Objectives

Intrepid would traverse six distinct lunar geologic regions and would address a host of key topics identified in NASA planning documents [LEAG, 2016; NASA, 2014; NAC, 2007; NRC, 2007; 2011] as high science priorities: the origin of magnetic anomalies and associated albedo formations (swirls), the range of chemistries of magmatic source regions, the main controls on eruption styles, mixing systematics during impact crater ray formation, the range of compositional heterogeneities of the lunar crust (including the characteristics and origin of Procellarum KREEP Terrane, or PKT), when (or whether?) volcanism shut off, and other key questions. The Intrepid mission concept has three key scientific themes with twelve specific objectives:

1. Evolution of the lunar interior and nature of the Procellarum KREEP Terrane:
 - a. Determine the cause of extended volcanism in the Procellarum region
 - b. Determine the cause of the lunar crustal asymmetry
 - c. Determine the origin of nonmare volcanism
 - d. Determine composition of deep mantle from pyroclastic deposits
 - e. Characterize decline of core dynamo and magnetic field over time
2. Diversity of styles of magmatism:
 - a. Characterize flood basalt emplacement from rilles, flows, and vents
 - b. Determine origin(s) and composition(s) of cones, domes and shields
 - c. Characterize the compositions and physical state (grain size, glass content) of pyroclastic materials
 - d. Determine the nature of intrusive volcanism and relation to effusive deposits
3. Post-emplacement modification of magmatic materials:



- a. Test hypotheses of crater impact formation, ballistic sedimentation, ray formation, and physical properties of regolith outward from impact
- b. Determine target material influence on crater characteristics and impact mechanics
- c. Characterize variations in space weathering across a variety of geologic regions and ages (relationship to radiation environment, H abundance, magnetic anomalies, swirls)

To achieve these objectives, Intrepid would traverse 1800 kilometers over four years (three years nominal, plus one year margin), and acquire thousands of chemical, reflectance, imaging, magnetic, radiation, and solar wind observations. This ambitious concept requires detailed planning of stops and a disciplined science and operations team to stay on schedule and keep costs manageable. The selected suite of instruments minimizes rover and operation complexity while ensuring that the measurements needed to address science objectives are acquired. Acquiring the observations and addressing the core questions in the given time requires pre-planning stops and measurement points along with a high degree of rover autonomy – a new paradigm for planetary rover operations (see ConOps discussion in section 3).

Measurement objectives include: elemental abundances to 3% absolute (Si, O, Fe, Mg, K, Al, Ca, Ti, Th, S, H); magnetic field strength, orientation and polarity to 2% absolute accuracy; solar wind composition and flux to 10% absolute; galactic cosmic rays and solar energetic particle flux to 10% absolute, landform morphology and color at scales from 100 μm and up (SNR >100), and ultraviolet to near-infrared spectral reflectance (300 nm to 1400 nm) absorptions at meter scale (mineralogy, maturity) (SNR >100).

Traverse: Six Key Lunar Geologic Regions

The nominal traverse (Figure 1-1 and Appendix B.1.5) is wholly contained within the PKT and starts south of—and zigzags across—the Reiner Gamma formation, heads north through the Marius Hills volcanic complex, across a stretch of Oceanus Procellarum basalts, then over the Aristarchus plateau, around Aristarchus crater, and finishes at an Irregular Mare Patch 45 km from Aristarchus crater. Throughout the 1800 km traverse, the Intrepid rover would investigate these six regions and provide much needed ground truth and

key measurements required to retire the Intrepid objectives; this traverse represents the only place on the Moon with the required diversity of units and ages (Appendix B.1.7).

Reiner Gamma (RG), an ancient volcanic plain (~3.5 to 3.3 Gyr), contains one of the strongest so called “magnetic anomalies” on the Moon and the associated albedo feature known as a “swirl” [Blewett *et al.*, 2011; Hood and Williams, 1989]. At RG, the main science objectives are to determine the nature of the remanent lunar magnetic field and elucidate its role in moderating space weathering of the regolith and its suitability for radiation protection of surface assets [Bell and Hawke, 1982; Blewett *et al.*, 2011; Blewett *et al.*, 2010; Garrick-Bethell *et al.*, 2011; Garrick-Bethell and Kelley, 2019; Glotch *et al.*, 2015; Kramer *et al.*, 2011b; McCauley, 1967a; b; 1968; Neish *et al.*, 2011; Pinet *et al.*, 2000; Whitaker, 1999]. Space weathering (or maturation) is a process where the physical state, color and albedo of the surface evolves with time (~500 myr time scales) due to exposure to the space environment. These two objectives are achieved with

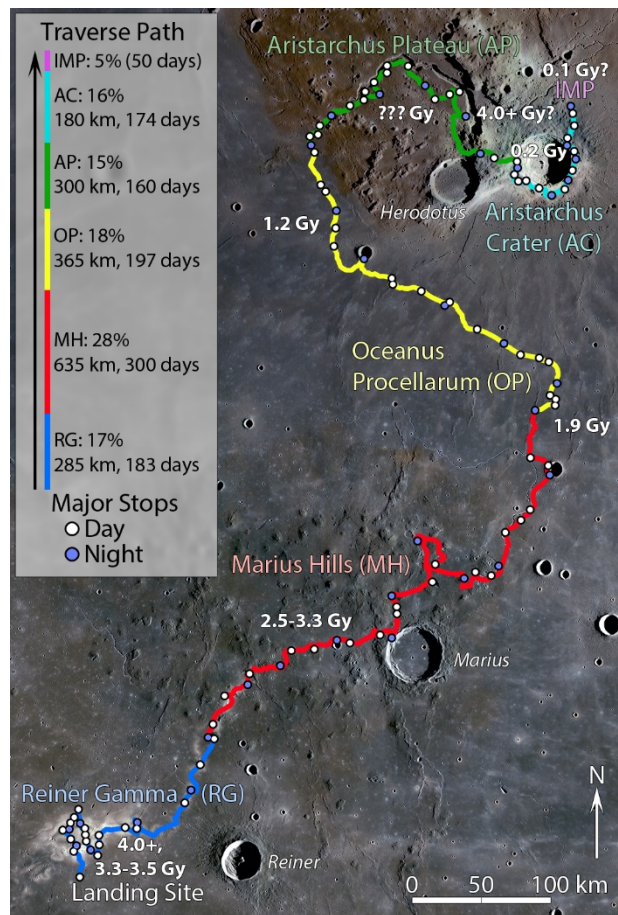


Figure 1-1. Intrepid traverse map (Appendix B.1.5).



three main observational objectives: 1) characterize the magnetic field across the RG traverse to 2 nT resolution at a 5-meter sampling rate with 50-m spatial location accuracy, 2) measure variations in the strength and composition of solar wind constituents as a function of magnetic field strength and orientation across the RG traverse, and 3) characterize the state of maturation of the regolith across the swirl. The magnetometer and electrostatic analyzer would provide the necessary measurements to retire the first two objectives. The optical maturity of the surface would be measured with two key absorptions in the UV to visible range [Denevi *et al.*, 2016; Denevi *et al.*, 2014] and the visible to near-infrared [Blewett *et al.*, 2011]. These key measurements would be supplemented with the geochemical measurements provided by the Alpha Particle X-Ray Spectrometer (APXS) and Gamma Ray Neutron Spectrometer (GRNS) and mineralogic estimates from spectral reflectance absorption features (300 to 1400 nm) measured with the Point Spectrometer (PS). The RG area consists of basaltic flood lavas with ages estimated as 3.3 Gyr [Hiesinger *et al.*, 2011], the oldest volcanic materials to be sampled during the Intrepid mission.

The Marius Hills (MH) complex is a unique lunar volcanic complex, with the highest concentration of blocky lava flows, domes, and cones on the Moon [Campbell *et al.*, 2009; Head and Gifford, 1980; Lawrence *et al.*, 2013; McCauley, 1976a; b; Whitford-Stark and Head, 1977]. While this unique and large grouping of volcanic landforms remains somewhat enigmatic, previous workers generally agree that there were four main volcanic episodes (cf. Lawrence *et al.* [2013]). The first episode built the large scale (250 km) low relief dome that forms the foundation of the complex, then the small domes (1-10 km) were formed, followed by the cones. Finally, these constructs were embayed by mare-like basaltic eruptions. Intrepid would also investigate tectonic landforms (ridges and faults) in this region to elucidate their relation to specific volcanic landforms. Previous studies classified domes and cones based on small-scale roughness and flank slopes, but the cause of these landform distinctions is still debated (compositional, eruption conditions, percent crystallinity etc.). Intrepid would investigate “type” volcanic landforms within the complex to test hypotheses of eruption conditions and styles vs. magma physical properties as the magma source regions evolved. The ages of these major events are not well-constrained and the area has been subdivided into several units based on visible

to near-infrared color properties [Lawrence *et al.*, 2013] and age estimates for these units range from < 1 Gyr to 3.3 Gyr. Because of the small size of the units the uncertainty on these ages is high; however, the largest effusive unit (Flamsteed), which seems to embay the domes and cones, is dated at 2.5 Gyr [Boyce, 1976]. Documenting the chemistry of the various units (domes, cones, mare flows) within the MH would help ascertain their relative ages.

The Oceanus Procellarum (OP) traverse stretches from MH to the Aristarchus Plateau. Intrepid would traverse mare basalts that erupted over a broad span of lunar history (~2.5 Gyr in MH to 1.9 Gyr (P51) and 1.2 Gyr (P 60) within Oceanus Procellarum [Hiesinger *et al.*, 2011; Stadermann *et al.*, 2018; Wilhelms and McCauley, 1971]. Orbital remote sensing indicates that these flows are of different ages yet have major element chemistries that are indistinguishable with existing observations [Besse *et al.*, 2011; Heather *et al.*, 2003; Stadermann *et al.*, 2018; Weitz and Head III, 1999] and thus are only separable by crater density (relative age). The detailed chemistry returned by Intrepid (impossible to obtain from orbital platforms) would show whether the units are compositionally distinguishable, lending greater insight to the evolution of magma source regions over time. In particular, remote sensing is not clear on the possible relationship between extended volcanism and the content of radiogenic heat-producing elements (Th, K), but Intrepid measurements would unambiguously test for a relationship.

Orbital observations of the OP basalt region are confounded by rays from Aristarchus crater that mixed material ejected from the crater into the regolith. Intrepid observations would: 1) show how magma source regions evolved over time (locally and relative to other areas visited by Intrepid), 2) examine the significance of mixing in ray materials, and 3) investigate mare tectonism (Appendix B.1.8). Perhaps the most significant contribution of this OP traverse is determining if the basalts are intrinsically rich in KREEP elements, particularly the radiogenic heat-producing elements. Remote sensing observations suggest these OP basalts (both P51 and P60) contain 3 to 6 ppm Th [Lawrence *et al.*, 2007]; however, the Th signal may be contamination from Aristarchus crater ejecta, and not intrinsic to the basalts. By measuring the composition of materials in ray shadow areas and excavated from depth at a series of young impact craters (25-200 m diameters) we can test if the Th is native to the basalts or not.



Finally, the OP traverse includes a traverse up one of the few lunar shield volcanoes (10 km diameter). The relative paucity of this type of volcanic landform is a mystery, and understanding its origin requires a comparison of its chemistry and physical properties relative to the nearby flood basalt deposits.

The traverse then extends across Aristarchus Plateau (AP), which is a crustal block thought to have been uplifted during the formation of the Imbrium basin [Zisk *et al.*, 1977]. The plateau is covered by one of the largest pyroclastic deposits on the Moon [Gaddis *et al.*, 2003] and the widest and deepest sinuous rille [Hurwitz *et al.*, 2013b]. The pyroclastic deposit may contain volatile elements in quantities up to several hundred ppm [Milliken and Li, 2017], possibly representing an ore grade deposit [Hawke *et al.*, 1991]. The APXS and GRNS spectra, HLI images, and color stereo observations would: 1) elucidate the range in chemistry of the pyroclastic deposits, 2) measure the range of composition of the basalt beneath the deposit (revealed in rille walls and crater ejecta), and 3) disentangle the mixing of Aristarchus crater ejecta with local material in the ray-formation process (ejecta shadowed areas vs. rays). Characterizing this massive pyroclastic deposit (vertically and laterally) would provide insight to deeper mantle source regions [Grove and Krawczynski, 2009] relative to the mare basalt that were sourced from the upper mantle (Appendix B.1.9).

Next, Intrepid would traverse the southeastern rim of Aristarchus Crater (AC), a ~40 km Copernican crater (<300 Myrs age; [Zanetti *et al.*, 2017]) that excavated material from the crustal block of AP. Of great interest is the unusual layering revealed in the central peak, which originates from more than 5 km depth [McEwen *et al.*, 1994]. The materials seen in the heterogeneous central peak also drape the crater rim and are thus accessible to the full suite of Intrepid instruments, enabling an unprecedented look at crustal variations. Also, while crossing ponded deposits of AC impact melt, Intrepid would investigate the rate of regolith development and document the recent cratering history on the ejecta blanket. By sampling the granular (or blocky) ejecta and impact melt rocks, Intrepid would test the hypothesis that impact melt is a homogenized sample of the target material [Grieve, 1975]. AC is one of the best locations on the Moon to test this hypothesis because there are large-scale compositional variations and Intrepid would cross several of these units and sample numerous impact melt deposits. If the hypothesis is correct, all the

impact melt deposits would have the same composition and fall on a mixing line of all the granular materials. The most important objective on the AC traverse is determining the nature of the PKT and the associated non-mare rocks (identified from orbit). From the OP traverse Intrepid would have determined if basalts are KREEP-rich or simply contaminated with ejected Aristarchus material. But what is this Aristarchus material? From low resolution (approximately the diameter of the crater) orbital gamma ray observations, it is known that the crater and ejected material contain some of the highest levels of Th on the Moon, potentially in excess of 15 ppm [Lawrence *et al.*, 2007]. What is the range of rock types associated with this crater, and which rocks contain Th and other KREEP-rich components? Answering these questions would allow the first constrained test on the origin of KREEP and possibly other petrologically evolved rock types (granite / rhyolite or monzogabbro / monzodiorite). These questions are among the most significant outstanding questions of lunar petrology (Appendix B.1.11, Hess [1989]).

The traverse culminates at the Aristarchus Irregular Mare Patch (IMP) that is found within the AC ejecta blanket. More than 70 IMP deposits were identified and proposed to be the youngest volcanic landforms (<100 Myrs) on the Moon [Braden *et al.*, 2014]. If the young ages of IMPs are confirmed, they would provide clear evidence that internal heat sources persisted significantly past 1 billion years ago [Braden *et al.*, 2014; Schultz *et al.*, 2006]. An alternative hypothesis is that the IMPs are composed of a magmatic foam that erupted ~3.5 Gyr and these foams had extreme porosity (90%), which renders IMPs resistant to typical degradation processes [Qiao *et al.*, 2018; Wilson and Head, 2017]. In situ exploration with Intrepid can test the magmatic foam hypothesis with high-resolution images of key landforms, particularly the form of impact craters that are predicted to have different shapes when formed in volcanic foams. As the rover passes over the contact between the AC ejecta and the IMP, compositional and morphologic indicators would reveal the stratigraphic relation between the two units, and thus which is younger. Additionally, images of the landforms at the centimeter scale provide the means to determine the nature of regolith formed in magmatic foams (if the IMP is older) or the eruptive processes of young volcanics and early regolith development (if the IMP is younger).



Science Overview

Some objectives require observations collected from much or all of the Intrepid traverse. For example, remanent magnetism records the strength of the early formed core dynamo magnetic field. Over time, the dynamo declined such that there is no longer a measurable global magnetic field [Mighani *et al.*, 2020; Tikoo *et al.*, 2014; Tikoo *et al.*, 2017]. Intrepid would measure remanent magnetism in materials as old as 4 Gyr (or older) in the form of intrusions, most notably at the Reiner Gamma magnetic anomaly (see above; if the dike hypothesis is correct) and possibly at ejected material from AC. Intrepid would characterize remanent magnetism of basalt units with ages of 3.3 Gyr (RG), 2.5 Gyr (MH), 2 to 3 Gyr (AP), 1.9 Gyr (OP), 1.7 Gyr (MH), 1.2 Gyr (OP), and possibly as young as <0.2 Gyr (IMP). This time series of remanent magnetism would not only reveal the evolution of the core but may enable estimating ages of units too small or rough for Crater Size Frequency Distribution (CSFD) analysis (domes, cones, IMP, etc). There should be a strong correlation between CSFD ages from the large dated basaltic plains and their magnetic signatures. If true, this correlation can be exploited for relative dating.

Intrepid's four-year mission and payload suite would document the radiation environment at the surface over a broad range of geologic regions and a substantial portion of the solar cycle, which feeds forward to long duration human exploration planning. In addition, along the traverse, Intrepid would analyze new (post-2009) surface features (craters, splotches) identified in LROC temporal image pairs, providing insight into the cratering process [Speyerer *et al.*, 2016].

Multiple measurements suggest that even at low latitudes, the abundances and locations of hydrogen, water, or hydroxyl vary with local time, increasing during the colder night hours and returning to low levels during the day (e.g., Hendrix *et al.* [2019]; Livengood *et al.* [2015]; Sunshine *et al.* [2009]). However these results have been controversial, both because of the large volumes of H that would have to migrate diurnally implied by neutron spectroscopy [Livengood *et al.*, 2015], and the complications of photometric corrections for reflectance spectroscopy [Hendrix *et al.*, 2019; Sunshine *et al.*, 2009]; measurements of H (to 50 ppm accuracy) from Intrepid have the potential to resolve this debate. Additionally, traverses across regions of varying maturity could provide a quantitative measure of differences in space weathering, where

implanted solar wind H is thought to result in the formation of OH/H₂O within mature materials like agglutinates (e.g., Bandfield *et al.* [2018]), and swirls have been observed to have shallower OH/H₂O absorption bands [Kramer *et al.*, 2011a; Kramer *et al.*, 2011b]. Additionally, there are indications of indigenous water in the Aristarchus pyroclastic deposits [Milliken and Li, 2017], a potentially valuable in-situ resource, and Intrepid could ground-truth these orbital observations.

Regolith vs. Outcrop

The surface of the Moon is covered by regolith — a layer of fragmented and unconsolidated rock predominantly formed as the product of hypervelocity impacts across a broad range of sizes [Shoemaker *et al.*, 1967; 1968; 1969]. The vast majority of orbital remote sensing observations are sampling the regolith, and the same would be true for Intrepid. Regolith formation essentially pre-processes the samples thus reducing the time to collect a measurement and the complexity of required instrumentation (no drilling, grinding or digging is required). As a result the time required at an Intrepid stop is significantly less than that of current Mars missions, which often must prepare samples from exposed outcrop before acquiring many key measurements [McSween *et al.*, 2009; Wdowiak *et al.*, 2003]. Only in a few cases would Intrepid encounter outcrop (in-place rock), perhaps some of the volcanic constructs and impact melt deposits. In those cases, the arm would place the APXS directly on the sample as it does for regolith sampling. Weathering rinds on lunar samples are typically <100 microns in thickness and the bulk chemistry of affected materials is not changed and thus would not affect the APXS (or GRNS) measurements [Keller and McKay, 1997].

The Third Dimension

Intrepid would take advantage of the fact that impact events overturn the local stratigraphy, such that the deepest excavated material is deposited on or near rim and shallower material is deposited outward from the rim (to ~1 crater radius). This sampling strategy was validated by the Apollo astronauts many times, and in fact the core science rationale for the Apollo 14 mission depended on a radial traverse of Cone crater [Swann *et al.*, 1977]. As a general rule of thumb, the deepest material is excavated from about one-tenth the diameter of the crater. By visiting the rims of craters of various diameters (50 m, 100 m ...) Intrepid can sample the underlying stratigraphy at depths (5 m, 10 m ...) and through time (deeper material is generally older



material). It may be possible to trace the lateral extent of a partially buried unit through its geochemical fingerprint, or discover previously unknown units with no outcrops. For example, a buried high-Ti mare underneath a younger low-Ti mare would be readily identifiable from excavated materials, as would the thickness of the younger mare. This capability is crucial for mapping out local changes in the chemistry source regions over time. The meter scale images returned by the LROC NAC allow identification of safe spots on the rims of craters to obtain these measurements (Appendix B.1.10).

Expected Significance and Traceability to NASA Goals and Objectives

Overall, the Intrepid traverse enables a wealth of transdisciplinary observations addressing themes highlighted in guiding documents such as *Vision and Voyages for Planetary Science in the Decade 2013-2023* [NRC, 2011]. The V&V document includes three research goals for the inner planets that would be directly addressed by Intrepid: 1) Understand the origin and diversity of terrestrial planets, 2) Understand how the evolution of terrestrial planets enables and limits the origin and evolution of life, and 3) Provide critical context and information for future human exploration (Table 1-1). The next decadal survey, which would guide exploration objectives for the years 2023 to 2032, is currently in progress; themes that the Intrepid mission would be highly relevant to include: planetary-scale differentiation and thermal evolution; understanding the origins of planetary asymmetries (e.g., compositional, structural, thermal); diversity of mantle processes and magmatism; and post-emplacement modification of geologic materials (Table 1-1 and Appendix B.1.2).

Intrepid's objectives are also fully aligned with key NASA planning documents [LEAG, 2016; NAC, 2007; NRC, 2007], and observations from Intrepid can retire many outstanding science questions (Table 1-2).

The significance of the proposed Intrepid observations should not be underestimated. Intrepid observations would enrich our inventory of magmatic compositions and eruption mechanisms and test key hypothesis, current interpretation assumptions and methods. Further, by associating previously unavailable sub-pixel composition, texture, and morphology, Intrepid observations would increase the value of existing orbital remote sensing datasets. For example, calibrating and interpreting binned Lunar Prospector gamma and neutron

spectrometer elemental estimates relies on ties to geochemistry from Apollo sample locations (e.g. Lawrence *et al.* [2002]). Thus, adding more calibration points from large relatively homogeneous basaltic areas (i.e. OP traverse) and unusual compositions (i.e. RG and AP) would improve calibration fits. Sub-pixel sharpening methods that rely on accurate knowledge of an instrument's spatial response function and have been used in conjunction with the Lunar Prospector gamma ray observations (as well as other applications) to investigate Th abundance at the Aristarchus plateau (using the Pixon method [Lawrence *et al.*, 2007]). Intrepid observations would provide a definitive test of the method.

Instrument Suite and Measurements

The heart of the Intrepid investigation is a robust set of observations obtained by 8 instruments (plus the passive lunar retroreflector). The payload was selected to acquire the magnetic, radiation, solar wind, geochemistry, mineralogy, and landform observations required to meet the science objectives while maintaining high-TRL and a simple ConOps.

TriCam: TriCam consists of three cameras mounted side-by-side (10 cm separations) on the mast. Two Bayer pattern 3-color (Figure 1-3) stereo cameras each have a field-of-view (FoV) of 50° horizontal by 37.5° vertical, providing 3D context around the rover while also supporting arm operations. FarCam [Robinson and Ravine, 2012] is mounted between the two stereo cameras and is an adaptation of the 100 mm focal length MSL MastCam instrument modified to meet lunar requirements. It is a monochrome imaging system (FoV 6.7° by 5.0°) providing high resolution (5 cm at 1 km) images for geologic context and close-up inspection of landforms the rover cannot access. FarCam also serves as the telescope of the Point Spectrometer; there is a fiber optic pickup on the FarCam focal plane. TriCam shares a common electronics box (commanding, compression, and buffering) with the Hand Lens Imager and Point Spectrometer. All components of TriCam have heritage with Malin Space Science Systems E-Cam, MSL, and LRO imaging systems.

PS: The Point Spectrometer provides spectral reflectance (16 bands, Figure 1-3) across the wavelength range 300 to 1400 nm enabling mineralogic abundance estimates (clinopyroxene vs orthopyroxene, spinel, glasses, olivine, shocked plagioclase, and maturity). Spectra would have a spot size of 3 m at 100 m. The fiber optic pickup on

Table 1-1. Science Traceability Matrix. Note that the Laser Retro-Reflector is not required to meet or address any Intrepid science objectives.

Themes (Science Goals)	Science Objectives	Physical Parameter	Measurement Requirements (Observable)	Instrument Requirements	Instrument Capability	Instrument Accommodation Requirements				
<p>1. Evolution of the lunar interior</p> <p><i>V&V 2011: Origin and diversity of terrestrial planets and their interiors; How planetary bodies differentiate and evolve, bulk composition of the planets to understand their formation and evolution</i></p> <p><i>2023 Decadal: Evolution of planetary interiors</i></p>	(1.1) Determine if extended volcanism in Procellarum volcanic terrain was due to: (a) mantle heterogeneity, (b) mantle overturn, (c) radioactive-element abundances (heating), or (d) migration of melting deeper with time	Mineralogy: relative abundance pyroxene (Opx,Cpx), olivine, ilmenite over >3 Gyr (Figure 1-3)	#1 UV-Vis-NIR spectral reflectance (absorption bands)	<p>Satisfies # 6,9,10,15,17 RGB stereo imaging</p> <ul style="list-style-type: none"> FOV: ±60° at 2 m – 20 m in front of rover IFOV: 50 cm at 1 km SNR > 80 with < 75° incidence angle 	<p>Driven by: #6</p> <p>RGB color stereo imager</p> <ul style="list-style-type: none"> FOV: >180° (mosaicking) at 2 m – 100 m IFOV: 2.2 × 10⁻⁴ radians SNR >120 with <75° incidence angle 	<p>Mast-mounted RGB stereo FarCam stereo Point spectrometer</p> <ul style="list-style-type: none"> Yaw: ±90° Pitch: -60° – +15° Pointing accuracy: ±2° Height: > 1.4 m above surface 				
	(1.2) Test whether crustal asymmetry (1) was caused by a degree-1 overturn, (b) was caused by a large, early Procellarum basin impact, or (c) does not exist (average crust covered by basalt)	Major- and trace-element chemical composition (Figure 1-4)	#2 X-ray spectra (0.8 – 14 keV) resolve Na, Mg, Al, Si, P, K, Ca, Ti, Cr, Mn, Fe, Ni, Zr lines #3 Gamma-ray spectra (0.5 – 9 MeV). Quantify the gamma-ray flux for the following elemental lines: O, Mg, Al, Si, K, Fe, and Th				<p>Satisfies # 9,15,17 Monochrome stereo imaging</p> <ul style="list-style-type: none"> FOV: ±60° at 2 m – 20 m in front of rover IFOV: 10 cm at 1 km SNR >80 with <75° incidence angle 	<p>Driven by: #9</p> <p>FarCam monochrome stereo imager</p> <ul style="list-style-type: none"> FOV: >180° (mosaicking) at 2 m – 100 m IFOV: 5 × 10⁻⁵ radians SNR >120 with <75° incidence angle 		
	(1.3) Test hypothesis that non-mare volcanism exposed by Aristarchus Crater formed through bimodal volcanism and basaltic underplating vs. extended fractional crystallization	Subsurface density variations	#4 Static gravitational acceleration	<p>Satisfies # 1,6,10,16,18 Spectral reflectance</p> <ul style="list-style-type: none"> 300 nm – 1400 nm; 16 bands FOV: < 2° FWHM < 40 nm SNR > 80 with <75° incidence 	<p>Driven by: #1</p> <p>Point spectrometer</p> <ul style="list-style-type: none"> 16+ bands FOV < 0.3° FWHM < 30 nm SNR > 120 with < 75° incidence angle 					
	(1.4) Determine composition of the deep mantle from pyroclastic glasses on Aristarchus Plateau	Major- and trace-element chemical composition (Figure 1-4) Grain size, physical state, visible color of pyroclastic materials	#5 X-ray spectra, Gamma-ray spectra as defined in #2, #3 #6 Three-band visible color reflectance				<p>Satisfies: # 6, 10 RGB hand lens imaging</p> <ul style="list-style-type: none"> 3-band visible color imager Pixel scale: 50 microns SNR >80 	<p>Driven by: #6</p> <p>Hand Lens Imager</p> <ul style="list-style-type: none"> RGB color Pixel scale: 15 microns SNR > 120 		
	(1.5) Test slow decline vs. fast decline hypothesis of core dynamo	Magnetic field	#7 Vector magnetic field within volcanic units of different ages	<p>Satisfies # 2,5,8,13,14 X-ray spectra</p> <ul style="list-style-type: none"> 0.8 keV – 16 keV 300 eV at 6.4 keV below -5 °C FWHM: 200 eV below -15 °C 	<p>Driven by #13,#14</p> <p>APXS</p> <ul style="list-style-type: none"> 0.8 keV – 25 keV 200 eV at 6.4 keV below -5 °C FWHM: < 150 eV below -15 °C 					
<p>2. Diversity of styles of magmatism</p> <p><i>V&V 2011: Characterize planetary surfaces; Identify the major volcanic features and their distribution, composition, and timescales</i></p> <p><i>2023 Decadal: Diversity of styles of magmatism</i></p>	(2.1) Test for relationships among flood basalt emplacement, vents, and rilles	Major and trace element chemical composition (Figure 1-4)	#8 X-ray spectra, Gamma-ray spectra as defined in #2, #3			<p>Satisfies # 3, Gamma-ray & Neutron spectra</p> <ul style="list-style-type: none"> 0.5 MeV – 9 MeV Neutron effective area > 30 cm² at 0.01 eV 	<p>Driven by #3</p> <p>GRNS</p> <ul style="list-style-type: none"> 0.4 MeV – 10MeV Neutron effective area: 50 cm² at 0.01 eV 	<p>GRNS</p> <ul style="list-style-type: none"> 0.4 MeV GRNS: fixed to rover, <70 cm from surface with clear view to the surface. 		
	(2.2) Test whether volcanic construct morphology is caused by (a) composition (Si/Fe, volatile content) or (b) effusion dynamics (e.g., composition would be the same, but grain size might differ)	Landform morphology (flow features to whole edifice, meter scale) Grain size, physical state, visible color of pyroclastic materials	#9 3-D shape from (length, width, position) #10 Three-band visible color reflectance						<p>Satisfies # 4,7,8,18,19,21 Magnetic field</p> <ul style="list-style-type: none"> Magnetic field: ±1000 nT Precision: 2nT Sampling rate: 1 Hz 	<p>Driven by: #7</p> <p>Magnetometer</p> <ul style="list-style-type: none"> Magnetic field: ±100,000 nT Precision: 0.2 nT Sampling rate: 1 Hz
	(2.3) Test whether the driving parameter in the Aristarchus pyroclastic deposit was (a) volatile content, (b) major element composition, or (c) fragmentation dynamics (associated with bead size and deposit thickness)	Subsurface density variations	#11 Static gravitational acceleration							
	(2.4) Test hypothesis that intrusive bodies of subvolcanic rock occur in relation to specific effusive volcanic eruption styles	Subsurface density variations Major- and trace-element chemical composition (Figure 1-4)	#12 Static gravitational acceleration #13 X-ray spectra, Gamma-ray spectra as defined in #2, #3	<p>Satisfies # 21 Radiation absorption</p> <ul style="list-style-type: none"> Absorbed energy: 75 keV – >10 MeV TID max resolution: 20 μrad TID max range: 50 krad – ∞ 	<p>Driven by #21</p> <p>ARMAS</p> <ul style="list-style-type: none"> Absorbed energy: 60 keV – >15 MeV TID max resolution: 14 μrad TID max range: 100 krad 					
<p>3. Post emplacement modifications</p> <p><i>V&V 2011: How planetary surfaces are modified by geologic processes; Determine impact flux over time; Understand limits and origins of life through volatile distributions and impact flux; Context and input for human exploration</i></p> <p><i>2023 Decadal: Post emplacement modifications of planetary materials</i></p>	(3.1) Determine if impact crater rays are (a) primarily caused by addition of primary ejected material or (b) by the excavation of fresh material by secondary crater formation and the ballistic sedimentation process	Major- and trace-element chemistry as function of depth Distribution and angularity of blocks (cm to 10 m diameter) Regolith maturity (320/450 nm and 970/750 nm features) (Figure 1-3)	#14 X-ray spectra, Gamma-ray spectra as defined in #2, #3 #15 3-D shape (length, width, angularity, position) #16 UV-Vis-NIR spectral reflectance (absorption bands)			<p>Satisfies # 4,11,12 Acceleration measurement</p> <ul style="list-style-type: none"> Sampling interval: 100 m distance Sensitivity: 100 mGal 	<p>Driven by #4</p> <p>LN-200S</p> <ul style="list-style-type: none"> Sampling rate: up to 400 Hz Sensitivity: 10 mGal 	<p>LN-200S: Accurate transformation of IMU position relative to rover COM</p>		
	(3.2) Determine target material influence on crater characteristics and impact mechanics	Distribution in crater ejecta in relation to crater shape relative to composition of materials	#17 3-D shape (length, width, position)							
	(3.3) Test origin of strong magnetic anomalies hypotheses. Determine variations in space weathering across a variety of materials and ages (relationship to radiation environment, H abundance, magnetic anomalies)	Regolith maturity (320/450 nm and 970/750 nm features) (Figure 1-3)	#18 UV-Vis-NIR spectral reflectance (absorption bands)							
		Magnetic field	#19 Vector magnetic-field variations at RG magnetic anomaly							



the focal plane of FarCam is routed to the detectors in the warm electronics box. The PS requires the most development of all the instruments, however it is entirely built of high TRL components, including the detectors.

GRNS: The Gamma Ray Neutron Spectrometer provides the primary geochemical measurements for Intrepid with integration collected while in motion and when stopped. It returns Si, O, Fe, Mg, K, Al, Ca, Ti, Th to better than 3%, and it enables estimates of H abundance to 50 ppm (from neutron absorption) (Appendix B.1.14). The instrument senses elements throughout the top 30 cm of regolith. The ARMAS provides simultaneous measurements of the Galactic Cosmic Ray environment which improves the GRNS calibration ensuring the 3% absolute accuracy is met (see Appendix B.1.12).

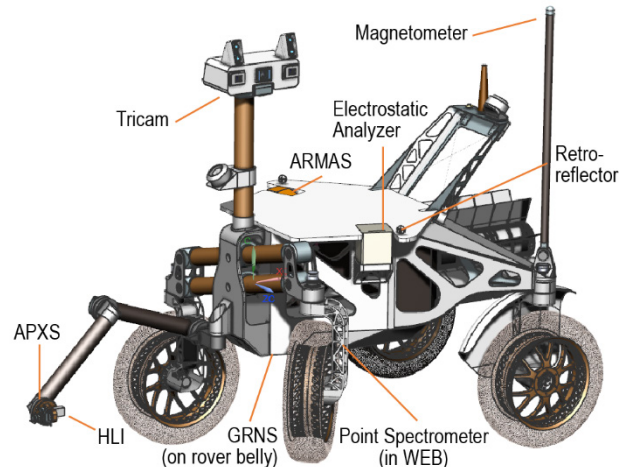


Figure 1-2. Rover schematic showing instrument accommodation.

Table 1-2. Intrepid relevance to key NASA exploration documents (Region Abbreviations: RG – Reiner Gamma; MH – Marius Hills; OP – Oceanus Procellarum; AP – Aristarchus Plateau; AC – Aristarchus Crater; IMP – Irregular Mare Patch). The “(all)” notation under region indicates that all the regions would contribute some understanding to the particular question while the called out region(s) are the most significant contributors.

SCEM Goals (2007, 2018), LER Science Objectives (2016), & NAC Report (2007)	Contribution	Region
SCEM 1d. Assess the recent impact flux. (LER: Sci-A-7, Sci-A-8, Sci-B-1) (NAC mGEO-6)	Significant	RG, OP (all)
SCEM 1e. Study the role of secondary impact craters on crater counts. (LER: Sci-B-1, Sci-A-8) (NAC mGEO-6)	Significant	RG, OP (all)
SCEM 2a. Determine the thickness of the lunar crust (upper and lower) and characterize its lateral variability on regional and global scales. (LER: Sci-A-5, Sci-A-8, Sci-A-9) (NAC mGEO-2)	Significant	MH, OP, AP, AC, IMP
SCEM 2d. Characterize the thermal state of the interior and elucidate the workings of the planetary heat engine. (LER: Sci-A-5, Sci-A-8, Sci-A-9) (NAC mGEO-2)	Incremental	IMP
SCEM 3a. Determine the extent and composition of the primary feldspathic crust, KREEP layer, and other products of planetary differentiation. (LER: Sci-A-5, Sci-A-8, Sci-A-9) (NAC mGEO-2, 5)	Significant	MH, AP, AC, IMP (all)
SCEM 3b. Inventory the variety, age, distribution, and origin of lunar rock types. (LER: Sci-A-8) (NAC mGEO-2, 5)	Significant	MH, AP, AC, IMP (all)
SCEM 3c. Determine the composition of the lower crust and bulk Moon. (LER: Sci-A-5, Sci-A-8, Sci-A-9) (NAC mGEO-2)	Incremental	MH, AP, AC, IMP (all)
SCEM 3d. Quantify the local and regional complexity of the current lunar crust. (LER: Sci-A-5, Sci-A-8, Sci-A-9) (NAC mGEO-2, 5)	Significant	AC
SCEM 5a. Determine the origin and variability of lunar basalts. (LER: Sci-A-6, Sci-A-8, Sci-A-9) (NAC mGEO-2, 5)	Significant	MH, AP, IMP (all)
SCEM 5b. Determine the age of the youngest and oldest mare basalts (LER: Sci-A-8) (NAC mGEO-2) (NAC mGEO-2)	Significant	MH, OP, IMP
SCEM 5c. Determine the compositional range and extent of lunar pyroclastic deposits (LER: Sci-A-6, Sci-A-8, Sci-A-9) (NAC mGEO-2, 4, 14)	Significant	MH, AP, AC, IMP
SCEM 5d. Determine the flux of lunar volcanism and its evolution through space and time. (LER: Sci-A-6, Sci-A-8) (NAC mGEO-2)	Significant	MH, OP, IMP
SCEM 6c. Quantify the effects of planetary characteristics (composition, density, impact velocities) on crater formation and morphology. (LER: Sci-A-7) (NAC mGEO-6)	Significant	AP, AC, IMP
SCEM 6d. Measure the extent of lateral and vertical mixing of local and ejecta material. (LER: Sci-A-4, Sci-A-7) (NAC mGEO-6)	Significant	OP, AP
SCEM 7b. Determine physical properties of the regolith at diverse locations of expected human activity (LER: Sci-A-4, FF-C-5) (NAC mGEO-10)	Significant	MH, AP
SCEM 7c. Understand regolith modification processes (including space weathering), particularly deposition of volatile materials (LER: Sci-A-4, FF-C-5) (NAC mGEO-11, 12)	Significant	RG, AP (all)
SCEM 8b. Determine the size, charge, and spatial distribution of electrostatically transported dust grains and assess their likely effects on lunar exploration and lunar-based astronomy (LER: Sci-A-1, D-22, Sci-C-3) (NAC mGEO-10)	Incremental	RG (all)

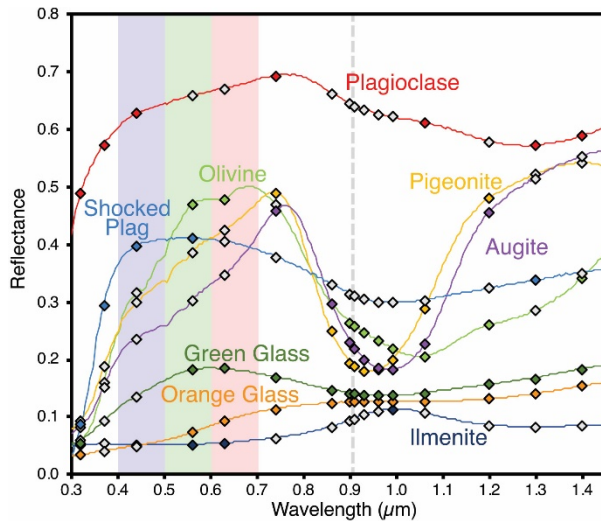


Figure 1-3. Spectra of lunar mineral separates from Apollo samples 15555 and 70035 (crushed and sieved to <45 μm size fraction; Isaacson et al., 2011), and lunar orange and green volcanic glass from the RELAB library, shocked plagioclase from Pieters (1996). Solid lines indicate lab spectra and diamonds show PS bandpass centers. Solid RGB color indicate sensitivity of HLI and SCI. Vertical line separates CCD (left) and InGaAs (right) detectors.

APXS: The arm mounted Alpha Particle X-ray Spectrometer provides close-up elemental abundances (Si, O, Fe, Mg, K, Al, Ca) to ≤3% accuracy in one hour integrations, and all elements with atomic numbers between 11 and 40 (Na through Zr) in 4 hrs. The APXS requires temperatures <0°C; a cryocooler would maintain the detector at its operating temperature during most of the day (with some exceptions due to rover position, local topography and time of day). The instrument senses elements in the top 2 cm of the target (regolith or rock) which complements the GRNS measurements which sense the top 30 cm of the target (see Appendices B.1.12 and B.1.13).

HLI: The Hand Lens Imager is mounted on the arm and has active focus and active illumination (for close up targets), providing flexibility to image the surface at 20 micron pixel scale night and day (15 micron at 22.5 mm). The pixel scale was selected due to the average grain size of most lunar soils between 45 and 100 microns [Heiken et al., 1991]. Its Bayer pattern 3-color capability is a powerful tool for investigating color differences known to exist within lunar pyroclastic beads [Heiken et al., 1991]. HLI also serves a critical outreach function, imaging the rover and Earth (in color).

Mag: The Magnetometer is a dual ring-core tri-axial fluxgate instrument that would determine

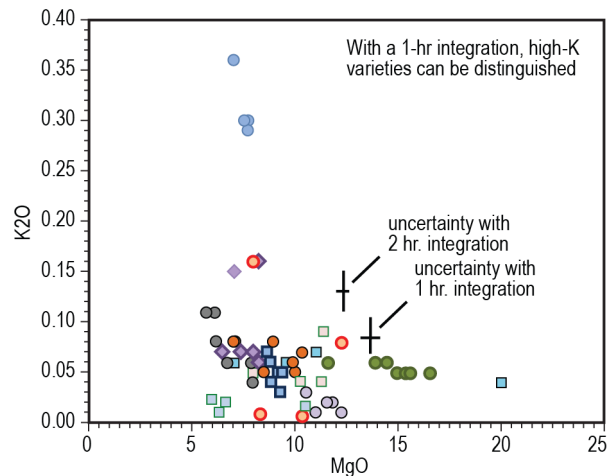


Figure 1-4. Weight percent oxides for Apollo and Luna basalt groups measured in the laboratory compared to the expected analytical uncertainty (precision) for the APXS. TiO₂ and FeO are two of the main parameters, along with K₂O and MgO, to discriminate lunar mare basalt groups.

the strength, orientation, polarity and depth of the Reiner Gamma remanent magnetic field [Hemingway and Garrick-Bethell, 2012; Hood and Schubert, 1980; Kurata et al., 2005] and thus allow definitive testing of current formation models (review in Robinson et al. [2018]). Determination of the characteristics of the 3D magnetic field at Reiner Gamma also provides the means to determine the nature of the associated albedo patterns known as swirls. Over the course of the mission as Intrepid traverses across progressively younger basalts the Mag would measure their remanent magnetism and thus determine the decay rate of the core dynamo (Mighani et al. [2020] and references therein).

ESA: The ElectroStatic Analyzer measures ions (200 eV to 20 keV; 9% accuracy) impinging on the surface. Its key roles are determining the shielding effects of the RG magnetic anomaly as the rover passes through the field, providing the means to determine the relative importance of solar wind in space weathering processes (across the whole traverse) and the utility of magnetic anomalies to protect future surface assets.

ARMAS: The Automated Radiation Measurements for Aerospace Safety records the Total Ionizing Dose (TID) from all sources including heavy ions, alphas, protons, neutrons, electrons, and gamma rays, provided they be energetic enough to deposit at least 60 keV in the sensor and up to 15 MeV, (range of interest for deep penetration into a material). ARMAS would provide critical information regarding the primary



and secondary radiation environment. Key information for planning future human exploration of the Moon as well as extending our characterization the space weathering environment and its effect on surface materials. Additionally, ARMAS would play a significant role in calibrating the GRNS observations. ARMAS requires mostly unobstructed zenith omnidirectional viewing.

LRR: The Laser Retro-Reflector is passive, using no power and producing no onboard data. It simply reflects laser shots back to an orbiting spacecraft as part of ranging geophysics experiments, which can also supply precise geographic coordinates of the rover. The LRR is not required to meet any Intrepid objectives.

IMU: The LN-200S Inertial Measurement Unit is not strictly a science instrument but it allows estimates of the local gravity field, which in turn are used to estimate density contrasts in the subsurface (Lewis et al., 2019). This capability provides the ability to detect dikes and subsurface voids. For example, a dike that begins at the base of the crust (~30 km depth) and extends to within 0.5 km of the surface, width of 250 m, and a density contrast of 500 kg/m³ (density difference between the upper crust (2550 kg/m³, Wieczorek et al., 2013) and the bulk densities of Apollo lunar basalts (~3010–3247 kg/m³) would produce a gravity anomaly of ~600 mGal. This signal is detectable with margin (IMU/accelerometer performance ~10 mGal).

Outreach Opportunities

The Intrepid mission enables a unique opportunity to infuse science into the public consciousness through formal education programs, a series of outreach events, immersive and interactive experiences, as well as continuous tracking exercises reaching a broad web audience. Intrepid’s steady progress would be displayed on an interactive webpage with daily image updates and activities that invite frequent return visits. With the near-real-time communication between Intrepid and Earth, there would be opportunities for the public to take LIVE pictures from the mast cameras. A simplified engineering model of Intrepid would be exhibited at schools, museum events, and Arizona State University and JPL open house events enabling the public to experience how the rover operates; including its autonomy and hazard avoidance capabilities. To further increase our reach, including under-served populations, small science kits focused on each leg of the traverse can be provided to public libraries (similar to: <https://tinyurl.com/yxsslry7>) and partner schools for STEM events similar to the solar eclipse kits provided to the STAR Library Education Network in 2017 (<https://tinyurl.com/y9mr87y5>). From these kits, people can track the rover’s progress (location and science) and from the phase of the Moon assess the rover’s lighting conditions (see Appendix B.1.16).

Table 1-3. Intrepid instrument suite. Power and mass estimates from high TRL instruments, except Point Spectrometer. Note: TriCam, PS and HLI share same electronics box inside rover – only one rover interface for power and data for these three instruments (instrument capabilities, not requirements).

Instrument	Key Parameters	Data	Peak Power (W)	Standby Power (W)	Mass (kg)
ARMAS	60 keV to >10 MeV	~300 kBytes / hr	0.3	0.3	1
Magnetometer	±100,000 nT range, 0.2 nT resolution	60 kBytes / hr	1.7	1.7	0.5
Gamma Ray Neutron Spectrometer	3% accuracy in 1 to 12 hrs depending on element	4 kBytes / obs.	4	4	3
TriCam Stereo RGB Imager + BW FarCam (electronics shared with PS, HLI)	50° FoV, 8 mm pixel scale @ 10 m 6.7° FoV, 5 cm pixel scale @ 1 km	Up to 8.6 Mbytes / obs.	12	9	5.9 (3.5 kg on mast)
Point Spectrometer uses FarCam telescope	300 to 1400 nm 16 bands 30 cm spot size @ 10 m	~35 Bytes / obs.	4	4	2 (1 kg on mast)
Hand Lens Imager	2 cm to infinity focal range 15 µm pixel scale @ 23mm	5.4 MBytes/ obs.	12	1	0.6
Alpha Particle X-ray Spectrometer	3% elemental (Z between 11 and 40) abundance in 4 hrs	~30 kBytes/ obs.	8	8	2.3 (0.9 on arm)
Electrostatic Analyzer	200 eV to 20 keV	500 kBytes/hr	2	2	4.2
Laser Retro-Reflector	Visible from nadir pointed orbiting laser	0	0	0	0.5
Totals				30	19.8



2 HIGH-LEVEL MISSION CONCEPT

Concept Maturity Level

The Intrepid concept as presented in this study is at CML 4, per the definitions presented in the PMCS ground rules. An initial CML 3 trade-space analysis was completed by a dedicated study team at the outset of this work. The initial rover trade space was culled down to two potential architectures; Radioisotope Power System (RPS) and solar powered, during this first phase of the study. Each option was then defined at the assembly level and was estimated for mass, power, data volume, link rate, and cost by Team X using JPL’s institutionally endorsed design and cost tools. Following this an in-depth configuration, design and operations refinement effort was conducted by the study team. Risks were also compiled as part of this study.

Technology Maturity

The Intrepid rover design benefits from significant prior art, robust engineering processes and design practices, and a large body of knowledge generated in developing and successfully operating Mars rovers over the last two decades. It leverages experience from past and current lunar rovers (Apollo LRV, Lunokhod, Yutu) and builds on current lunar development activities including the VIPER lunar rover, as well as significant advances in capabilities from other space and terrestrial applications. As is the case with any new mission concept, the Intrepid rover will need specific engineering developments and the application of key technologies.

Lunar Dust Environment: Lunar dust is a potential hazard with unique challenges posed by abrasive particles, electrostatic charging of surfaces, and differential charging effects over the day/night cycle. Our current understanding of lunar rover dust challenges is built on experience gained from past lunar surface missions and is informed by continuing technology efforts as well as current plans for the upcoming commercial (CLPS) lander and VIPER rover missions. Given that dust deposition in the lunar environment primarily results from the interactions of the wheels with terrain, the system is designed to keep all dust-sensitive surfaces well above height of the wheels to minimize dust accumulation at Intrepid’s low mobility speed (<1 km/hr). Further, Intrepid’s payload does not require contact with the terrain. While engineering development activities and validation to mitigate dust remain and are

planned for, especially for the long-distance traverse, there are no new technologies that are anticipated beyond what has been employed by prior missions (including Mars) and those being addressed by the upcoming VIPER rover.

Science Instruments: The Intrepid rover mission objectives are met using instruments that have space flight heritage (Table 2-1). The HLI and APXS are based on those currently in use on MSL. ARMAS has flown on high altitude balloons, sounding rockets, Unity Space Ship Two, New Shepard and CubeSats. All components of TriCam have heritage with MSSS ECAM, MSL and LRO imaging systems. While standard engineering will be needed to adapt these instruments to the Intrepid mission, none of them require new technologies. Only the point spectrometer and its integration with the FarCam will require flight qualification since it is based on a new combination of existing product-line elements.

Mobility and Manipulation System: Similar to the LRV, the Intrepid rover is a four-wheel-drive, all-wheel-steered vehicle with compliant wheels. Unlike the LRV, it uses a front rocker suspension. While a front rocker configuration has not thus far been used in a planetary rover, it is a non-actuated, well understood mechanism involving no new technology. Intrepid’s 0.8 m compliant wheels are similar in both size and design to the LRV mesh wheels. NASA Glenn Research Center has conducted a detailed design, development, and testing campaign (currently at TRL 6 for Mars environment) that improved this design to extend durability and traversability (rocks and craters). Further maturation of the wheel design and materials for the lunar environment for this mission will be needed (See Appendix C.1).

Table 2-1. Instrument Heritage Table.

Instrument	Heritage
Hand Lens Imager	MSL MAHLI
Alpha Particle X-Ray Spectrometer	MSL APXS
ARMAS Lunar	LRO CRaTER
Gamma Ray Neutron Spectrometer (GRNS)	MESSENGER, Lunar Prospector and others
Electrostatic Analyzer (ESA)	THEMIS (ESA)
TriCam: Stereo RGB cameras and BW FarCam	MSL, LRO LROC, MSSS ECAM and others
Point Spectrometer (PS) that uses FarCam telescope	MSL and SELENE
Magnetometer	MESSENGER and others
Laser Corner Reflector	SpacEL Beresheet



Intrepid has a 5 degree-of-freedom robotic arm with a joint configuration similar to Mars rover arms as well as arms currently in development for lunar applications. The actuators for both the mobility system and robotic arm leverage existing Mars Curiosity and Perseverance rover actuator designs.

Avionics: The rover flight compute element and avionics for the vision system and motor control are based on current engineering developments at JPL (currently on-track to achieve TRL 5 by September of 2021). Other avionics (e.g., instrument interface, battery and power management, radio) have flight heritage and are not new technology. The rover sensor suite uses flight-proven cameras, optics, IMUs, and sun sensors.

Autonomy: Based on the trade described in the next Section, the Intrepid rover requires, in the nominal case, reliable autonomous surface operations with ground oversight in nominal cases and human-directed actions in off-nominal cases. Autonomous operations comprise mobility, instrument placement, and system management. Autonomous mobility leverages flight-operational capabilities on MER and MSL, which have been further advanced for faster traverse on the Perseverance rover. Unlike Mars though, the availability of continuous, low latency communications (8 hr per day at high bandwidth and 16 hr at low bandwidth) allows ground operators to more rapidly interrogate, diagnose, and respond to faults (a physical or logical cause, which explains a failure) or failures (the unacceptable performance of an intended function) that cannot be resolved by the rover’s autonomous system. Onboard lunar global localization, a technology funded by NASA STMD’s Game Changing Development with a start in fiscal 2021, resets unbounded growth in rover position error after long-traverse segments.

Similar to autonomous mobility, autonomous instrument placement and system management (resource/activity planning and system-health management) leverage decades of technology development and demonstrations on terrestrial prototypes [Backes et al., 2005; Fleder et al., 2011; Pedersen et al., 2005; Wettergreen, 2008]. Aspects of these capabilities have also been or will soon be demonstrated in flight [Chien et al., 2004; Kim et al., 2009; Maimone et al., 2006].

Critical to the operations of the Intrepid rover is the system integration of

several functional elements into an autonomous system and the maturation of all its constituents to achieve the necessary overall reliability for this long-distance mission. Over the years, both space and terrestrial applications have incrementally increased their level of autonomy. The MER and Curiosity rovers have enhanced their mobility with autonomous navigation. The Perseverance rover transitioned autonomous navigation from an enhancing capability to an enabling one, resulting in increased performance. Terrestrial autonomous driving, which was boosted through DARPA’s off-road and urban challenges [Buebler et al., 2009; Iagnemma and Buebler, 2006], similarly increased in performance (mean-distance between faults) through focused and sustained industrial investment. Similarly, Intrepid would need a focused technology investment for the integration and maturation of the several proven functions to a higher degree of performance as discussed in Section 4.

Thermal Management: The thermal management system uses high-TRL component technologies in a new configuration that may need engineering development. Specifically, the thermal switches that provide for radiator turn-down are a new technology element. These switches provide a variable conduction path between the components internal to the WEB and radiators. They are passively actuated based entirely on differences in coefficients of thermal expansion of their selected materials, as shown in Figure 2-1.

The on/off conductance ratio is 5 to 0.002 W/K through a given switch, which is 20× better than the switches flown on MER. Multiple switches are configured in parallel, depending on the heat load to be transferred. These switches, developed at JPL, are currently at TRL 7 having completed flight qualification and life testing.

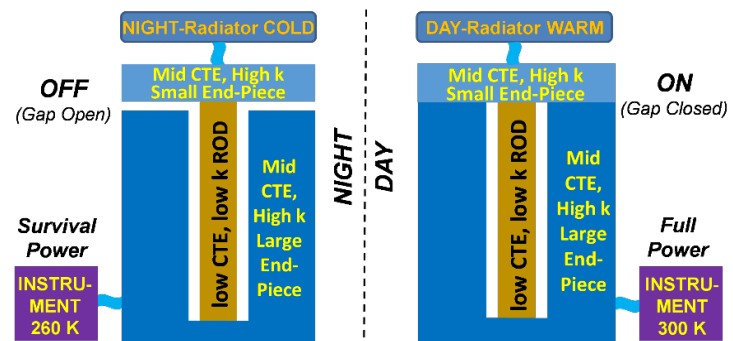


Figure 2-1. Thermal switch design.



Key Trades

The trades for the design and operation of the Intrepid rover are driven by the knowledge of the lunar environment, the traverse distance, energy budget, and communication constraints with considerations for maximizing heritage and technology maturity. The key performance objective is achieving the desired science with sufficient margin. Trades are further detailed in the appendices.

Mobility

Table 2-2 captures Intrepid’s key mobility requirements and expected terrain characteristics. For the mobility trade, key drivers are robustness and durability, long-traverse distance, energy efficiency, low power, and the ability to traverse expected terrain.

Based on these requirements and constraints, we examined mobility designs with different wheel/steering configurations, suspension (passively compliant or actuated) [Nesnas et al., 2000], and wheel types and sizes, leveraging Apollo wheel-design data (see Appendix C). Table 2-3 summarizes the individual mobility trades. The selected architecture is four-wheel drive, all-wheel steering with a passive, single-rocker suspension that balances the weight of the vehicle among its four wheels. The wheels are large for better traction and narrow to reduce mass. Compliant wheel rims improve traction and reduce wear [Asnani et al., 2009].

Autonomy

For the autonomy trade, key constraints that drive the viability of operation modes include: (1) communication availability of the Deep Space Network (DSN), (2) bandwidth of Near Earth Network (NEN) and commercial lunar communication, and (3) the cadence of required rover

motions (traverse and instrument placement). To identify the required level of autonomy, we examined trades ranging from ground-based human control, similar to the joystick operations of the Lunokhod rover, to onboard autonomous control for mobility, instrument placement and system management. Table 2-4 summarizes the autonomy-related trades. Throughput analyses based on sensors dataflow, onboard computation performance, and communication bandwidths showed that this mission has to rely on the onboard decide mode for a significant portion of its nominal operations and on the human-decide mode for handling contingencies. Furthermore, after the first four weeks of 24/7 mission operations, the project transitions to a normal workday schedule, where both traverse and arm operations would inevitably fall outside the workday schedule. Therefore, a significant portion has to be conducted through autonomous operations.

Power Source

The choice of power source for the rover was one of the first major trades to be addressed in the study. The original concept assumed radioisotope power would be required for overnight survival and limited night-time operations and early designs planned on incorporating a single MMRTG,

Table 2-2. Key Mobility Requirements and Constraints.

	Requirements		Comments
	Rover	Distance	1800 km
Daytime speed (avg)		14 cm/s	Nominal speed will be at max speed to compensate for slower traverse due to unexpected situations
Daytime speed (max)		28 cm/s	
Nighttime speed		1.4 cm/s	
Environment	Characteristics		Comments
	Surface properties	Regolith	Largely ubiquitous
	Max slope	15°	From 3x3 grid (5 m/px) DTM
	Rock distribution (area coverage)	1%	Most of the traverse route
		10%	Around crater rims
Crater distribution (areal coverage)	~10%	Diameter: 5 m < ϕ < 250 m (for ϕ < 35 m, depth not measurable from orbit; but traversable; otherwise, need to be avoided)	

Table 2-3. Mobility Trades, Selection, and Rationale.

	Key Trades	Selection	Rationale
Type	Wheeled vs. tracked	Wheeled	Lower mass, larger ground clearance and lower risk of rock entrapment
	Configuration	<u>Drive + steering wheels:</u> 3-wheel (1 steering) 4-wheel (0 steering) 4-wheel (2 steering) 4-wheel (4 steering) 6-wheel (4 steering) 6-wheel (6 steering)	4-wheel (4-steering)
<u>Suspension:</u> Active vs. passive vs. spring-loaded		Passive	Balanced weight on wheels, lower mass and volume in rover body, simpler mechanism, fewer failure modes, adequate for expected terrain difficulty and rock traversal
Dual-sided rocker vs. single-sided rocker		Single-sided rocker	
Wheels		<u>Diameter:</u> Large vs. small Narrow vs. wide (large: ~1½ x MSL) (narrow: ½ x MSL)	Large Narrow
	Rigid vs. compliant	Compliant	Improved mobility in soft regolith and over rocks, improved wear resistance (Table C-10)



Table 2-4. Autonomy-related Trades, Selection, and Rationale.

	Key Trades	Selection	Rationale
Operation Modes	<ul style="list-style-type: none"> • Human control: operators joystick every action • Human decide: ground computers assess situation w/ humans deciding on actions • Ground compute: computers assess situation and decide w/ limited async human oversight • Onboard decide: onboard computer controls w/ limited async human oversight 	<p>Main: Onboard decide</p> <p>Backup: Human decide</p>	<p>DSN availability of 8 every 24 hours, limited bandwidth of commercial communication, and need to drive for hundreds of hours (Earth day/night) left the onboard-decide mode as the only viable option for nominal operations to meet traverse rate. Slower operations can use human-decide mode. (Table C-11-13)</p>
Sensors	<p><u>Exteroceptive</u></p> <ul style="list-style-type: none"> • Cameras (stereo) • LIDARs (flash, spinning) • Star tracker • Sun sensor <p><u>Proprioceptive</u></p> <ul style="list-style-type: none"> • Inertial • Resolvers, encoders, hall effect • Motor currents 	<p>Stereo cameras + Sun sensor</p> <p>IMU + hall-effect (all) + resolvers (arm / steer only) + current</p>	<p>Lower power and mass; mature capability; wide field-of-view. No illumination needed with longer exposures at night from Earth-shine</p> <p>IMU complement visual odometry for low textured terrains, provides vehicle tilt; hall-effect sensors and resolvers are more reliable than encoders at high temperatures. Resolvers for absolute angles. Currents to estimate torque</p>
Compute	<p><u>Main Processor:</u></p> <ul style="list-style-type: none"> • LEON3 (dual-core) / Sphinx • LEON4 (quad-core) / Sabertooth <p><u>Aux Processor:</u></p> <ul style="list-style-type: none"> • Virtex 5 	<p>LEON 4 Sabertooth</p> <p>Virtex 5</p>	<p>Quadruple compute and more I/O of LEON4 vs. LEON3</p> <p>Mars 2020 heritage</p>

similar to the MSL and Mars 2020 rovers. At the start of the PMCS effort it was decided that the team should also investigate the possibility of using solar power for daytime operations, carrying sufficient batteries to ensure survival and limited science data taking over the lunar night. This particular RPS/solar power trade resulted in development

of both rover options to a similar level of detail, although for science and operational reasons the RPS powered rover has been retained as the baseline concept for the Intrepid mission. While the solar powered option should also produce a viable long-range, long-duration rover, the limitations on its ability to perform significant science at multiple locations over the long lunar night would result in a significant increase (essentially double) in needed mission duration to achieve the science objectives.

A further trade related to the RPS option was the choice of RPS. The Study Groundrules provided a number of choices including MMRTGs, NextGen RTGs in a variety of sizes, and the DRPS. Given the significant amount of driving involved in the Intrepid mission and the mobility power required while driving the team initially baselined an 8-GPHS NextGen RTG providing ~200 W (BOM). In the course of development of the rover design and concept of operations it was found that the 200 W unit would unacceptably impact the ability to complete the long-distance drives required, and the decision was made to adopt the 12-GPHS NextGen unit with ~300 W (BOM) as the baseline. This choice allows the rover to execute the baseline concept of operations without the need for frequent interruptions for battery charging.

Solar array trades considered the use of deployable wings versus a fixed design. The angled fixed array design was determined to provide the simplest implementation, assuring sufficient illumination and power independent of rover heading or local solar time.

Finally, consideration was given to a hybrid system, using a smaller RPS for base power and nighttime activities, supplemented by a solar array to provide extra power for long drives during day light operations. This option is possible and could be attractive in the absence of the larger RPS options, but was not necessary given the availability of the modular NextGen RTG.

3 TECHNICAL OVERVIEW

Intrepid builds on a history of rover developments from the Apollo LRV through Mars 2020 and existing instrument designs to support this high-value science mission.

Instrument Payload Description

The payload for Intrepid comprises nine instruments. Detailed discussion of the instrument complement can be found in Section 1.

Flight System

Overview

The rover design for Intrepid evolved from two primary driving requirements that flowed from a carefully developed concept of operations provided by the science team. The rover:

- Shall be capable of driving >1800 km across the lunar surface



- Shall operate for 4 years in the lunar environment (RPS) or 7 years (solar)

Both of the above requirements drove the trades on the mobility design and autonomy (including sensor selection and compute) as described in Section 2 of this report and Appendix C. Additional requirements that drove the rover design include the following. The rover:

- Shall support instruments as defined by science team
- Shall return sufficient mission data to Earth

Two versions of the rover were developed in parallel for the study (Figure 3-1); one using RPS for power and thermal control and one using solar power combined with batteries for overnight survival. While it was recognized that the solar option would necessitate a major change in the mission concept of operations and duration to achieve the science goals, it was felt by the team that it would provide a valuable comparison of design options that might be applicable to future missions. System mass and power modes for the two rover variants are shown in Tables 3-1 and 3-2. The RPS-powered rover shows robust mass margin (41%) against the assumed 500 kg allocation. The solar-powered rover mass margin is lower, at 21% for this allocation, but still significant. Both variants show substantial power margins of >40% for worst-case modes. Rover characteristics are summarized in Table 3-3.

Subsystems

Subsystem elements for Intrepid were derived from proven, heritage designs as well as product lines currently in late stages of development.

Mobility/ Manipulation

The mobility system is designed for the expected terrain types along the 1800 km route (see Appendix C.1, Table C-2) with slopes not exceeding 15° and speeds not exceeding 1 km/hr. The mobility system uses a four-wheel drive, all-wheel steering configuration with a passive one-sided rocker suspension. On the RTG version, the rocker is on the front (i.e. on the mast side) and opposite on

Table 3-1. Intrepid Rover Mass Table.

	Mass (kg)					
	RTG Option			Solar Option		
	CBE	Cont.	MEV	CBE	Cont.	MEV
Instruments	19.8	10%	21.8	19.8	10%	21.8
C&DH	16.0	14%	18.3	16.0	14%	18.3
Telecom	7.6	11%	8.4	7.6	11%	8.4
GNC	6.3	10%	7.0	6.3	10%	7.0
Power	61.7	31%	81.1	135.5	42%	192.9
Thermal	12.3	28%	15.7	13.1	15%	15.1
Structures	76.7	23%	94.4	86.6	23%	106.5
Mobility	78.3	30%	101.7	78.3	30%	101.7
Harness	17.4	30%	22.6	30.9	30%	40.2
Rover Total	296.0	25%	371.0	394.1	30%	511.9
Lander Allocation (MPV)			500			500
Margin (MPV-CBE)/MPV			41%			21%

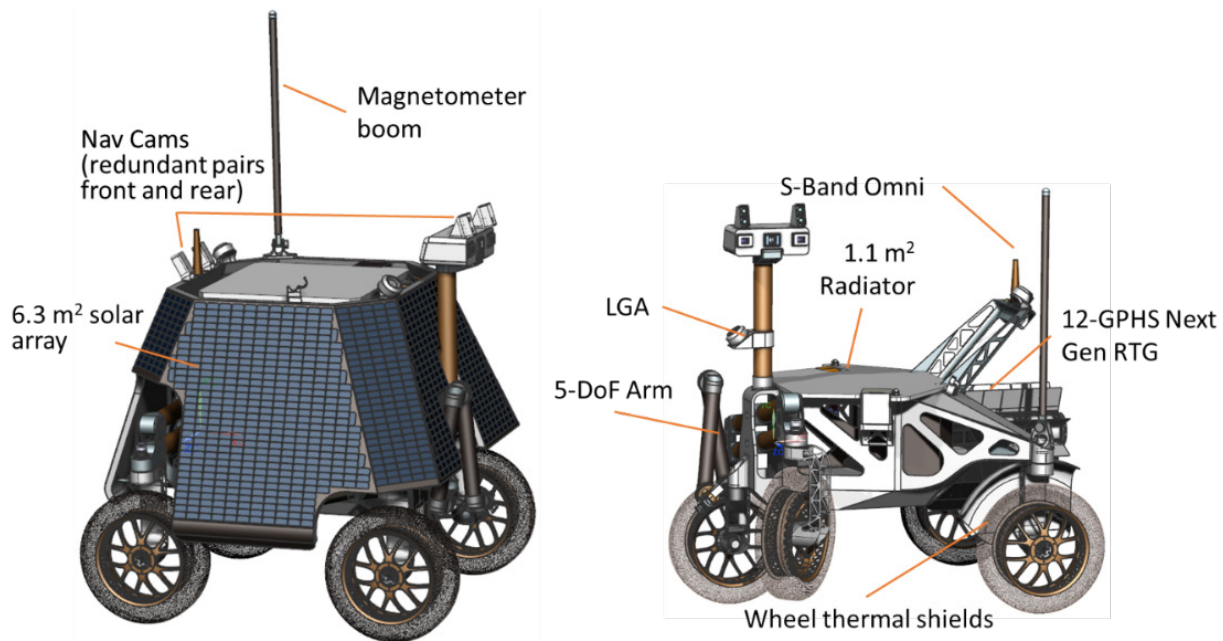


Figure 3-1. The Intrepid Rover study developed complete designs for options utilizing radioisotope power (right) and solar/batteries (left).



the solar. However, the rover is designed to drive in either direction supported by front and back stereo cameras. The rover can also drive sideways at different angles. The rover has >0.6 m ground clearance and large-diameter compliant wheels to improve rock traversal, traction on regolith, and energy efficiency [Asnani et al., 2009; Nuttall Jr., 1965; Sutob et al., 2012]. The 0.8 m-diameter wheels use a mesh structure, similar to the LRV, to traverse rocks that are less than 30 cm in height and drive through smaller craters not apparent in orbital data (<5 m in diameter with a slopes below 10°).

The robotic arm is designed to place two instruments: the APXS and HLI on selected rock and regolith targets. Targets are either selected by the science team or autonomously by the rover. For the former, the required lateral placement accuracy is ±5 cm of the target identified in an image acquired from 1 m away. For the latter, the required lateral placement accuracy requirement is ±15 cm of the centroid of the rock face, typically >60 cm in diameter. Both cases require a 2 cm ±1 cm offset from the surface, and ±30° from the surface normal [VanBommel et al., 2017]. As such, there is no requirement for contacting the surface. The arm has five degrees of freedom; a shoulder pitch and yaw, an elbow pitch, and a wrist pitch and yaw. The wrist pitch points the instrument on the target. The arm is also designed to be capable of imaging under the rover.

All mechanisms use Mars-heritage brushless DC motors with planetary gear boxes. The actuators are sealed from the environment using sintered metal filters and a rotary seal at the output. All actuators use hall-effect sensors in lieu of encoders as they are more tolerant to the higher daytime temperatures. The steering and arm actuators also use resolvers for measuring absolute joint angles. The drive-wheel and arm actuators use magnetic detents in lieu of brakes to reduce power. Steering actuators require neither, allowing smooth steering while driving.

Table 3-2. Intrepid Power Modes.

Subsystem	Power Modes – RTG ¹					Solar	
	Traverse Day (W)	Traverse Night (W)	Science Imaging (W)	Telecom DTE (W)	Charge (Safe) (W)	Night Sleep (W)	Dawn Warmup (W)
Instruments	8	8	22	8	0	0	0
GNC	10	6	2	0	0	0	10
C&DH	29	29	29	29	1	1	13
Power	14	11	10	10	5	1	14
Mobility	60	18	0	0	0	0	0
Telecom	41	41	41	41	6	0	41
Thermal	0	7	0	0	10	19	90
Rover total	162	120	103	88	21	21	167
Contingency	69	52	44	38	9	9	72
MEV Power	231	172	147	126	30	30	239
Avail. Power ²	274	274	274	274	274	Bat.	278
Margin	41%	56%	62%	68%	92%	-	40%

¹All modes except “Traverse Night” also applicable to Solar option

²Represents EOM power from RTG, EOM with minimum 1.3 m² illuminated area on solar array

Table 3-3. Flight System Element Characteristics Table.

Flight System Element Parameters	Value/Summary, Units
General	
Design Life (RTG/Solar)	48/84 months
Structure	
Structures material	Aluminum and composite
Number of deployed structures	1 (magnetometer boom)
Mobility/Articulation	
Control method	4-wheeled rover, 4-wheel steering
Control reference	Solar, terrain recognition
Slope capability	15 degrees
Driving speed on flat terrain av./max.	0.5/1.0 km/hr
Number of articulated structures	15 (4 wheels, 4 steering, 5 dof arm, 2 axis tri-cam head)
Thermal Control	
Type of thermal control used	Passive/heat pipes/radiators/electric heaters/thermal switches
Command & Data Handling	
Rover housekeeping data rate	2 kbps
Data storage capacity	128,000 Mbits
Maximum storage record rate	700 kbps
Maximum storage playback rate	700 kbps
Power	
Type of array (solar option)	Body mounted
Array size (solar option)	6.3 m ² total, 1.3 m ² min. illuminated
Solar cell type (solar option)	Multi-junction
Expected power generation at Beginning of Life (BOL) and End of Life (EOL)	RTG: 300 W BOL, 273 W EOM Solar: minimum 317 W BOM, 280 W EOM
Average power consumption	239 W (driving mode)
Battery type	Li-ion
Battery storage capacity	RTG: 20 amp-hr, Solar: 612 amp-hr



For this application, torques on the wheels and arm can be sufficiently inferred by measuring current in the motor winding.

Autonomous Surface Operations

To ensure meeting the science objectives within the mission duration the rover must follow the pre-planned traverse. It must also select and safely place instruments on regolith and rock targets along the route. Because of limited high-bandwidth communication windows, an Earth-based operations schedule, and required traverse distances and number of instrument placements, these activities must be executed autonomously and reliably with ground oversight to track progress, re-adjust the plan, and support fault handling (for more details, see Table 2-5 and Table C-13 in Appendix C.2). Staying on the timeline requires a pose knowledge uncertainty of better than 100 m per 30 km for the planned traverse.

The rover’s sensors, avionics, and software are designed to support onboard autonomous operations with ground oversight. The rover has two redundant stereo camera pairs (Mars 2020 EECAM) mounted on a pan-tilt mast and a second redundant pair mounted on the rear of the rover at a comparable height, making bidirectional driving fully redundant. With a height of 1.5 m above the ground, dust covers were deemed unnecessary. All engineering cameras have 90° field-of-view lenses and a ~25-cm baseline to enable bi-directional surface navigation without mast articulation. Short exposures (~10 – 20 ms) allow imaging-while-driving during the lunar daytime (similar to the Perseverance rover). At night, long exposures (tens of seconds) use earthshine rather than an illuminator to image while stationary, an acceptable strategy since night driving is limited in distance and speed. The mast-mounted cameras also support autonomous manipulation operations. The rover also uses an Adcole pyramid-type coarse Sun sensor and redundant heritage LN200 IMUs for navigation purposes.

In nominal situations, autonomous operations use vision-based waypoint navigation that respects keep-in and keep-out zones to reach targets of interest. For focused investigations, targets are selected by ground operators while for others, they are selected by onboard algorithms. Before instrument placement, the rover uses its stereovision and models to assess collision and thermal hazards, position and orient the rover, and use arm-mounted fiducials to place the instruments at the proper off-

set distance from the target. Resources and activities are managed onboard and monitored by the system-health manager (fault protection), which has to detect and identify all faults/failures but only respond to a subset. The onboard autonomous system handles both nominal and off-nominal conditions through the same execution mechanisms. For off-nominal situations that cannot be handled onboard, operations fall back on ground-in-the-loop control. Table 3-4 summarizes the onboard and ground needed for functions for autonomous operations.

Command & Data Handling (C&DH)

Intrepid’s C&DH subsystem consists of three assemblies: a compute element, an instrument interface and a motor driver. All are JPL-designed and have heritage traceable to flight units. A block diagram of the C&DH system is shown in Figure 3-2.

The compute element is built around redundant GR740, Quad-core LEON4 processor boards, redundant power supplies and a fault management unit that facilitates timer, sleep functions, and swap-over between the processor boards. Redundant navigation interface boards are connected to the processors to implement the specific interfaces required for the Intrepid architecture. The redundant instrument interface units are built around the GR712 Dual-core LEON 3

Table 3-4. Onboard and ground activities.

Onboard and Ground Functions	
Onboard Rover	<p><u>While driving</u></p> <ul style="list-style-type: none"> • Surface navigation (stereo imaging, 3D mapping, hazard assessment (rocks, craters), path planning, path following) • Dead reckoning pose estimation (visual/inertial/wheel odometry ego-motion estimation)
	<p><u>While stopped</u></p> <ul style="list-style-type: none"> • Global localization (Sun/Earth sensing, crater detection from rover and registration with orbital imagery) • Safe target selection for instrument placement (thermal hazard assessment, arm (self) and environment collisions) • Arm instrument placement on selected targets (collision-free motion planning)
	<p><u>Both</u></p> <ul style="list-style-type: none"> • Reliable operations (mean-distance between faults > 6 km; mean-time between failures > 24 hours) • System health management (monitoring devices and activities, assessing health, limited diagnosing and response) • Activity and resource planning, scheduling and execution
Ground	<p><u>24/7 Operations (first 4 weeks)</u></p> <ul style="list-style-type: none"> • Full DSN coverage and continuous oversight • Checkouts and shakedown of remaining bugs • Rapid fault response (min 1-hour turn around)
	<p><u>Workday schedule (remaining 4 years)</u></p> <ul style="list-style-type: none"> • Ground-based monitoring and health assessment • On-call fault diagnosis and response (min 24-hour turn around)

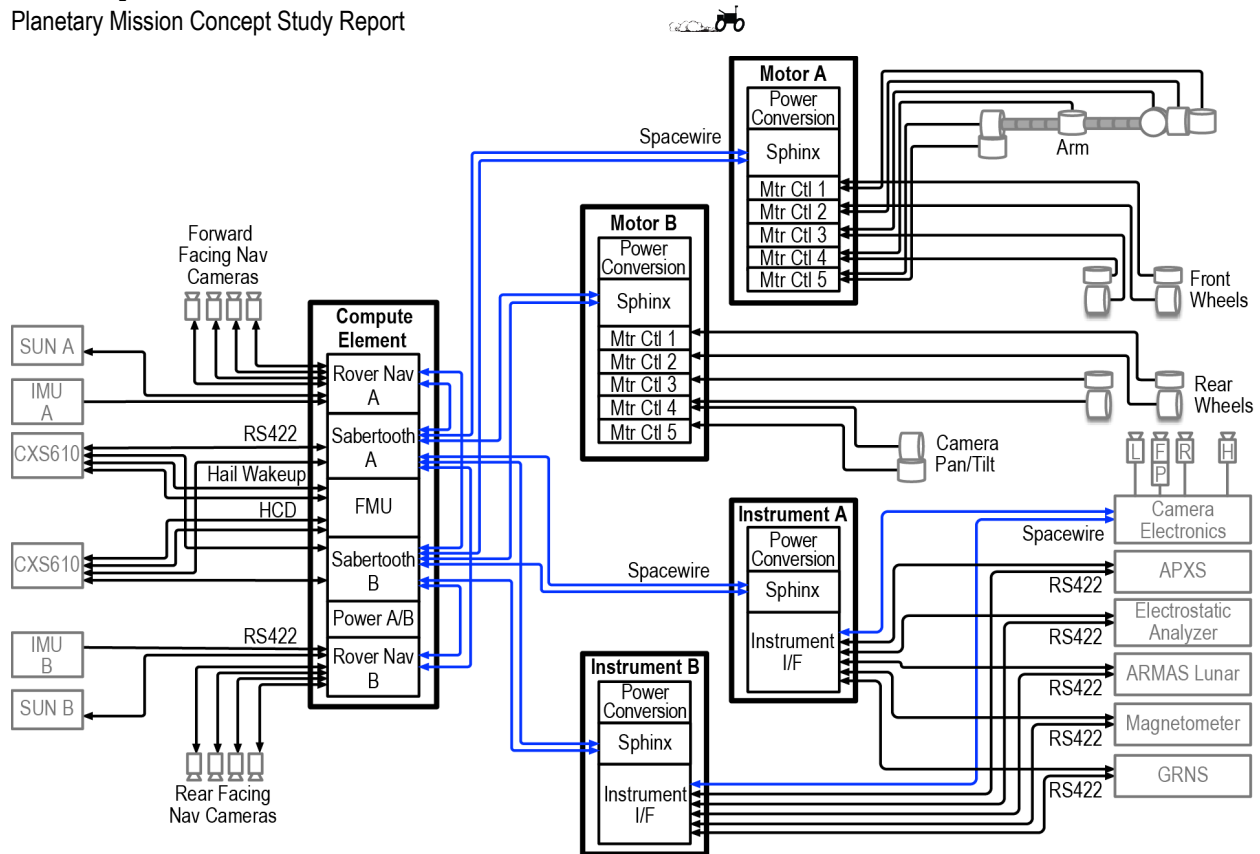


Figure 3-2. Intrepid C&DH Block Diagram.

processor and control and collect data from the science instruments. The motor driver was developed for the Europa Lander and is similarly built using the same processing board as the instrument interface. It controls the mobility, arm, and mast. Each motor control board can control one motor at a time so the current configuration supports ten simultaneous motor operations.

The Intrepid Flight Software (FSW) for the compute element is direct heritage from JPL’s Psyche FSW product with modifications from the Mars 2020 rover software. The FSW heritage includes not only the flight code, but also the software development and management processes required for a class B flight software deliverable. Over 99% of the inherited flight software is written in the C programming language. The remainder is written in assembly to cover niche areas in SUROM and operating system routines. The basic FSW architectural principles have remained the same for years with successful architectural reuse across MSL, M2020 and Psyche missions.

The FSW for the motor controller and instrument interface units is built from the F⁷ (F Prime) programming language developed at JPL to facilitate software development for embedded applications. A C++ framework for basic features

such as message queues, threading and OS abstraction, and an evolving collection of generic components for commands, memory management and event logging are supported by a suite of tools for testing. F⁷ is deployed in Mars Helicopter, Lunar Flashlight and Near-Earth Asteroid Scout and has flown on the ASTERIA CubeSat.

Telecom

The telecommunications subsystem supports all mission uplink and downlink requirements using S-band frequencies and components with flight heritage. To support maximums Direct-to-Earth (DTE) downlink data rates of 100 kbps while driving and 700 kbps while parked, an L3 Harris CXS-610 transponder with integrated 5W SSPA and S-band diplexer will generate the downlink signal that will be directed through one of two types of S-band low-gain antennas onboard the rover. One helix antenna provides hemispherical coverage referenced from the rover top deck to be used while driving. While parked, one of two identical patch-excited cup antennas placed on opposite sides of the rover will provide a higher gain and more directional radiation pattern necessary for a 700 kbps downlink data rate from the lunar surface. The link analyses for the parked and driving DTE links hold at least 3dB margin to a 34m DSN station with the



effects of lunar hot body noise included. An uplink data rate of up to 2 kbps for commanding is achievable at all times during the mission from a 34m DSN station with greater than 3 dB link margin. Comparable links to an 11.3 m Near Earth Network (NEN) station provide rates of 10 kbps while moving and 50 kbps stationary.

Power

The 12 GPHS module Next Generation RTG option provides sufficient power for all operating modes at end of mission per Table 3-3. As such, the battery for the RTG options is sized to absorb power transients. The RTG option includes three power control modules to support the ~300W capability at beginning of mission (BOM) as well as provide the battery charge/discharge control interface.

The solar array option consists of a fixed pyramidal array structure of 29% efficient solar cells encompassing the rover, with a minimum effective illuminated area over the course of a lunar day of 1.3 m², exceeding the 1.07 m² array required for the worst case 313-hour illuminated period to achieve energy balance. A 612 Ah battery is provided for one hour of night science plus 395 hours of night heater power. The solar array option includes two power control modules to manage power bus voltage via solar array string switching and battery charge/discharge management.

Power electronics is based on a SmallSat avionics architecture currently in development at JPL. This includes variations of RTG and solar array power control functionality as well as power distribution for loads and pyro events. This distribution functionality has a fault tolerant control interface to C&DH. Further, switches can be placed in parallel to mitigate stuck open faults, or in series to mitigate stuck on faults.

Thermal

The thermal control subsystem is required to maintain hardware within allowable flight temperatures (shown in Table C-20 in Appendix C.3). The system is challenged by not only the need to survive the lunar night, but also the lunar day where regolith temperatures and high solar angles combine into extreme hot scenarios at equatorial latitudes. Building on

past rover experience, Intrepid employs a Warm Electronics Box (WEB) design, as illustrated in Figure 3-3.

During the lunar day, a radiator that is parallel with the top of the WEB is employed to reject heat from rover internals. Barring articulation or complex orientation restrictions for the rover, such a zenith-facing radiator provides the best performance throughout the lunar day with the design allowing some degradation depending on rover tilt angles and terrain features. For the solar powered option, a propylene loop heat pipe (LHP) is employed to transfer waste heat from WEB internals (which are mounted relatively close the ground for stability) to the radiator which is located above the solar arrays to permit a clear view to sky. The LHP also minimizes the WEB penetration since only two tubes (6 mm vapor line and 4 mm liquid return line) are needed for heat transport under worst-case hot conditions.

To conserve heater power during the lunar night, WEB internals are thermally co-located and insulated with MLI. The thermal path to the radiator via the LHP is essentially removed if hardware temperatures drop below -10 °C through the action of a set of passive thermal switches. Each switch is capable of turning down its thermal conductance from 5 to 0.002 W/K. Furthermore, by removing the load from the LHP evaporator, the LHP will also shut itself off without requiring power for further reduction on overall thermal

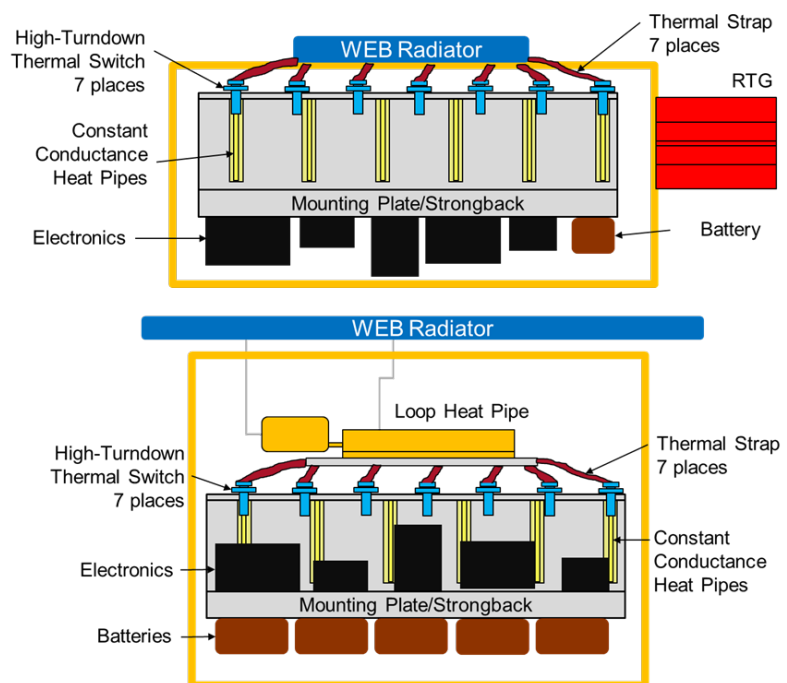


Figure 3-3. Rover WEB layout for RTG version (top) and Solar (bottom).



conductance. This feature is especially important for the solar powered option where survival heating during the lunar night is a significant driver on battery mass. Note that as shown in Figure 3-3, the LHP will not be needed in the RTG option due to relatively short distance between the hardware and radiator.

Mobility and arm actuators are allowed to freeze during the night and are warmed prior to use to their minimum operating AFTs. Those elements external to the WEB, such as instruments, have local thermal control consisting of heaters to maintain nighttime temperatures and a local zenith-facing radiator to maintain temperatures during the day. Note that some operational scenarios may dictate that instruments are powered down to prevent overheating.

Structures

The structure configuration employs a lightweight approach using a combination of carbon fiber composite struts, aluminum brackets, and aluminum honeycomb panels for both the solar and RPS versions. These materials are compatible with all radiation and thermal conditions during the traverse. Details of structure and rover configuration are presented in Appendix C.4.

The RPS version incorporates a honeycomb chassis, as well as metal outriggers using aluminum metal sheet bending techniques for both rear wheels, instruments and cameras. The chassis provides mechanical attachments as well as space for the thermal system. The rocker system on both versions is made of large-diameter hollowed composite rods and metal fittings. The rest of the rocker mechanisms, as well as the attachment to the chassis are made of machined aluminum parts. The radiator is mounted on top of the chassis and all electronics are placed on a horizontal plate accessible from the bottom to facilitate integration and thermal performance.

The solar version uses the same structural configuration for the mobility system, but it has a different chassis design using a three-dimensional composite-strut truss. The internal web, holding electronics on top and batteries underneath, is mechanically connected through composite bipods to the chassis. That chassis has two aluminum-machined panels (front and end) used as interface to multiple components such as robotic arms, leg outriggers and solar panels struts. The solar cone is made of lightweight honeycomb composite panels and glued solar cells.

Instrument Accommodation

Both RPS and solar versions present similar instrument accommodations. The ARMAS instrument is located on a hollowed bracket allowing views of both the sky and the ground. The electrostatic analyzer is located on the top part of the rover for a clear zenith view. The GRNS is located on the belly. The robotic arm is attached to the front of the rover to ensure the necessary access for the APXS and HLI, and the TriCam imagers are co-located in a mast-mounted pan/tilt camera head. The magnetometer is located on a deployable composite boom on both versions.

Concept of Operations

The Intrepid mission ConOps baselines the RTG-powered rover option to meet all science objectives in a 4-year mission.

The Intrepid surface ConOps relies on pre-planning, autonomy, and streamlined operations; a very different operational scenario than previous rover missions. These differences, identified in Table 3-5, enable an order of magnitude increase in the distance covered by the rover per month, while maintaining a robust science return. The pre-determined, onboard traverse plan includes day and night Focused Investigation stops (FI, n=133), Interval Stops, and in motion observations to fulfill the measurement objectives (Table 3-6). The ConOps also relies on a multi-layer margin strategy: flexible stop points, repeat observations at a single location, and multiple stops at like landforms.

In motion: The Mag, GRNS, ESA, and ARMAS will collect measurements continuously and imaging data will be acquired on a set cadence of one set of TriCam Stereo, 4x4 downsampled FarCam frame, and PS observations approximately every 80 m (~10 minutes) along the traverse.

One-hour Interval Stops: Intrepid will downlink science data and collect a fully automated suite of observations: a 360° stereo panorama with an even sampling of point spectra, one-hour stationary GRNS integration, and an APXS/HLI measurement of an arbitrary patch of regolith in front of the rover, with TriCam observations to provide context for arm placement. Should the rover stop as a result of an anomaly, a similar sequence of observations (or a subset) will be acquired.

Focused Investigation (FI) Sites: Intrepid will follow pre-defined measurement scripts, with a focus on long-duration GRNS and APXS measurements (up to 48 and 12 hours per integration, respec-



tively), at one or more pre-planned specific or relative locations within a few-km-wide area. Examples include radial traverses of crater ejecta or interrogating regolith or boulders at the base of a volcanic landform. Typical APXS measurements will be acquired by placing the APXS on the regolith, at the center of a boulder, or by positioning on regolith within 1 meter of an identified boulder. APXS measurements will be supplemented by HLI grain-scale RGB color images of rocks and regolith, acquired from within 2 cm of surface documenting the spot where the APXS integration occurred. Additionally, FI sites often include extensive acquisition of images and spectra for providing geologic context and measurements of inaccessible terrain, and when long GRNS integrations require staying at a point for >24 hours, the movement of the Sun allows repeat TriCam and PS observations to form a photometric sequence with varying incidence and phase angles (phase angle varying much more than incidence) to help constrain soil properties. Most daytime FI sites require between 12 and 74 hours of science acquisition activities. The locations and activities of these stops are planned ahead of arrival but exact positioning can be changed by the rover after arrival at a stop. For example if a specific boulder identified from orbit for an APXS integration turns out to be inaccessible the rover finds another nearby boulder or if one is not accessible it simply defaults to a regolith integration.

Nighttime Focused Investigation Sites: Upon arrival at a night site, while the Sun is still up, Intrepid will drive to each night measurement site laying down tracks to follow after sunset (with earthlight sufficient illumination for tracks following after sunset). Night operations consist of single extensive FI sites that emphasize long duration, high-signal-to-noise GRNS and APXS integrations, with repositioning of the rover limited to a few hundred meters at a time (for example, an eight-sample-point radial traverse of the ejecta of a 10 km crater). Night operations will also include long-exposure earthlight imaging of landforms, and imaging related to testing dust levitation hypotheses (dawn/dusk horizon glow, new dust deposits on rover [Colwell et al., 2009; Rennison and Criswell, 1974; Stubbs et al., 2007]).

Traverse Plan

The Intrepid traverse route was entirely pre-planned based on Lunar Reconnaissance Orbiter Camera (LROC) images (0.5 to 2 m/px) and other relevant datasets (Appendices B.1.5 and B.2). The

Table 3-5. Why Intrepid ops is more efficient than Mars ops.

Attributes		Intrepid	Typ. Mars Rover
Mission	One-way light time	1.3 sec	3–21 mins
	Command mode	Monthly plan updates	Daily sequencing
	Rover autonomy	>60% of the time (full operations)	<10% of the time (traverse only)
	Available cmd cycles per day	~1000 for anomaly response	1 due to light time & planning cycle
	Science complexity	Pre-planned, onboard	Developed daily
Activities	Typical speed	0.5 km/h	0.02 km/h (TBC)
	Distance/month	50 km	3.0 km (MER)
	Inst. place/24 h	2-5 coarse targets	2-3 precise targets
	Observations while in motion	GRNS, MAG, ESA, ARMAS, TriCam, PS	MSL: REMS, RAD, DAN
	Nighttime ops	Minimal motion	None
Planning & Sequencing	Traverse planning	Pre-planned	Daily
	Sci planning	Pre-planned	Daily
	Resource management	Robust resource margins	Must plan to severe resource limits
	Commanding	Flexible task plan (network)	Custom integration of 100s of cmds daily
	Arm Operations	Auto target selection and arm placement	Multistep sampling over multiple sols
	Plan robustness	Auto-adapt plan to situation and faults	Halt the ground if plan cannot be executed
	Rover downlink assessment	Real time situational awareness of rover	Assessment only after 100s of cmds
	Science downlink assessment	Available daily but not required	Must complete daily to inform next uplink
	Anomaly diagnosis & response	Autonomous on rover or realtime on ground	1 step per 24 hours

Table 3-6. Definitions of terms used in this section.

Term	Definition
Interval Stop	One-hour stop every 4 hours of driving for a fully automatic set of baseline observations.
FI Site	A Focused Investigation (FI) Site is an area with several pre-planned locations for investigation.
Night Stop	FI site visited at night with additional points and longer duration measurements.
Way-point	Navigation target on the lunar surface that the rover must pass through to traverse desired terrain units or avoid large-scale obstacles.
Region	One of six major sections of the traverse described in Section 1
Region Team	Science team sub-group in charge of science planning and operations for a Region.



route was chosen to ensure the science objectives are met with margin and that large hazardous regions are avoided over the entire 1800 km traverse; smaller-scale hazards rely on onboard surface navigation to assess and avoid. Our notional traverse achieves the mission goals in three years of operations (detailed in Appendix C.5), leaving one full year of margin for unforeseen events. On a typical lunation, Intrepid starts travelling shortly after dawn, stopping at 2-3 FI sites for 24-72 hours each. By dusk, the rover has travelled ~50 km with ~30 Interval Stops, and has arrived at a night FI site where it will take measurements of ~8-10 locations in a 1-2 km area over the course of the night.

Traverse Flexibility: The vast majority of traverse decisions and science targets will be made prior to arriving at a site. A small, focused ‘Region Team’ for each region will evaluate the incoming datasets and will have the ability to make small modifications to waypoints and stay times in exceptional circumstances. The Region Team will be responsible for traverse modifications and must decide on modifications without exceeding the allocated time for the whole Region. While there is some flexibility built into the operations plan, a rigorous schedule must be followed to ensure mission success.

If a Region Team decides that further investigation of a feature is needed beyond what is initially scheduled, they must replan the remainder of the Region traverse within the allocated time frame while achieving all the pre-determined science goals. Fortunately, most of the planned FI sites target a geographically convenient example of a type of feature, not a unique feature, and so could be replaced with alternate locations nearby for the same science return. Such substitutions also allow significant flexibility in the traverse to handle schedule changes due to mobility anomalies. A major task of the science team prior to the beginning of each Region traverse is the identification of alternate FI sites and traverse routes as backup options.

Due to the fixed cadence of night stops, each traverse Region must start at the scheduled time of the lunar day, so any lengthening of a prior Region (for science or operational reasons) must be an integer number of lunations. In the case of extraordinary discoveries, the Region Team could request that the full science team allocate an extra lunation to their Region from the one-year reserve. Major schedule slips due to operational anomalies can also be corrected using one of those 12 unallocated lunations, if replanning based on previously selected alternate FI sites is not sufficient.

How does Intrepid get to the Moon?

In the timeframe of the Intrepid mission it is currently in NASA’s planning that a variety of commercial services will be available through the Commercial Lunar Payload Services (CLPS) program. The first lander delivery systems in this program are currently in development and are projected to be capable of landed payloads up to 200-300 kg. The next step in the CLPS progression is for mid-range payload capability such as the services recently contracted for delivery of NASA’s VIPER rover. Recognizing that this capability will be available in the timeframe of the Intrepid mission the team has worked with NASA’s CLPS office to define a rough accommodation volume, mass and cost for the Intrepid delivery.

The accommodation envelope is estimated as having a deck footprint of approximately 2.5 x 2.5 m, and the team has also assumed a height allocation of 2.5m above the lander deck. Mass limits are broad, but an allocation of 500 kg has been assumed for the study.

One additional assumption plays into the mission schedule. Conservatively, the Intrepid study team has assumed that the commercial lander may execute a low energy trajectory to the Moon with a transfer duration of three months.

Uplink/Downlink Conops

Intrepid uplink and downlink relies on two communications networks (Table 3-7) The first is a continuously-available link between the rover and commercial stations in the Near Earth Network (NEN), providing 10 kbps of downlink while the rover is moving and 50 kbps when the rover is stationary (to 11.3 m ground station). The lower end of this capability exceeds the needs for realtime rover health and safety assessment with a margin of 900%. The NEN-downlinked data will feed into a pipeline that provides data to the operators with expected latency of <1 minute between the Moon and the rover operations center. The second capability is a daily DSN pass of 8 hours, which the rover can utilize at 100 kbps when moving and 700 kbps when stationary. This pass is sufficient to periodically clear all data from the rover buffer and to create a robust data margin for the mission, as shown in Figure 3-4. Science data is not required for tactical decision making or anomaly resolution, so a latency of hours to Earth days is acceptable. Intrepid carries 128 Gbits of memory, while the maximum expected use case is 96 Gbits, which occurs when the traverse plan requires the rover to be moving for several consecutive DSN passes.



Rover Ops

The rover is commanded via a pre-planned task plan that captures the intent of the science team but can be modified onboard based on the situation that the rover encounters during the execution of its traverse and instrument placement activities. The primary activities that the rover will be conducting include autonomous traversing, autonomous target selection on regolith or a rock based on the aforementioned intent captured in the up-linked task plan and autonomous instrument placement on that target. Telemetry from the rover is continuously recorded onboard and downlinked during rover traverse and while stopped, with the latter being at higher bandwidth. Anomalies are handled hierarchically, first onboard the rover and later on the ground. Rover resources, which are less constrained than Mars rover resources, are continuously monitored by the system health manager and used in replanning to respond to onboard fault conditions. When the rover is unable to handle a fault, it will halt its operations and call home for further assessment of the situation and for intervention. Response to faults is critically handled with a rapid-turn around by having on-call subsystem engineering teams with access to rover state and ability to interrogate the rover in near real-time to diagnose faults.

Ground operators monitor progress and assess the health of the rover 24/7, providing oversight of the rover’s onboard autonomous operations.

Table 3-7. Mission Operations and Ground Data Systems Table (DSN and NEN).

Downlink Information	Surface Checkout	Balance of Mission
Contacts/wk (DSN)	21	7
Contacts/wk (NEN)	-	14
Number of Weeks for Mission Phase	4	208
Downlink Frequency Band	S	
Telemetry Data Rate (DSN) kbps	100 – 700	
Telemetry Data Rate (NEN) kbps	-	10 – 50.
Transmitting Antenna Type(s) and Gain(s), DBi	Omni, 0, LGA, 7	
D/L Receiving Ant. Gain (DSN), DBi	56.4	
D/L Receiving Ant. Gain (NEN), DBi	44.8	
Transmit Power Amplifier Out, W RF	5	
Total Daily Data Volume, (MB/day)	2000	
Uplink Information		
Number of Uplinks per Day	3	1
Uplink Frequency Band	S	
Telecommand Data Rate, kbps	2	
Receiving Antenna Type(s) and Gain(s), DBi	Omni, 0, LGA, 6	

Updates to the strategic plan are anticipated at a much lower frequency compared to Mars operations. When necessary, changes to the pre-planned activities are transmitted to the rover to update the active plan that the rover is executing. When situations call for ground operators to take over (Table 2-4 – *Human decide* backup option), the near real-time communication allows operators to make their decisions based on the latest estimates of rover states and do not have to rely on projections, which simplifies operations.

Ground Ops

Two operation centers will be established to support Intrepid; a Rover Operations Center (ROC) at JPL and a Science Operations Center (SOC) at ASU. The two teams will focus on largely independent daily activities, with sufficient flexibility in the science plan that essentially no interaction between the teams is required for tactical traverse corrections, rover parking, or arm placement. Due to the generous resource margins and autonomous system design, the instrument commanding is treated as *non-interactive*, meaning that the instruments can be commanded directly from the SOC without rover modeling or sequence integration to check for interference issues.

The primary objective of the ROC is to ensure that the rover faithfully executes the onboard plan. At all times, two members of the ROC team will be responsible for monitoring the realtime telemetry for rover health and safety and to triage problems. If the rover is unable to autonomously resolve a fault, it will cease activity, hail the ground, and begin a data dump using the available

Intrepid Downlink Budget (Tbits)

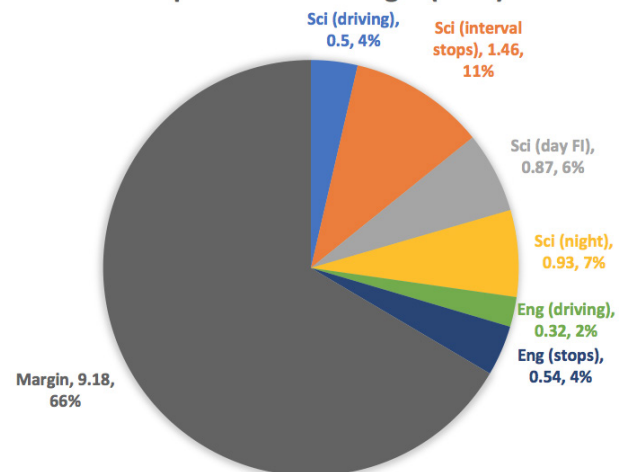


Figure 3-4. Data volume generation for the mission has 66.5% margin against the total mission downlink capacity.



bandwidth. The realtime monitors at the ROC will identify if it is a known, benign issue, in which case they can clear the fault following established protocols. Otherwise, they will alert the rover response team to join an anomaly meeting within an hour, and begin preparing discussion material as contextual data is downloaded. Under this approach, the expected latency to initiate an anomaly response is 1 hour. When the anomaly is resolved, the appropriate commands are transmitted to the rover via the NEN to clear the fault and recommence surface operations.

The primary objective of the SOC is to ensure quality science data is returned by Intrepid and that mission science objectives are met. This objective is achieved by daily examination of the high-level instrument data after each DSN pass, identifying if instrument parameters need to be adjusted or if an instrument needs to be taken offline for anomaly resolution. Due to the survey nature of the mission, the traverse may continue while an instrument anomaly is worked without significant impact to the overall science return of the mission. Additionally, the SOC monitors traverse progress towards the next nighttime science site. If the timeline reserve for the lunation is diminishing, then the SOC team has the option of shortening inter-

mediate science integrations or eliminating a daytime stop altogether. This descope requires rapidly finalizing an updated plan to the ROC for validation, from where it will be uplinked to supersede the onboard plan. The timeline for this process is expected to be 24 hours. Finally, the SOC will be responsible for leading a monthly process to examine mission progress and update the traverse plan as necessary, with the ROC providing plan validation for the rover.

A Day in the Life

The following describes a Lunar Day in the life of Intrepid (operations at Marius Hills focused investigation stops 8 to 11; Figure 3-5):

- Intrepid will reach stop MH8, next to a low albedo moated dome, prior to nightfall (mid-afternoon). While still in daylight, Intrepid will traverse up the SW flank, ensuring the rover is fully on the dome for the first measurement; the rover will then work back along its tracks during the rest of the night. Planned observations at MH8: 7 GRNS integrations, 28 arm placements (APXS integrations and HLI context images), 24 stereo panoramas (6 daylight in color, 18 nighttime in black-and-white), and 3 daylight FarCam mosaics. MH8 night stop planning includes 110 unallocated hours.

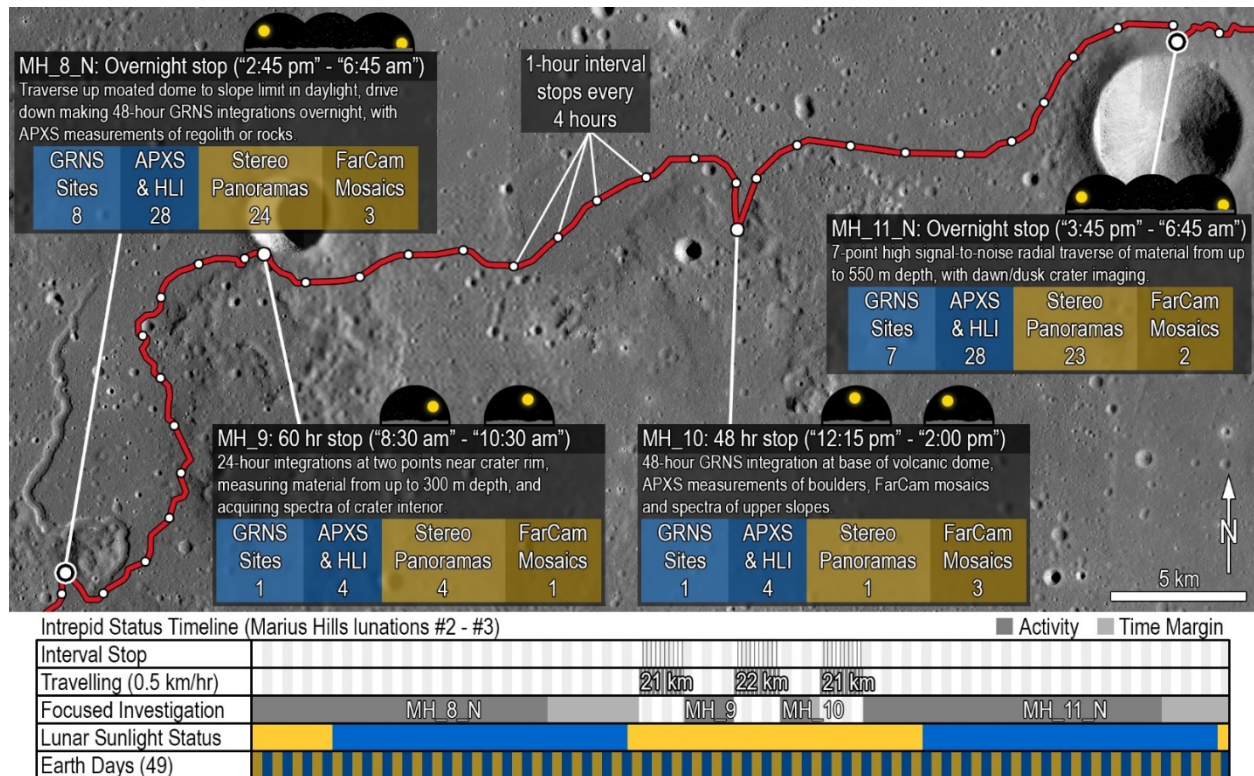


Figure 3-5. A day in the life of Intrepid.



- Intrepid will start from MH8 when the Sun is 10° above the horizon, and drive for 52 hours (21 km) to reach MH9 in mid-morning (Sun ~37° above the horizon). MH9 is close to the contact between a crater and an irregular dome. Intrepid will sample two points 1 km apart, both with 24-hour integrations: the crater rim, and ejecta mixed with local dome materials. Planned observations at MH9 (60 hours allocated): 2 GRNS integrations, 4 arm placements at different sampling locations, 4 panoramas and 1 FarCam mosaic.
- Intrepid will drive 55 hours (22 km) from MH9 to reach stop MH10, near a notch in an irregular dome, just past local noon. At MH10, Intrepid will drive up slope about 500 m from the initial stop location to sample local dome materials. Planned observations at MH10 (48 hours allocated): 1 GRNS integration, 4 arm placements, 1 panorama and 3 FarCam mosaics. If time is short, the stop duration could be reduced to 24 hours.
- Starting from MH10, Intrepid will reach the night stop MH11 near the crater Marius E after 52 hours (21 km), in mid-afternoon (Sun ~35° above the horizon). At MH11, Intrepid will drive upslope 500 m to the rim, acquire interior panoramas at two points 500 m apart along the rim of the crater interior, then backtrack along the rim during night for composition measurements, before getting a dawn panorama from the 1st rim location. Planned observations at MH11: 7 GRNS, 28 arm placements, 23 panoramas (6 daytime, 15 night) and 2 FarCam mosaics. Traverse and science operations plan includes a margin of 80 hours.

Risk List

The Intrepid concept takes a conservative approach to engineering, mission planning and operations, informed by experience from past lunar and Mars missions. New technology is limited and the operating environment and traverse is well understood. Significant risks identified by the team are shown in Table 3-8.

Table 3-8. Intrepid’s adoption of existing technologies and proven instrument designs facilitates a high-performance mission with manageable risks.

Risk	C*	L*	Mitigation
Next Gen RTG not available in time for launch	3	2	<ul style="list-style-type: none"> • Design could be adapted to use MMRTGs with likely impact to mission duration required to meet baseline science objectives • Solar-powered option could be adopted with commensurate increase in mission duration to meet baseline science objectives • Mission opportunity is not time-critical and could accommodate some slip in Next Gen schedule
Accommodation of lunar dust environment requires additional qualification and design changes to ensure reliable operation for the span of the mission	3	1	<ul style="list-style-type: none"> • Seal all exposed joints: use three-stage seal derived from Mars rovers. • Use no-contact instruments: no science instrument requires contact or interaction with the surface. • Raise sensitive surfaces and instruments: all sensitive surface such as optical/thermal surfaces are designed 3x higher than the wheels to mitigate the effect of dust and debris. Place instruments at least 1 m above regolith. Solar panels (solar option) extend outboard of wheels to reduce dust. • Account for dust in performance analysis and design: all thermal and solar cell analyses assume a monolayer of dust at all times
Reliability of autonomous operations cannot be made sufficiently high to ensure execution of mission within allotted time	2	2	<ul style="list-style-type: none"> • Mature and integrate all required autonomous capabilities in unison on a prototype rover with same mobility, manipulation, sensors, and avionics leverage flight-relevant components (hardware and software) • Conduct extensive field-testing complemented with a validated simulation to collect adequate statistics for characterizing the long-distance traverse, manipulation, and system-level performance. • Adjust the plan and functions that have to occur autonomously onboard vs. with ground assistance and plan for increased ground engagement for functions that have lowest autonomous reliable performance. • Include significant margin and flexibility in mission plan to allow for anomaly resolution in operations
Rover encounters lunar terrain with unexpected trafficability features	2	2	<ul style="list-style-type: none"> • Rover mobility test plan will encompass worst case terrain types • Mobility system designed with multiple ways to detect mobility problems and back out of hazardous areas • Timeline includes margin for alternate route planning should hazardous terrains be encountered on planned path
WEB thermal design (solar option) does not perform as expected	2	2	<ul style="list-style-type: none"> • Thermal design and testing begin early in Phase A. • Battery capacity currently includes margin above design principles. Mass margin could allow additional battery capacity.

* C=Consequences; L=Likelihood, in accordance with the NASA 5x5 Table. Consequence and Likelihood criteria defined per SOMA Cost Threat Matrix (ref. Discovery 2014 Transition Briefing, 3/3/2017). Consequence criteria (C): cost impact to complete Phases A-D: 1=Very Minimal (<\$10M). 2=Minimal (\$10-20M). 3=Limited (\$20-40M). 4=Moderate (\$40-80M). 5=Significant (\$80-\$120M). 6=Very Significant (>\$120M). Likelihood criteria (L): % probability of occurrence; 1=Unlikely (<10%). 2=Possible (10-30%). 3=Likely (30-60%). 4=Very Likely (60-75%). 5=Almost Certain (>75%).

4 DEVELOPMENT SCHEDULE AND SCHEDULE CONSTRAINTS

The Intrepid development schedule benefits from lessons learned from past rover missions and is cognizant of the requirements of a mission using RPS.

High-Level Mission Schedule

Figure 4-1 presents a feasible high-level schedule for the Intrepid mission. The mission complexity falls in the range of a New Frontiers-class development. The reference schedules used for this study were derived from the JPL mission schedule database, informed by recent rover developments and the unique schedule features associated with the use of radioisotope power systems.

The Intrepid mission has no direct analogies; it is similar to the MER and MSL/2020 missions, but significantly simplified in that Intrepid is a single-element design, relying on the CLPS provider for cruise and landing. The mobility range for Intrepid is significantly beyond that of previous rover missions, and that is reflected in the number of field tests planned to begin early in the development cycle.

No major schedule drivers or long-lead items need to be addressed beyond the proposed schedule. Table 4-1 provides key phase durations for the project. Since this mission is targeted as a New Frontiers competed mission, all instruments and flight elements are planned to be delivered at the beginning of system-level integration and test.

Technology Development Plan

As identified in Section 2, two technologies need to be matured to higher technology readiness levels: (i) reliable integrated autonomous rover operations and (ii) the point spectrometer instrument.

Autonomous surface operations leverage several Mars-heritage autonomous functions but need to provide integrated mobility, target selection, instrument placement, and resource/health management relying on the strategic science plan and *without daily tactical planning*. Furthermore, it needs to provide this integrated functionality at a higher reliability than Mars rovers whose activities are planned every sol (martian day). The performance

Table 4-1. Key Phase Duration Table.

Project Phase	Duration (Months)
Phase A – Conceptual Design	14
Phase B – Preliminary Design	15
Phase C – Detailed Design	22
Phase D – Integration & Test	23
Phase E – Primary Mission Operations	50
Phase F – Extended Mission Operations	6
Start of Phase B to PDR	8
Start of Phase B to CDR	23
Start of Phase B to Delivery of Instrument #1-9*	37
Start of Phase B to Delivery of Flight Element #1	54
System Level Integration & Test	17
Project Total Funded Schedule Reserve	6 (120 days)
Total Development Time Phase B - D	61

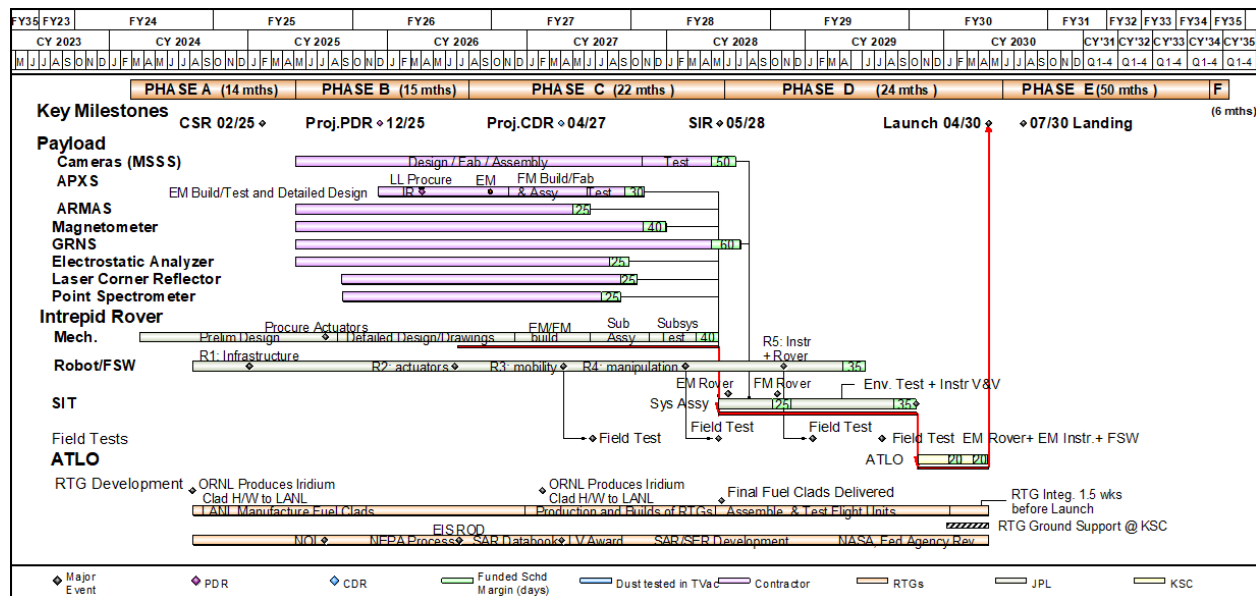


Figure 4-1. Notional High-Level Schedule Assuming a 2030 Launch.



metric needed for Intrepid to complete its mission is a combination of mean-distance-between-faults and fault-recovery response time. With a continuous communication link and accounting for an Earth-based operations schedule, a preliminary model provided insight into the reliability performance metrics needed for this mission. Parametric data for this model was based on fault rates and response times of prior Mars missions adjusted for the cadence of lunar communication. A Monte-Carlo statistical analysis indicated that for **minor faults** Intrepid needs a mean distance-between-faults of > 6 km with a response time of less than 24 hours (a conservative estimate for the continuous lunar communication, albeit, at times, at lower rate) and for **major faults** a mean distance-between-faults of 16 km with a response time of less than 72 hours (see more details in Appendix C – Autonomy Reliability). This level of reliability for autonomous operations would allow Intrepid to complete its baseline science in a manner consistent with the current concept of operations and within the planned three-year period, leaving the remaining one year as unallocated margin.

Ground-operation tools, matured for Mars rovers, are expected to have the needed functionality to support the rapid response. The plan is to adapt and integrate flight-matured autonomous

functions that include surface navigation (Mars 2020: 3D perception, hazard assessment, motion planning, visual/wheel/ inertial odometry), instrument placement (MER/ research development: target tracking, approach, rover positioning, hazard assessment (self- and surface collision), arm deployment), and activity/ resource planning (Mars 2020), with system health management and global localization into an autonomous system and deploy it in simulation and on a prototype rover with relevant sensing, mobility, controls, and compute avionics. Initial maturation of the integrated autonomy capabilities for long-duration, long-distance, instrument operations, and fault recovery can be demonstrated in simulation (e.g. the Mars 2020 rover simulation used for autonomous navigation) as well as on existing rover prototypes. To validate the required Intrepid performance, a combination of flight-relevant rover prototype and validated high-fidelity Intrepid simulation and would be necessary. The use of the relevant prototype in relevant environments to validate the simulation is similar to the approach adopted by the Mars 2020 mission for entry, descent and landing and for autonomous rover traverse. Table 4-2 provides a development plan for a focused technology program, which is similar to the multi-year programs that preceded MER, MSL and Mars 2020. Trends to

Table 4-2. Technology Development Plan.

Justification (completed activities)	Maturation Plan (work to go)	Duration	ROM Cost	
Reliable Integrated Autonomous Operations				
Intrepid needs integrated and reliable autonomous operations for traverse, target selection, instrument placement, and system management. Preliminary models long-traverse indicate that Intrepid requires the following mean-distance-between-faults (MDBF) with fault-recovery response time (RT): MDBF > 6 km w/ RT < 24 hours MDBF > 16 km w/ RT < 72 hours	Phase I: Pre-Phase A (FY21–24) (feasibility assessment) Integrated Autonomy Framework: set up autonomy framework for integration of all functions Function adaptation: adapt/update Perseverance rover autonomy functions (surface navigation (perception, hazard assessment, pose estimation, path planning, mobility), instrument placement (target selection, self- and terrain-collision, arm motion planning), activity planning, and system health into framework Global localization: develop from TRL 3 to 6; funded by NASA STMD GCD ('21–24); Fallback: use ground-based localization techniques used in current Mars missions every 10 km.	4 years 2 years 3 years	\$5.0M \$2.0M \$2.5M	
	Demonstration: demonstrate integrated functions in existing simulation or on existing rover prototype (ROM: \$0.5 M, 1 year)	3 years	Funded	
	Phase II: Pre-Phase A (FY23–FY26) (reliability assessment) Durable Wheels: mature and validate wheel design for temperature range and distance Rover prototype: develop prototype rover with similar mechanical configuration, sensing, and avionics (compute elements, camera interface and motor controls). SW Bench top: set up equivalent bench top system for software/autonomy development	4 years 2 years 3 years	\$10.0M \$1.4M \$3.5M	
	Simulation: increase fidelity of simulation and validate against field campaigns MOS/GDS: mature MOS/GDS tools to support rapid anomaly identification and resolution	1 year	\$0.8M	
	Validation campaigns: conduct 10s of km of autonomous driving to collect statistics to mature integrated capabilities and validate simulation; fully characterize reliability; inform hw changes in time Fallback: extend mission duration to accommodate the achievable reliability performance metrics	3 years	\$2.3M	
		2 years	\$1.0M	
		2 years	\$1.0M	
	Instrument Development			
	Point Spectrometer	Before PDR MSSS led activity integrated with cameras, likely a DALI/ MattSSE	3 years	



reduce mean-distance-between-interruptions have been well-documented for the autonomous vehicle industry [Yoshida, 2020], which similarly, complemented on-road testing on relevant hardware with high-fidelity simulations.

The point-spectrometer design is well understood and uses components from an existing product line. As the current TRL is at 4, the instrument would have to be fabricated and flight qualified for operations on the Moon. NASA has instrument development programs (e.g. PICASSO and MatISSE) that can be exercised for the flight qualification for TRL 6. We also propose a phase A activity for any residual activities to get to TRL 6 prior to PDR.

Development Schedule and Constraints

The development schedule including Phases C and D is shown in Figure 4-1 for the baseline RTG option. The schedule represents a relatively

straightforward completion of design and transition to I&T through launch operations for a rover of this type. Instrument development is complete for all instruments prior to start of Phase D. The critical path runs through the rover mechanical system which is necessary to begin I&T. Rover field tests to validate mobility and autonomy continue throughout these phases and feed into FSW builds. The RTG development line is representative of the typical activities associated with an MMRTG mission and may need to be revisited should there be any changes associated with use of the NextGen RTG.

Note that the schedule is tied to a launch date in April of 2030, representing an early opportunity for execution of this mission given the timing of NextGen RTG development with availability no earlier than 2030. It should be noted that the Intrepid mission schedule is flexible and can be adapted to any CLPS payload opportunity in this timeframe.

5 MISSION LIFE-CYCLE COST

The Intrepid mission cost, estimated by JPL's institutional cost models and validated by independent cost modeling, appears to fit comfortably within the expected New Frontiers (NF) cost range.

Costing Methodology and Basis of Estimate

Intrepid developed its cost estimate using JPL's cost estimation process for early formulation. The Intrepid team initiates this process by describing the project in a technical data package (TDP) containing the science requirements, technical design, instrument design, and project schedule. An initial estimate is generated using JPL Institutional Cost Models (ICM) in a focused Team X session that allows the Intrepid team to perform subsequent design-to-cost trades.

This study of the Intrepid mission generated cost estimates for 2 options, an RTG and a solar powered rover. The RTG option has a four-year mission duration while the solar option is seven years. Team X has estimated Intrepid's total mission lifecycle cost to be \$1,511M and \$1,547M FY25 respectively, as detailed in Table 5-1. Phase A-D cost estimates range from \$888M to \$1.05M, consistent with a NF-class implementation for Intrepid. The estimates are organized by NASA's standard Work Breakdown Structure (WBS).

Team X estimates are generally model-based, and were generated after a series of instrument and mission-level studies. The costs presented in this

report are ROM estimates and do not constitute an implementation or cost commitment. It is possible that each estimate could range from as much as 20% higher to 10% lower. The costs presented are based on Pre-Phase A design information, which is subject to change.

The instruments were estimated using the NICM System Tool which primarily relies on mass and power. Lifetime also impacts cost for ARMAS, GRNS and Electrostatic Analyzer. The rover was estimated assuming an in-house build.

Flight software was assessed based on analogy to the MSL and Mars2020 rover missions. One key difference and a significant cost driver is that the Intrepid rover will require a high degree of autonomy to drive for long distances without ground in the loop.

The RTG is based on the NextGen RTG with 12 general purpose heat source modules. The \$70M cost is derived from the "Groundrules For Mission Concept Studies in Support of Planetary Decadal Survey", Appendix A, Nov. 2019.

No planetary protection costs were assumed for this mission concept.

Reserves were applied at 50% for Phase A-D development (excluding LV) as required by NASA for this study and 15% for Phase E (excluding tracking costs).

The LV value of \$200M is based on the expected delivery cost for a medium class CLPS lander as estimated by the NASA CLPS Program



Office. For the RTG option, an additional \$20M is included for RTG handling by the launch service provider.

As another step to validate these costs, JPL’s business organization evaluated Intrepid with parametric models supplemented with analogies and wrap factors based on historical data. The cost models used include SEER and TruePlanning for Phase B-D, and SOCM for Phase E. Launch system and Phase E tracking costs were a passthrough from Team X. Phase A costs were assumed to be \$5M based on an escalated value of the Phase A cost from the NF 4 AO. The details for each of the cost model estimates is provided in Appendix D.

Table 5-1 shows the mission cost breakdown for the JPL Team X cost estimate, as well as the average from the cost model estimates. The flight system cost shows a significant difference between the two estimates with the cost model estimate being lower. One factor that contributes to this difference is the flight software. SEER and TruePlanning can model software based on lines of code. Since this information was not available in Pre-Phase A, a factor was applied to the hardware costs based on a historical average. Because of Intrepid’s requirement for autonomous driving, this is not well represented by historical data and is underestimated in the cost model results.

For WBS 10, the opposite occurs with the cost model estimate higher than Team X. This is primarily observable with the TruePlanning estimate. A possible explanation is that Team X carries the cost for a mechanical integration testbed and the driving tests for the mobility system as part of WBS 06 whereas TruePlanning captures this under WBS 10. Because of this mapping difference, it is better to compare WBS 06 and 10 together.

Cost Estimate(s)

The Intrepid team has adopted the Team X cost as the more conservative estimate. To create a mission cost funding profile, historical missions were analyzed to define representative profiles by phase. The analogous mission set includes the

Table 5-1. JPL Team X and cost model estimates for Intrepid (FY25\$M).

WBS Element	RTG Option		Solar Option	
	Team X	Cost Models	Team X	Cost Models
Phase A Concept Study	Incl. below	5.0	Incl. below	5.0
01/02/03 PM/PSE/SMA	83.1	86.7	80.4	82.0
04 Science	37.3	17.1	37.3	16.2
05 Payload	73.4	86.1	80.4	86.1
06 Flight System	426.1	344.1	361.6	300.9
07 Mission Ops	33.3	21.9	33.3	21.3
09 Ground Data System	36.1	22.4	36.5	20.5
10 Project System I&T	33.2	56.4	35.4	59.5
Total Dev. w/o Reserves	722.5	639.7	664.8	591.5
Development Reserves	326.2	319.9	332.4	295.8
Total A-D Development Cost	1,048.7	959.6	997.2	887.3
01 Project Management	6.7	2.5	11.1	4.2
04 Science	71.7	90.0	119.4	147.9
07 Mission Operations System	104.9	107.7	122.2	151.7
09 Ground Data System	32.9	30.9	56.4	52.5
Total Ops w/o Reserves	216.2	231.0	309.1	356.4
Operations Reserves	26.2	28.4	40.6	47.7
Total E-F Operations Cost	242.4	259.4	349.7	404.1
08 Launch System	220.0	220.0	200.0	200.0
Total Cost	1,511.1	1,439.0	1,546.9	1,491.4

MER and MSL rovers, and a selection of competed Discovery and New Frontiers missions. Normalized percentage spreads were then used to phase the Team X estimate over the duration of 60 months for Phase B-D development and similarly for the 4 - 7 year duration for Phase E. The base year profile was then escalated to real year dollars using the JPL Composite Inflation Index.

Table 5-2 and Table 5-3 shows the total mission cost funding profile for the Intrepid options. The RTG option has a Phase A start date of April 2024 and the Solar option has a Phase A start date of Mar 2023.

Potential Cost Savings

In addition to developing a cost estimate for the Intrepid concept, Team X also provided feedback on potential ways to lower costs. Team X findings include:

- For the 4 cameras, the project may be able to leverage using common readout and camera architectures.
- Consider foreign contributions for the instruments.
- Reuse of the same components in multiple locations could potentially save some cost (e.g., actuators and actuator housings).



Table 5-2. Total Mission Cost Funding Profile for the RTG Option. (FY costs¹ in Real Year Dollars, Totals in Real Year and FY25 Dollars.)

Item	FY24	FY25	FY26	FY27	FY28	FY29	FY30	FY31	FY32	FY33	FY34	Total (RY\$M)	Total (F25\$M)	
Cost														
Phase A Concept Study	2.1	2.9	-	-	-	-	-	-	-	-	-	4.9	5.0	
Technology Development	-	-	-	-	-	-	-	-	-	-	-	-	-	
Phase B-D Development ²	-	56.6	193.2	244.4	149.6	82.8	33.9	-	-	-	-	760.5	717.5	
Phase B-D Reserves	-	25.7	87.8	111.1	68.0	37.7	15.4	-	-	-	-	345.8	326.2	
Total A-D Development Cost	2.1	85.2	281.0	355.5	217.7	120.5	49.3	-	-	-	-	1,111.2	1,048.7	
Launch services	-	-	37.7	38.7	39.8	40.9	42.1	43.3	-	-	-	242.6	220.0	
Phase E Science	-	-	-	-	-	-	13.4	17.7	18.2	18.7	19.3	87.4	71.7	
Other Phase E Cost	-	-	-	-	-	-	27.1	35.7	36.7	37.8	38.8	176.1	144.5	
Phase E Reserves	-	-	-	-	-	-	4.9	6.5	6.6	6.8	7.0	31.9	26.2	
Total Phase E Cost	-	-	-	-	-	-	45.4	59.9	61.6	63.3	65.1	295.3	242.4	
Education/Outreach														
Other (specify)														
Total Cost	2.1	85.2	318.7	394.2	257.5	161.4	136.8	103.2	61.6	63.3	65.1	1,649.1	1,511.1	
¹ Costs should include all costs including any fee												Total Mission Cost	1,649.1	1,511.1
² MSI&T - Mission System Integration and Test and preparation for operations included														

Table 5-3. Total Mission Cost Funding Profile for the Solar Option. (FY costs¹ in Real Year Dollars, Totals in Real Year and FY25 Dollars.)

Item	FY23	FY24	FY25	FY26	FY27	FY28	FY29	FY30	FY31	FY32	FY33	FY34	FY35	Total (RY)	Total (F25\$M)
Cost															
Phase A Concept Study	2.4	2.4	-	-	-	-	-	-	-	-	-	-	-	4.8	5.0
Technology Development	-	-	-	-	-	-	-	-	-	-	-	-	-	-	-
Phase B-D Development ²	-	50.7	172.9	218.6	133.8	74.1	30.3	-	-	-	-	-	-	680.5	659.8
Phase B-D Reserves	-	25.5	87.1	110.1	67.4	37.3	15.3	-	-	-	-	-	-	342.8	332.4
Total A-D Development Cost	2.4	78.7	260.0	328.8	201.3	111.4	45.6	-	-	-	-	-	-	1,028.1	997.2
Launch services	-	-	-	34.3	35.2	36.2	37.2	38.3	39.4	-	-	-	-	220.5	200.0
Phase E Science	-	-	-	-	-	-	52.9	13.8	14.2	14.6	15.0	15.4	15.9	141.7	119.4
Other Phase E Cost	-	-	-	-	-	-	84.1	21.9	22.5	23.2	23.8	24.5	25.2	225.1	189.7
Phase E Reserves	-	-	-	-	-	-	18.0	4.7	4.8	5.0	5.1	5.2	5.4	48.2	40.6
Total Phase E Cost	-	-	-	-	-	-	155.0	40.4	41.5	42.7	43.9	45.1	46.4	415.0	349.7
Education/Outreach															
Other (specify)															
Total Cost	2.4	78.7	260.0	363.0	236.5	147.6	237.8	78.6	80.9	42.7	43.9	45.1	46.4	1,663.6	1,546.9
¹ Costs should include all costs including any fee												Total Mission Cost	1,663.6	1,546.9	
² MSI&T - Mission System Integration and Test and preparation for operations included															

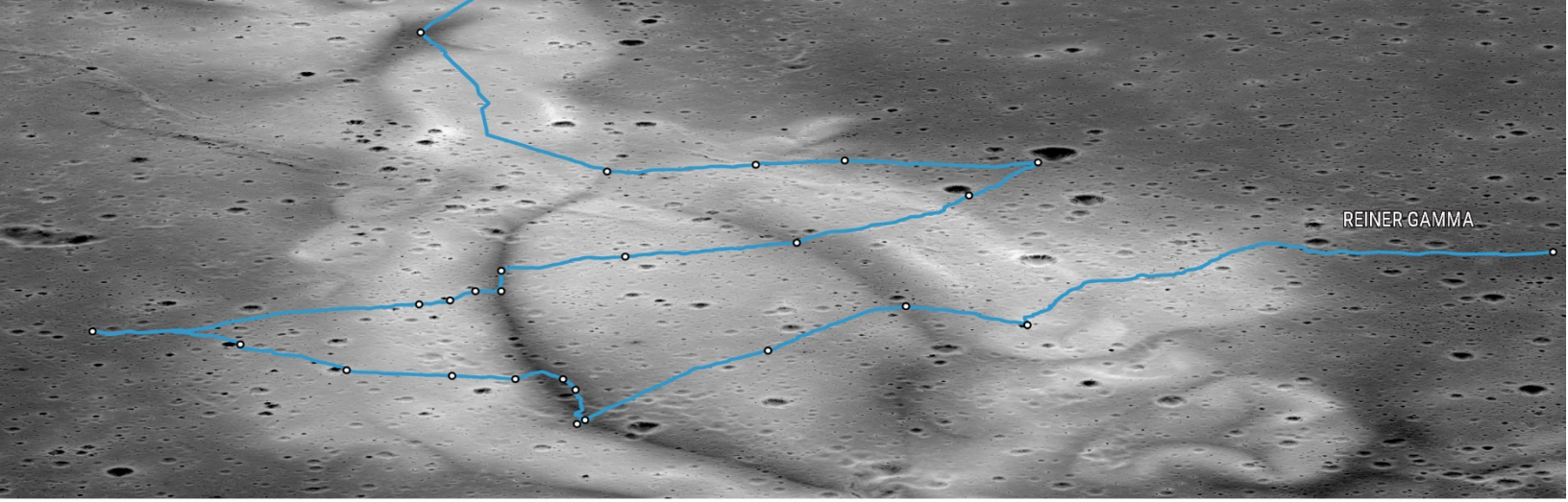


A ACRONYMS

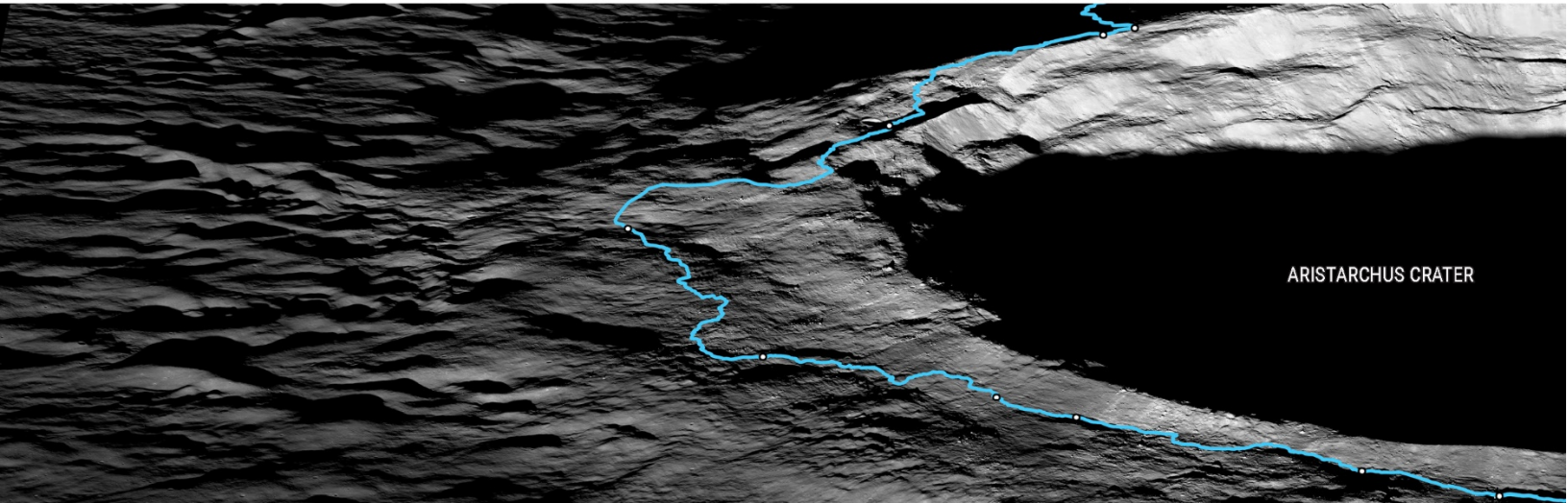
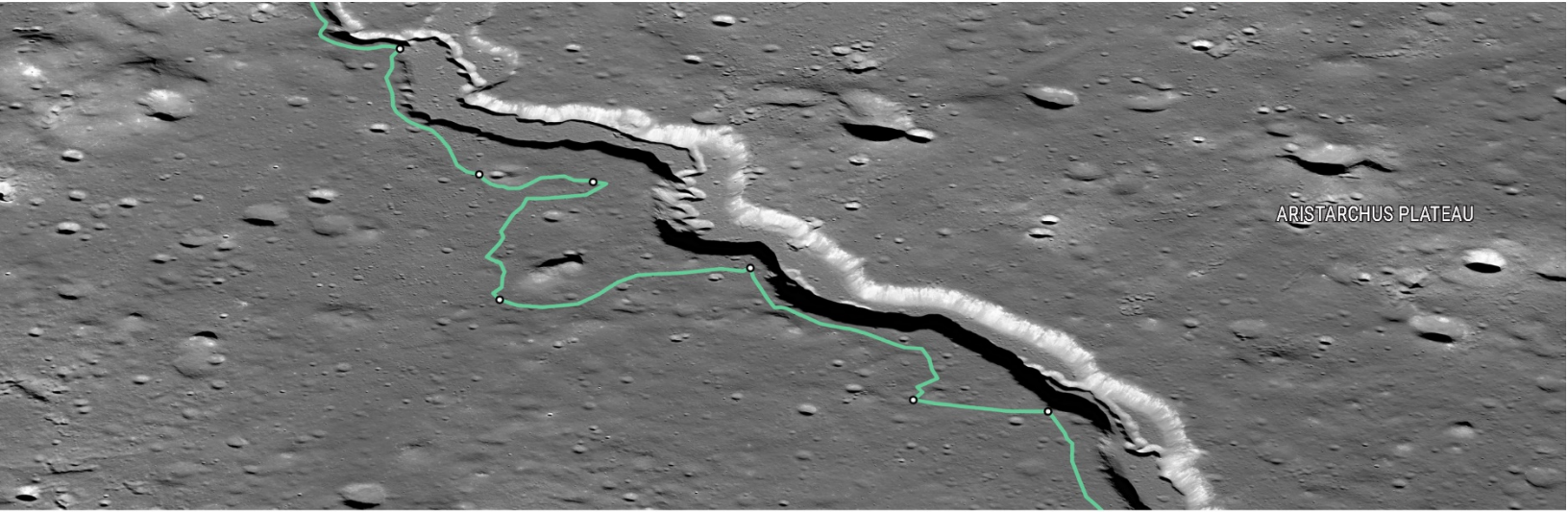
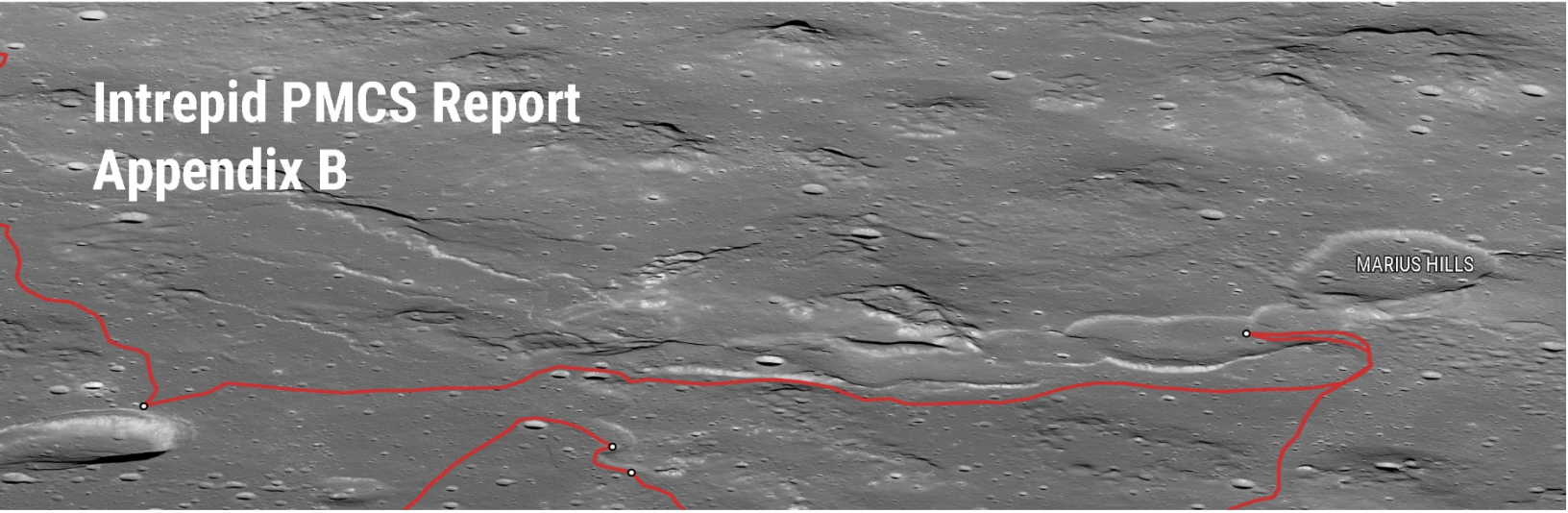
AC	Aristarchus Crater	FI	Focused Investigation
AFT	Allowable Flight Temperature	FOV	Field of View
AO	Announcement of Opportunity	FSW	Flight Software
AP	Aristarchus Plateau	FWHM	Full width half maximum
APXS	Alpha Particle X-Ray Spectrometer	FY	Fiscal Year
ARMAS	Automated Radiation Measurements for Aerospace Safety	GCR	Galactic Cosmic Ray
ASU	Arizona State University	GNC	Guidance, Navigation, and Control
B/W	Black and White	GPHS	General Purpose Heat Source
BOL	Beginning of Life	GRAIL	Gravity Recovery and Interior Laboratory
BOM	Beginning of Mission	GRNS	Gamma Ray Neutron Spectrometer
BW	Black and White	GVC	Gruithuisen Volcanic Complex
C&DH	Command & Data Handling	HLI	Hand Lens Imager
CBE	Current Best Estimate	HST	Hubble Space Telescope
CCD	Charge-coupled Device	I/F	Interface
CDR	Critical Design Review	I/O	Input/Output
CG	Center of Gravity	I&T	Integration and Test
CLPS	Commercial Lunar Payload Services	ICM	Institutional Cost Model
CML	Concept Maturity Level	IFOV	Instantaneous field-of-view
CMOS	Complementary metal-oxide-semi- conductor	IMP	Irregular Mare Patch
CRaTER	Cosmic Ray Telescope for the Effects of Radiation	IMU	inertial measurement unit
CSFD	Crater Size Frequency Distribution	InGaAs	Indium-Gallium-Arsenide
D/L	Downlink	IR	Infrared
DALI	Development and Advancement of Lunar Instrumentation	JPL	Jet Propulsion Laboratory
DARPA	Defense Advanced Projects Research Agency	K2O	Potassium oxide
DC	Direct Current	LGA	Low Gain Antenna
DEM	digital-elevation map	LHP	loop heat pipe
DRPS	Dynamic Radioisotope Power System	LIDAR	Light Detection and Ranging
DSN	Deep Space Network	LRO	Lunar Reconnaissance Orbiter
DTE	Direct-to-Earth	LROC	Lunar Reconnaissance Orbiter Camera
DTM	Digital Terrain Model	LRR	Laser Retro-Reflector
EDL	Entry, Descent, and Landing	LRV	Lunar Roving Vehicle
EECAM	Enhanced Engineering Camera	LSSM	Local Scientific Survey Module
EM	Engineering Model	LV	Launch Vehicle
EOL	End of Life	M2020	Mars 2020 mission
EOM	End of Mission	MAHLI	Mars Hand Lens Imager
EOS	Earth Observing System	MatISSE	Maturation of Instruments for Solar System Exploration
eV/eV	electronvolt	MAV	Mars Ascent Vehicle
EVA	Extra-Vehicular Activity	MDBF	mean-distance-between-faults
		MEL	Mass Equipment List
		MER	Mars Exploration Rover
		MeV	Mega Electronvolts (million electronvolts)



MEV	Maximum Expected Value	RHU	Radioisotope Heater Unit
MgO	Magnesium Oxide	ROC	Rover Operations Center
MH	Marius Hills	ROM	Rough Order of Magnitude
MIMU	Miniature Inertial Measurement Unit	RPS	Radioisotope Power System
MLI	Multi-Layer Insulation	RT	response time
MMM	Moon Mineralogy Mapper	RTG	Radioisotope Thermoelectric Generator
MMRTG	Multi-Mission Radioisotope Thermoelectric Generator	RY	Real Year
MPV	Maximum Possible Value	SDD	Silicon Drift Detector
MSI&T	Mission System Integration and Test	SELENE	Selenological and Engineering Explorer
MSL	Mars Science Laboratory	SfM	Structure from Motion
MSSS	Malin Space Science Systems	SMA	Safety & Mission Assurance
MUX	Multiplexer	SNR	signal-to-noise ratio
NA	Not Applicable	SOC	Science Operations Center
NAC	Narrow Angle Camera	SOCM	Space Operations Cost Model
NASA	National Aeronautics and Space Administration	SOMA	Science Office for Mission Assessments
NE	Northeast	SSPA	Solid State Power Amplifier
NEN	Near Earth Network	STEM	Science Technology Engineering Mathematics
NF	New Frontiers	STM	Science Traceability Matrix
NICM	NASA Instrument Cost Model	STMD	Space Technology Mission Directorate
NS	Neutron Spectrometer	SUROM	Start Up Read Only Memory
NW	Northwest	SW	Southwest
OH/H ₂ O	Hydroxide / water	TBD	to be determined
OP	Oceanus Procellarum	TDP	Technical Data Package
OS	Operating System	THEMIS	Time History of Events and Macroscale Interactions during Substorms
PBC	Power Bus Control	TID	Total Ionizing Dose
PCB	Printed Circuit Board	TiO ₂	Titanium dioxide
PDR	Preliminary Design Review	TRL	Technical Readiness Level
PEL	Power Equipment List	UV	ultraviolet
PI	Principal Investigator	UV/IR	Ultraviolet/Infrared
PICASSO	Planetary Instrument Concepts for the Advancement of Solar System Observations	V&V	Visions and Voyages
PKT	Procellarum KREEP Terrane	VIPER	Volatiles Investigating Polar Exploration Rover
PM	Project Management	WBS	Work Breakdown Structure
PMCS	Planetary Mission Concept Study	WEB	Warm Electronics Box
PRT	Platinum Resistance Thermometer	WFOV	Wide Field of View
PS	Point Spectrometer		
PSE	Project Systems Engineering		
RF	Radio Frequency		
RG	Reiner Gamma		
RGB	Red Green Blue		



**Intrepid PMCS Report
Appendix B**





B DESIGN TEAM STUDY REPORT

B.1 INTREPID MISSION CONCEPT: FREQUENTLY ASKED QUESTIONS

B.1.1 HOW WOULD INTREPID HELP US BETTER UNDERSTAND THE SOLAR SYSTEM, NOT JUST THE MOON?

The Moon provides a cornerstone upon which our understanding of many planetary processes is based because we have documented samples from nine locations (Apollo and Luna) that ground the extensive remote sensing datasets collected over the past sixty years. As such, our detailed knowledge of the Moon informs our understanding of how planets evolve, including crustal formation, volcanic activity, alteration by the space environment, and the influence of impact bombardment through time. The Intrepid traverse provides an opportunity to investigate the regional complexities of the lunar crust as well as sample various eruption mechanisms and magmatic compositions. Intrepid's traverse was selected because it samples the Procellarum KREEP Terrane, a large-scale compositional anomaly not sampled by previous surface operations. The merged results of Intrepid ground observations and the results of the previous sixty years of lunar science would fuel the paradigm shifting results from Intrepid, and thus improve our understanding of key geologic processes across many bodies in the Solar System.

Intrepid would contribute to understanding planetary processes throughout the Solar System in many ways. Mercury also underwent widespread volcanic resurfacing to build much of its crust (e.g., *Strom et al.* [1975] *Denevi et al.*, 2009, 2013, 2018; *Whitten et al.* [2014]; *Byrne et al.* [2018]). Like Oceanus Procellarum, Mercury's vast northern volcanic plains are also not clearly linked to any single impact basin (e.g., *Head et al.* [2011]), and are related to nearby pyroclastic deposits, vents, and rille-like features (e.g., *Hurwitz et al.* [2013a]; *Byrne et al.* [2013]; *Goudge et al.* [2014]); knowledge of these processes at Oceanus Procellarum would directly benefit our interpretations of Mercury's geologic history. Flood basalt emplacement was also important in the building of crusts of Earth, Mars (e.g., *McEwen et al.* [1999]; *Elkins-Tanton et al.* [2005]), and likely Venus (e.g., *McKenzie et al.* [1992]). On the Moon, the process of basaltic crust building was arrested before engulfing the whole body, providing a snapshot in

time of processes that also occurred early in the histories of Mercury, Venus, and Mars.

Crustal dichotomies are also important features of Mercury (younger smooth plains concentrated in the low-lying northern/Caloris hemisphere vs. older crustal materials; (e.g., *Hawke II et al.* [2018]) and Mars (the northern lowlands vs. southern highlands; e.g., *McGill and Squyres* [1991]). The crustal dichotomies on Mercury and Mars have, like the Moon, been suggested to result from either impact events or endogenic effects such as mantle overturn. Gathering evidence on the Moon that can help to explain these basic, first-order features of the terrestrial planets would be a key contribution of Intrepid.

Intrepid's progress toward revealing the modification of the surface of airless bodies would also have direct implications for understanding surface processes on Mercury and asteroids. Investigating the process of ballistic sedimentation at the Moon would provide a baseline for understanding Mercury, where the higher impact velocities and larger secondary craters mean ballistic sedimentation has been an even more important process [*Chapman et al.*, 2018], and the lack of large compositional contrasts complicate discerning between the contributions of local and distal material. Going in the other direction, the Moon can similarly provide a comparison for the asteroid belt, where impact mixing is likely less effective owing to lower impact velocities and gravitational acceleration, and primary ejected material may be more important. Variations in space weathering due to changes in the radiation environment and magnetic field strength also provide a direct tie to understanding how space weathering varies with distance from the Sun and in locations like Mercury (e.g., *Domingue et al.* [2014]) and possibly Vesta [*Blewett et al.*, 2016; *Fu et al.*, 2012], where a magnetic field may partially shield the surface.

B.1.2 HOW ARE INTREPID'S SCIENCE OBJECTIVES TIED TO CURRENT PLANETARY SCIENCE DECADE SURVEY THEMES AND WHY SHOULD INTREPID BE RECOMMENDED AS A NEW FRONTIERS MISSION FOR THE COMING DECADE?

The Intrepid mission would acquire vital new data that would directly address several scientific themes identified in *Vision and Voyages for Planetary Science in the Decade 2013-2023* [NRC, 2011] that



are as yet unresolved. The V&V document includes three research goals for the inner planets that are fully relevant to Intrepid: I) Understand the origin and diversity of terrestrial planets, II) Understand how the evolution of terrestrial planets enables and limits the origin and evolution of life, and III) Provide critical context and information for future human exploration (V&V Table 1-2). The next decadal survey, which would guide exploration objectives for the years 2023 to 2032, is currently in progress. Current submissions to the *Planetary Science and Astrobiology Decadal Survey 2023-2032* include a number of white papers that might guide scientific themes in the coming decade of exploration that are also aligned with Intrepid's objectives [see references below]. We identify four themes common to a number of submitted white papers that suggest the following objectives: A) planetary-scale differentiation and thermal evolution; B) understanding the origins of planetary asymmetries (e.g., compositional, structural, thermal); C) diversity of mantle processes and magmatism; and D) post-emplacement modification of geologic materials.

Within the V&V theme of understanding the origin and diversity of terrestrial planets, Intrepid's objectives are intimately aligned with the goals: (1) constraining the bulk composition of the planets to understand their formation and evolution (I-II, A-C above); (2) characterize planetary interiors to understand how they differentiate and evolve (I, A, C); and (3) characterize planetary surfaces to understand how they are modified by geologic processes (I-III, B-D). Similar themes are likely to be echoed in the 2023-2032 report. Intrepid would address current and future Decadal objectives through its investigation of the lunar interior and its evolution over 4 billion years. (1) Constraining the bulk composition of the Moon is achieved through understanding the major components of the crust, mantle, and core; to this end, Intrepid's mineralogical and geochemical measurements would fundamentally improve our understanding of the components and variety of rock types making up the Moon's crust and mantle. (2) Pathways to understanding the Moon's differentiation and evolution are closely intertwined with questions about its structural and compositional global asymmetry, and the origin of the PKT. Intrepid's traverse, in tandem with mineralogy and geochemistry measurements, would provide a time sequence of rock types and geologic events in the PKT that would

elucidate its structure and composition, e.g., distribution of KREEP rich materials, over time.

Characterizing planetary surfaces and identifying the major volcanic features along the Intrepid traverse, and assessing their distribution, composition, and timescales would reveal clues to the diversity of styles of magmatism on the Moon, associated with the PKT. The V&V document highlights questions about the major surface features on each of the inner planets, as well as understanding the distribution and timescales of volcanism. Measurements to be made by Intrepid are recommended key measurements in the V&V document, and would include in-situ measurements of rock and regolith types, that represent major advances in, and would provide a much more detailed view of, the surface to inform the geologic and magmatic evolution of the Moon. Intrepid's measurements would investigate processes relevant to all of the terrestrial planets, specifically testing relationships between flood basalts and other volcanic deposits, testing relationships between intrusive and extrusive magma, assessing the role of volatiles as a driving parameter for volcanic eruptions, and providing constraints on physical models. Altogether, Intrepid's measurements would provide insight to the compositions and physical state of the interior over 4 billion years of lunar history exposed at the surface.

(3) The myriad geologic processes that have processed surface materials would also be investigated along Intrepid's unprecedented traverse. In addition to characterizing the volcanic processes that have modified the lunar surface, Intrepid's imaging and compositional measurements would directly investigate the impact flux over time, investigate ballistic sedimentation process during impact cratering, and determine target material influences on cratering mechanisms. The Moon is a natural laboratory for studying impact processes because of their high degree of preservation on the Moon's surface. Additional information about ejecta emplacement and environmental effects of impacts gained through Intrepid's observations might be applied to improve models of the Solar System's earliest impactors and their effects on limiting the origins of life and volatile distributions. Additional spectral measurements would determine variations in space weathering on a variety of regolith types and over time, and provide a comprehensive test the origin of the strong magnetic anomaly. This capability is far beyond what can be achieved at a single landing site, such



as the upcoming Commercial Lunar Payload Services (CLPS) flight in the near-future. To understand the evolution of a planetary body over time, it is critical to gain measurements over a long and representative section of its history, and the traverse selected for Intrepid is a unique occurrence of deposits ideally suited to this goal for the Moon. Only a long-duration rover paradigm for exploration, like Intrepid, can be so complete and detailed in its exploration of large, Decadal-scale objectives.

Finally, as stated in V&V, the Moon is the next logical step in the continued human exploration of the Solar System. Intrepid would collect additional context and input for future human exploration while also bridging the gap between samples and remotely sensed data through ground-truth. The scale of Intrepid's traverse is beyond what is currently technologically possible for a single human mission. The Intrepid rover is designed for much more rapid and long-duration exploration than the VIPER rover currently in design for an upcoming mission to the Moon's south pole. However, the long-lived Intrepid rover could be adapted for future exploration and science in support of or in tandem with a future human presence on the Moon's surface or cis-lunar space.

The science conducted by Intrepid is distinct from what has been previously proposed and recommended as high priority science for the New Frontiers program – specifically the Lunar Geophysical Network [NASAEM, 2020]. The magnitude of Intrepid's investigations far exceed any current vision for smallsats, cubesats, the CLPS program, and any vocalized plans for international exploration of the Moon [ISECG, 2018]. In summary, Intrepid is a robust and highly efficient exploration pathway to address scientific goals on a scale only rivaled by the wealth of information provided by samples returned by Apollo. However, Intrepid would dive into questions that cannot be addressed by the Apollo samples alone, investigating a much wider range of samples than can possibly be returned to Earth, including materials that are unsampled and unvisited by previous explorers.

2023-2032 Decadal Submitted White Papers

1. Constraining the bulk composition of the planets to understand their formation and evolution:

- a. *Exploring end-member volcanism on the Moon at the Aristarchus Plateau* (Jawin et al.) - evolution of the interior via non-mare volcanism
 - b. *The Importance of Planetary Volcanism and Key Investigations for the Next Decade* (Kerber et al.) - sampling diversity of magma compositions, tracing volcanic volatiles
 - c. *End-member volcanism in the absence of plate tectonics: Silicic volcanism on the Moon* (Valencia et al.) - evolution of the interior via non-mare volcanism
 - d. *Origin and Evolution of the Moon's Procellarum KREEP Terrane* (Jolliff et al.) - evolution of the interior via lava composition
2. Characterize planetary interiors to understand how they differentiate and evolve:
- a. *Exploring end-member volcanism on the Moon at the Aristarchus Plateau* (Jawin et al.) - connecting morphology and composition with style of volcanism
 - b. *The Importance of Planetary Volcanism and Key Investigations for the Next Decade* (Kerber et al.) - connecting lava morphologies to processes, tracing volatiles
 - c. *End-member volcanism in the absence of plate tectonics: Silicic volcanism on the Moon* (Valencia et al.) - connecting morphology and composition with style of volcanism
 - d. *Origin and Evolution of the Moon's Procellarum KREEP Terrane* (Jolliff et al.) - connecting morphology and composition with style of volcanism
3. Characterize planetary surfaces to understand how they are modified by geologic processes:
- a. *Science Case for a Lander or Rover Mission to a Lunar Magnetic Anomaly and Swirl* (Blewett et al.) – magnetic anomalies
 - b. *Investigating Impact Processes at all Scales: The Moon as a Laboratory* (Costello et al.) – impact stratigraphy and flux, understanding ray formation and secondary crater population
 - c. *Assessing the Recent Impact Flux in the Inner Solar System: 1 Ga to Present* (Ghent et al.) – impact stratigraphy and flux, understanding ray formation and secondary crater population
 - d. *Exploring the Bombardment History of the Moon* (Bottke et al.) – impact stratigraphy and flux, understanding ray formation and secondary crater population



B.1.3 CAN THE PROPOSED INTREPID MEASUREMENTS BE OBTAINED FROM AN ORBITER?

No, almost none of the Intrepid measurements can be obtained from an orbiter because of the high resolution nature of most observations.

Among the more compelling examples are the measurements obtained by the APXS and GRNS during impact crater radial traverses. Impacts overturn the target stratigraphy, exposing deeper materials closest to the crater rim. As the rover approaches an impact crater, the GRNS continuously measures the elemental abundance of the regolith integrated over a depth of about 30 cm. At each stop along the way the APXS measures elemental abundance integrated over a depth of about 2 cm. These measurements would reveal the amount of mixing between the substrate and overlying ejecta at the beginning of the traverse and then both instruments would measure progressively deeper and deeper into the pre-existing substrate while approaching the rim (ejecta reflects the overturned stratigraphy). Near the rim (~1/10 of crater radius to the rim) the GRNS and APXS would measure the composition of regolith composed of materials excavated from the deepest reaches of the crater, thus revealing the geochemical variations through time of volcanic materials (the APXS would also measure the chemistry of blocks to compare with the regolith measurements). These meter to centimeter scale, high-precision, high-accuracy elemental measurements simply cannot be obtained from orbit by any existing instruments.

B.1.4 IF THE ROVER IS DESIGNED TO TRAVERSE 1800 KM IN ORDER TO MEET ITS OBJECTIVES, THEN ISN'T IT LIKELY TO LAST MUCH LONGER? WHAT ABOUT LAST SIX MONTHS AND / OR EXTENDED MISSION?

The historic record of NASA planetary rovers far exceeding their planned lifespan raises the question of what options exist for Intrepid if it reaches the end of its nominal traverse at the Aristarchus IMP in good health. While details of a mission extension are beyond the scope of this report, excellent opportunities exist for additional high-science-return destinations for the Intrepid rover. The Gruithuisen Volcanic Complex (GVC), interpreted as a center of silicic volcanism [Glotch *et al.*, 2010], is 400 km north of the Aristarchus IMP. The route to GVC allows a second look at the

young mare P60 (1.2 Gyr; [Hiesinger *et al.*, 2003]) and then passes through the Prinz Volcanic complex (3.5-3.7 Gyr; [Hiesinger *et al.*, 2003]). Next Intrepid would cross a moderately high titanium (>5 wt%) mare unit that is spectrally similar to the nearby P40 (2.1 Gyr) unit. Here Intrepid would densify its temporal coverage of the mare materials. Within the GVC there are two large silicic domes (Gamma and Delta) easily accessible from the embaying mare. There are several places on Gamma where Intrepid could traverse up onto the flank for at least a kilometer, ensuring excellent opportunities for detailed characterization of this enigmatic class of volcanic landform. After departing the GVC Intrepid would head west towards the Mairan T dome (350 km traverse) and associated compositional anomalies. Note that this region is embayed by another very young mare unit (P58, 1.3 Gyr; [Hiesinger *et al.*, 2003]) which is thought to be the target of an upcoming sample return mission by China. Here, Intrepid could provide valuable context information for the returned sample. Together, these destinations would make up an extended traverse about 80% as long as the primary mission, with new regions every few months of travel, and at the end leave the rover within reach of further destinations in northern Oceanus Procellarum.

B.1.5 HOW DETAILED ARE THE CURRENT TRAVERSE PLANS? HOW CAN YOU BE SURE YOUR PLANNED MEASUREMENTS WOULD OBTAIN THE DESIRED RESULTS? WON'T THE MISSION BECOME SIDE-TRACKED BY UNEXPECTED DISCOVERIES?

The Intrepid mission concept relies on extensive pre-planning of both the nominal traverse and contingency paths, so that even in the case of anomalies that throw off the schedule, a human operator can select the appropriate alternate plan to stay on schedule without needing a major meeting of the science team to re-plan on the fly. This pre-planning is possible due to high-quality existing orbital measurements of the entire traverse. Lower-resolution (10s to 100s of meter pixel scale) multispectral datasets inform the general path of the traverse and key science sites, while meter-scale LROC NAC images cover the full traverse. Additionally, over 30% of the traverse (as of March 2020) is covered with stereo NAC observations allowing the creation of 2-to-5-meter-scale digital terrain models enhancing science



planning and hazard avoidance. Hazards not identified from orbital datasets are handled onboard the rover, enabled by recent developments in autonomy capabilities, thus minimizing communication and human analysis delays in the driving process.

A commonly expressed concern with the Intrepid mission concept is that observations would reveal some major unforeseen discovery outside the science objectives, but its tight adherence to schedule would prevent any follow-up of that discovery. It is true that the broad scope of the Intrepid mission means that interesting (but out-of-science-scope) local discoveries simply are not a priority unless they fundamentally overturn our understanding of the Moon (in which case, if the entire science team agrees that it is truly revolutionary, time can be pulled from the one-year reserve to follow up). However, such unforeseen discoveries would not derail the mission. Intrepid would document these discoveries and move on. An unexpected discovery may be the impetus for another mission, but Intrepid would stay on course and retire its objectives in the given time frame. With that said, there is some capability to follow up on unexpected discoveries built into the concept of operations, though the pace of the mission, extremely short command cycle, and tight schedule would make follow-ups more akin to how Apollo astronauts reacted to new discoveries than to the highly detailed discovery follow-ups typical of martian rover missions.

If a discovery is identified while the rover is still at the location, it can be followed up immediately. The mission as planned has large data and power margins, and long periods when the rover is simply stationary, allowing the GRNS and APXS to integrate, so commands could easily be uploaded to acquire additional high-resolution images and spectra of the area. If the regional science team decides it is worth adjusting the schedule for the rest of the lunation (or reducing the length of GRNS and APXS integrations) to gain a few hours of time, they could command Intrepid to drive closer and acquire additional images and spectra. Arm operations to get hand lens images or APXS measurements would require more time, but on the order of hours, not days as often happens with martian missions. This speed results from three factors: 1) The short command cycle between the Earth and the Moon, 2) onboard autonomy that supports rapid and safe arm placement, and 3) a low-complexity instrument suite compared to Mars rovers.

In cases where a discovery is made after the rover has moved on, the regional science team has the option to adjust the locations of future stops to make another investigation of a similar feature, or possibly even to abandon multiple stops from the rest of the region's traverse plan in order to gain the time to turn around and go back, but this would be an extreme circumstance and a very unlikely outcome. Most likely the team would want to start planning a future mission, such as a CLPS lander/rover, to visit that site with an instrument suite optimized to follow up on Intrepid's pioneering discovery.

The following four figures (Figures B-1 to B-4) show the full nominal traverse used in this report, with stops labeled for cross-referencing with the science objectives and observation plan in Table B-7. Stops with an “N” suffix are overnight stops, with at least 400 hours available for acquiring data over an area of a few km, while other stops occur during daylight, with durations ranging from 24-78 hours. Traverse colors indicate the traverse region (blue=Reiner Gamma, red=Marcius Hills, yellow=Oceanus Procellarum, green=Aristarchus Plateau, light blue=Aristarchus Crater).

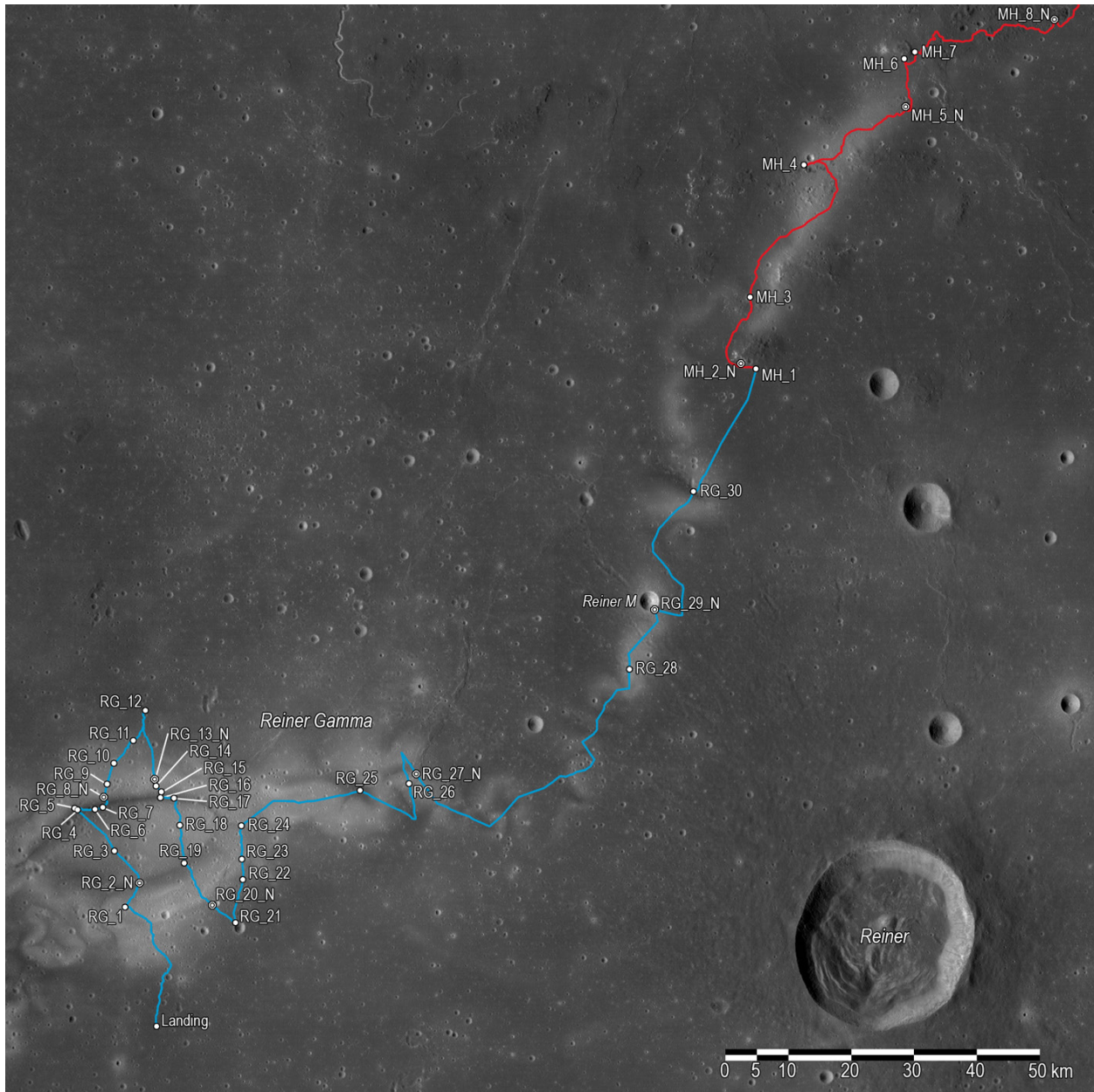


Figure B-1. Map of Intrepid traverse of the Reiner Gamma (blue) and early Marius Hills (red) regions. While near the Reiner Gamma magnetic anomaly, the traverse zig-zags across the swirl to get a detailed magnetic profile, with Focused Investigation stops concentrated on high albedo, low albedo, and albedo contacts. In the swirl-influenced portion of the Marius Hills region, the traverse continues zig-zagging the albedo anomaly, but the stops are focused on specific volcanic features. See Table B-7 for details of each stop.

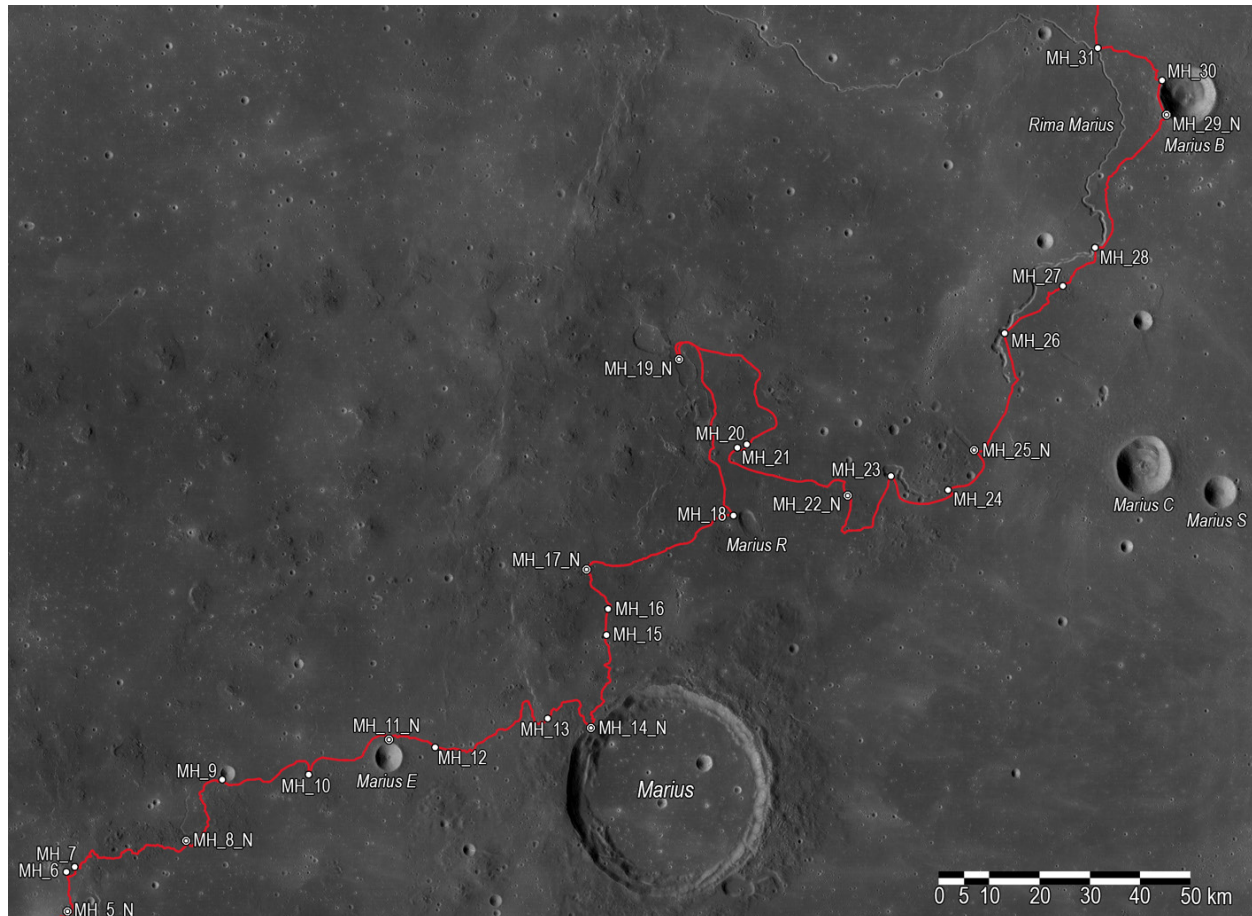


Figure B-2. Map of the post-swirl portions Marius Hills region traverse. While traversing the core of the volcanic complex, Intrepid would visit numerous volcanic domes (10), cones (6) and large scale vents (3), as well as craters (100 m to 20 km diameters) that excavated material from within this enigmatic volcanic region. Towards the end of the region, Intrepid would characterize its first lunar rille, Rima Marius, starting from its vent and downstream more than 75 kilometers. See Table B-7 for details of each stop.

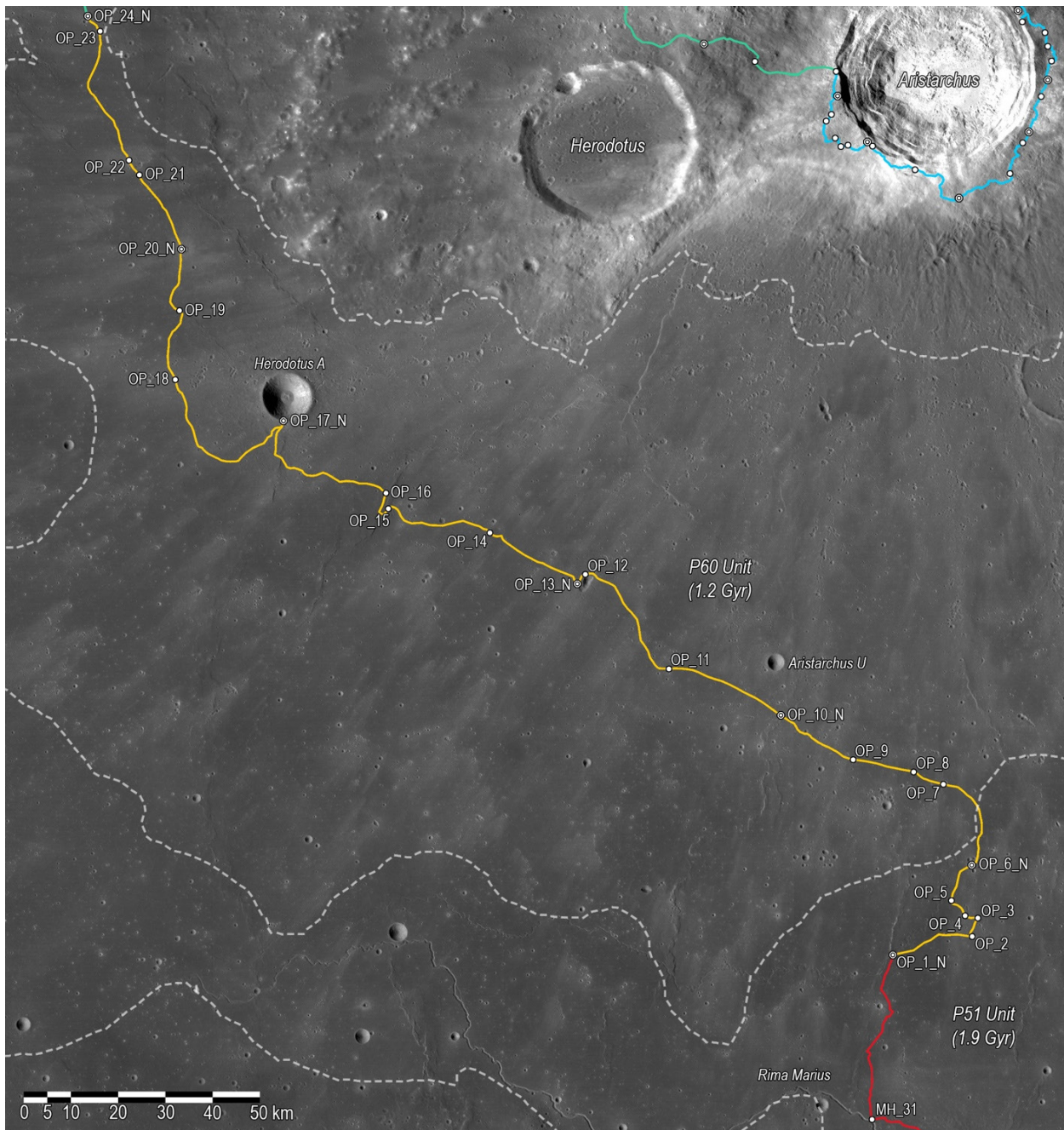


Figure B-3. Map of the Oceanus Procellarum region traverse. In this section Intrepid investigates regolith/ejecta interactions (nature of crater rays) and the chemistry of two of the youngest mare units on the Moon, P60 and P51 (Hiesinger et al., 2003), with a stop at the summit of an unusual standalone shield volcano (stops OP_12 and OP_13_N), and a few craters that potentially excavated material from beneath these young mare units. Intrepid would also determine if the mare units are themselves KREEP rich or are simply contaminated with KREEP materials from the Aristarchus crater event, a high-level question readily answered with the elemental observations collected over the entire Oceanus Procellarum traverse. See Table B-7 for details of each stop.

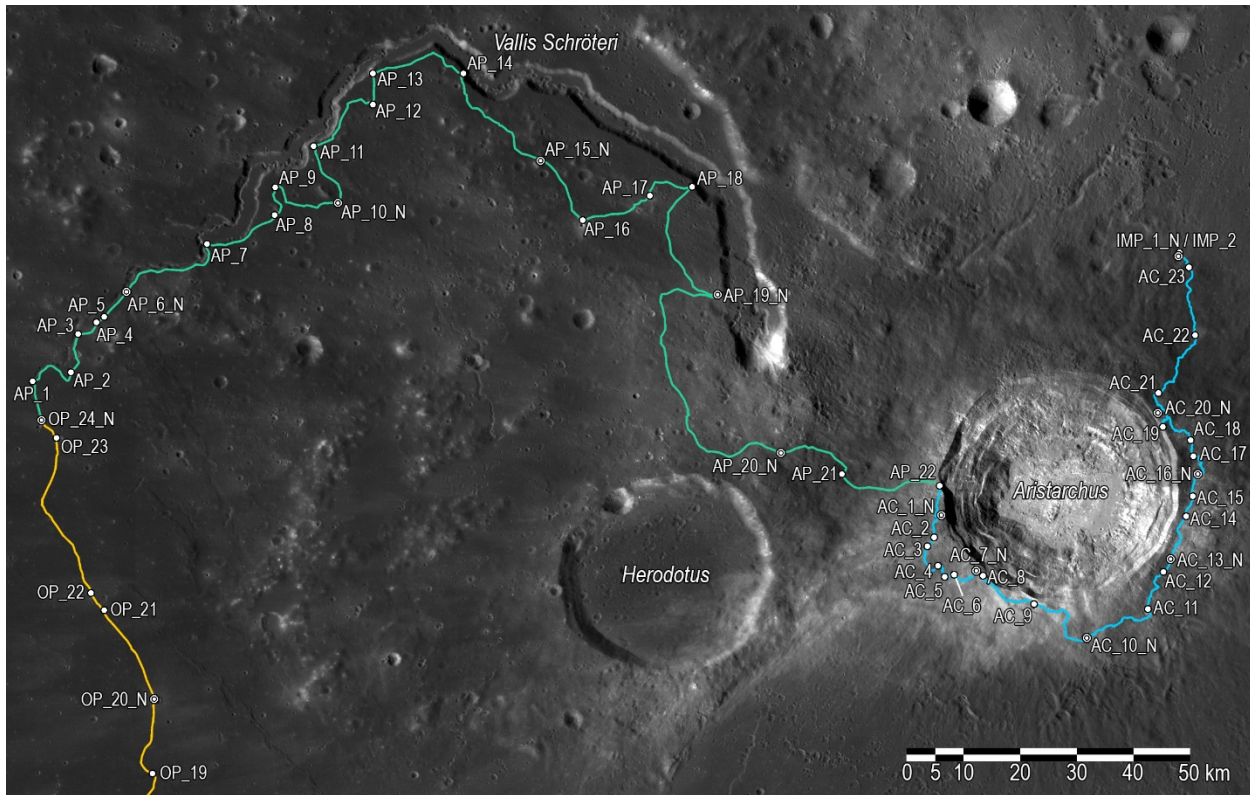


Figure B-4. Map of Intrepid traverse of the Aristarchus Plateau, Aristarchus Crater, and Aristarchus Irregular Mare Patch regions. On the Aristarchus Plateau, Intrepid would investigate pyroclastic deposits and the Vallis Schröteri rille, with stops split between focusing on chemistry (including material excavated from depth by recent craters) and morphological and spectral studies of the rille. The traverse speed would slow dramatically around Aristarchus crater, as the rover navigates the roughest terrain on the entire traverse. A benefit of the slower speed is higher-resolution GRNS measurements while in motion and more densely spaced interval stops, important here due to the multiple fine scale compositional units crossed on the SE ejecta. Major stops would focus on these units (ejecta material that originated from different subsurface units), with a few stops reaching close enough to the rim to investigate the crater interior. Finally, Intrepid would wrap up its 1800 km traverse at the Irregular Mare Patch (volcanic deposit) that is inferred to superpose the Aristarchus ejecta blanket, implying an age of <200 Myr age. See Table B-7 for details of each stop.

B.1.6 WHAT IS SPACE WEATHERING AND WHY WOULD ONE EXPECT THE REINER GAMMA MAGNETIC ANOMALY TO MODERATE SPACE WEATHERING? WHAT IS THE MEANING OF OPTICAL MATURITY AND ITS IMPORTANCE?

Mysterious albedo patterns, called swirls, have captured the imagination of the scientific community since the invention of the telescope. Apollo era measurements hinted that swirls may be associated with local magnetic anomalies (Hood et al., 1979), and this idea was confirmed with the Lunar Prospector mission [Hood et al., 2001; Richmond et

al., 2003]. Analysis of lunar soil samples revealed that over time solar wind, galactic cosmic rays, and micrometeorite impacts alter the albedo and color of surface soil grains, a process known as space weathering, leading to the hypothesis that local magnetic structures act as shields that impedes space weathering resulting in relatively less space weathering in regions with the strongest localized magnetic fields. The state of maturity of a surface is estimated from several spectral reflectance features in the visible and near-infrared range thus obtaining the moniker *optical maturity*; the more mature a soil, the more it is space-weathered.

To this day, the origins of the magnetic anomalies and associated swirls remain enigmatic [Robinson et al., 2018 and references therein]. An



alternate hypothesis posits that the swirls are depositional in nature [Garrick-Bethell *et al.*, 2011; Pieters *et al.*, 2014] owing to solar wind induced electric fields interacting with the local magnetic fields [Jarvinen *et al.*, 2014; Saito *et al.*, 2012] to attract fine-grained dust lofted from afar. These models can be tested by characterizing the field strength, polarity, and orientation across the structure and the composition and state of maturity of the regolith [Robinson *et al.*, 2018].

B.1.7 IT IS CLEAR THAT INDIVIDUAL OBSERVATIONS ARE KEY TO ANSWERING QUESTIONS WITHIN A REGION, BUT WHY, TOGETHER, ARE THESE REGIONS KEY FOR UNDERSTANDING LUNAR GEOLOGY AS A WHOLE?

Most of the Intrepid objectives address changes over time and/or the spatial variability (chemistry, mineralogy, morphology, maturity) of volcanic processes and the derived products. The Intrepid traverse was specifically selected as the shortest route to obtain the required observations to address the twelve objectives (Table B-1). To shorten the mission to one or two regions would decimate the science return. It is the total sum of the observations through four Gyr of time across only 1800 kilometers of volcanic terrain that returns the decadal science proposed here.

B.1.8 HOW WOULD INTREPID BE ABLE TO DISTINGUISH BETWEEN CRATER RAY MATERIAL AND MARE BASALTS?

Orbital color observations at the 200-meter pixel scale show that Aristarchus rays affect much of the OP traverse (Figure B-5); however, rays are somewhat discrete (boundaries are fuzzy) and Intrepid would make multiple ray crossings (and would pass through “ray shadows”, areas with little to no ray material). During these crossings the GRNS would measure the chemistry along the path and a key indicator would be the relative amounts of K and Fe. If the K and Fe are not correlated with the local albedo (as seen from orbit and the rover) then the K is native to the basalt and the existence of KREEP rich basalts would be confirmed. Likewise, if the K is related to higher albedo (and thus ray material) and not Fe content then we would know that the local basalts are not KREEP rich. This result would be checked with crater radial traverses, that is, measuring the chemistry as a function of distance from the rims of impact craters (and thus depth beneath the surface).

During impact events the original stratigraphy is overturned [Shoemaker, 1959] such that the deepest excavated material lies close to the rim while the shallower material lies outward from the rim (the continuous ejecta extends out roughly 1 crater radius from the rim). Rocks and debris right on the rim are representative of the underlying materials and less affected by ray material (especially larger rocks), and for craters formed after the Aristarchus event the amount of Aristarchus material would be even less (or non-existent).

Table B-1. Some objectives require observations from the full traverse (all six regions) while others require observations from fewer regions. Mission progresses from left to right.; “x” indicates regions where required measurements are acquired.

	Reiner Gamma	Marius Hills	Oc. Proc.	Arist. Plateau	Arist. Crater	IMP
1.1 Extended volcanism Proc region	x	x	x	x	x	x
1.2 Crustal asymmetry		x	x	x	x	
1.3 Origin of nonmare volcanism		x?			x	
1.4 Deep mantle composition		x		x		x?
1.5 Decline of core dynamo	x	x	x			x
2.1 Flood basalt emplacement	x	x	x	x		
2.2 Origin domes, cones, shields		x	x			x
2.3 Pyroclastic processes		x		x		x?
2.4 Nature of intrusive volcanism	x			x	x	
3.1 Crater formation and processes	x	x	x	x	x	x
3.2 Target material influence	x	x	x	x	x	x
3.3 Space weathering	x	x	x	x	x	x

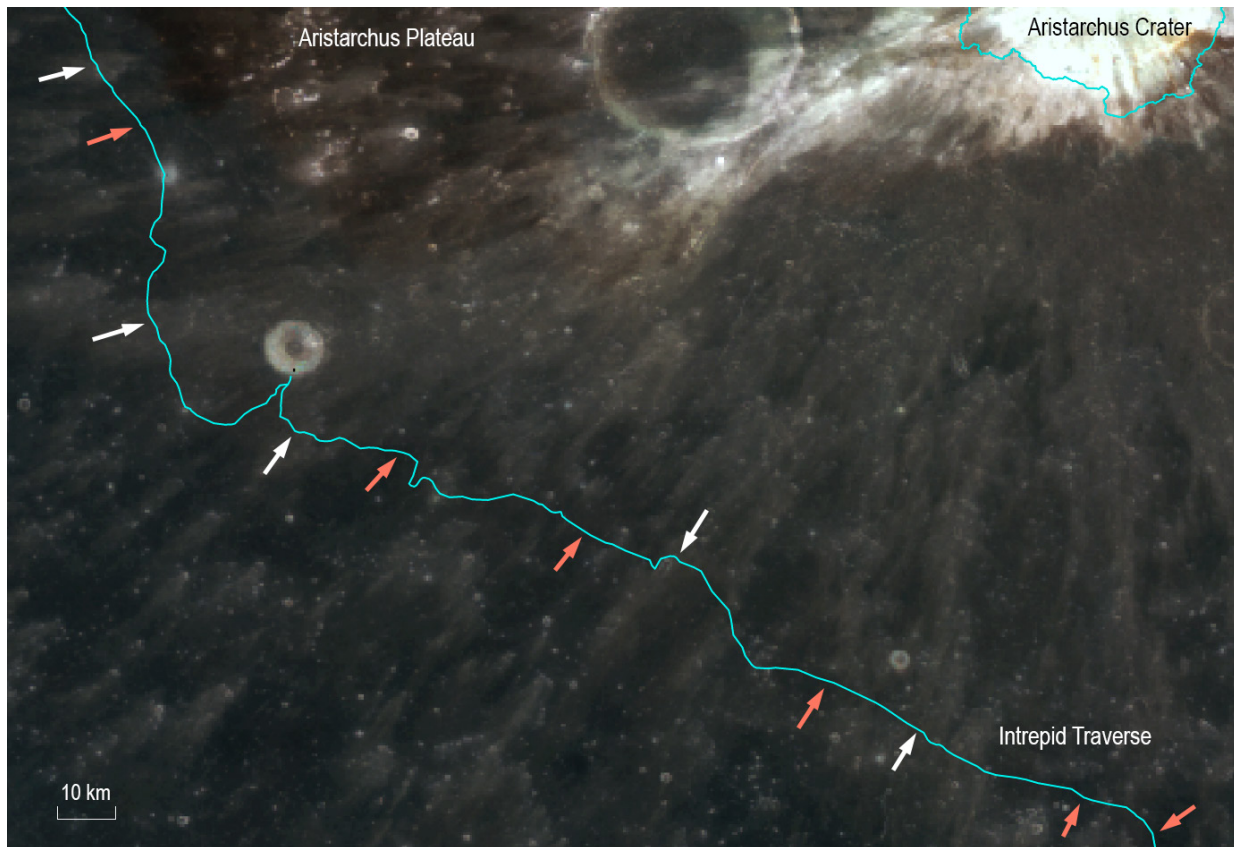


Figure B-5. LROC WAC color composite (red 689 nm, green 415 nm, blue 321 nm) of rays crossing Oceanus Procellarum basalts. White arrows indicate Intrepid ray crossings and salmon arrows indicate ray shadowed areas.

Also it should be noted that the current thought is that rays are mostly the result of overturned local material from relatively small amounts of foreign material striking and churning the surface [Melosh, 1989 and references therein]. By measuring the chemistry of rocks (APXS) and regolith (GRNS and APXS) at the rims of small craters (25 to 200 m diameter), Intrepid can determine the true chemistry of the basalts (depths of excavation ranging from 3 to 20 meters) and the amount of contamination (material ejected from Aristarchus crater). Also, the Intrepid spectral reflectance observations would characterize the state of maturity.

B.1.9 WHY DO PYROCLASTIC DEPOSITS PROVIDE INSIGHT TO THE DEEP MANTLE?

Pyroclastics or volcanic glasses are a special kind of volcanic product because they travel very rapidly to the lunar surface from their origin by partial melting in the mantle. We know this because they have few if any crystals in them. The volcanic glasses tell us in a very direct way about the composition and conditions in the mantle where they

formed by partial melting of magma ocean cumulates. Laboratory experimental petrology can determine the depth of melting using multiple-saturation experiments, and these can be designed using basalt and volcanic glass compositions measured (from deposits on the Aristarchus Plateau) by the Intrepid APXS. Experience with the Apollo-collected orange and green volcanic glasses tells us that these melts came to the surface from great depths, 250 to 500 km [Grove and Kravczynski, 2009], and possibly as deep as 1000 km [Longhi, 2006].

B.1.10 IS IT POSSIBLE TO SAFELY OR EASILY ACCESS EXCAVATED DEEPER REGIONS (THROUGH CRATER RADIAL TRAVERSES) DESPITE THE DENSITY AND SIZE OF BLOCKS CLOSE TO THE CRATER RIM?

The Intrepid traverses were planned from several datasets, the most important being the LROC Narrow Angle Camera (NAC; Robinson *et al.* [2010]). Pixels scales range 25 cm to 150 cm across the region of the traverse (typically 100



cm). Owing to the longevity of the LRO spacecraft, images with a wide variety of incidence angles exist for the same areas in many cases. Images with small incidence angles (Sun high above the horizon) enhance reflectance (albedo) differences whereas those with large incidence angles (Sun near the horizon) bring out topographic details. LROC also obtains stereo observations that enable photogrammetric reduction of stereo pairs to Digital Terrain Models (DTM). The pixel sampling of the DTMs is typically 3x that of the stereo images; a 1 meter pixels scale stereo set results in a 3-meter pixel- scale DTM.

The small incidence angle images are particularly suited to identifying the youngest craters (high albedo, Copernican age) and locating pyroclastic deposits because of their low reflectance.

The large incidence angles allow mapping of hazards along the traverse, blocks and depression, down to the pixel scale. A block with a diameter the size of the pixel is detectable in large incidence angle images. For example a 50 cm diameter block in a 50 cm pixel scale, 75 incidence angle image would appear as one bright pixel (Sun facing side) with a 2-pixel shadow (dark pixels). While the block cannot be resolved per se, it is clear that it exists, or rather a positive feature exists that is interpreted as a block.

The NAC DTMs provide topographic slope, a critical factor when mapping a traverse route. While complete stereo coverage along the entire 1800 km traverse does not exist, key areas with the most challenging terrain have been acquired and processed into DTMs. For example, we have studied NAC DTMs for key domes and cones in the MH region where we know the terrain would be rugged from coarser global terrain models of the region derived from LROC WAC and Selene Terrain Camera stereo images. Furthermore, NAC stereo has been collected and processed for the whole of the Aristarchus crater rim traverse (3 to 4 meter topographic postings). From these high resolution DTMs, we have identified optimal traverses that avoid surface hazards and steep slopes while still traversing important geologic units.

Interpretations of these data are grounded in the surface observations of the Apollo astronauts. We have compared the NAC images and DTMs to Apollo sites, specifically looking at steeper and blockier areas (for example: Camelot crater, Cone crater, Lee-Lincoln scarp, North Ray crater, Spur

crater to Station 6, Van Serg crater) visited by astronauts that calibrate our interpretations of similar-appearing regions along the Intrepid traverse.

Finally, onboard autonomy would allow Intrepid to negotiate block fields as long as there are 3 meters of separation between blocks with diameters >20 cm. In cases where the path near the rim is blocked, Intrepid would simply measure blocks and regolith at that point. An important component of the sampling strategy is collecting observations from many similar spots – any one spot is not crucial to answering any questions. Intrepid would simply measure (and document) what it can and move on to the next stop.

B.1.11 HOW CAN INTREPID UNIQUELY IDENTIFY KREEP RICH MATERIALS?

KREEP rich materials were first identified from small samples of erratic (origin unknown) materials found in Apollo samples and were shown to have relatively high concentrations of thorium (Th), potassium (K) and phosphorous (P). The Procellarum KREEP Terrane (PKT) was predominantly delimited from Lunar Prospector orbital gamma-ray measurements of Th [Jolliff *et al.*, 2000]. It is here in the PKT that Intrepid would identify which materials are KREEP rich and which are not, with no ambiguity. The GRNS can measure K and Th to 4 ppm and 6 ppb, respectively, for relevant lunar materials (see next question).

The APXS can measure P (phosphorus) as well as K (potassium) at the expected levels that these elements occur in KREEP-rich or silicic materials with no difficulty. The MER APXS measured concentration values as low as 0.1 wt.% K₂O and 0.15 wt.% P₂O₅. The high-K mare basalts that we expect to find in Oceanus Procellarum all have at least this much K and P, and most are likely to have 3-4 times as much based on remote sensing. KREEP basalts and silicic or granitic materials have 1-2 orders of magnitude more K and at least 1 order of magnitude more P. These levels would be readily measured with the APXS. Independent measurements of other rare earth elements (REE) do not matter. The GRS would measure thorium and in most lunar samples, Th concentrations are tightly and linearly correlated with REE concentrations, so knowledge of the Th concentration gives a good estimate of the REE. P is also a very good indicator of REE concentrations, because the REE are highly concentrated in the phosphate

minerals apatite and merrillite in nearly all lunar rocks.

Note: it is known from Apollo samples that surface rocks have a weathering rind or patina. However, that material is only on the scale of 100 microns thick and has the same elemental composition as its host rock, so this patina would not affect the APXS measurements.

B.1.12 WHAT IS THE ACTUAL ACCURACY/PRECISION OF THE GRNS AND APXS ELEMENTAL ANALYSES?

For both instruments the sensitivity varies by element, and the accuracy varies with integration time. The APXS, because it has its own radiation source, requires much shorter integration times than the GRNS for the same level of accuracy.

ARMAS measurements enhance the scientific interpretation of GRNS observations. Galactic cosmic ray (GCR) variations must be removed from GRNS measurements for correct interpretation; the GCR correction factor can be large (many tens of percent). Accordingly, though GRNS produces its own internal GCR correction, the ARMAS direct measurement of GCR is both independent and complementary to establishing this important correction factor. At this time we do not have detailed models (or real observations) to allow us to estimate the actual increase in precision that ARMAS would allow but personal communication from David Lawrence indicates the increase would be significant. Note that the GRNS estimates presented here (Table B-2 and Figure B-7) do not consider the ARMAS enhancement.

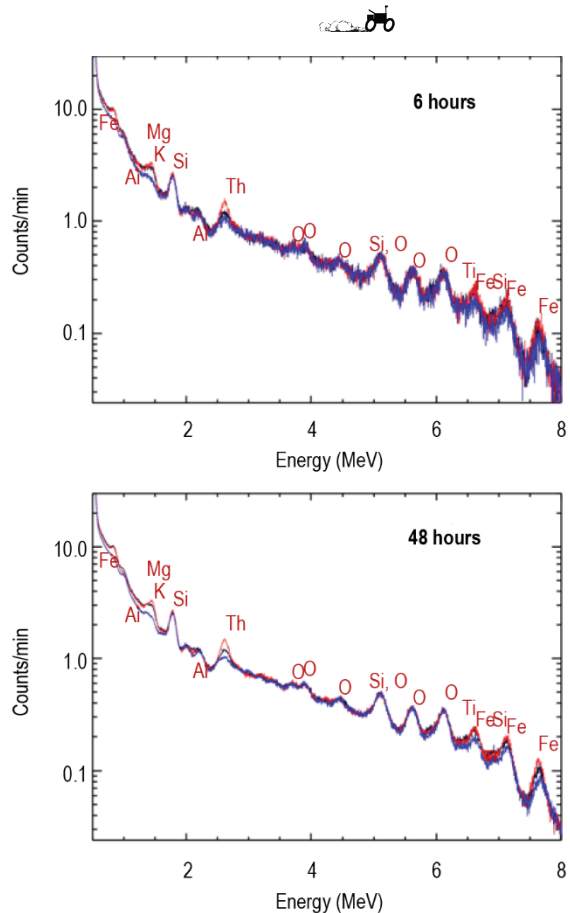


Figure B-6. GRNS element energy lines and sensitivity for two integration durations (upper panel vs. lower panel). The black, red, and blue lines are calculated using the chemical compositions of Apollo 11, Apollo 12, and Apollo 16 soils and regolith breccias from Haskin and Warren, 1991.

Table B-2. Key GRS (GRNS) measured elements for lunar science and uncertainties as a function of integration time. Relative uncertainty is translated to absolute uncertainty by multiplying the concentration by the relative uncertainty. For example in this table the absolute uncertainty for Si is 19.6 ± 0.6 wt% for a 6 hour integration and 19.6 ± 0.4 wt% for a 48 hour integration (19.6×0.029). Sample values are the lowest for each element of concentrations reported for Apollo 11, Apollo 12, and Apollo 16 soils and regolith breccias from Haskin and Warren, 1991.

Element wt%	Sample Value	GRS			
		6 hr		48 hr	
		% 1-sigma relative	% 1-sigma relative	1-sigma absolute	1-sigma absolute
Si	19.6	2.9	2	0.6	0.4
Al	6.4	8.2	4	0.5	0.3
Fe	3.7	16.4	8	0.6	0.3
Mg	3.6	14.4	7	0.5	0.3
O	42.4	6.2	3	2.6	1.3
K (ppm)	800	4.1	2.1	4	2
Th (ppb)	160	6.2	3	6	3

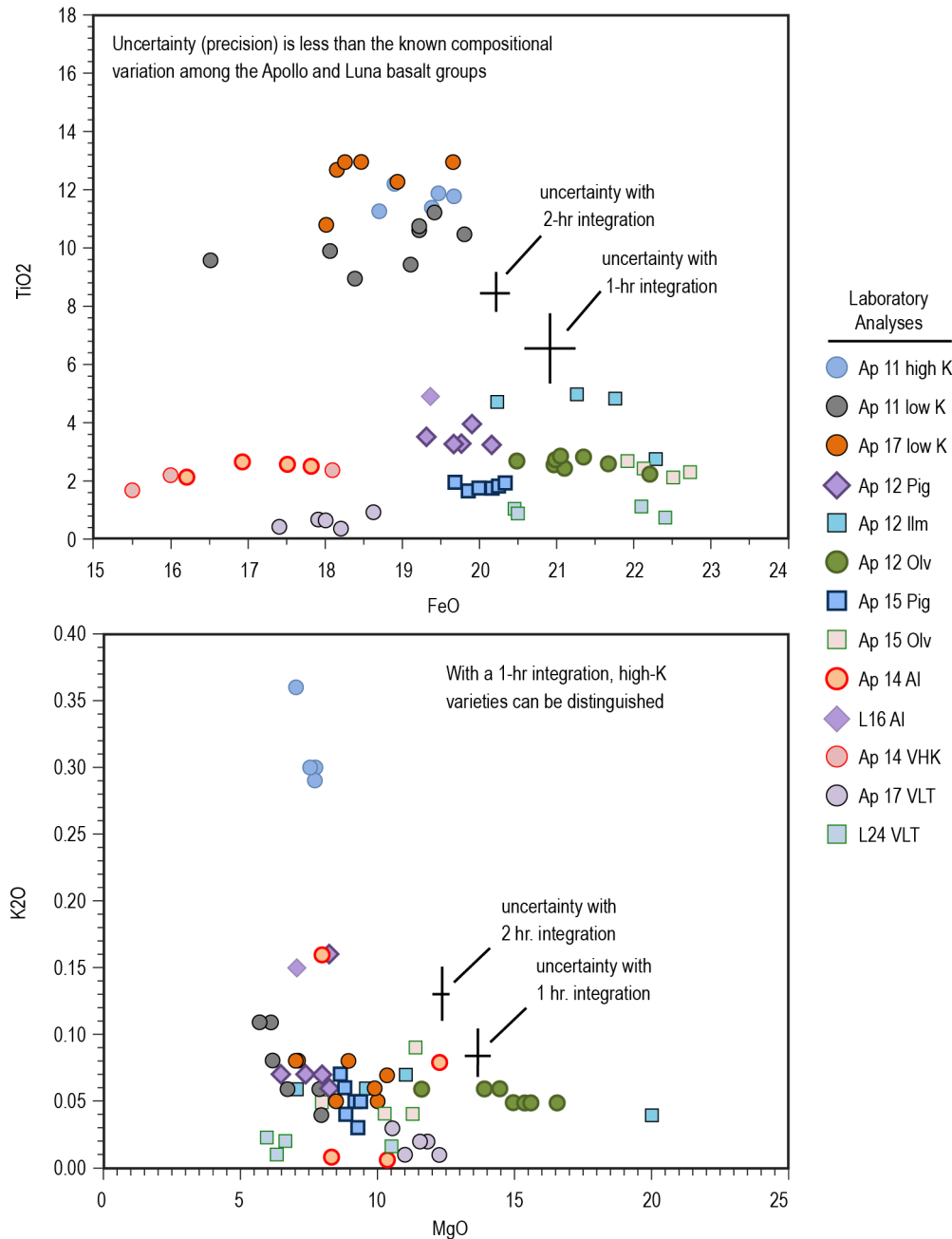


Figure B-7. Weight percent oxides for Apollo and Luna basalt groups measured in the laboratory compared to the expected analytical uncertainty (precision) for the APXS with 1-hour and 2-hour integration times. TiO₂ and K₂O are two of the main parameters, along with major-element oxides FeO and MgO, to discriminate lunar mare basalt groups.



Table B-3. Key APXS measured elements for lunar science and uncertainties as a function of integration time (example composition of **Apollo sample 12009 olivine basalt**). Note that the APXS returns concentration values for all elements with atomic masses between 11 and 40 (Na through Zr) as long as the element is present above its detection limit.

Oxide wt%	Sample Value	APXS			
		1 hr	4 hr	1 hr	4 hr
		+/- % relative	+/- % relative	+/- absolute	+/- absolute
SiO ₂	45	1.4	1	0.6	0.5
TiO ₂	2.9	18	9	0.5	0.3
Al ₂ O ₃	8.6	2.9	1.7	0.2	0.1
Cr ₂ O ₃	0.55	23	16	0.1	0.1
FeO	21	1.2	0.7	0.3	0.1
MnO	0.28	14	4	0.0	0.0
MgO	11.55	2.8	1.7	0.3	0.2
CaO	9.42	1.4	1	0.1	0.1
Na ₂ O	0.23	33	14	0.1	0.03
K ₂ O	0.06	16	12	0.01	0.01
P ₂ O ₅	0.07	18	9	0.01	0.01

B.1.13 WHAT ARE THE LIMITATIONS OF THE APXS MEASUREMENTS?

The performance of the APXS Silicon Drift Detector (SDD) is reduced due to fast neutron degradation damage caused by its Cm-244 source. This type of degradation is most significant after installing the radioactive source, and most of the damage occurs during the first year. This effect can be mitigated by lowering the temperature of the SDD during operations. For example, for the APXS instruments used on MER to achieve an acceptable detector resolution, an operating temperature of $<-10^{\circ}\text{C}$ was required after ~ 1 year, and $<-25^{\circ}\text{C}$ was required after ~ 6 years. For this reason the Intrepid implementation of the APXS would include a cryocooler that keeps the detector temperature within its working range except under the most taxing of thermal conditions.

The Cm-244 source has a half-life of 18.1 years; after four years of operation, slightly longer integration times may be needed to account for this decay.

B.1.14 WHAT IS THE SPECIFIC GOAL OF THE NS PORTION OF THE GRNS IN TERMS OF HYDROGEN?

Multiple measurements suggest that even at low latitudes, the abundances and locations of hydrogen, water, or hydroxyl vary with local time, increasing during the colder night hours and returning to low levels during the day (e.g., *Sunshine et al.* [2009]; *Livengood et al.* [2015]; *Hendrix et al.* [2019]). However, these results have been controversial,

both because of the large volumes of H that would have to migrate diurnally implied by neutron spectroscopy [*Livengood et al.*, 2015], and the complications of photometric corrections for reflectance spectroscopy [*Hendrix et al.*, 2019; *Sunshine et al.*, 2009]; measurements of H (to 50 ppm accuracy) from Intrepid have the potential to resolve this debate. Additionally, traverses across regions of varying maturity could provide a quantitative measure of differences in space weathering, where implanted solar wind H is thought to result in the formation of OH/H₂O within mature materials like agglutinates (e.g., *Bandfield et al.* [2018]), and swirls have been observed to have shallower OH/H₂O absorption bands [*Kramer et al.*, 2011a; *Kramer et al.*, 2011b]. Additionally, there are indications of indigenous water in the Aristarchus pyroclastic deposits [*Milliken and Li*, 2017], which are a potentially valuable in-situ resource, and Intrepid could provide ground truth for these remote sensing observations.

B.1.15 HOW WOULD THE LOCAL GRAVITATIONAL FIELD ESTIMATES BE OBTAINED WITHOUT A GRAVIMETER?

The LN-200S Inertial Measurement Unit is not strictly a science instrument but it allows estimates of the local gravity field, which in turn are used to estimate density contrasts in the subsurface [*Lewis et al.*, 2019]. This capability enables the detection of local density anomalies such as dikes intruded into fractured materials and subsurface



voids (magma chambers, lava tubes). For example, a dike that begins at the base of the crust (~30 km depth) and extends to within 0.5 km of the surface, width of 250 m, and a density contrast of 500 kg/m³ (density difference between the upper crust (2550 kg/m³, *Wieczorek et al.* [2013]) and the bulk densities of Apollo lunar basalts (~3010–3247 kg/m³) would produce a gravity anomaly of ~20 mGal. This signal is detectable with margin (IMU/accelerometer performance is ~10 mGal for a single measurement, and can be further improved by averaging multiple measurements).

B.1.16 HOW WOULD THE INTREPID TEAM ENGAGE THE PUBLIC IN THIS MISSION CONCEPT?

The Intrepid mission is a fantastic opportunity to bring the excitement of lunar exploration to a very broad and inclusive audience! Outreach activities would take the form of both formal in-class educational exercises and informal education events ranging from school events, museum/planetarium exhibits, and open house events. Additionally, an interactive website would track the progress of Intrepid as it traverses four billion years of lunar history. The website would bring to life rover operations with daily pictures and related science activities.

The Intrepid website would include information for all ages, to simple tools and downloadable booklets to help locate Intrepid when looking at the Moon, interactive Intrepid driving simulations, to recent measurements for users wanting more in-depth information regarding the current science. The thorough “Where is Intrepid?” page would include detailed maps derived from LROC NAC images, the planned traverse, as well as images and data collected by instruments on Intrepid during current and previous stops.

To strengthen school curriculum and teachers’ background knowledge, ASU provides workshops for elementary and secondary teachers from around the state, yielding unique teaching opportunities involving math, science, and art. For Intrepid, these opportunities would occur at ASU and partner institutions, demonstrating the technology behind the Intrepid rover (design, instruments, and autonomy) as well as the science being conducted in each segment of the traverse as teaching elements for the upcoming school year.

As part of the informal education efforts, a simplified engineering model of Intrepid would

be exhibited at schools, museum events, and open house events at ASU and JPL. These demonstrations would highlight enabling technologies and ongoing science results (what is happening in real time, also seen on the Intrepid webpage). Recent panoramic mosaics would be paired with 3D technology allowing the public to experience the Moon from the rover’s point of view. These panoramas may be hours to just a few days old and give the person an immersive and current view of the Moon. Furthermore, the downlink budget allows public opportunities to take their own LIVE image and see those images in a matter of minutes.

The Intrepid mission is unique in that one can look up at the Moon and by glancing at a simple guide identify where Intrepid is currently exploring. Observers would also see under what illumination conditions the rover is working (dawn, noon, dusk, night). These simple traverse guides along with simple science kits would be provided to partner libraries across the United States. In 2017, in support of the solar eclipse that crossed the country, organizations partnered with NASA to provide local libraries with solar eclipse kits that provided information about the eclipse event itself and solar glasses for the public. Library events tied to the landing of the Intrepid rover and mission milestones, would be designed to reach underserved populations that otherwise may not have access to college campus science nights or museum exhibits.

Finally, Intrepid covers just over a mile on average each Earth day, facilitating activities where people of all ages can “Walk with Intrepid.” This activity integrates science and engineering with physical fitness. Each day, people would be able to log their walk and hike distances to track how far they have traveled virtually on the lunar surface with Intrepid. As milestones are reached, a virtual travel sticker, similar to the ones that cover an old-fashioned travel trunk, can be collected at each focused investigation site and provide an opportunity to keep up to date with the mission in real time and learn about the investigations being carried out by Intrepid of the past four billion years of lunar history.



B.2 TRACKING THE TRAVERSE: INTREPID CONOPS PLANNING DETAIL

The Intrepid ConOps relies on traverse preplanning for efficient operations and realization of the Intrepid science goals. The traverse path selection was an iterative process of picking Focused Investigation sites and allocating timed instrument measurement combinations at each stop (making sure science measurement objectives were met). The final traverse required 12 observation modes (for the whole payload), 133 focused stops, and over 900 interval stops. This level of detail is needed to provide the implementation team with realistic engineering requirements as well as ensure a robust science return (data collection and downlink rates, power, thermal etc. as a function of time over the 1800 kilometer traverse). A database was required to cohesively represent, track the operations via Observations codes, compute relevant statistics at sites, and also list distances and times between sites. Multiple operational modes make up the Observation code at each site (Table B-7). The operational modes (Table B-4) represent sequences of instrument operations (depicted with “swim lane” charts; Figures B-7 to Figure B-22). Together the Observation code and Operational modes represent a clearly defined hierarchy of instrument operations. Expected data volumes used in this report are computed based on Table B-5. Data volumes for individual instruments are listed in Table B-6, which can be used for recomputing overall data volume and data volume statistics if the current instrument observations are altered.

B.2.1 INSTRUMENT OBSERVATIONS USED TO PLAN THE INTREPID TRAVERSE

Tables B-4, B-5, and B-6 summarize the instrument observations in each operational mode and the corresponding data volumes and integration times. Table B-4 lists the number of observations per instrument over the timespan of each operational mode and depicts the corresponding data volume for each operational mode. Data volume for the stops (Focused Investigation stops and Interval stops (here listed as engineering or eng. stop) varies between 180 MBytes to 850 Mbytes. Table B-6 lists the data volume of each observation for each instrument. Note that for GRNS, ARMAS, Mag and ESA the data volume acquired per second is listed.

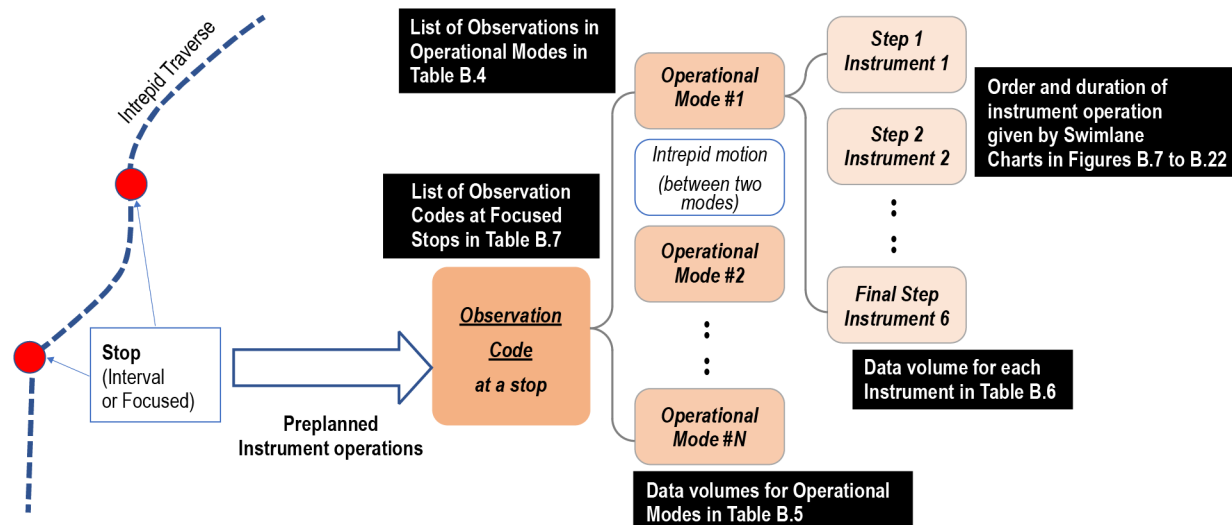


Figure B-8. Encoded hierarchy for tracking traverse and ConOps planning.



Table B-4. Operational Modes – Number of Observations per Instrument.

Mode Overview	Drive Sampling (10 min.)	Drive Extra (Every min.)	Eng. Stop (every 4 hrs)	Site Survey 1 (Color stereo emphasis)				Site Survey 2 (Hi Res BW emphasis)			Site Survey 1 (no arm, Color stereo emphasis)				Site Survey 2 (no arm, Hi Res BW emphasis)		Far-Cam Pan (60 deg, 4 row)	Rover mosaic	Night site survey (48 hrs)
MODE	1	2	3	4.12	4.24	4.36	4.48	5.12	5.24	5.48	6.12	6.24	6.36	6.48	7.12	7.48	8	9	12
PS	1	1	50	45	90	90	135	82	164	246	45	90	90	135	82	246	100	0	0
FarCam	0	0	4	8	8	8	8	68	128	188	4	4	4	4	64	184	100	0	8
FarCam L	0	1	18	18	36	36	54	9	18	27	18	36	36	54	9	27	0	0	0
Stereo BW	0	0	0	0	0	0	0	0	0	0	0	0	0	0	0	0	0	0	54
Stereo RGB	0	0	18	18	36	36	54	9	18	27	18	36	36	54	9	27	0	0	0
Stereo BWL	1	1	0	0	0	0	0	0	0	0	0	0	0	0	0	0	0	0	0
APXS	0	0	1	1	2	3	4	1	2	4	0	0	0	0	0	0	0	0	4
HLI	0	0	1	1	2	3	4	1	2	4	0	0	0	0	0	0	0	90	4
GRNS	1	1	1	1	1	1	1	1	1	1	1	1	1	1	1	1	1	1	1
MAG	1	1	1	1	1	1	1	1	1	1	1	1	1	1	1	1	1	1	1
ARMAS	1	1	1	1	1	1	1	1	1	1	1	1	1	1	1	1	1	1	1
ESA	1	1	1	1	1	1	1	1	1	1	1	1	1	1	1	1	1	1	1

Stereo: Includes two image frames per observation.

FarCam L/Stereo BWL: Full resolution images, 90% quality jpeg.

Stereo RGB/Stereo BW: Both are raw CCD data; "BW" indicates that color data is not expected to be spectrally useful.

APXS: Acquired only when temperature is acceptable.

GRNS/MAG/ARMAS/ESA: # observations is duty cycle, always 100%.

Table B-5. Most Commonly Used Operational Modes – Data Volume.

	MODE	Data Vol. (Mbyte)	Time (h)
Drive Sampling (10 min interval)	1	3	-
Eng Stop (every 4 hrs)	3	183	1
Site Survey 1 (Color stereo emphasis)	4.12	199	12
	4.24	374	24
	4.36	386	36
	4.48	561	48
Site Survey 2 (Hi Res BW emphasis)	5.12	295	12
	5.24	566	24
	5.48	850	48
Site Survey 1 (no arm, Color stereo emphasis)	6.12	180	12
	6.24	348	24
	6.36	352	36
	6.48	520	48
Site Survey 2 (no arm, Hi Res BW emphasis)	7.12	276	12
	7.48	809	48
FarCam Pan (60 deg, 4 row)	8	298	2
Rover mosaic	9	659	4
Night site survey (48 hrs)	12	493	48

Table B-6. Instrument Data Volume per Observation.

Instrument Observation	Data Volume per observation (MByte)
PS	0.064
FarCam	2.9
FarCam L	1.1
Stereo BW	7.8
Stereo RGB	7.8
Stereo BWL	2.2
Stereo RGBL	6
APXS	0.032
HLI	7.3
GRNS	0.000064 / s
MAG	0.000012 / s
ARMAS	0.000025 / s
ESA	0.000006 / s



B.2.2 COMMON OPERATIONAL MODES

Time lines (or “swim lane”) charts below represent the sequence and duration of Intrepid instrument operations for each operational mode (represented by the mode number and total number of hours). Parallel ‘lanes’ indicate unique instrument activity and the horizontal axis indicates the time since the start of the operational mode. Intrepid observation code at a focused site includes multiple operational modes and short local traverses.

Mode 4, 12 hours

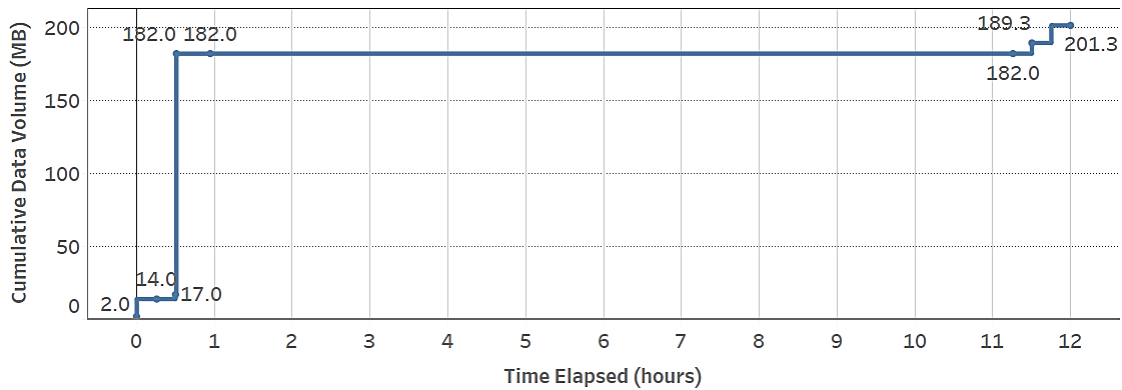
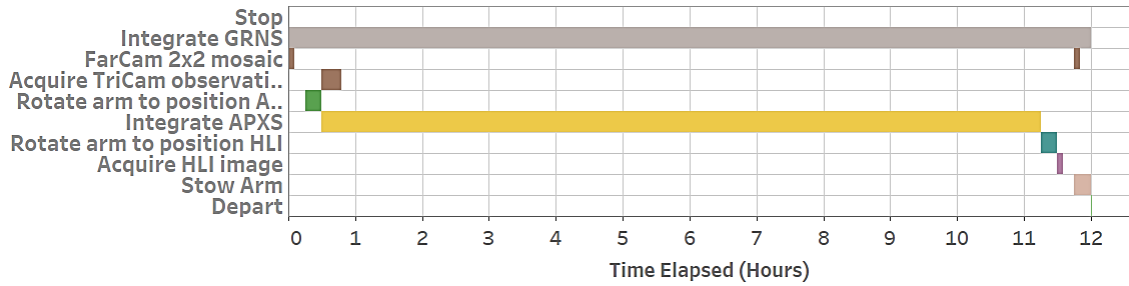


Figure B-9. Swimlane chart for mode 4.12. Observations with color stereo emphasis, requires 2 arm rotations.



Mode 4, 24 hours

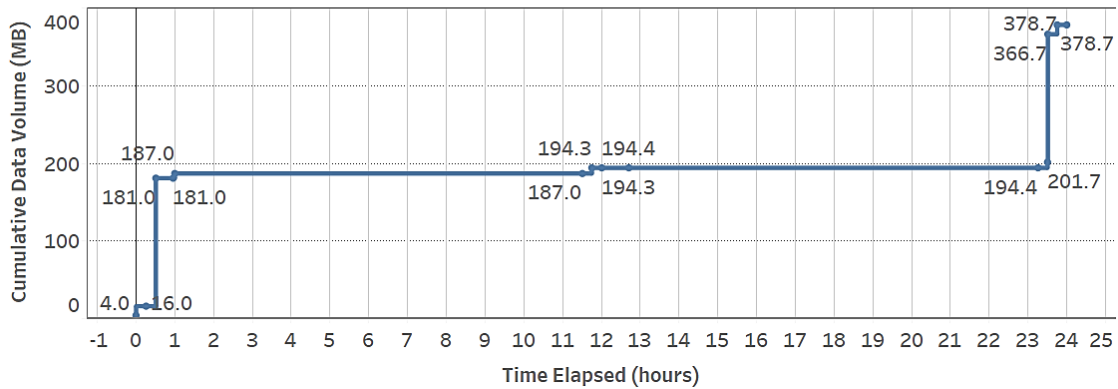
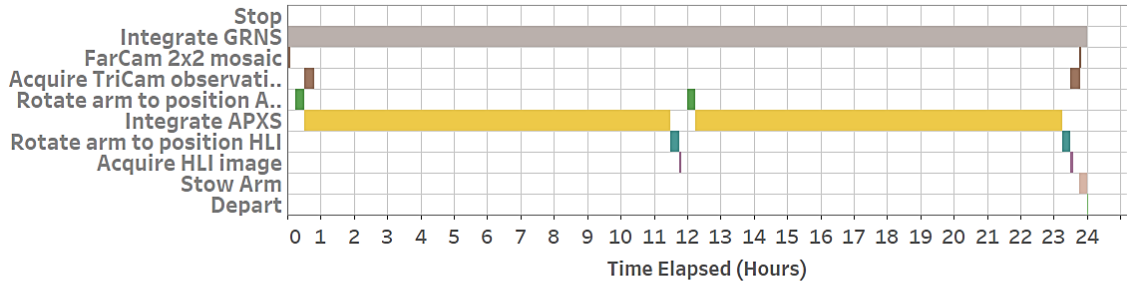


Figure B-10. Swimlane chart for mode 4.24. Observations with color stereo emphasis, requires 2 arm rotations.

Mode 4, 36 hours

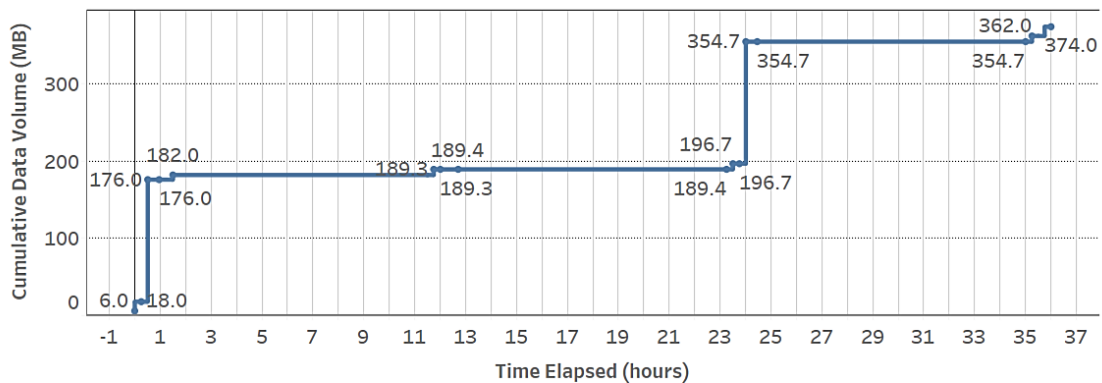
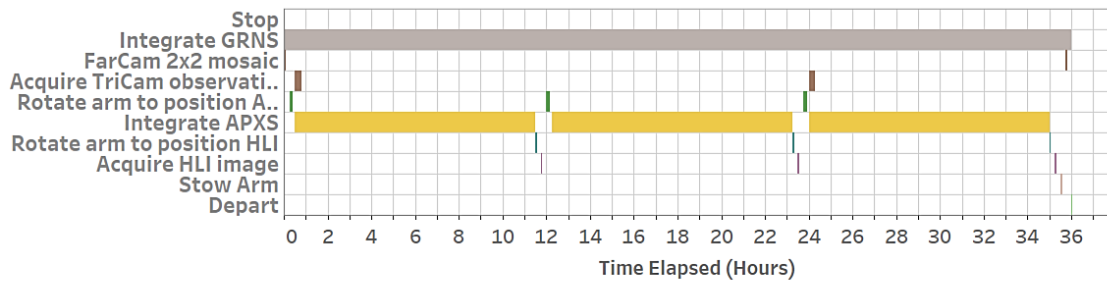


Figure B-11. Swimlane chart for mode 4.36. Observations with color stereo emphasis, requires 2 arm rotations.



Mode 4, 48 hours

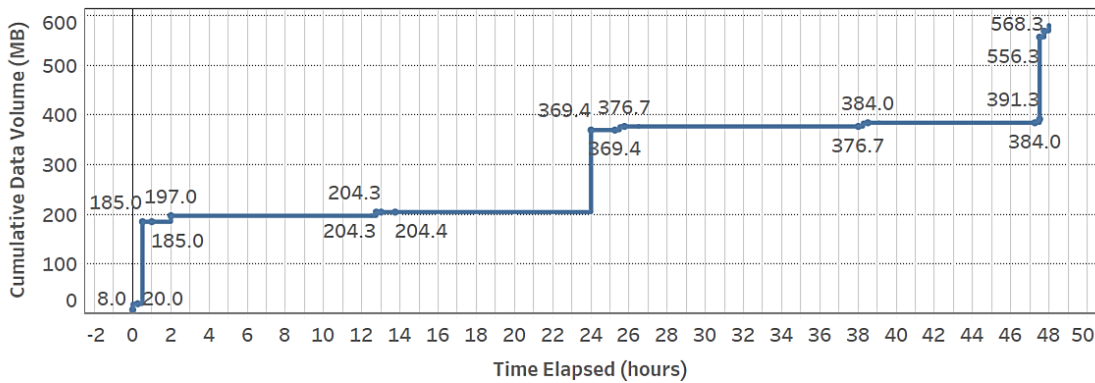
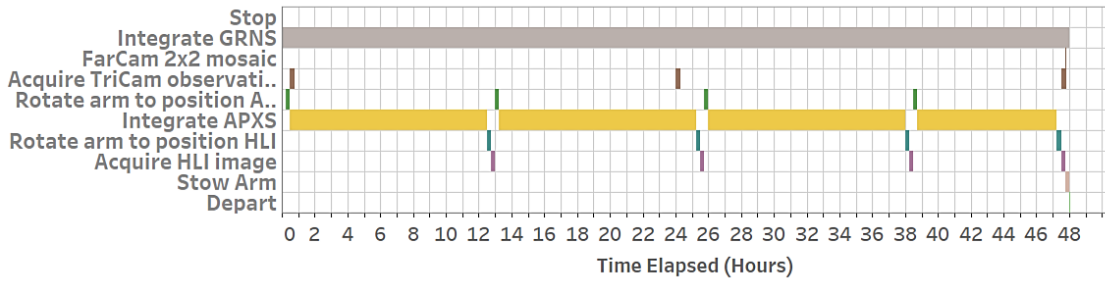


Figure B-12. Swimlane chart for mode 4.48. Observations with color stereo emphasis, requires 2 arm rotations.

Mode 5, 12 hours

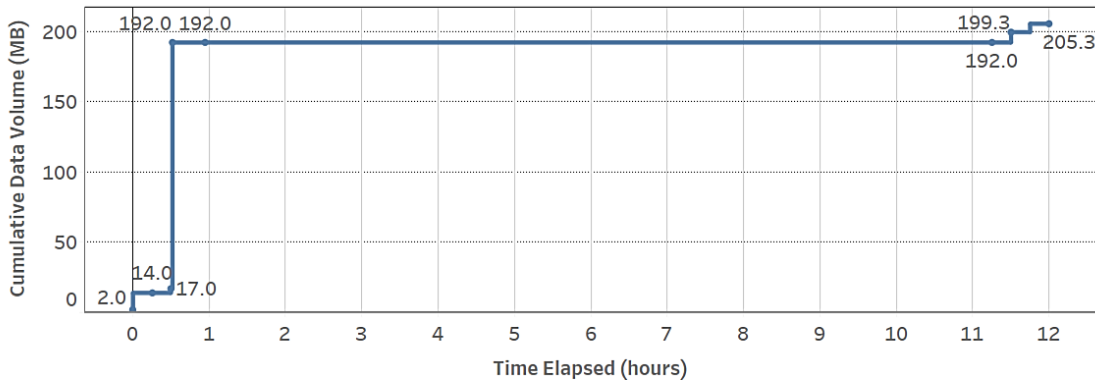
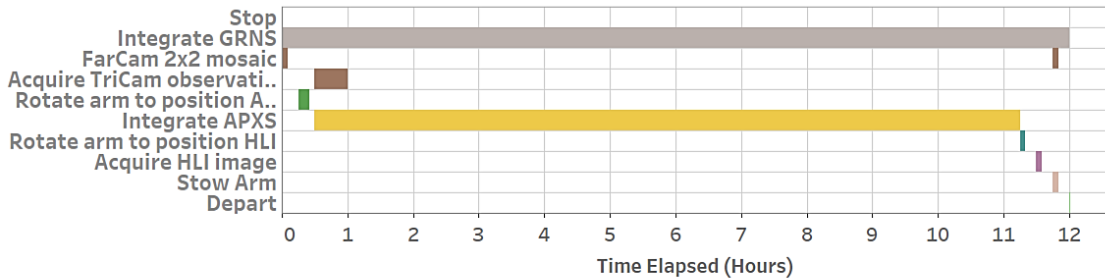


Figure B-13. Swimlane chart for mode 5.12. Observations with high resolution BW emphasis, requires 2 arm rotations.



Mode 5, 24 hours

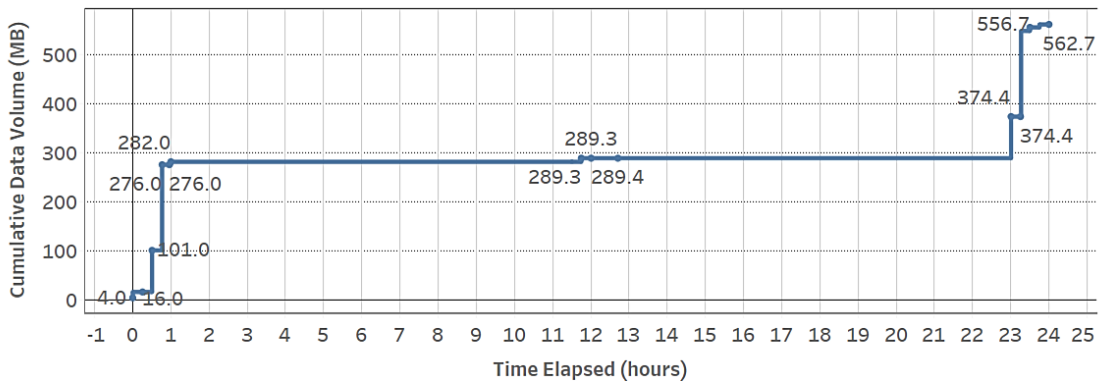
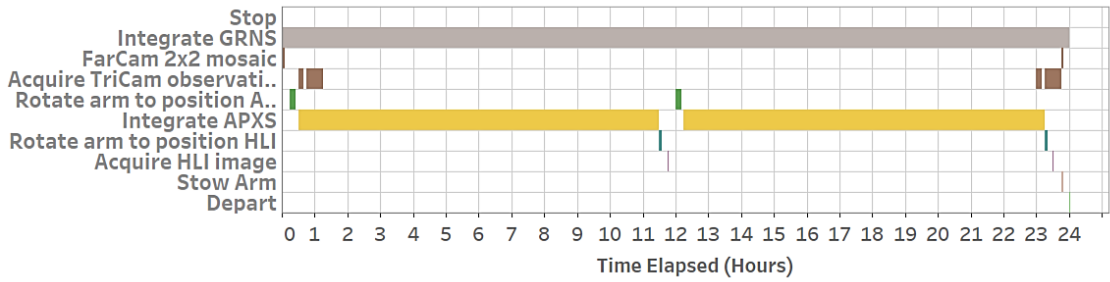


Figure B-14. Swimlane chart for mode 5.24. Observations with high resolution BW emphasis, requires 2 arm rotations.

Mode 5, 48 hours

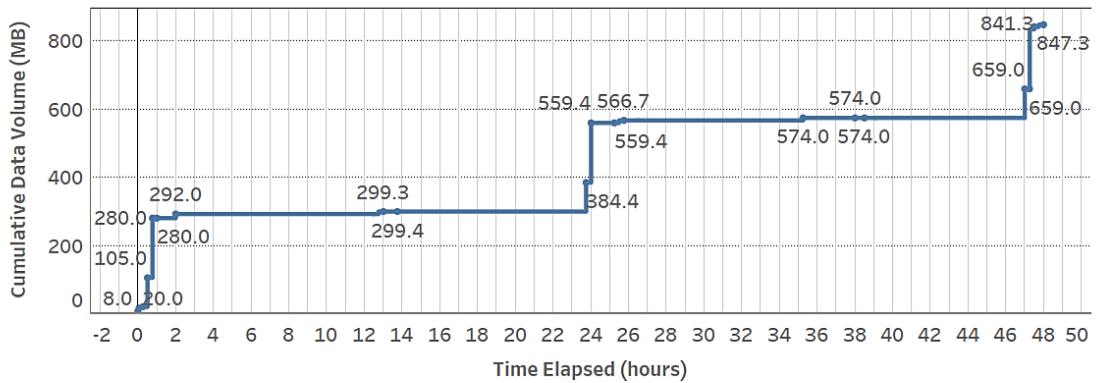
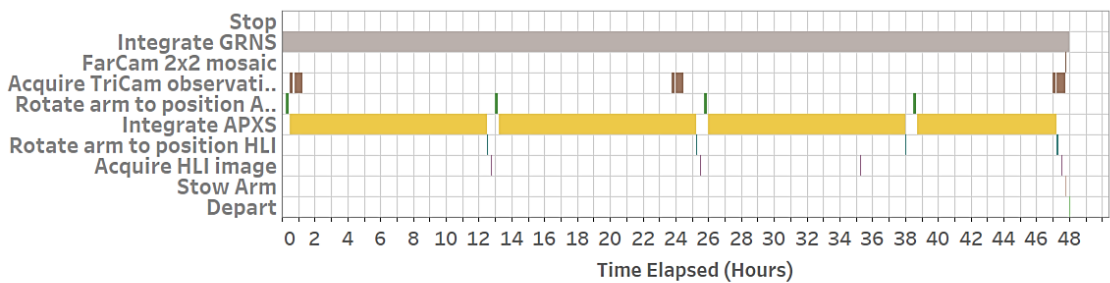


Figure B-15. Swimlane chart for mode 5.48. Observations with high resolution BW emphasis, requires 2 arm rotations.



Mode 6, 12 hours

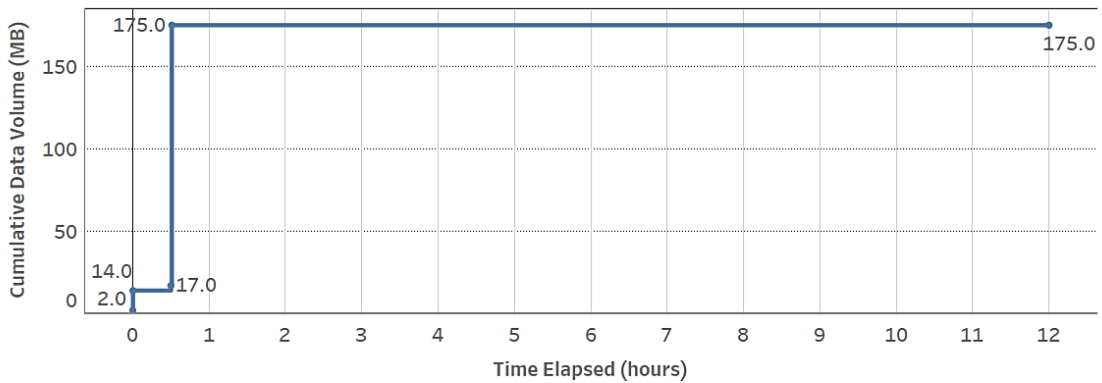
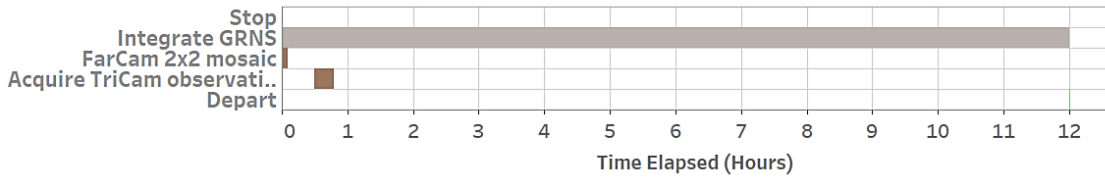


Figure B-16. Swimlane chart for mode 6.12. Observations with color stereo emphasis, no arm rotations required.

Mode 6, 24 hours

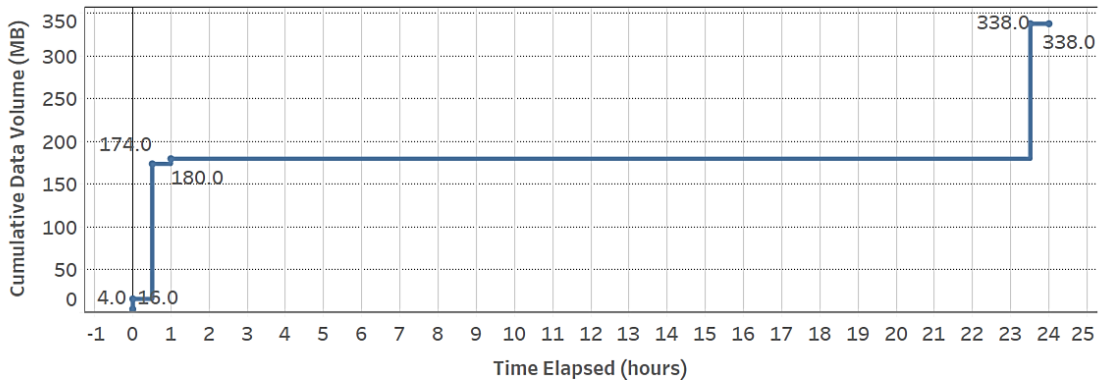
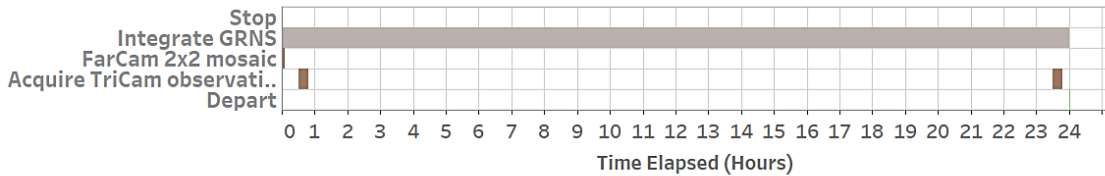


Figure B-17. Swimlane chart for mode 6.24. Observations with color stereo emphasis, no arm rotations required.



Mode 6, 36 hours

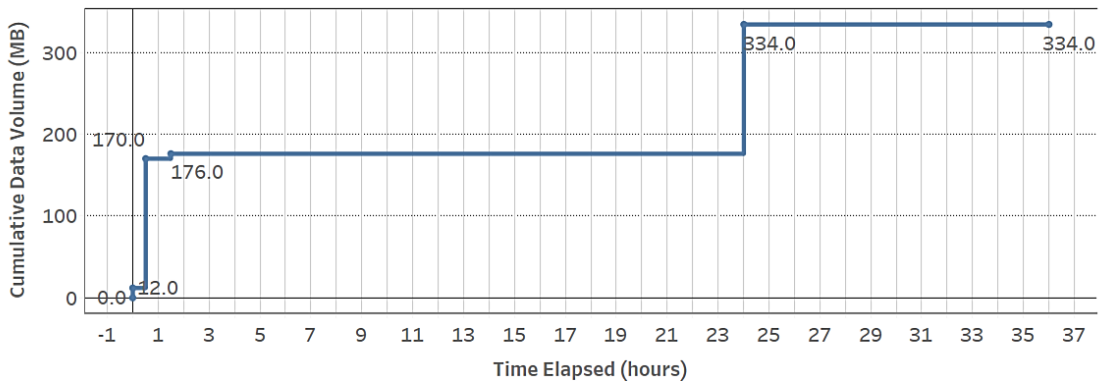
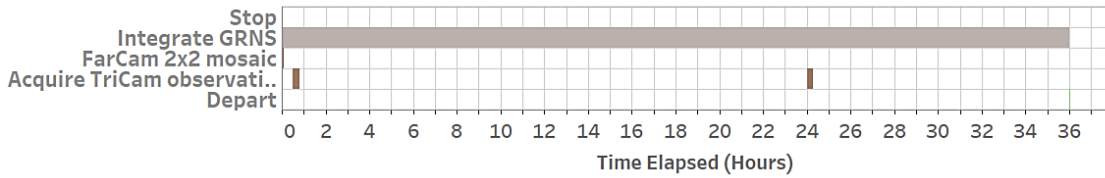


Figure B-18. Swimlane chart for mode 6.36. Observations with color stereo emphasis, no arm rotations required.

Mode 6, 48 hours

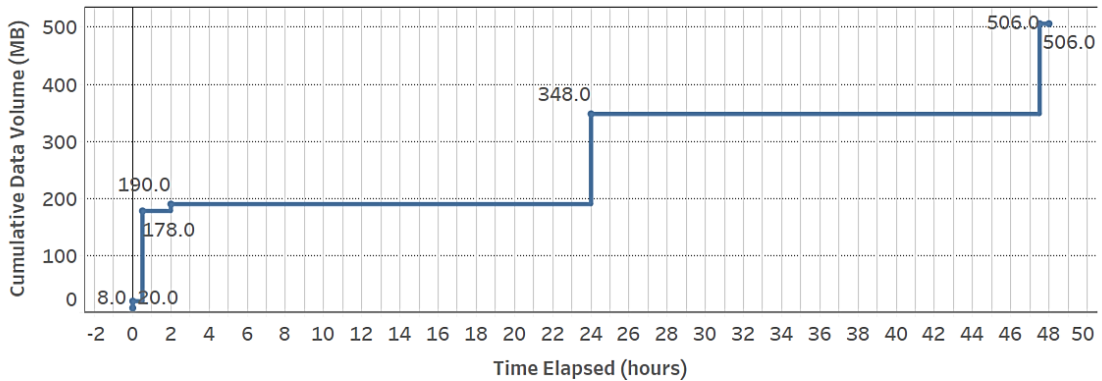
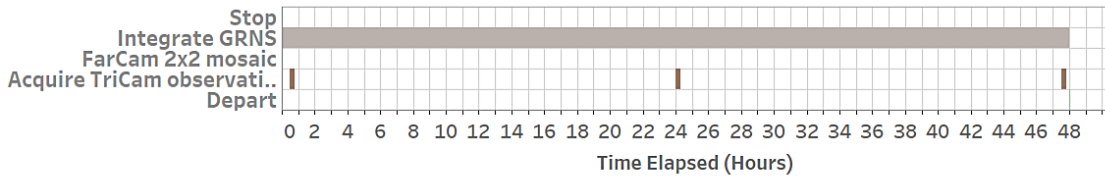


Figure B-19. Swimlane chart for mode 6.48. Observations with color stereo emphasis, no arm rotations required.



Mode 7, 12 hours

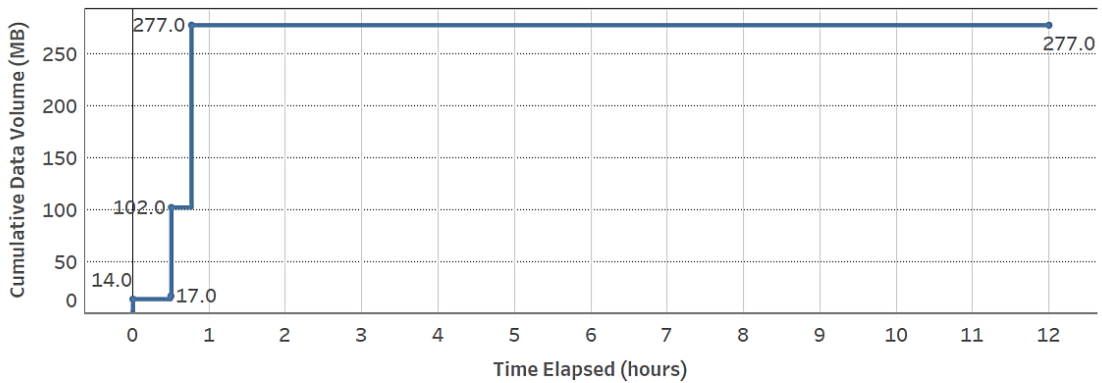
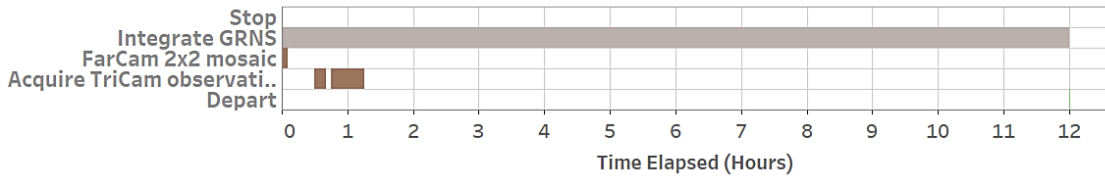


Figure B-20. Swimlane chart for mode 7.12. Observations with high resolution BW emphasis, no arm rotations required.

Mode 7, 48 hours

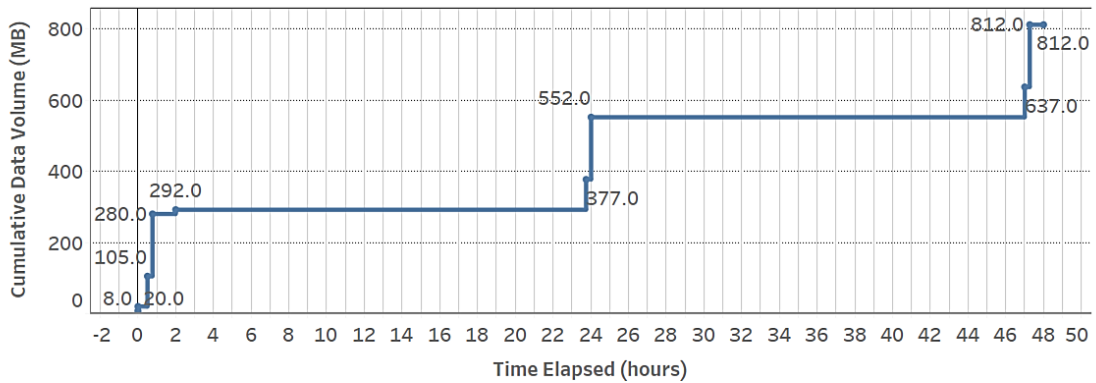
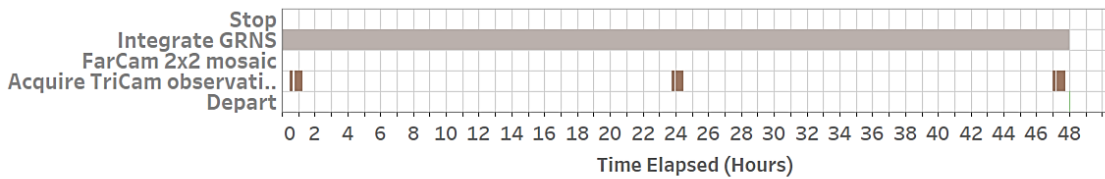


Figure B-21. Swimlane chart for mode 7.48. Observations with high resolution BW emphasis, no arm rotations required.



Mode 8, 2 hours

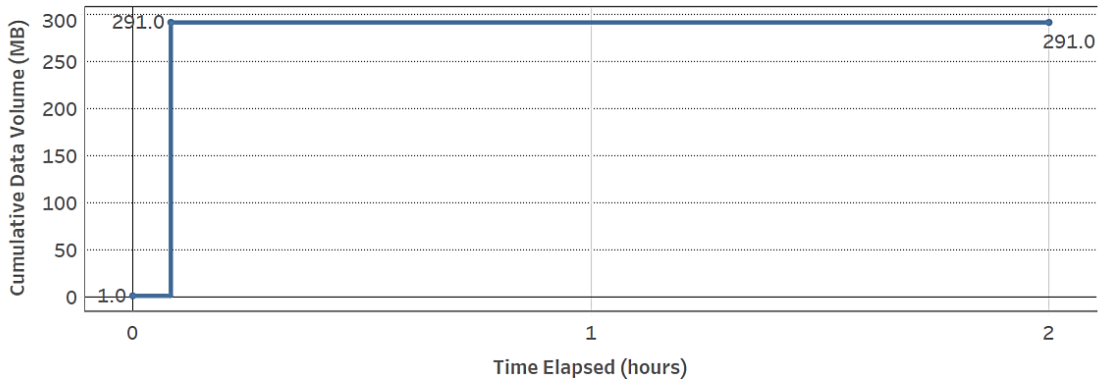
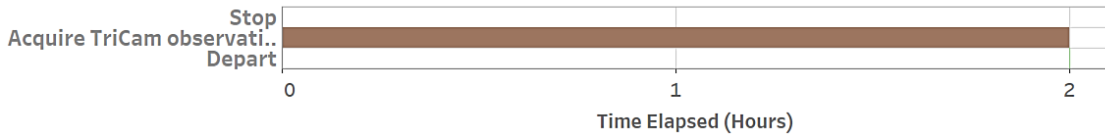


Figure B-22. Swimlane chart for mode 8.2. Acquire Farcam panorama.

Mode 9, 4 hours

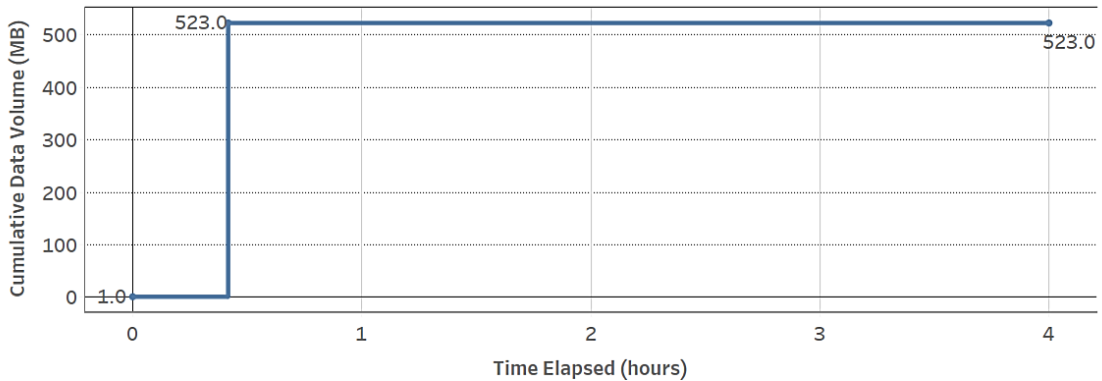
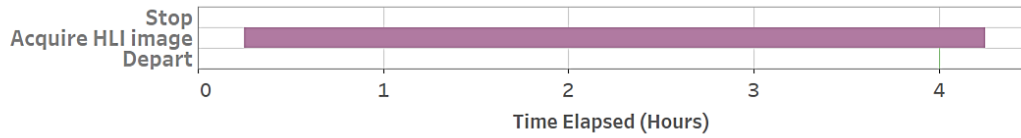


Figure B-23. Swimlane chart for mode 9.4. Acquire rover mosaic with HLI.



Mode 12, 48 hours

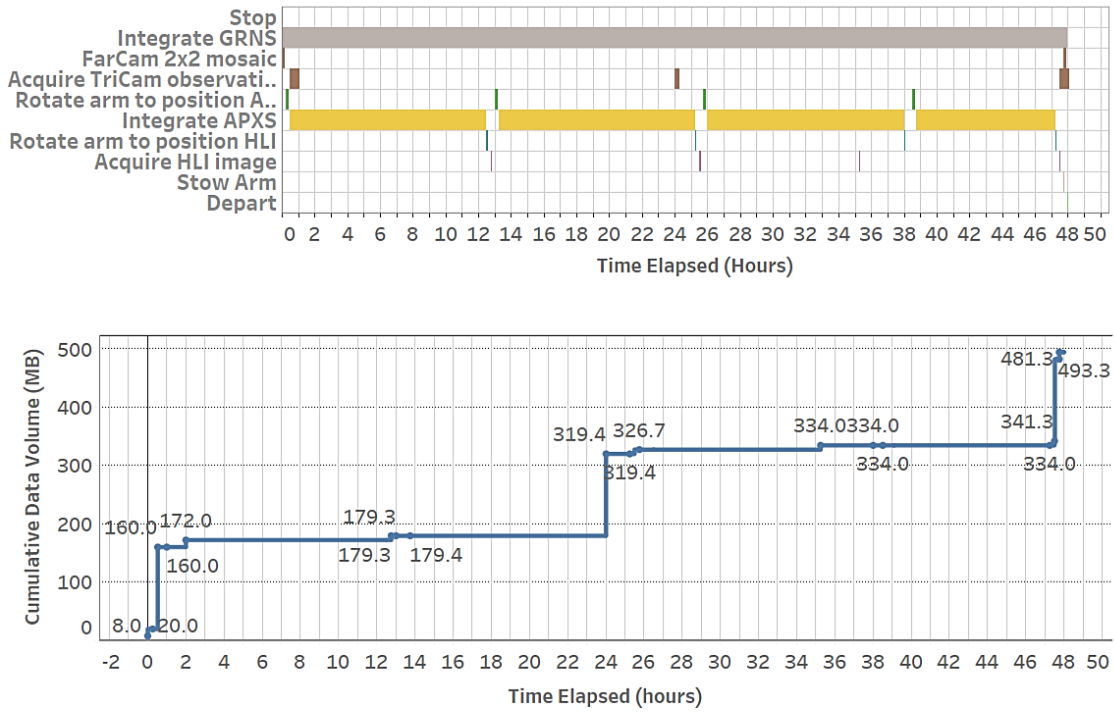


Figure B-24. Swimlane chart for mode 12.



Table B-7. Intrepid Focused Science Stops – Description and Observation Codes.

Focused Stop ID	Lat	Lon	Dist (km)	Speed (kph)	Drive Time (h)	Arrival Solar Time	Stop Time (h)	Description	Objectives / notes	Observation Code
Landing	6.457	-58.893	0	0	0	6.70	140	Landing site, Oceanus Procellarum basalts	Rover commissioning activities, begin traverse!	4.12h,25m,7.12h,100m,4.12h,9.4h,500m,5.12h,2000m,4.48h
RG_1	7.065	-59.061	23.8	0.4	59.5	13.46	26	420 meter diameter fresh crater	Determine chemistry of soil 100 m from rim and at rim for depth profile	4.12h,100m,4.12h
RG_2_N	7.189	-58.983	4.6	0.4	11.5	14.73	471	Center of "dark lane"	Magnetics and chemistry of dark lane; first drive 250 meters past stop (north) and then backtrack to stop laying down tracks for night driving.	4.48h,50m,12.48h,50m,12.48h,50m,12.48h,50m,12.48h,8.2h
RG_3	7.351	-59.118	6.7	0.4	16.75	7.27	24	60 meter diameter fresh crater near center of bright area	Determine chemistry of rock and soil at rim for depth profile	4.24h
RG_4	7.559	-59.321	9.2	0.2	46	9.64	49	125 meter fresh crater near the center of dark lane	Determine chemistry of rock and soil at rim for depth profile	4.24h,30m,6.24h
RG_5	7.568	-59.332	0.5	0.2	2.5	11.38	24	35 meter fresh crater near edge of dark lane	Determine chemistry of soil at rim for depth profile	6.24h
RG_6	7.563	-59.221	3.6	0.4	9	12.50	48	45 meter fresh crater in the center of the dark lane	Determine chemistry of soil at rim for depth profile	6.48h
RG_7	7.574	-59.184	1.2	0.4	3	14.23	24	35 meter fresh crater in the dark lane	Determine chemistry of soil at rim for depth profile	6.24h
RG_8_N	7.624	-59.177	2.2	0.1	22	15.78	440	74 meter fresh crater on the boundary between bright and dark material. Drive speed from 7 to 8 was slow to better sample the transition (dark vs. bright) with MAG and GRNS.	Magnetics and chemistry across contact (dark and bright); first drive 250 meters past stop (north) and then backtrack to stop laying down tracks for night driving.	5.48h,50m,12.48h,50m,12.48h,50m,12.48h,50m,12.48h,8.2h
RG_9	7.690	-59.158	2.1	0.4	5.25	6.88	24	33 meter fresh crater in bright material	Determine chemistry of rock and soil at rim for depth profile	5.24h
RG_10	7.800	-59.122	3.6	0.4	9	8.00	37	440 meter diameter very blocky fresh crater	Determine chemistry of rock and soil 100 m from rim and as close as possible to rim for depth profile. Fairly blocky crater so closest approach may be ~80 meters from rim.	4.12h,100m,4.24h
RG_11	7.910	-59.019	5	0.2	25	10.10	67	540 meter diameter fresh crater at the margin of the bright zone	Approach rim about 250 m west of formal stop point, then head to stop, then circumvent boulders to southeast and integrate down rim 50 meters	6.12h,8.2h,100m,8.2h,100m,6.36h,100m,6.12h



Focused Stop ID	Lat	Lon	Dist (km)	Speed (kph)	Drive Time (h)	Arrival Solar Time	Stop Time (h)	Description	Objectives / notes	Observation Code
RG_12	8.067	-58.953	5.8	0.2	29	13.35	24	Turning point; note we backtrack along tracks to stop at (7.956,-58.961)	Measure environment traversing 3 kilometers off swirl (maximum traverse distance from swirl center). Much of return trip towards RG_13 follows outbound tracks providing repeatability test	6.24h
RG_13_N	7.714	-58.905	11.6	0.4	29	15.14	459	Center of high albedo zone	Measure environment from off to on swirl, backtrack 250 meters from formal stop for night activities tracks.	4.48h,50m,12.48h,50m,12.48h,50m,12.48h,50m,12.48h,50m,12.48h,8.2h
RG_14	7.680	-58.896	1.2	0.4	3	6.80	49	330 meter diameter crater on edge of bright zone	Determine chemistry of rock and soil from two places on rim for depth profile. First stop on rim 75 meters from formal stop, then proceed to that stop.	4.12h,8.2h,75m,4.36h,8.2h
RG_15	7.651	-58.868	1.3	0.4	3.25	8.57	53	380 meter crater at the edge of the dark zone	Determine chemistry of rock and soil from two places on rim for depth profile. First stop on rim 75 meters from formal stop, then proceed to that stop.	4.12h,8.2h,75m,6.36h,8.2h
RG_16	7.623	-58.872	0.9	0.2	4.5	10.52	24	Center of the dark lane	Slow drive from 15 to 16 to better resolve transition from bright to dark unit	6.24h
RG_17	7.619	-58.798	2.3	0.4	5.75	11.53	24	Center of the dark lane	Measure environment of dark lane (along traverse from 16 to 17 and at stop)	6.24h
RG_18	7.480	-58.767	4.7	0.4	11.75	12.74	24	65 meter diameter crater in bright material	Determine chemistry of soil at rim for depth profile	6.24h
RG_19	7.287	-58.742	6.3	0.4	15.75	14.08	37	Center of the dark lane	Environment of dark lane	6.12h,100m,6.24h,8.2h
RG_20_N	7.078	-58.592	8.3	0.2	41.5	16.74	412	1 km diameter degraded crater at the edge of the dark lane	Note the slow traverse across bright filament (dark to bright to dark). Drive 100 m past formal stop then backtrack 200 m for night activities.	6.48h,8.2h,300m,12.48h,50m,12.48h,50m,12.48h,50m,12.48h,8.2h
RG_21	6.985	-58.468	4.9	0.4	12.25	7.11	37	1800 meter diameter degraded crater	Measure soil and rock 100 m from rim, then same at rim for depth profile	4.12h,100m,4.24h
RG_22	7.204	-58.427	7.1	0.4	17.75	8.97	24	110 meter diameter moderately fresh crater	Determine chemistry of rock (if possible otherwise soil) and soil from rim for depth profile.	4.24h
RG_23	7.307	-58.433	3.3	0.4	8.25	10.06	9	Wrinkle ridge in bright area	Two stereo sequences of wrinkle ridge (north and south from summit), requires 4 positions	8.2h,25m,8.2h,25m,8.2h,25m,8.2h
RG_24	7.478	-58.437	5.4	0.4	13.5	10.82	12	Narrow dark lane	Measurements on narrow dark lane	6.12h



Focused Stop ID	Lat	Lon	Dist (km)	Speed (kph)	Drive Time (h)	Arrival Solar Time	Stop Time (h)	Description	Objectives / notes	Observation Code
RG_25	7.656	-57.798	20.8	0.4	52	12.99	24	Small dark patch	Traverse down center of bright zone, stop in "closed-depression" of low albedo contours	6.24h
RG_26	7.693	-57.537	15.7	0.4	39.25	15.13	9	Wrinkle ridge morphology (high albedo)	Two stereo FarCam sequences of wrinkle ridge (north and south from summit), requires 4 positions	8.2h,25m,8.2h,25m,8.2h,25m,8.2h
RG_27_N	7.742	-57.497	9.2	0.4	23	16.22	427	Wrinkle ridge morphology (high albedo)	Traverse across dark lane back to bright material, measure transition.	8.2h,7.48h,50m,12.48h,50m,12.48h,50m,12.48h,50m,12.48h,8.2h
RG_28	8.275	-56.356	53.9	0.4	134.75	11.26	24	Center of small high albedo patch south of Reiner M crater	First long traverse (54 km). characterize bright region in tail.	6.24h
RG_29_N	8.578	-56.216	11.2	0.4	28	13.02	521	3100 meter Reiner M crater	Arrive at rim about 300 meters west of formal stop acquire stereo panorama, move to station, then 300 meters east complete stereo panorama	6.12h,8.2h,300m,8.2h,6.12h,300m,8.2h,50m,12.48h,50m,12.48h,50m,12.48h,50m,12.48h,8.2h
RG_30	9.180	-56.011	28.1	0.4	70.25	9.08	24	Secondary crater or volcanic feature investigation in small dark lane (high TiO2 mare)	Determine origin of positive relief feature, continue investigation of RG tail (dark lane)	4.24h,8.2h
MH_1	9.806	-55.672	21.9	0.4	54.75	11.75	24	Notch on south side of dome 1	First dome investigation!	6.24h,8.2h
MH_2_N	9.835	-55.757	3	0.4	7.5	12.81	528	Variegated cliff face dome 1	Early arrival, trace night route along base of cliff (~1.2 km) in daylight documenting material shedding downslope (blocky outcrop), backtrack during night (lots of day and night measures)	6.24h,8.2h,200m,4.24h,8.2h,200m,12.48h,100m,12.48h,100m,12.48h,100m,12.48h,200m,8.2h
MH_3	10.172	-55.706	15.1	0.4	37.75	7.98	12	400 meter diameter fresh crater on the north side of volcanic dome 2	Traverse across degraded dome and stop near rim of 400-m crater, geochemistry of boulder or regolith near rim	4.12h
MH_4	10.845	-55.417	31.9	0.4	79.75	11.09	61	Low albedo deposits (U-shaped cone 1) adjacent to 1200 meter diameter fresh crater	Traverse across tail of RG, investigate enigmatic low-albedo deposits (M188607499L), stop just before dark unit for 12 hr integration, then move on deposit	4.12h,100m,4.48h
MH_5_N	11.138	-54.868	21.1	0.4	52.75	14.94	465	1000 meter diameter U-shaped cone 2	Traverse up into cone through south breach and document, traverse out during night (note that traverse from MH_4 to MH_5 is last distinct portion of RG swirl)	8.2h,6.48h,50m,12.48h,50m,12.48h,50m,12.48h,50m,12.48h,100m,12.48h,100m,4.48h,8.2h



Focused Stop ID	Lat	Lon	Dist (km)	Speed (kph)	Drive Time (h)	Arrival Solar Time	Stop Time (h)	Description	Objectives / notes	Observation Code
MH_6	11.387	-54.878	9.7	0.4	24.25	7.52	78	Large irregular dome 3	Drive up to summit from formal stop (1.2 km), integrate 48 hrs then back track to formal stop (assume 100 m/hr, 12 hrs), NAC pan at summit.	8.2h,1400m,4.48h,200m,6.12h
MH_7	11.420	-54.823	4	0.4	10	10.50	48	Wrinkle ridge scarp	Stop 200 meters shy of ridge, 200 meters onto ridge looking up scarp, and then again at summit of ridge looking at dome: acquire FarCam panorama	8.2h,400m,8.2h,600m,6.24h
MH_8_N	11.585	-54.073	30.9	0.4	77.25	14.74	471	Low albedo moated dome 4	Traverse up SW flank until local slope exceeds 10 degrees for stop point, then work tracks back during dark	8.2h,6.48h,100m,4.48h,8.2h,100m,12.48h,100m,12.48h,100m,12.48h,100m,12.48h,200m,12.48h,200m,8.2h
MH_9	11.975	-53.829	20.8	0.4	52	8.46	60	Contact between 2900 meter diameter crater and irregular dome 5	Detour 1 km south from formal stop for dome site, integrate 24 hrs then move back to rim of crater (should be spectacular view into crater!)	4.24h,1200m,8.2h,4.24h
MH_10	12.004	-53.247	21.8	0.4	54.5	12.34	48	Notch in irregular dome 6	Drive up slope about 500 m from formal stop	6.48h
MH_11_N	12.234	-52.708	20.8	0.4	52	15.73	442	5500 meter diameter crater Marius E	Drive up slope 500 m from formal stop to rim, acquire interior panorama, traverse 500 m along rim for dusk panorama interior, backtrack during night to 1st rim spot for dawn panorama	8.2h,6.48h,500m,4.48h,8.2h,50m,12.48h,50m,12.48h,50m,12.48h,100m,12.48h,100m,12.48h,100m,8.2h
MH_12	12.178	-52.400	10.6	0.4	26.5	7.60	24	400 meter diameter crater	Measure boulder and/or regolith as close to rim as possible (careful - don't drive in!)	4.24h
MH_13	12.364	-51.643	32.8	0.4	82	11.19	24	300 meter diameter fresh crater on wrinkle ridge summit	End of drive traverse through an ancient leveed channel, provides convenient topographic friendly ramp. Stop near crater at contact of uplifted rim and surrounding volcanics for measurements, rim rocks likely sample Marius crater ejecta	6.24h
MH_14_N	12.307	-51.354	15.2	0.4	38	13.29	514	40 kilometer diameter Marius crater	Panorama at formal site then traverse east along rim for 2 km establishing night backtrack route. What a view!	8.2h,6.48h,2000m,4.48h,8.2h,50m,12.48h,50m,12.48h,50m,12.48h,100m,12.48h,100m,12.48h,100m,8.2h
MH_15	12.892	-51.247	23.6	0.4	59	8.70	36	980 meter diameter crater north of Marius	Sample rim materials for depth profile	4.36h



Focused Stop ID	Lat	Lon	Dist (km)	Speed (kph)	Drive Time (h)	Arrival Solar Time	Stop Time (h)	Description	Objectives / notes	Observation Code
MH_16	13.062	-51.237	5.3	0.4	13.25	10.37	36	1040 meter diameter crater north of Marius	Sample rim materials for depth profile	6.36h
MH_17_N	13.309	-51.379	10.8	0.4	27	12.50	537	Moated cone 3 north of Marius	Circumnavigate central depression (2.5 km) and then backtrack at night. Afternoon stop at highest point.	8.2h,6.48h,200m,4.48h,8.2h,200m,12.48h,200m,12.48h,200m,12.48h,200m,12.48h,200m,8.2h
MH_18	13.653	-50.392	33.6	0.4	84	9.54	48	Likely vent (>3 km diameter)	Approach vent edge as close as possible, appears to gradually taper down.	4.48h
MH_19_N	14.643	-50.758	43.9	0.4	109.75	14.89	466	Floor of large vent complex	Stop inside depression, backtrack out at night, morning panorama looking back into depression	8.2h,6.48h,100m,4.48h,8.2h,100m,12.48h,100m,12.48h,100m,12.48h,100m,12.48h,100m,8.2h
MH_20	14.108	-50.304	40.3	0.4	100.75	10.11	36	Scarp 1	Sample chemistry downstream from vent	6.36h
MH_21	14.085	-50.366	2.6	0.4	6.5	11.55	49	Scarp 2, 175 meter fresh crater	Depth profile, 50 m from rim and as close to rim as possible	6.24h,50m,6.24h
MH_22_N	13.783	-49.624	30.6	0.4	76.5	15.80	439	Dome 7	Drive past formal stop point 2 km and then back for night tracks	6.48h,250m,4.48h,8.2h,250m,12.48h,250m,12.48h,250m,12.48h,250m,12.48h,250m,8.2h
MH_23	13.906	-49.332	24.8	0.4	62	8.80	76	Rille vent	Measure 3 locations on vent rim	4.24h,200m,4.24h,200m,4.24h
MH_24	13.819	-48.950	16.9	0.4	42.25	12.80	48	Dome 8	Drive up (north) a few hundred meters from formal stop, Sample chemistry of dome	6.48h
MH_25_N	14.071	-48.775	12.8	0.4	32	15.51	448	Volcanic-tectonic depression	Drive up (NW) depression 2 km for night tracks	6.48h,250m,4.48h,8.2h,250m,12.48h,250m,12.48h,250m,12.48h,250m,12.48h,250m,8.2h
MH_26	14.817	-48.568	27.2	0.4	68	9.00	24	Marius rille assessment point 1	First look into Marius rille	4.24h
MH_27	15.116	-48.177	16.4	0.4	41	11.20	24	Small dome 9	Chemistry of small dome	6.24h
MH_28	15.361	-47.960	11.4	0.4	28.5	12.98	24	Marius rille assessment site 2	Characterize flow thicknesses exposed in rille far wall	6.24h
MH_29_N	16.204	-47.482	34.1	0.4	85.25	16.68	413	Marius B 11 km diameter	Measure depth profile of local mare deposits	6.48h,250m,4.48h,8.2h,250m,12.48h,250m,12.48h,250m,12.48h,250m,12.48h,250m,8.2h



Focused Stop ID	Lat	Lon	Dist (km)	Speed (kph)	Drive Time (h)	Arrival Solar Time	Stop Time (h)	Description	Objectives / notes	Observation Code
MH_30	16.424	-47.512	7.2	0.4	18	7.31	53	Marius B 11 km diameter	Sunrise observations into Marius B crater, radial traverse off crater down to mare.	4.24h,500m,4.24h
MH_31	16.626	-47.944	17.5	0.4	43.75	10.59	36	Marius rille assessment site 3	Mid-morning observations of west wall of rille	4.24h
OP_1_N	17.741	-47.798	38.2	0.4	95.5	15.04	462	Wrinkle ridge and rille intersection	Complex intersection of rille and ridge, several FarCam panoramas, local chemistry. Drive up to rille and head east along rim daylight for 2 km for night tracks	8.2h,6.48h,250m,8.2h,250m,8.2h,4.48h,8.2h,250m,12.48h,250m,12.48h,250m,12.48h,250m,12.48h,250m,12.48h,250m,8.2h
OP_2	17.865	-47.228	17.6	0.4	44	8.19	37	Fresh crater pair (500 and 280 meter) in Aristarchus ejecta maxima	Measure depth profile and surface mixing	4.24h,50m,4.12h
OP_3	17.988	-47.188	4.3	0.4	10.75	9.81	36	Edge of bright ray material from Aristarchus	Measure local mixing	4.36h
OP_4	18.008	-47.279	2.8	0.4	7	11.26	36	Center of bright ray material	Measure local mixing	6.36h
OP_5	18.108	-47.379	4.5	0.4	11.25	12.86	36	Edge of bright ray material	Measure local mixing	6.36h
OP_6_N	18.351	-47.235	9	0.4	22.5	14.84	468	Crossing bright ray material	Drive past formal stop point 1 km, traverse back to 1 km before stop point and then start night operations (traverse across Aristarchus ray)	6.48h,250m,4.48h,250m,12.48h,250m,12.48h,250m,12.48h,250m,12.48h,250m,12.48h,250m,8.2h
OP_7	18.898	-47.433	21.8	0.4	54.5	8.55	49	850 meter crater	Depth profile and surface mixing	4.24h,100m,4.24h
OP_8	18.985	-47.646	6.8	0.4	17	10.78	23	Wrinkle ridge stop	Look south to distinct wrinkle ridge landforms	8.2h,500m,8.2h,200m,8.2h,6.12h
OP_9	19.065	-48.081	12.7	0.4	31.75	12.63	24	580 meter diameter crater	Measure depth profile	6.24h
OP_10_N	19.364	-48.596	17.7	0.4	44.25	14.95	465	Wrinkle ridge	Drive past formal station 1 km then back 1 km before formal station. Acquire FarCam panorama looking south at 1 km beyond point before turning back, then FarCam pan at 1 km before looking southwest	8.2h,2000m,8.2h,4.48h,250m,12.48h,250m,12.48h,250m,12.48h,250m,12.48h,250m,12.48h,250m,8.2h
OP_11	19.680	-49.399	25.4	0.4	63.5	8.85	24	500 m crater	Depth profile at rim	4.24h
OP_12	20.319	-49.995	28.4	0.4	71	12.07	72	Shield volcano stop 1	Stop about 1.5 km before formal stop at rim, then go to formal stop for stereo panorama of caldera interior and geochemical characterization	6.36h,6.36h



Focused Stop ID	Lat	Lon	Dist (km)	Speed (kph)	Drive Time (h)	Arrival Solar Time	Stop Time (h)	Description	Objectives / notes	Observation Code
OP_13_N	20.255	-50.052	2.7	0.4	6.75	14.73	471	Shield volcano stop 2	Go to rim just south of formal stop, then during night back track towards laying down night tracks	8.2h,6.48h,200m,4.48h,8.2h,200m,12.48h,200m,12.48h,200m,12.48h,200m,12.48h,200m,8.2h
OP_14	20.605	-50.679	21.6	0.4	54	8.53	24	Ghost crater	Characterize composition of regolith in area shielded from Aristarchus ejecta	4.24h
OP_15	20.769	-51.405	23.1	0.4	57.75	11.30	14	Wrinkle ridge pass 1	Several FarCam panoramas while traversing ridge	8.2h,500m,8.2h,500m,8.2h,500m,8.2h,500m,8.2h,500m,8.2h
OP_16	20.872	-51.422	6.7	0.4	16.75	12.34	24	Wrinkle ridge 2	FarCam panorama and other measurements	6.24h
OP_17_N	21.362	-52.153	33	0.4	82.5	15.95	435	Herodotus A (10 kilometer diameter) crater and tectonic feature on south flank	What lies below these basalts? Acquire dusk imaging inside crater then backtrack downslope for radial profile.	8.2h,6.48h,200m,4.48h,8.2h,200m,12.48h,200m,12.48h,200m,12.48h,200m,12.48h,200m,4.48h,8.2h
OP_18	21.645	-52.927	37.2	0.4	93	9.85	36	Middle of Aristarchus ray material west of Herodotus A	Measure local mixing	4.36h
OP_19	22.107	-52.896	15.4	0.4	38.5	12.37	14	Tectonic feature northwest of Herodotus A	Series of FarCam mosaics of fresh wrinkle ridge	8.2h,250m,8.2h,250m,8.2h,250m,8.2h,250m,8.2h,250m,8.2h
OP_20_N	22.528	-52.882	14.2	0.4	35.5	14.05	491	960 meter fresh crater with blocky material	Traverse as close to rim as possible laying down night route, radial traverse for depth profile	8.2h,6.48h,50m,12.48h,50m,12.48h,50m,12.48h,50m,12.48h,100m,12.48h,100m,4.48h,8.2h
OP_21	23.028	-53.184	17.6	0.4	44	8.19	36	Just off Aristarchus ray	Relatively uncontaminated local basalts	4.36h
OP_22	23.127	-53.262	3.7	0.4	9.25	9.72	36	Aristarchus ray	Local mixing	4.36h
OP_23	24.003	-53.469	29.5	0.4	73.75	13.44	48	1100 meter diameter crater near terminus of rille	Measure depth profile, rim	6.48h
OP_24_N	24.103	-53.555	4	0.4	10	15.40	451	Terminus of Schroters rille	Highly mixed zone (AC ejecta), proceed along traverse in 100 m increments night sampling	8.2h,6.48h,100m,12.48h,100m,12.48h,100m,12.48h,100m,12.48h,100m,12.48h,100m,4.48h,8.2h
AP_1	24.323	-53.607	6.9	0.4	17.25	7.28	36	Rille assessment point 1	Two 180 deg panoramas across rille with rover moved for far field parallax	8.2h,500m,8.2h,4.24h
AP_2	24.373	-53.381	9.8	0.4	24.5	9.33	24	50 meter fresh crater radial traverse	Sample rim of crater	4.24h



Focused Stop ID	Lat	Lon	Dist (km)	Speed (kph)	Drive Time (h)	Arrival Solar Time	Stop Time (h)	Description	Objectives / notes	Observation Code
AP_3	24.590	-53.339	7.3	0.2	36.5	11.38	36	Rille assessment point 2	Two 180 degrees panoramas across rille with rover moved for far field parallax	8.2h,500m,8.2h,4.24h
AP_4	24.656	-53.224	4.2	0.2	21	13.31	24	Ash assessment, nearby 30 meter diameter fresh crater	Constrain ash thickness	6.24h
AP_5	24.687	-53.182	1.5	0.2	7.5	14.38	36	750 meter diameter crater in-spection	Crater may be pre-ash, so finding boulder on rim is best chance of peek at subsurface.	6.36h
AP_6_N	24.829	-53.049	5.7	0.4	14.25	16.08	431	Rille assessment point 3	Two 180 degrees panoramas across rille with rover moved for far field parallax, dusk and dawn. Drive past stop 1 km then backtrack 2 km for night tracks	8.2h,250m,8.2h,250m,8.2h, 250m,8.2h,250m,8.2h,250 m,8.2h,250m,4.48h,8.2h
AP_7	25.099	-52.569	18.9	0.4	47.25	8.30	53	Primary secondary rilles bifurcation point	Two 180 degrees panoramas across rille with rover moved for far field parallax.	4.24h,500m,4.24h
AP_8	25.262	-52.166	13.1	0.4	32.75	11.20	48	70 meter diameter crater with apparent excavated basement material	High-reflectance ejecta on NE rim	6.48h
AP_9	25.419	-52.164	6	0.2	30	13.85	24	Ash assessment site 2, relatively sheltered from AC ejecta	Relatively pristine ash deposit	6.24h
AP_10_N	25.334	-51.788	13.5	0.4	33.75	15.80	439	Ash assessment site 3, relatively sheltered from AC ejecta	Relatively pristine ash deposit, small forward increments at night	8.2h,6.48h,50m,12.48h,50 m,12.48h,50m,12.48h,50m, 12.48h,50m,12.48h,100m,1 2.48h,100m,4.48h,8.2h
AP_11	25.653	-51.933	11.5	0.4	28.75	7.67	31	Rille assessment site 4	Two 180 deg panoramas across rille with rover moved for far field parallax	8.2h,500m,8.2h,4.24h
AP_12	25.890	-51.581	14.7	0.4	36.75	9.97	37	60 m diameter fresh crater, depth profile (ash thickness)	Constrain ash layer thickness on high reflectance ejecta near rim	4.12h,50m,4.24h
AP_13	26.061	-51.579	5.2	0.4	13	11.66	31	Rille assessment site 5	Two 180 deg panoramas across rille with rover moved for far field parallax	8.2h,500m,8.2h,6.24h
AP_14	26.061	-51.040	17.1	0.4	42.75	14.16	31	Rille assessment stop 6	Two 180 deg panoramas across rille with rover moved for far field parallax	8.2h,500m,8.2h,6.24h
AP_15_N	25.571	-50.582	22.4	0.4	56	17.11	401	High albedo mound	Traverse to summit (1 km) and follow tracks down for night observations (sample pre-ash terrane)	8.2h,6.48h,100m,12.48h,10 0m,12.48h,100m,12.48h,10 0m,12.48h,100m,12.48h,10 0m,12.48h,100m,4.48h,8.2h
AP_16	25.232	-50.329	13	0.4	32.5	7.80	49	700 meter fresh crater atop ash	Stop about 100 m shy of rim, then go towards rim for radial depth profile (rim ejecta may expose sub-ash material)	4.12h,100m,4.36h



Focused Stop ID	Lat	Lon	Dist (km)	Speed (kph)	Drive Time (h)	Arrival Solar Time	Stop Time (h)	Description	Objectives / notes	Observation Code
AP_17	25.372	-49.928	12.6	0.4	31.5	10.53	37	190 m diameter fresh crater on AC ray	Investigate substrate (lower ash or substrate), first stop 50 m from rim, then at rim	4.12h,50m,4.24h
AP_18	25.421	-49.678	8.9	0.4	22.25	12.53	31	Rille assessment stop 7	Two 180 degrees panoramas across rille with rover moved for far field parallax	8.2h,500m,8.2h,6.24h
AP_19_N	24.813	-49.527	24.2	0.4	60.5	15.63	444	Rille assessment stop 8, including Cobra Head vent	Two 180 degrees panoramas across rille with rover moved for far field parallax, then head along traverse at 50 m increments	8.2h,500m,8.2h,6.48h,50m,12.48h,50m,12.48h,50m,12.48h,100m,12.48h,150m,12.48h,150m,4.48h,8.2h
AP_20_N	23.918	-49.148	53.2	0.2	266	15.71	442	Cobra spatter cone assessment	Note slower speed to account for potentially rougher terrain. Investigate mixing of AC ejecta and local spatter deposits	8.2h,6.48h,50m,12.48h,50m,12.48h,50m,12.48h,50m,12.48h,50m,12.48h,50m,4.48h,8.2h
AP_21	23.798	-48.784	13.7	0.2	68.5	9.02	34	First site Aristarchus crater proximal ejecta, probable first view of far rim	Determine local geology (Copernican ejecta on spatter cone) and take an incredible panoramas, drive forward 500 m five times collecting panoramas looking east, integrate 24 hrs at final stop.	8.2h,500m,8.2h,500m,8.2h,500m,8.2h,500m,8.2h,500m,4.24h,8.2h
AP_22	23.733	-48.202	17.8	0.2	89	13.19	48	Rim of Aristarchus crater	Measure composition of rim materials, image interior of crater with lighting from west. Dense FarCam and PS mosaics of central peak and east and southeast interior.	6.48h
AC_1_N	23.567	-48.191	6.7	0.2	33.5	15.95	435	Impact melt pool near rim	Take it easy! Chemistry of melt sheet and boulders and regolith properties. Slowly follow tracks out at 25 m increments. Also spectacular sunset panorama into crater. Plot out key boulders during daylight. Is impact melt really homogenized sample of target material?	8.2h,6.48h,25m,12.48h,25m,12.48h,25m,12.48h,25m,12.48h,25m,12.48h,25m,4.48h,8.2h
AC_2	23.444	-48.236	7.3	0.2	36.5	7.94	24	Impact melt deposit #2 (2.5 km from rim), AC_2 through AS_8 show up as 1-micon band anomalies (low) in MMM maps, and higher silica in Diviner maps	Test impact melt homogenization hypothesis, composition of boulders	4.24h
AC_3	23.394	-48.272	2.7	0.2	13.5	9.21	24	Rough ejecta (4 km from rim)	Characterize ejecta composition.	4.24h



Focused Stop ID	Lat	Lon	Dist (km)	Speed (kph)	Drive Time (h)	Arrival Solar Time	Stop Time (h)	Description	Objectives / notes	Observation Code
AC_4	23.281	-48.211	7.7	0.2	38.5	11.32	37	Leveed melt flow #3 (5 km from rim)	Test impact melt homogenization hypothesis, primary impact melt flow features	4.12h,50m,4.24h
AC_5	23.220	-48.169	3	0.2	15	13.08	24	East edge of melt field	Test impact melt homogenization hypothesis, primary impact melt flow features	4.24h
AC_6	23.233	-48.116	1.8	0.2	9	14.20	37	Granular eject (maybe) by 170 m diameter crater	Test impact melt homogenization hypothesis, composition of boulders (reference for other sites this day)	6.12h,50m,6.24h
AC_7_N	23.252	-47.981	6.3	0.2	31.5	16.52	418	Rim of Aristarchus #2	Drive past 500 meters then backtrack 1000 m. At far point acquire FarCam mosaic. Chemistry of ejecta and impact melt (boulders, granular, melt)	8.2h,500m,8.2h,1000m,6.48h,250m,12.48h,250m,12.48h,250m,12.48h,250m,12.48h,250m,12.48h,250m,4.48h,8.2h
AC_8	23.227	-47.944	1.5	0.2	7.5	6.95	49	Rim of Aristarchus #3	Test impact melt homogenization hypothesis, composition of boulders	8.2h,4.24h,50m,4.24h
AC_9	23.066	-47.638	13	0.2	65	10.81	49	Rim of Aristarchus #4	Test impact melt homogenization hypothesis, composition of boulders	8.2h,6.24h,50m,6.24h
AC_10_N	22.873	-47.326	15.7	0.2	78.5	15.13	459	Impact melt (#4)	Backtrack 1500 m to start activities (into boulder field). Chemistry of boulders vs. ejecta and impact melt (boulders, granular, melt)	8.2h,4.48h,50m,12.48h,50m,12.48h,100m,12.48h,200m,12.48h,250m,12.48h,250m,4.48h,8.2h
AC_11	23.039	-46.959	16.8	0.2	84	9.54	48	High reflectance material on melt	Color boundary stop	4.48h
AC_12	23.248	-46.866	10.5	0.2	52.5	12.95	49	Edge of red ejecta stream	1-micron anomaly (high) in MMM maps	6.24h,100m,6.24h
AC_13_N	23.319	-46.824	3.1	0.2	15.5	15.13	459	Red ejecta stream	Drive 300 meters past formal spot than retreat 500 m. Lots of boulders and melt deposits to sample.	8.2h,4.48h,50m,12.48h,50m,12.48h,50m,12.48h,50m,12.48h,100m,12.48h,100m,4.48h,8.2h
AC_14	23.560	-46.732	10.6	0.2	53	8.49	48	White unit	Sample low Si (Diviner) low 1-micron unit (MMM)	4.48h
AC_15	23.674	-46.691	4.5	0.1	45	11.64	49	Bouldery stop on color unit	Test impact melt homogenization hypothesis	6.24h,25m,6.24h
AC_16_N	23.798	-46.661	5	0.1	50	15.00	463	Bouldery stop on color unit	Drive past 250 meters then backtrack 500 m to start activities (into boulder field). Chemistry of boulders vs. ejecta and impact melt (boulders, granular, melt)	8.2h,4.48h,50m,12.48h,50m,12.48h,50m,12.48h,50m,12.48h,100m,12.48h,100m,4.48h,8.2h
AC_17	23.901	-46.688	6.9	0.1	69	9.04	48	Away from color anomaly	Moderate silica and 1-micon unit	4.48h



Focused Stop ID	Lat	Lon	Dist (km)	Speed (kph)	Drive Time (h)	Arrival Solar Time	Stop Time (h)	Description	Objectives / notes	Observation Code
AC_18	23.993	-46.705	3.5	0.2	17.5	11.25	24	Impact melt (#5)	Impact melt composition	6.24h
AC_19	24.066	-46.870	10.6	0.2	53	13.86	48	Rim of Aristarchus #5	Crater interior characterization (TriCam, PS)	6.48h,8.2h
AC_20_N	24.146	-46.899	5.6	0.2	28	16.44	420	Rim of Aristarchus #6	Drive past 500 meters (to rim) then back-track 1000 m. At far point acquire FarCam mosaic. Chemistry of ejecta and impact melt (boulders, granular, melt)	8.2h,500m,8.2h,1000m,6.48h,250m,12.48h,250m,12.48h,250m,12.48h,250m,12.48h,250m,12.48h,250m,4.48h,8.2h
AC_21	24.254	-46.896	5.5	0.2	27.5	7.63	24	2.5 km from rim (bye-bye AC)	Depth profile of AC	4.24h
AC_22	24.585	-46.677	16.2	0.4	40.5	9.82	37	Rim of 360 m diameter crater (14 km from AC rim)	Depth profile of AC, sample 50 m from rim, then rim	4.12h,50m,4.24h
AC_23	24.968	-46.713	15.9	0.4	39.75	12.41	24	Average ejecta 23 km from rim (near IMP)	Depth profile of AC, approach to IMP	6.24h
IMP_1_N	25.034	-46.774	4.3	0.2	21.5	13.96	494	IMP	Drive 500 m past then backtrack for night tracks	8.2h,4.48h,50m,12.48h,50m,12.48h,50m,12.48h,50m,12.48h,100m,12.48h,100m,4.48h,8.2h
IMP_2	25.051	-46.770	0.6	0.2	3	6.80	310	Daylight investigation of IMP	Drive into IMP taking multiple panoramas	4.12h,8.2h,25m,4.12h,8.2h,25m,4.48h,8.2h,25m,4.48h,8.2h,25m,8.2h,25m,8.2h,25m,8.2h,25m,8.2h,4.48h



B.3 JPL TEAM X REPORT

This appendix provides the Executive Summary from the Team X Intrepid Study Report (June, 2020). Note that rover detailed design activities by the Intrepid Team continued following this study, resulting in values for some parameters (e.g., total mass) being slightly different from those in the body of the report.



2325 & 235: Lunar Intrepid

Study Lead – John Elliott, PI – Mark Robinson

Facilitator – Troy Hudson

April 6th – 9th, June 11, 2020





Data Use Policy



- The information and data contained in this document may include restricted information considered Jet Propulsion Laboratory (JPL)/California Institute of Technology (Caltech) Proprietary, Proposal Sensitive, Third-party Proprietary, and/or Export Controlled. This document has not been reviewed for export control. It may not be distributed to, or accessed by, foreign persons.
- The data contained in this document may not be modified in any way.
- Distribution of this document is constrained by the terms specified in the footer on each page of the report.



Team X Participants



- **Troy Hudson** (Facilitator)
- **Aron Wolf** (Attitude Control System - ACS)
- **Karen Lee** (Command and Data System - CDS)
- **Roger Klemm** (Command and Data System - CDS)
- **Amanda Ho** (Configuration)
- **Mason Takidin** (Cost)
- **Sherry Stukes** (Cost)
- **Serena Ferraro** (Deputy Systems)
- **Gregory Welz** (Ground Systems)
- **Melora Larson** (Instruments)
- **Christopher Landry** (Mechanical)
- **Matthew Spaulding** (Mechanical)
- **Ronald Hall** (Power)
- **William Smythe** (Science)
- **Ian Trettel** (Software)
- **Kareem Badaruddin** (Systems Verification Integration and Testing - SVIT)
- **Alan Didion** (Systems)
- **Thaddaeus Voss** (Telecommunications)
- **Eric Sunada** (Thermal)



ACS	Attitude Control System	HEOMD	Human Exploration and Operations Mission Directorate
ARR	ATLO Readiness Review	HW	Hardware
ATLO	Assembly, Test and Launch Operations	IMU	Inertial Measurement Unit
BOL	Beginning of Life	I&T	Integration and Testing
BTE	Bench Test Equipment	KSC	Kennedy Space Center
BWG	Beam Wave Guide	LGA	Low-Gain Antenna
CAD	Computer Aided Design	LV	Launch Vehicle
CBE	Current Best Estimate	MEL	Master Equipment List
CC	Contamination Control	MEV	Maximum Expected Value
C&DH	Command and Data Handling	MLI	Multi-Layer Insulation
CDR	Critical Design Review	NEN	NASA Engineering Network
CDS	Command and Data System	NGRTG	Next Generation Radioisotope Thermoelectric Generator
CLPS	Commercial Lunar Payload Services	PDR	Preliminary Design Review
ConOps	Concept of Operations	PEL	Powered Element List
DOD	Depth of Discharge	P/L	Payload
DSN	Deep Space Network	PPT	PowerPoint
EOL	End of Life	PSE	Project System Engineering
EOM	End of Mission	RPS	Radioisotope Power System
FSW	Flight Software	RTG	Radioisotope Thermoelectric Generator
FTE	Full Time Equivalent	SVIT	Systems Verification Integration and Testing
FY25	Fiscal Year 2025	SW	Software
GRAIL	Gravity Recovery and Interior Laboratory	V&V	Verification and Validation
GSE	Ground Support Equipment	WBS	Work Breakdown Structure



Executive Summary

Author: Troy Lee Hudson

Email: Troy.L.Hudson@jpl.nasa.gov

Phone: (818) 203-1021





Executive Summary

Study Overview



- Study Goals
 - Assess the design and estimate the cost of a long-distance lunar rover concept selected by NASA for study under the pre-Decadal Planetary Mission Concept Studies
 - Solicitation: NNH18ZDA001N-PMCS
 - Lunar Intrepid is sponsored in part by HEOMD
- Study Objectives
 - From customer provided design (MEL, CAD, power modes, instrument compliment), provide a technical design assessment (fixing where necessary) for Rover and Ground segments only (study does NOT include commercial lander for lunar delivery), and estimate mission cost. Team-X shall produce a MEL and cost estimate for each option.
 - Option 1 is 4 years, NGRTG powered, and includes night-time traverses
 - Option 2 is 7 years, solar powered, without night-time traverses

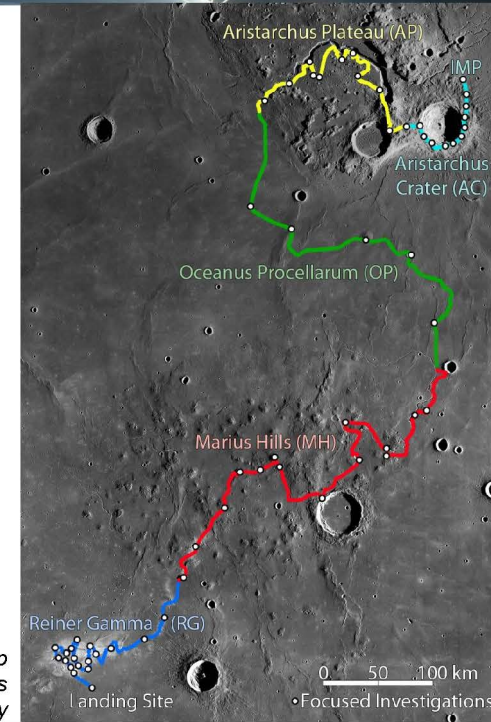


Executive Summary

Mission Architecture and Assumptions



- Lunar Intrepid is a semi-autonomous long-distance (1800 km) lunar rover to be delivered to the lunar surface by a commercial lander (not studied) for a 4 or 7 year traverse covering varied terrains spanning more than 4 Byr of lunar history. The rover carries a suite of instruments for analyzing lunar surface characteristics (composition and morphology) and environmental sensors (magnetic fields, solar wind). The latter address HEOMD goals for the mission.
 - The operational concept includes a pre-defined traverse and fixed suite of measurements at pre-defined sites. This is a significant difference from more familiar (i.e., martian) rover operations.
- Mission Lifetime after lunar deployment: 3 years nominally expected for Option 1, but 4 assumed (50 months) to provide margin. The delivery system (lander and egress) were not included in this study.
- In Option 2, to acquire the nighttime data in Option 1, the mission length was extended to 7 years and a two new power modes were added for nighttime sleep and lander warmup after sunrise.
- The study assumed constraints for the delivery system:
 - Assumed mass cap of 500 kg
 - Assumed volume envelope of 2 to 2.5 m cubed.
 - Daily data volume ~16 Gb per *terrestrial* day



The pre-defined 1800 km traverse and stop locations pass through multiple terrains spanning 4 Byr of lunar history

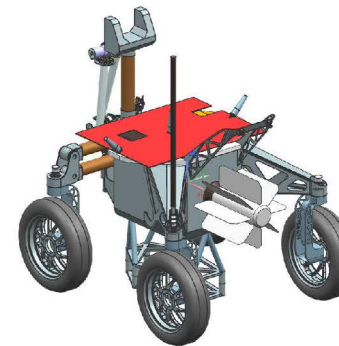


Executive Summary

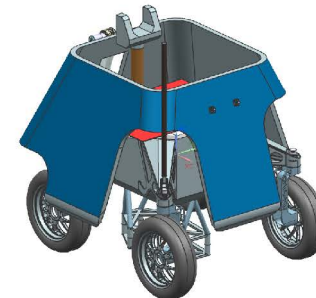
Mission Architecture and Assumptions



- The RTG option failed closure using a 200 W RTG (daytime traverse power was driving mode), but was closed with a 300-W RTG.
- Cost and Schedule Assumptions:
- Cost Target: \$1.1B FY25 A-D; New Frontiers Class B
 - \$200 M (FY25) for launch services and lunar delivery
- Phase A start 2024, Launch 5/2030 for RTG option, 4/2029 for solar option



Intrepid Option 1:
Next Generation RTG
300 W.
Allows limited night
time traverses in
addition to night time
data collection.

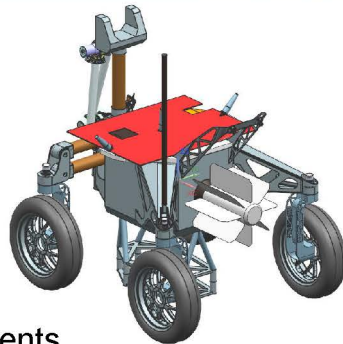


Intrepid Option 2: Solar.
No night time traverses or
mobility; at night only pre-placed
instrument data collection.



Executive Summary

Design Summary – Option 1



- **Instruments**

- Cosmic Ray Detector (ARMAS)
- Magnetometer
- Stereo and telescopic cameras (TriCam)
- Element abundance (GRNS & APXS)
- Microscope-reflectance (HLI)
- Low-energy solar wind (ElectAnalyzer)
- Laser Corner Reflectometer
- Point Spectrometer

- **CDS**

- Sabertooth/Sphinx dual-string (cold) avionics
- 16 Gbytes on-board storage

- **Ground Systems**

- Ground Network = DSN, augmented with NEN/equivalent
- 8.5 Tb over 4 years

- **Telecom**

- 2x S-band directional LGAs
- 1x S-band omni LGA
- 2x S-band transponders w/SSPAs, diplexers, etc.

- **ACS**

- Rover- ACS functions performed by cameras as necessary

- **Structures**

- Primary Structure Mass MEV = 41.0 kg
- Secondary Structure Mass MEV = 3.6 kg
- LV allocation given as very rough guess = 500 kg
 - Delivery lander TBD
 - Scar mass included as “SC-side adapter”
- Mechanisms
 - Mobility system and arm provided by customer
 - No other deployables

- **Thermal**

- Heaters for external instruments during night only
- RTG waste heat is harvested to heat spacecraft internals

- **Power**

- Next-Generation RTG
- Small secondary battery for off-nominal scenario only
- SmallSat electronics w/RTG shunt

- **Software**

- Highly autonomous software, leveraging FSW core product line



Executive Summary

Design Summary – Option 2



Differences from Option 1 highlighted in orange

- **Instruments – same as option 1**
 - Cosmic Ray Detector (ARMAS)
 - Magnetometer
 - Stereo and telescopic cameras (TriCam)
 - Element abundance (GRNS & APXS)
 - Microscope-reflectance (HLI)
 - Low-energy solar wind (ElectAnalyzer)
 - Laser Corner Reflectometer
 - Point Spectrometer
- **CDS – same as option 1**
 - Sabertooth/Sphinx dual-string (cold) avionics
 - 16 Gbytes on-board storage
- **Ground Systems**
 - Ground Network = DSN, augmented with NEN/equivalent
 - 8.3 Tb over 7 years
- **Telecom – same as option 1**
 - 2x S-band directional LGAs
 - 1x S-band omni LGA
 - 2x S-band transponders w/SSPAs, diplexers, etc.
- **ACS – same as option 1**
 - Rover- ACS functions performed by cameras as necessary
- **Structures**
 - Primary Structure Mass MEV = 66.6 kg
 - Secondary Structure Mass MEV = 6.4 kg
 - LV allocation given as very rough guess = 500 kg
 - Delivery lander TBD
 - Scar mass included as “SC-side adapter”
 - Mechanisms
 - Mobility system and arm provided by customer
 - No other deployables
- **Thermal**
 - Heaters for night survival (large design driver)
- **Power**
 - Fixed solar array: 4.9 m2
 - Large battery for night survival (large design driver)
 - SmallSat electronics
- **Software – same as option 1**
 - Highly autonomous software, leveraging FSW core product line



Executive Summary

Option Comparison

	Option 1	Option 2
Total Cost (FY25, A-D, 50% res)	\$1.05B	\$1.00B
Launch Mass (at 30% JPL Margin)	415 kg	590 kg
Mass Margin (against 500 kg allocation)	17.1%	-18.0%
Instruments	NO DIFFERENCE BETWEEN OPTIONS: Cosmic Ray Detector (ARMAS); Magnetometer; Stereo and telescopic cameras (TriCam); Element abundance (GRNS & APXS); Microscope-reflectance (HLI); Low-energy solar wind (ElectAnalyzer); Laser Corner Reflectometer; Point Spectrometer	
Power	300 W Next Gen RTG	4.9 m ² Body-Fixed solar arrays; large battery (large design driver)
Thermal	Heat external instruments at night; harvest waste heat to keep S/C internals warm.	Heaters for night survival (large design driver)
Data Volume	8.5 Tb over 4 years	8.3 Tb over 7 years
Primary Structure Mass	41.0 kg	66.6 kg



Executive Summary

Total Cost Comparison

OPTION 1: RTG

COST SUMMARY (FY2025 \$M)	Generate ProPricer Input	Team X Estimate		
		CBE	Res.	PBE
Project Cost		\$1158.7 M	30%	\$1511.1 M
Launch Vehicle		\$220.0 M	0%	\$220.0 M
Project Cost (w/o LV)		\$938.7 M	38%	\$1291.1 M
Development Cost		\$722.4 M	50%	\$1048.7 M
Phase A		\$7.2 M	50%	\$10.5 M
Phase B		\$65.0 M	50%	\$94.4 M
Phase C/D		\$650.2 M	50%	\$943.8 M
Operations Cost		\$216.2 M	15%	\$242.4 M

OPTION 2: Solar

COST SUMMARY (FY2025 \$M)	Generate ProPricer Input	Team X Estimate		
		CBE	Res.	PBE
Project Cost		\$1173.9 M	32%	\$1546.9 M
Launch Vehicle		\$200.0 M	0%	\$200.0 M
Project Cost (w/o LV)		\$973.9 M	38%	\$1346.9 M
Development Cost		\$664.8 M	50%	\$997.2 M
Phase A		\$6.6 M	50%	\$10.0 M
Phase B		\$59.8 M	50%	\$89.7 M
Phase C/D		\$598.3 M	50%	\$897.5 M
Operations Cost		\$309.1 M	13%	\$349.7 M



Executive Summary

Conclusions, Risks, and Recommendations



- This design is fairly straightforward with low-complexity observations and simple deployment mechanisms (arm)
- A perceived (if not actual) technical hurdle will be the development and V&V of autonomy for this application.
- Assumptions about the capacity of the lunar delivery system (mass, volume) need to be vetted.
- Option 2 exceeds the **assumed** mass cap of 500 kg by 18%.
 - Most of this delta is battery mass from Power (57 kg vs 136 kg) and Structures (152 vs 184 kg) for solar panel mass and associated structure.



C SPECIAL TECHNICAL ANALYSES

C.1 MOBILITY

Requirements: We examined mobility trades for the requirements described in Table C-1. While terrain information at the scale of the mobility system is not available for the planned route, it can be inferred from available data and current knowledge of lunar surface formation process. This information includes data from the Apollo missions, full coverage of orbital imagery at 0.5 – 2 m resolution at different incidence angles from the Lunar Reconnaissance Orbiter Narrow Angle Camera (LRO NAC), derived high-resolution digital-elevation map (DEM) at 2 – 5 m scale for ~10% – 25% of the path, lower-resolution DEM from Kaguya Terrain Camera at 60 m scale for the entire path, thermal imaging from Diviner on LRO, and HST (Hubble Space Telescope) UV and RGB imagery of the lunar surface. For the mobility trades, we drew on mobility and navigation expertise from the lunar (Apollo) and martian surface missions. Table C-2 shows the terrain types along the rover’s route.

Based on test data from the Apollo program, mobility on 15°–20° is possible in lunar simulant [Freitag et al., 1970], which exceeds the maximum slope requirement for Intrepid. However, for angles exceeding 15°, slip would likely exceed 60%.

Mobility configuration: Based on the key requirements of distance, speed, and anticipated terrain properties (topography, regolith properties) (Table C-2), we examined vehicle designs with different wheel/steering configurations (skid-steered, Ackermann-steered, and omni-directional) and with different suspension types (passively and actively articulated). Figure C-1 shows examples of different mobility wheel configurations and suspensions with examples from both flight and research rovers [Nesnas et al., 2000].

Table C-1. Mobility Requirements.

Requirement		Comments
Distance	1800 km	Based on current planned route
Ave speed	0.5 km/hr	Nominal will be at max speed to compensate for slower traverse due to unexpected situations
Max speed	1 km/hr	
Max slope	15°	Based on 3x3 grid (5 m/px) DTM
Nominal regolith (largely ubiquitous)	Fine Coarse	30%: 40–100 μm angular fines 70%: mm – cm regolith
Worst terrain	Ash	10-m deep ash/glass surface
Nominal sinkage	2 – 5 cm	In regolith
Max sinkage	> 1m	Probably in OP ash
Crater distribution	10% 20%	Diameter: 5 m < φ < 35 m Diameter: φ < 5 m
Small crater slopes	7° – 8°	Depth = 0.17 φ (diameter) at formation w/ rapid degradation
Rock distribution (area coverage)	1% 10%	Most of the traverse route Around crater rims
Obstacle height	±0.25 m	Max traversable ± obstacle

Table C-2. Terrain types for mobility and navigation.

Type	Class	% of Path	Slope	Likely Regolith sinkage	Likely Rock Abund.		Regions	Analog / comments	Source
					< 1 m	> 1 m			
Mare	Flat compact	56%	< 5°	cms	Low	< 2%	MH, OP	Most Apollo/ Lunokhod/Yutu	6 m DTM
	Flat rocky compact	4%	< 5°	cms	High	2–12%	MH, OP	Small parts of Apollo traverses	
	Flat less compact	10%	< 5° rarely 8°	cms+	Low-	< 2%	RG	Apollo 16 EVA 1?	
	Sloped compact	4%	5°–15° typ < 10°	cms+	Low	< 2%	MH, OP	Small parts of Apollo traverses	
	Sloped w/ boulders	1%	5°–15° typ < 10°	cms+	High	2-15% typ lower	RG, MH, OP	Small parts of Apollo traverses	6 m DTM
Pyroclastic	Flat unknown	10%	< 5°	?	None	0%	AP	Apollo astronauts dug pyroclastic; like regolith w/o billions years of impacts like AP)	60 m DTM (qualitative)
	Sloped unknown	7%	5°–15°	?	None	0%	AP		
Crater	Crater ejecta	8%	5°–15° path < 12° exists for ¼ crater	?	Very high	< 10%	AC	No Apollo analog; Maybe cone (Apollo 14) and N. Ray (Apollo 16)	6 m DTM (qualitative)

Table C-3 captures the pros and cons of skid-steered vehicles that have four or more wheels, where none of the wheels can steer. Figure C-2 shows an example of how a skid-steered vehicle is amenable to walking out of entrapments. With an articulated suspension, the vehicle can lean forward and then use its link suspension to flip one wheel a time clockwise to overcome a difficult terrain. Wheels with walking abilities can be made smaller and lighter since the rover can walk out of trouble.

A variant of skid-steered and partially-steered vehicles is one with toe-in steering. In this configuration, the steerable wheels can toe in to allow the vehicle to rotate around a point at the center of the non-steerable wheels (Figure C-3). The advantage of toe-in steering is that it does not require a clear sweep volume for the motion of the steering, yet it allows turns-in-place without the slip experienced by skid vehicles. Table C-4 captures the pros and cons of this configuration.

Table C-5 looks at the trades of partially-steered vehicles. One of the key benefits of this configuration is that it can drive along arcs.

Partially steered vehicles allow the use of large wheels for the non-steered wheels, which have the advantage of improved trafficability over rocky and loose terrains and without loss of maneuverability (Figure C-4). Table C-6 captures the trades associated with the configuration of large non-steerable wheels and smaller steerable wheels. Figure C-5 shows a prototype that preceded the LRV with larger non-steerable front wheels.

Vehicles with all-wheel drive, whether four-wheeled, or six-wheeled and so on, are capable of omni-directional driving, also known as crabbing. This additional maneuverability that comes at a cost of additional actuation offers functional redundancy and can handle a loss of a steering wheel. The Spirit rover's maneuverability was impacted when the steering wheel froze at a fixed angle. In all-wheel-steering vehicles, one can

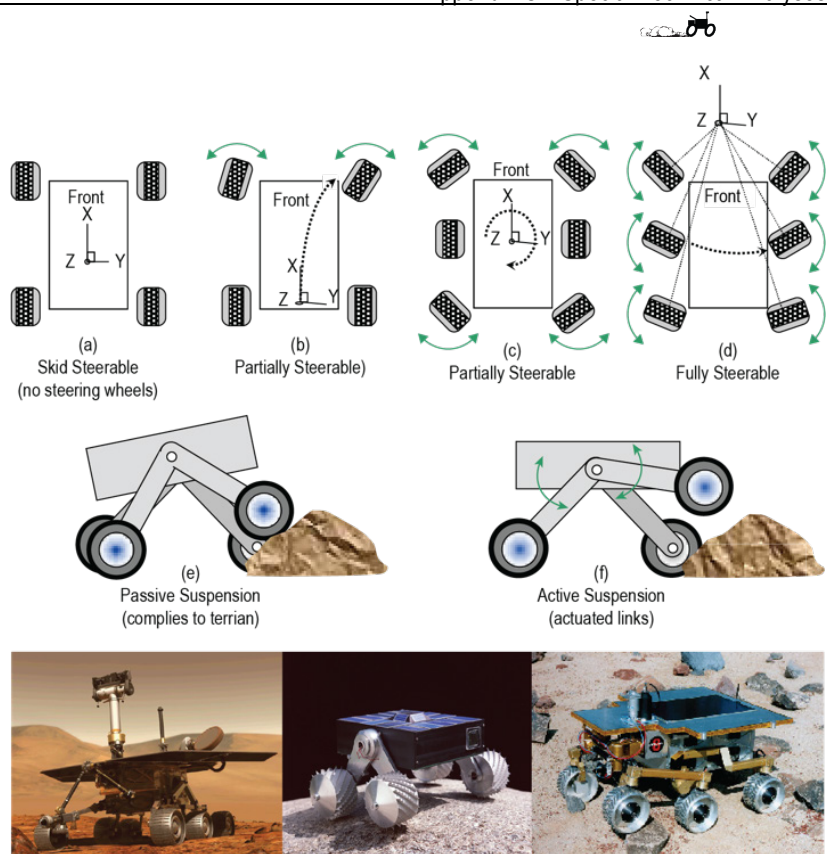


Figure C-1. Examples of different mobility configurations (drive wheels and steering) (top), active vs. passive suspension (middle), and examples from flight and research rovers (bottom). MER is a six-wheel-drive, four-wheel steering with passive suspension (bottom left), Nanorover is a four-wheel drive skid-steered vehicle with active suspension (bottom middle), and Rocky 8 is a six-wheel drive, six-wheel steering with passive suspension (bottom right).

overcome such constraint by orienting the vehicle along the direction of the failed steering angle and then driving. Figure C-6 shows two examples of all-wheel steered vehicles with different suspensions. Table C-7 outlines the trade related to all-wheel (omni-directional) vehicles. Figure C-7 depicts a six-wheel drive vehicle with all-wheel steering, which is capable of arc-crabbing by rotating the vehicle around any single point in the plane it drives on. Table C-8 examines the trades associated with six-wheel omni-directional vehicles, such as the Rock 8 rover shown in Figure C-1.

Wheel design: We also examined wheel types and sizes (stiff vs. compliant, small vs. large), leveraging Apollo wheel-design data (Table C-10) [Asnani et al., 2009; Bekker, 1985; Nuttall Jr., 1965]. Tracked vehicles were excluded from the trade due to their low-ground clearance, large mass, and risks associated with rock entrapment in the tracks of lighter versions.



Figure C-2. Four-wheeled skid vehicle with active suspension (amenable to walking).

Table C-3. Skid (no steering) pros and cons.

Pros	Cons
<ul style="list-style-type: none"> • Has fewer actuators (no steering actuators) • Is amenable to larger wheels (no sweeping volume needed for steering) • Has no steering failure • Is amenable to walking • Can steer and drive simultaneously (by differentially driving each side) 	<ul style="list-style-type: none"> • Cannot position vehicle predictably (but may be able to use control to compensate) • Experiences high sinkage during turn-in-place • Slides downslope when turning • Turning is friction dependent • Uses more power (may be negligible) • Turning is sensitive to small terrain variation. Cannot turn with rocks next to wheels (i.e. cannot steer wheels to roll over side rocks) • Experiences higher wheel wear from turning • <i>Has stability concerns if front/back wheels are closely placed*</i> • <i>Experiences high loads on frame (not quantified yet)*</i>

* There is disagreement on the team about these cons.



Figure C-2b. Compliant mesh tire referred to as the Spring Tire for its coil-spring interlocking mesh type design inspired by the Apollo LRV wheels.

Larger wheel diameters with narrower widths were favored over smaller wider wheels because of their superior traverse capabilities (traction, energy efficiency, and obstacle traversal) [Sutob et al., 2012].

They have lower coefficient of rolling resistance and a larger contact area for the same wheel width, offering improved traction.

Table C-4. Skid with toe-in steering pros and cons.

Pros	Cons
<ul style="list-style-type: none"> • Is amenable to using large wheels for better traversal • Enables turn-in-place for predictable pointing • Eliminates many cons of skid-steered vehicles 	<ul style="list-style-type: none"> • Does not offer more benefit over same design with full front-wheel steering • Increased number of actuators compared to skid while remaining a skid vehicle • Risks steering failure • Slides downslope when turning (unless you turn in place)

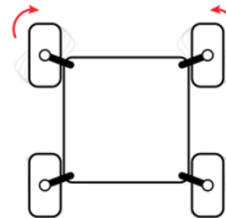


Figure C-3. Four-wheeled skid-steered vehicle with toe-in steering.

Large wheels, however, require large sweep volumes to support vehicle suspension and steering motions, which impact vehicle design. However, for long traverses, large wheels undergo fewer rotations, which extends their lifetime and reduces wheel wear.

When compared to a rigid wheel, compliant wheels have better performance in wear resistance and soft-regolith mobility and slightly better performance in rock traverses. Therefore, Intrepid baselined a compliant spring-tire design made of interwoven coil springs (Figure C-2b). This design has been in development for over a decade for both lunar and martian applications under the Constellation and Mars Exploration Programs [Benzing II et al., 2012; Creager et al., 2016; Creager et al., 2018; Kilkenny, 2017]. This technology is an evolutionary improvement over the Apollo Lunar Roving Vehicle (LRV) wheel intended to have increased durability and payload mass capability, but shares the high soft ground traction and energy efficient properties of the original LRV design. Spring-tire wheels of 43 cm and 70 cm diameter in four-wheel vehicles of 310 kg and 530 kg mass in lunar gravity have traction capabilities of 19° slope at 20% slip and a 23° at 60% slip (evaluated in loose GRC-3 lunar mobility simulant [He et al., 2013]).

The temperature environments encountered by Intrepid rover mobility system present a challenge for existing materials chosen for the compliant wheel, specifically the mesh material's ability to remain ductile and not exhibit brittle/fatigue type failure at the required -180°C. Proper material selection and design modifications are needed to meet Intrepid's mission requirements.

Table C-5. Partial steering pros and cons.

Pros	Cons
<ul style="list-style-type: none"> Improves maneuverability (allows arc drives) – all wheels moving in the rolling direction Improves directionality for driving on slopes Requires only partial steering Steering fails gracefully to skid steer 	<ul style="list-style-type: none"> Requires more actuation and complexity to support steering Needs large sweep volume for steering Is less amenable to large wheels (large sweep volume has to move with suspension)

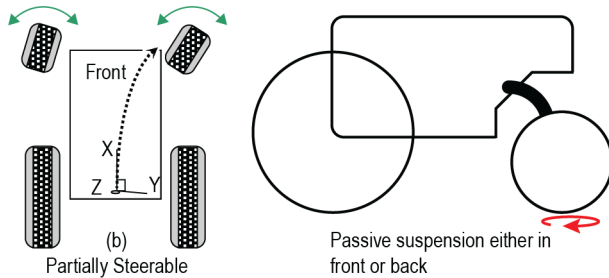


Figure C-4. Partially steerable vehicles with different sized wheels.

Table C-6. Partially steered: race car/tractor pros and cons.

Pros	Cons
<ul style="list-style-type: none"> Improves back-wheel rock traversal (rough terrain) Can house rear actuators inside thermally controlled electronics box Is volumetrically compact Improves maneuverability over skid; provides directionality for driving on slopes Has fewer actuators than fully-steerable Fails gracefully to skid steer Could be more energy efficient with larger wheels (requires further analysis) 	<ul style="list-style-type: none"> Has higher cost due to more actuator gear-train types Has more actuation and complexity than skid Needs large sweep volume for front steering Has some drawbacks to being asymmetric: <ul style="list-style-type: none"> Uneven performance for bi-directional mobility Could lead to higher structural mass May be more susceptible to tip over when compared to equal sized wheeled



Figure C-5. An example of a lunar rover prototype with different sized front and rear wheels: the Local Scientific Survey Module (LSSM) developed in 1965 by Brown Engineering (NASA).

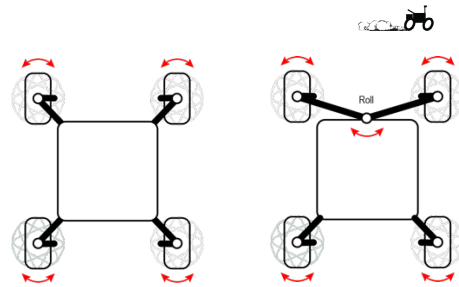


Figure C-6. Examples of a four-wheel drive, all-wheel steering with spring suspension (left) and a front rocker (right).

Table C-7. Crabbing (full steering, omni-directional) pros and cons.

Pros	Cons
<ul style="list-style-type: none"> Allows fine positioning Single steering failure does not affect mobility Allows direction changes on steep slopes Enhances mobility to get out of trouble (out of a rut if rover slides into it) 	<ul style="list-style-type: none"> Is not amenable to very large wheels Steering sweep requires large volume Has more actuation than partially steerable Forces either a higher center of gravity for large wheels or forces the wheels out to accommodate sweep volume for steering.

Table C-8. Crabbing (full steering, six wheels) pros and cons.

Pros	Cons
<ul style="list-style-type: none"> Additional drive wheels allow improved traction on steep, rocky and fine regolith terrains Allows fine positioning for arm placement Single steering failure does not affect mobility Allows direction changes on steep slopes Enhanced mobility to get out of trouble (out of a rut if rover slides into it). 	<ul style="list-style-type: none"> Not amenable to large wheels Requires more complex suspension design (larger mass) Steering sweep requires large volume Has more actuation than partially steerable Forces either a higher center of gravity for large wheels or forces the wheels out to accommodate sweep volume for steering.

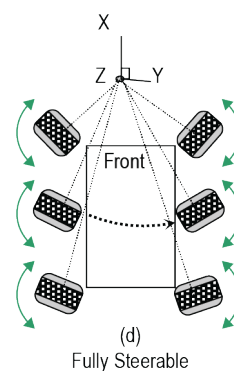




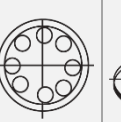
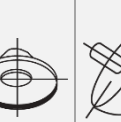
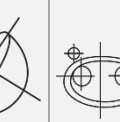


Figure C-7. Six-wheel drive vehicle with all-wheel steering.

The current design has been qualified for an operational temperature range of $-90\text{ }^{\circ}\text{C}$ – $+70\text{ }^{\circ}\text{C}$ for 20 km (60 km unmarginated) distance and $-135\text{ }^{\circ}\text{C}$ non-operational. The design is currently at TRL 6 for Mars applications and will be TRL 8 in 2023 for the Mars Sample Return mission. However, it needs to be qualified to



Table C-10. The Development of a Moon Rover [Bekker, 1985].

Criteria	Relative Value Factors								
		Rigid Wheel	Pneumatic Tire	Wire Mesh Tire	Metal-elastic Tires		Elliptical Wheel	Hemi-spherical Tire	Hubless Wheel
Mechanical Reliability	15	90.0	67.5	75.0	70.5	70.5	25.5	60.0	28.5
Weight	14	92.0	46.2	121.8	35.0	63.0	14.0	81.2	7.0
Soft Ground Performance*	14	53.0	101.5	101.5	121.1	121.1	114.8	116.4	121.1
Obstacle Performance**	10	68.0	74.0	74.0	64.0	64.0	68.0	74.0	64.0
Steerability	6	43.8	34.8	34.8	12.0	12.0	24.6	39.6	12.0
Ride Comfort	13	ZERO	104.0	117.0	39.0	65.0	78.0	26.0	39.0
Stability	8	64.0	56.0	56.0	22.4	45.6	34.4	56.0	22.4
Wear Resistance	8	24.0	12.0	42.0	48.0	48.0	48.0	42.0	48.0
Environment Compatibility	6	48.0	ZERO	36.0	42.0	42.0	36.0	36.0	18.0
Development Risk & Cost	6	64.0	8.0	48.0	48.0	48.0	24.0	32.0	16.0
Total	100	Eliminated	Eliminated	706.0	502.0	579.0	467.0	553.0	376.0

*Includes Slopes and Slip.

**Includes vertical obstacles and crevasses.

Table C-9. Wheel design.

Pros	Cons
Wheel diameter (large vs. small)	
<ul style="list-style-type: none"> • Larger contact length and area for same width (key) • Lower coefficient of rolling resistance • Lower wheel contact angle 	<ul style="list-style-type: none"> • Requires large clear volume for sweeping steering (larger accommodations) • Harder to turn larger wheels
Wheel width (narrow vs. wide)	
<ul style="list-style-type: none"> • Lower mass without with lower impact on mobility performance 	<ul style="list-style-type: none"> • Lower ground pressure, but that is no longer a good metric to use
Grouser (stiff vs. compliant)	
Third order effect	
Open questions	
Quantifying Impact of wheel diameter/width on power, energy, thermal, wear, mass	

-208°C – +140 °C and 1800 km for the Intrepid lunar mission.

Rover selection: Considering the traverse requirements (distance/speed) and the expected terrain properties (slopes, crater abundance, regolith, and other hazards) (Table C-2), designs with fewer wheels offered several advantages. They have: (1) enhanced maneuverability with fewer steering actuators, (2) lower mass with less complex mechanisms, and (3) lower power and higher

energy efficiency. As such, a four-wheeled design was favored over higher number of wheels, requiring only a single passive degree-of-freedom to ensure that all wheels contact the terrain and support equal weight on each wheel. While a three-wheeled vehicle conforms to the terrain without any suspension, it is less stable, risking tip over.

Among four-wheeled vehicles with large narrow wheels, three designs emerged as contenders for the baseline: (1) a four-wheeled vehicle with one-sided toe-in steering, (2) a four-wheeled vehicle with one-sided full-range steering, and (3) a four-wheeled vehicle with two-sided full-range steering. Each of these configurations offer non-skid steering for improved heading control, which is necessary for maneuvering on rocky crater rim slopes and for pointing and placing instrument on targets. The first two options allow even larger wheel diameters and fewer actuators since the wheels on one side do not steer.

However, option (3) with its all-wheel drive, all-wheel steering, and one-sided rocker is selected for the baseline because it affords some steering redundancy and has improved maneuverability for negotiating Aristarchus’ crater rim. The vehicle is designed to drive and steer in either direction. De-



scopes reduce the design to option (2). The baseline wheels have 0.8 m diameter wheels and the vehicle has >0.5 m ground clearance and is designed to traverse rocks less than 30 cm in height. Drive wheels use magnetic detent in lieu of brakes to reduce power draw and increase robustness to failures. Steering wheels do use brakes nor detent to minimize power draw and maintain smooth steering motions.

Table C-10b summarizes the trades, selections and rationale for that selection. The elaboration of the trade space, the selection, the rationale was informed by subject matter experts that drew from prior analyses, designs, implementations, and lessons learned.

Table C-10b. Summary of mobility trades, selection, and rationale.

	Key Trades	Selection	Rationale
Type	Wheeled vs. tracked	Wheeled	Lower mass, larger ground clearance and lower risk of rocks entrapment
Configuration	<u>Drive + steering wheels:</u> 3-wheel (1 steering) 4-wheel (0 steering) 4-wheel (2 steering) 4-wheel (4 steering) 6-wheel (4 steering) 6-wheel (6 steering)	4-wheel (4-steering)	Adequate stability (low tip-over risk) and best maneuverability at lower mass and power; resilient to single-steering failure.
	<u>Suspension:</u> Active vs. passive vs. spring-loaded Dual-sided rocker vs. single-sided rocker	Passive Single-sided rocker	Balanced weight on wheels, lower mass and volume in rover body, simpler mechanism, fewer failure modes, adequate for expected terrain difficulty and rock traversal
Wheels	<u>Diameter:</u> Large vs. small Narrow vs. wide (large: ~1½ x MSL) (narrow: ½ x MSL)	Large Narrow	Superior traction, energy efficient, enhanced obstacle traversal; fewer rotations and terrain contacts for longer life.
	Rigid vs. compliant	Compliant	Improved mobility in soft regolith and over rocks, improved wear resistance



C.2 AUTONOMY

To identify the required level of autonomy, we examined trades from ground-based human control, similar to the joystick operations of the Lunokhod rover back in the 1970s, to onboard autonomous control for mobility, instrument placement and system management. The trades are summarized in Table C-12.

Key constraints that determine the viability of operations modes include: (1) communication availability of the Deep Space Network (DSN), (2) bandwidth of anticipated commercial lunar communication, and (3) the cadence of rover motions (traverse and instrument placement) throughout the lunar day and night. Figure C-8 and Table C-11 summarize the required operations and operational constraints in a lunar day and night for two representative examples. Sustained *ground control* was deemed too cognitively taxing and not viable for the four-year operations period. *Ground decide* and *ground compute* modes were also not viable because they are unable to meet even the average traverse. Table C-13 estimates the throughput based on sensors’ dataflow, onboard computation performance, and communication bandwidths. As a result, this mission has to rely on *onboard decide* for a significant portion of

its nominal operations and on the *ground decide* for the remaining portions. Leveraging ground-based computing infrastructure (*ground compute*) to supplement the onboard computing does not offer an advantage due to the communication availability and bandwidth.

After mission operations transition to an Earth-based schedule, both traverse and arm operations would inevitably fall outside the normal operations schedule. Therefore, a significant portion has to be conducted through autonomous operations.

For the long-traverse distances, autonomous traverse would necessitate a level of reliability to ensure that the mean-distance-between-faults maintains an average traverse rate of 500 m/hour. Table C-14 captures the required capabilities for autonomous operations that encompasses surface navigation, localization, identifying safe regolith and rock targets for placing instruments and acquiring measurements. Throughout, the rover has to plan and manage its shared resources and monitor its health to achieve a TBD rate of faults for such operations.

Sensor selection and placement. Sensors are selected and mounted on the rover to support both autonomous and ground-assisted

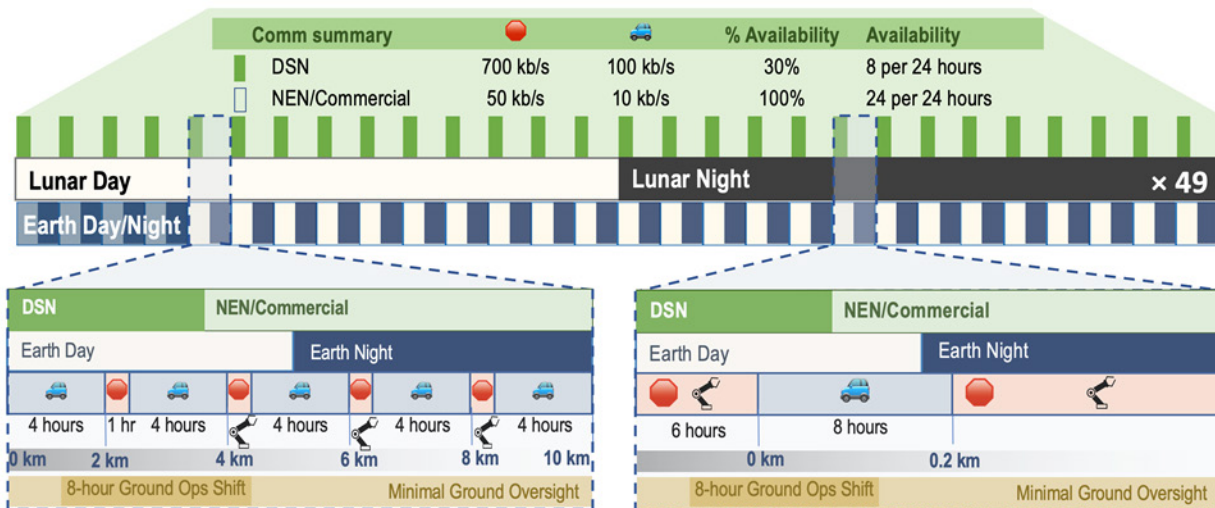


Figure C-8. Examples of operations from a lunar day and night across an Earth day that shows drive/arm operations with communication constraints and operation shifts.

Table C-11. Traverse Distances and Times During the Lunar Day and Night.

Period	Speed km/hr	Effective Speed km/hr	Driving distance (km)				Driving time (hr)				Avail. Time (hr)
			Ave.	Median	Min.	Max.	Ave.	Median	Min.	Max.	
Lunar day	0.5	0.4 4h🚗 + 1h🔦	51	53	20	93	128	133	50	233	315 RTG
Lunar night	0.05	0.05	0.9	0.7	0.2	2	18	14	4	40	354



operations, simplify operations, provide adequate sensing coverage with minimal articulation of the mast and arm, and offer robustness through functional of physical redundancy (see Redundancy Section).

Tables C-15 and C-16 examine the trades of passive (cameras) and active imaging (LIDAR).

Stereo cameras are selected over LIDAR options (both spinning and flash) for traverse and arm operations. Despite their superior 3D range and being agnostic to sun angle and shadows, LIDARs require higher power, have limited resolution in, at least, one dimension (vertical for spinning), and are currently at a lower TRL for lunar surface applications than cameras.

Redundant high-resolution stereo-camera pairs with 90° field-of-view lenses and a ~25-cm baseline are mounted on either end of the rover to accommodate driving in either direction as well as arm operations. The wide field of view allows rover navigation without the need to articulate and point the mast during nominal traverses. At the maximum traverse rate, short exposures (~10–20 ms) allow imaging-while-driving during the lunar daytime. At night, which requires short traverses and far fewer instrument placements, the rover relies on Earth shine for imaging to avoid the overhead (mass, power, cost, and complexity) of additional lights. Since night operations are infrequent, cameras use long exposures (tens of seconds) when the rover and arm are stationary. Table C-17 summarizes the night traverse requirements and Table C-18 provides information regarding exposure time for night driving using Earthshine. Night imaging requires 500× – 2000× longer exposures at full Earth and up to 10000× at half Earth (1–10 s).

With the cameras mounted at ~1.5 m off the ground, articulated covers for the camera lenses are not necessary. Arm motions are slow and do not require contact with the surface. Further assessment of the impact dust on lenses after prolonged exposure and the effects of sun

glints on the camera images is warranted. In addition to these perception sensors, the arm can be stowed such that the Hand-Lens Imager (HLI) can image the wheels on the arm-mounted side with only a rotation of the wrist pitch.

Table C-12. Operations modes and trades.

Mode	Downlink	Ground	Uplink
Human control	Stereo imagery and rover telemetry	Human assesses and controls rover, arm, and instruments	Actions for every step
<i>Sustained human control was deemed too cognitively taxing and not viable to sustain for the four-year operations (24/7).</i>			
Human decide	Stereo imagery and rover telemetry	Ground computer assesses and generates actions. Extensive synchronous human selection/oversight.	Actions for every step
Ground compute	Stereo imagery and rover telemetry	Ground computer assesses and generates actions autonomously. Limited asynchronous human oversight.	Actions for every step
<i>Human decide and ground compute modes were also not viable because they are unable to meet even the average traverse. Leveraging ground-based computing infrastructure (ground compute) to supplement the onboard computing does not offer an advantage due to the communication availability and bandwidth.</i>			
Onboard decide	Thumbnail imagery and rover telemetry	Onboard computer assesses and generates actions autonomously. Limited asynchronous human oversight.	Route plan and goals
<i>Onboard decide was the only viable option for nominal operations. Contingencies and off-nominal operations can leverage ground-based human decide option.</i>			

Table C-13. Assessing viability of ground-based compute mode.

Mode	Time for human confirmation (s)	Distance between onboard images (m)	Distance between images sent to ground (m)	Image Resolution (pixels)	Traverse Rate (m/hour)	
					Possible	Required
DSN Window: 8 hours per 24-hour period					Rate: 700 kb/s 100 kb/s	
Ground Compute	60	1.7–2.3	10-m drive steps	1280×960	238	Ave 500
				640×480	294	
Onboard decide	N/A	1.7-2.3	continuous drive	128×96 thumbnails	1,018	Max 1000
Commercial Window: 24/7 continuous					Rate: 18 kb/s 2.5 kb/s	
Ground Compute	60	1.7-2.3	10-m drive steps	1280×960	20	Ave 500
				640×480	69	
Onboard decide	N/A	1.7-2.3	continuous drive	128×96 thumbnails	1,018	Max 1000



Table C-19 captures the trade for inertial sensors which are using for pose (position and attitude) estimation of the rover. Selection favored low mass and power options.

In addition to the perception and inertial sensors, all actuators use hall-effect sensors in lieu of encoders to estimate and control wheel/joint motions. Hall-effect sensors are more tolerant to higher temperatures experienced by components outside the thermally managed electronics box. In addition to these relative position sensors, the steering and arm joints use resolvers on the joint outputs for absolute positioning. Torques on the wheels and arm are inferred from the motor winding currents and is sufficient since the arm does not require contact for instrument placement.

Arm operations and instrument placement.

The arm, which carries two turret-mounted instruments, the APXS and the HLI, has two primary functions: placing these instruments at centimeters distance above their targets and inspecting the rover, its wheels and underbelly using the HLI. Both the rover and the arm position and orient the instruments on either regolith or rock targets. The APXS places its head 2 cm above the surface. For rocks greater than 60 cm in diameter, the required lateral placement accuracy from rover-based images is ± 15 cm from the middle of the rock. Orientations errors of up to 30° can be tolerated by both instruments [VanBommel et al., 2017]. Targets are selected either by ground operators based on high-resolution orbital data with positional accuracy of > 1 m relative to the rover or by an onboard algorithm based on intent from ground operator. The science measurements do not necessitate surface preparation nor do they constrain a specific location or face on the rock for instrument placement. Therefore, onboard autonomy algorithms are driven only by engineering considerations such as lighting, thermal, and geometric consideration for safe placement and arm retraction in the event of a failure. Targets identified by ground operators or onboard algorithms from 10 m away will have a placement accuracy of < 5 cm [Fleder et al., 2011], well-within the science requirement. To minimize orientation errors in placement, the rover/arm has to match the two angles of the target surface normal. To match the first surface normal angle, the rover approaches the selected target along the surface vertical plane of the surface normal and deploys its

Table C-14. Autonomy Requirements.

	Requirement	Description
Surface navigation	Rate	1 km/hr max during daytime; 0.05 km/hr during nighttime
	Hazard assessment	Detection and avoidance for all hazards that include: <ol style="list-style-type: none"> 1. terrain topography (positive: untraversable rocks, negative: deep depressions or craters), 2. lateral slip toward a terrain hazard, 3. sink hazards in soft terrain, and 4. power/thermal hazards that occlude solar panels or block radiator
	Path planning	Route path around hazards
Instr. Placement	Target identification	Autonomous regolith patch or rock selection based on intent
	Approach target	Tracking and approach of selected target while avoiding navigation hazards along the way
	Hazard assessment	Hazard assessment at the target's vicinity prior to final positioning and placement <ul style="list-style-type: none"> • Assess lighting/thermal hazards from environment • Estimate surface normal of target patch • Maneuver rover to approach target to match surface normal and optimal sun angle • Assess clearance around target surface area for collision-free placement
System	Arm deployment and instrument placement	<ul style="list-style-type: none"> • Deploy arm and align other surface normal angle to turret's pitch angle • Place on regolith or small/large rock targets • Acquire measurements from multiple instruments • Retract and stow the arm
	Health management	Continuously monitor the health of the hardware and software components
	Resource management	Plan and schedule activities based on intent and available resources

Table C-15. Active imaging pros and cons.

Pros	Cons
LIDARs	
<ul style="list-style-type: none"> • High range • High accuracy at range • Works at night • Data can be used for science • Agnostic to shadow • Agnostic to sun angle • Could filter out dust (like snow from blizzard in terrestrial apps) 	<ul style="list-style-type: none"> • High power • Low TRL for lunar environment • Higher cost • Laser life • Localization accuracy • Dust accumulation on optics • Motion distortion
Spinning LIDAR	
<ul style="list-style-type: none"> • 360° coverage (no mast articulation) 	<ul style="list-style-type: none"> • Low vertical resolution • Moving parts
Flash LIDAR	
	<ul style="list-style-type: none"> • Small FOV



Table C-16. Passive imaging pros and cons.

Pros	Cons
Stereo vision	
<ul style="list-style-type: none"> • Low power • No moving parts • High heritage (TRL9 hw/sw) • High-density point cloud • Intensity + 3D data • Data can be used for science • Dust tolerant (quantified by MSSS) • Functional redundancy (SfM) 	<ul style="list-style-type: none"> • Texture dependent • Limited range • Dependent on incident/phase angles • Lens distortion for WFOV lenses • Requires calibration? • Requires large computation and memory for stereo • Motion smear/blur at higher speeds

Table C-17. Requirements for night driving.

Requirement	Value	Comment
Traverse distance	>2 km	Requires minimal operation at night possibly including < 100 m traverses
Traverse speed	50 m/h	

Table C-18. Camera exposure times for night driving.

Time of Day	Exposure (seconds)	Color Filter	Comment (all at full Earth – EarthShine)
Day (noon)	0.02	Y	Color LROC WAC (tested)
Night	40	Y	Factor of 2000x (tested)
Day (noon)	0.01	N	B/W camera (estimated)
Night	5–20	N	Factor of 500–2000 (est.)
Day (noon)	0.001	N	Broadband B/W camera (est.)
Night	1–3	N	With half Earth, est. at 10 s

Surveyor increased exposure by 800x from day to night.

Table C-19. Internal sensing. Limited options for low-mass, low-power, reliable long-duration Class B IMUs.

	Power	Mass	Rationale
MIMU	22 W ave 32 W max	4.5 kg*	High mass and power compared to other options. Used on M2020 EDL; baselined for MAV.
LN200**	15 W	0.6 kg	Has reliability problems; will be discontinued
ASTERIX 120	6 W × 3	6.5 kg	Large mass
SsirU	43 W max	5.5 kg	High cost; used for classified work
SmallSat IMUs	1.5 W ave 2 W max	0.06 kg	Not available in Class B (e.g. STIM300)
Accels only			Allows recovery of rover tilt, but without gyros, rover loses ability to accurately control its heading.

four-degree-of-freedom arm to place the instrument on the target, pitching its end effector to match the second surface normal angle.

System-level autonomy: The long traverse requires a level of TBD reliability that exceeds that of prior Mars missions. System health, shared resource and activities are managed using an

onboard autonomous system that can plan activities based on intent from the ground, available onboard resources, and the health of the components of the systems. Fault protect is integrated with the system manager to handle both nominal and off-nominal conditions through the same mechanisms. Robustness of performance both at the function and system levels for a range of uncertainties is critical to successfully meet the objectives of the mission.

Redundancy

The Intrepid rover features numerous physical and functional redundancy ensuring a robust system. In addition to the physical redundancy, 3D information can also be generated using a functional redundancy of structure-from-motion. The stereo cameras on both side of the rover have redundant pairs. The compute elements, motor controllers, and IMU are all redundant. For localization, the rover relies on both visual odometry as well as wheel and inertial dead reckoning.

Localization

This requires knowledge of rover position, which is coupled with knowledge of heading. Heading knowledge also serves antenna pointing, but this is not a driver with the relatively wide antenna beams (numbers?); therefore, heading knowledge requirements and trades were assessed as part of meeting position knowledge requirements

To meet science objectives, position knowledge error must be better than 3 m per 1,000 m of traverse in order to see science targets in rover imagery. However, tighter requirements derive from rover hazard avoidance processes. Rover navigation follows routes designated with orbital imagery and must respect human-specified keep-in and keep-out zones, which keep the rover safely away from navigation hazards that are visible from orbit. The most frequent hazards on the Moon are craters; absolute position knowledge on the order of the smallest crater reliably detectable from orbit (5 m diameter) is required at all times to respect these zones.

Potential sources of absolute position knowledge include radiometric sensing from transmitters on Earth or in lunar orbit, registration of digital elevation maps (DEMs) created onboard the rover to DEMs created from orbit, recognizing skyline landmarks, and recognizing crater landmarks near the rover. Between absolute position measurements, relative position updates are possible from wheel odometry, visual odometry, and an inertial measurement unit



(IMU). Potential sources of absolute heading knowledge include sensing directions to the sun, the Earth, and stars; relative heading updates are possible from an IMU and from wheel and visual odometry.

The solution that best meets requirements at the lowest cost is a combination of recognizing crater landmarks with the rover stereo cameras, measuring sun direction with an Adcole pyramid-type coarse sun sensor, and obtaining relative updates from wheel odometry, visual odometry, and a heritage LN200 IMU. When the sun is near zenith, absolute heading updates are still available from crater landmarks and can be obtained by observing direction to the Earth with the mast cameras. A star camera was deemed unnecessary and is relatively large. Other approaches to position measurement have inadequate accuracy and are available less frequently.



C.3 THERMAL CONTROL

Thermal control of low latitude rovers that must survive diurnal cycles is challenging due to the extreme cold and hot conditions, each of significantly long duration. This places an importance on the thermal analyses to accurately model the environmental conditions such that a high degree of model uncertainty does not drive an excessive need for system resources for rover survival.

Terrain features can have significant effects on the rover's thermal energy. Data from the Apollo program showed noticeable temperature increases when in view of distant hills. In the case of a rover with a scale factor on the order of nearby boulders and terrain features in combination with random tilts as it drives over an irregular surface, the thermal design must be coordinated with the operations plan to ensure a sufficiently high probability of success. This includes the ability to drive through unacceptable orientations that would otherwise result in high temperature limit violations.

Dust effects on thermo-optical properties of radiating surfaces must also be modeled accurately. An overly conservative approach would preclude a radiator design that receives an appreciable amount of solar flux while maintaining standard avionics temperature limits, thus requiring either an articulated radiator, dust mitigation provisions, or impractical orientation restrictions placed on the rover. Depending on the lander design, plume interaction analyses may be required to ensure an acceptably low amount of dust contamination on thermal control surfaces.

These environmental loads and influences must then be modeled onto the rover and its resulting thermal design. Heater energy predictions during the lunar night must be accurately predicted because of its driving effect on the power system and science-returning operability. Conservative, worst-case hot analyses are necessary for RPS hardware due to the strict interface requirements.

Lunar Surface Modeling. The effect of terrain features requires, at a minimum, representative cases to be run that include surface topography. Such cases are used to establish sensitivity analyses, or better yet, uncertainty quantification that can be used to assess temperature violation probabilities. Wider-swath topology data can be used to assess the effect of more distant terrain features. Custom scripts have been developed at JPL for translating Lunar Reconnaissance Orbiter

(LRO) data to finite element mesh for direct use in the Thermal Desktop® analysis software. Both higher resolution LRO data (LROC NAC data) and lower resolution data (WAC and SELENE TC + LRO WAC) are accessible by the JPL tool. A 2-D mesh is generated depending on the user-specified resolution. In Figure C-9, example snapshots of processed LRO surface data are shown at user specified lat/long, area, and discretization and a resulting surface temperature prediction.

The in-depth model of the regolith or basalt is a 1-D model with sufficient skin depth to negate edge effects and is based on the penetration depth of a periodic temperature wave corresponding to the diurnal. Based on properties given in reference *Hayne et al.* [2017], this penetration depth corresponds to 7 cm for regolith and 68 cm for basalt. The thermal model then simulates a depth 10x this amount for conservatism with a nodal resolution of 1/10th the skin depth.

Dust Effects. Thermal analyses assume sensitive thermal control surfaces are protected from ballistic impacts of regolith or basalt particles. Thermal control surfaces that lack any dust mitigation mechanisms are assumed to eventually be covered by a monolayer of lunar regolith dust regardless of orientation and location. The nature of the dust, most importantly the solar absorptivity and IR emissivity, can vary depending on location on the moon. For conservatism, assuming a darker, mare-type dust is prudent when performing worst-case analysis. Testing done by *Gaier et al.* [2013], of NASA Glenn Research Center has shown that second surface silverized Teflon films are less susceptible to dust degradation than white paints for radiator surfaces. Because of the lack of actual regolith from the mare for testing, we assume the JSC-1AF simulant properties. Testing by Gaier, et al., has shown that for such a monolayer over 5-mil silverized Teflon film, the solar absorptivity to IR emissivity ratio (α/ϵ) goes from 0.09/0.8 when pristine to 0.29/0.9 degraded.

For surfaces with lower IR emissivities, such as specular surfaces used on shields, JPL has found no reliable test data. And unlike for Martian dust, the particle size cannot be assumed sufficiently small as it is on Mars (~ 1 micron) to be effectively transparent to IR wavelengths. We are left to assume that particles are sufficiently large to not be IR transparent (> 10 microns) and that further testing is required to characterize the effects of dust on specular surfaces.

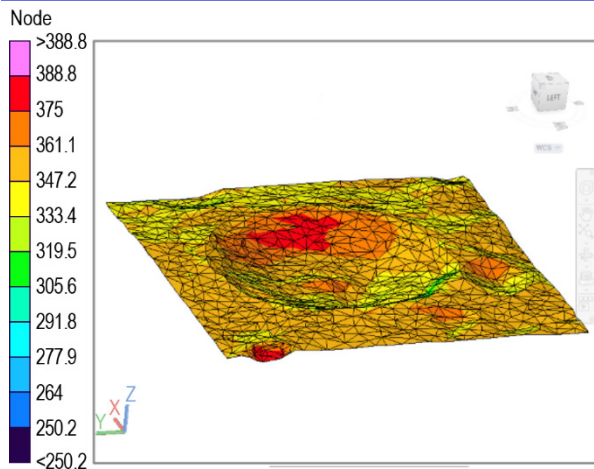
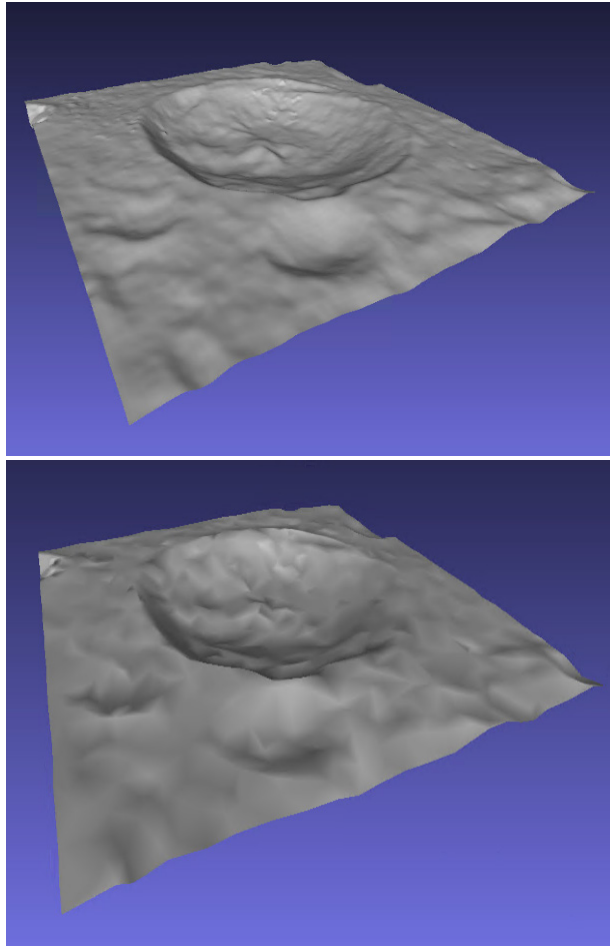


Figure C-9. LRO surface with 600,000 faces (a), reduced to 2,000 faces, and a predicted temperature contour for a given time of day.

Intrepid Thermal Analyses. The thermal design is most challenged by the solar powered option due to the sensitivity of battery mass to nighttime power usage, such as for heating, and the need to minimize it. Yet during the day, the

extreme hot conditions of direct sun on the radiator or, worse, an orientation that also includes a view to regolith will drive the need for a sizable radiator. The primary challenge then is to allow for adequate heat rejection during the day while minimizing it at night. To minimize thermal resources, hardware temperature limits that span a wide range are most helpful. Such is the case with external elements such as mobility actuators and structure. But batteries, avionics, and some instruments require much narrower temperature ranges to operate and will require special provisions for them to remain without employing excessive resources to do so. Table C-20 lists the driving temperature limits for Intrepid hardware.

The extreme environment of the lunar surface and temperature limits drive the following thermal design:

- Where possible, items with narrow temperature limits such as batteries, avionics, and motor controllers are placed in a central Warm Electronics Box (WEB) that is well insulated.
- External elements should be qualified to a wide temperature range to prevent excessive amounts of localized survival heating and heat rejection surfaces and accompanying orientation restrictions.
- To minimize costs associated with mechanisms for an articulated radiator, a zenith-facing radiator is used to reject waste heat dissipations from the WEB. Obstructions that are within view of this radiator should be minimized.
- To allow the radiator an unobstructed view to sky while maintaining a low CG with batteries and electronics mounted near the floor of the WEB, a loop heat pipe (LHP) is used to bridge the relatively long distance associated with the solar array option. An LHP is much more mass efficient than solid conductive couplings and allow for smaller penetrations through the WEB wall that minimizes heat leaks during the lunar night.
- To reduce the amount of heat leak at night, a set of thermal switches are used that passively de-couple the components from the LHP. These switches work on the principle of differences in the coefficient of thermal expansion between materials and have an on/off heat conductance ratio of about 5 W/K to 0.002 W/K.

A block diagram schematic of the solar powered Intrepid thermal design is shown in Figure C-10.



The RPS powered Intrepid rover does not require a LHP because of the shorter distance between WEB components and the radiator. A block diagram schematic of its thermal design is shown in Figure C-11.

The radiator is sized based on maintaining internal WEB components below 50 °C with a silverized Teflon coating whose properties are degraded by 100% coverage by a monolayer of lunar dust. The radiator surface area is sized at 1.1 m² and is capable of rejecting 150 W internal dissipation. Figure C-12 shows radiator size as a function of solar altitude angle for various heat loads.

The LHP utilizes a 12-inch evaporator to lift up to 150 W of load using propylene as the working fluid. The analysis assumes a 70 W/K LHP conductance. The LHP is not deliberately shutdown with a heater on the compensation chamber in order to minimize nighttime heating power, which would drive the battery sizing. The possible operation of the LHP in a reflux mode is the only driver given that dissipations on the evaporator will be sufficiently small with the thermal switches in the off-mode. Despite this, there is sufficient turn-down provide by the thermal switches to tolerate this small heat leak. The propylene is not expected to reach its freeze temperature of 88 K during the lunar night.

External Elements. The actuators are expected to tolerate temperatures down to 90 K during the night while not operating. Prior to use, they will be heated by external heaters. The solar powered version of Intrepid might be required to adhere to

Table C-20. Intrepid Temperature Limits.

Intrepid Hardware	Allowable Flight				Protoflight or Qual			
	Operational		Nonoperational		Operational		Nonoperational	
	min	max	min	max	min	max	min	max
Sabertooth Board	-20	50	-30	50	-35	70	-45	70
Motor Controller Board	-40	50	-40	50	-55	70	-55	70
Power Board	-40	50	-40	50	-55	70	-55	70
Telecom and MUX Board	-20	50	-30	50	-35	70	-45	70
IMU	-39	51	-47	65	-54	71	-62	85
Li-Ion Battery	-20	50	NA	NA	-30	70	NA	NA
Motor Winding	-70	135	-100	135	-85	155	-120	155
Gearbox	-55	135	-131	91	-70	135	-146	111
APXS Sensor Head Housing	-170	-5	-170	50	-185	70	-185	70
APXS Electronics Housing	-45	50	-45	50	-60	70	-60	70
FarCam	-55	50	-120	50	-70	70	-135	70
GRNS Detector	-30	30	-35	50	-45	50	-50	70
GRNS Electronics	-30	30	-35	50	-45	50	-50	70
SW Suprathermal Sensor	-30	30	-50	60	-45	50	-65	80
SW Suprathermal Electronics	-30	40	-50	60	-45	60	-65	80
Solar Wind Sensor	-30	40	-50	60	-45	60	-65	80
Solar Wind Electronics	-30	40	-50	60	-45	60	-65	80
Engineering Camera Detector	-20	40	-40	70	-35	60	-55	90
Engineering Camera Electronics	-45	55	-40	70	-60	75	-55	90
EECAM (CMOS, Optics, Elec)	-55	50	-120	50	-70	70	-135	70

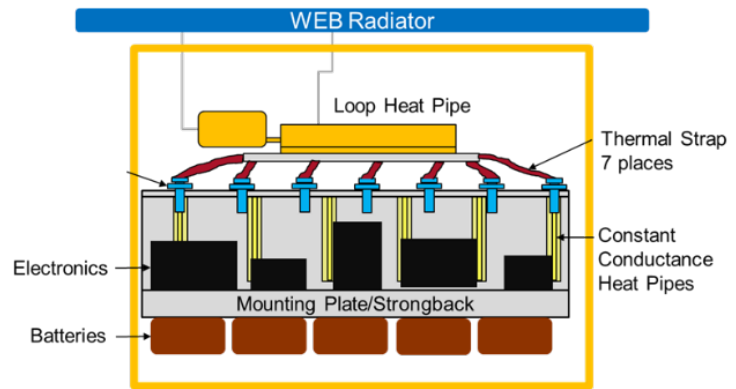


Figure C-10. Solar rover thermal control schematic.

this mode and warm-up times can be significant. Assuming a shadowed mobility actuator as shown

in Figure C-13 below, heating times using a 15 W heater can be over 7 earth hours. If unheated allowed to warm by the sun, it would require over 13 earth hours.

RTG Temperature. The extreme hot conditions during the lunar daytime drives RTG temperatures beyond the upper MMRTG limit of 473 K (200 °C). Peak temperatures occur with the RTG directly exposed to a 10 AM sun and reach as high as 513 K (240 °C), and require the higher temperature limits afforded by a next generation RTG. The harsh daytime temperatures of the regolith and/or shielding from it, will drive a significant reduction in view factor to cold space. Combined with direct solar loads during certain times of the day, the temperatures cannot be maintained colder without a method to remove the heat via a heat pipe or pumped fluid loop to a remote radiator. Both a heat pipe option and actively pumped loop will add cost and complexity. The heat pipe being susceptible to orientation/configuration restrictions and the active pump system adding significant mass, volume, and about 30 W of pump power.

Solar Array Temperature. Solar array temperatures were analyzed and are expected to have wide swings due to the diurnal. Temperatures can range from as high as 140 °C at around 900 lunar time and drop as low as -208 °C (65 K) during the night.

Instrument Thermal Control. The instrument with the most restrictive upper temperature limit is the APXS sensor head with an upper allowable of -5 °C. Note that the internal sensor temperature is held colder by a built-in thermoelectric cooler and that the temperature limit applies to its hot-side interface. Maintaining this temperature with passive thermal control is not possible without a dedicated, shielded radiator that is accompanied by highly restrictive orientation requirements. At best, a passive thermal system with a zenith-facing radiator can operate during limited morning and afternoon windows.

Figures C-15 and C-16 shows a scenario of the APXS sensor head located over a local shaded area of regolith. Still, the sensor can only remain below the -5 °C limit until about 0915 lunar time.

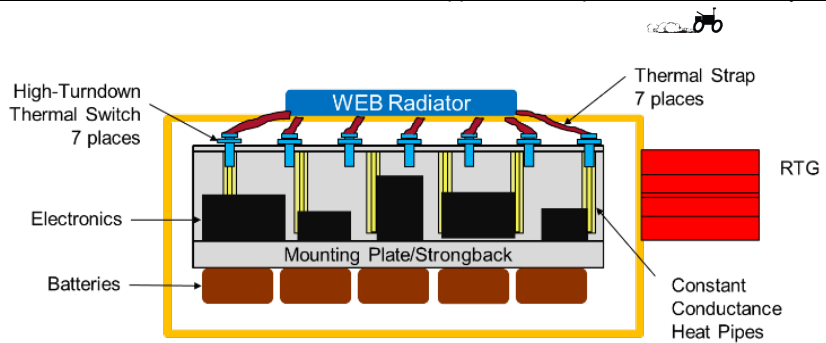


Figure C-11. RTG rover thermal control schematic

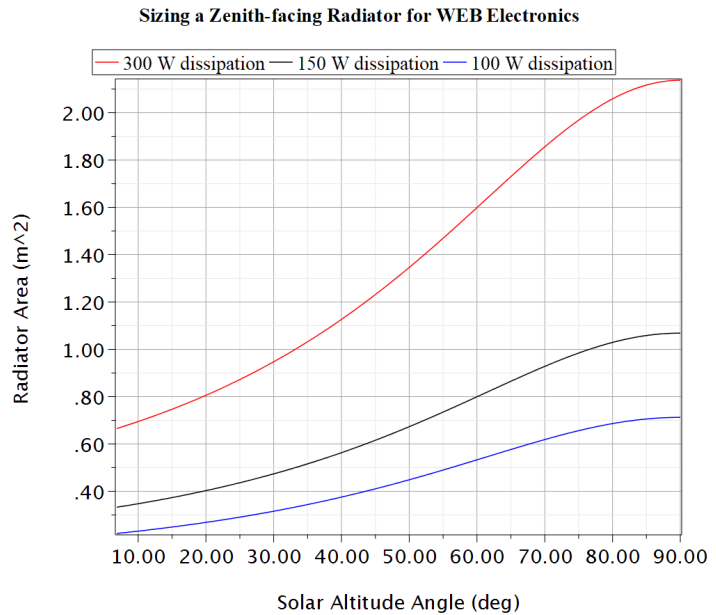


Figure C-12. Radiator size as a function of solar angle.

To provide greater science opportunities, a Ricor K508 cryocooler that can operate under warm conditions is baselined for the APXS (Figure C-17). It requires 8 W of input power that corresponds to a cryocooler heat sink temperature of 52 °C which may be supplied by a local radiator.

Thermal Architecture—Solar Power Option. The concept level thermal analysis described above was used to extrapolate a thermal point design from which MEL and PEL inputs can be estimated for thermal hardware. A cut-away view of the WEB is shown below (Figures C-18 and C-19). The loop heat pipe liquid return and vapor lines can be seen running from the evaporator/reservoir assembly to the elevated radiator above. The lines are then bonded to the

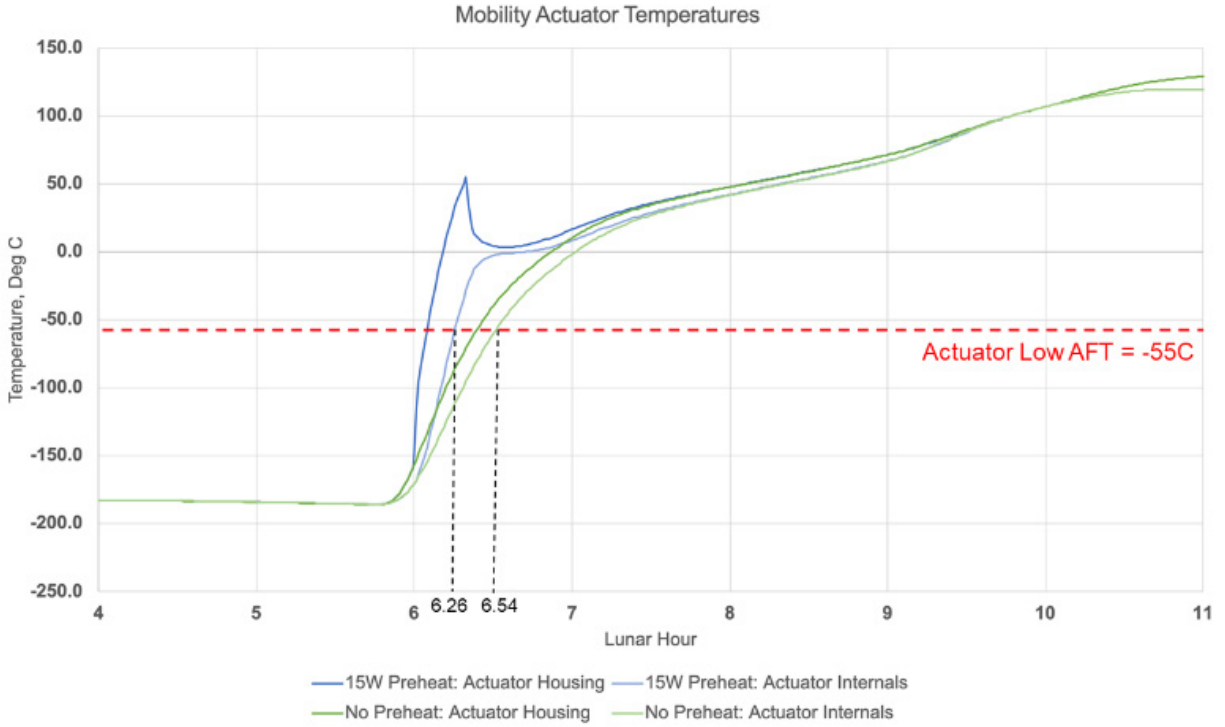


Figure C-13. Heating of shadowed mobility actuator.

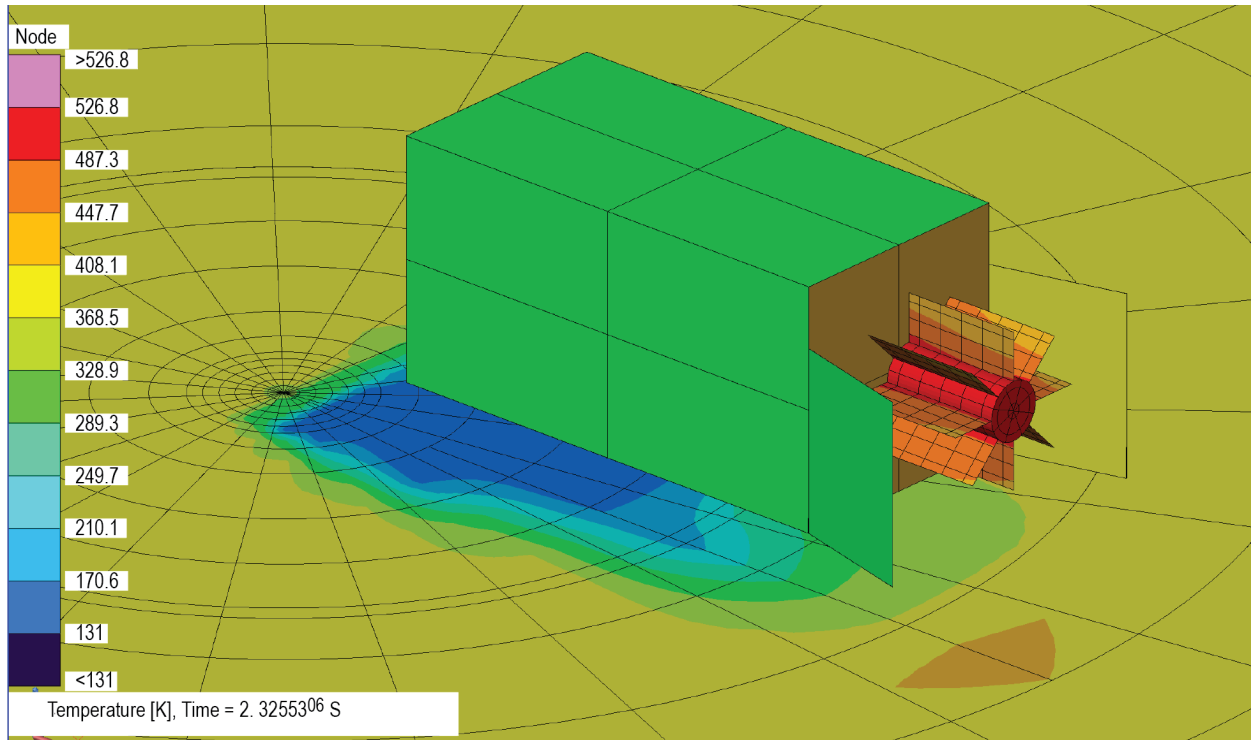


Figure C-14. Thermal modelling of MMRTG.

underside of the radiator in a serpentine configuration. The thermal switches provide the necessary isolation during the lunar night such that only 11 W of power (any combination of heating + internal dissipations) to maintain internal WEB components above -20°C . The radiator is shown to scale at the 1.1 m^2 baseline size.

Thermal Architecture—RPS Powered Option. The RPS thermal architecture affords a simpler design: The radiator can be located closer to the WEB internals and still maintain a largely unobstructed

view to space. A loop heat pipe is no longer necessary and thermal switches can be mounted directly to the radiator with a flexible thermal strap. There is less thermal isolation during the night, which drives a need for about 20 W of power (any combination of heating + internal dissipations) to maintain internal WEB components above -20°C . Figure C-20 shows the cut-away view of the WEB and Figure C-21 shows detail of the thermal switches mounted to the radiator.

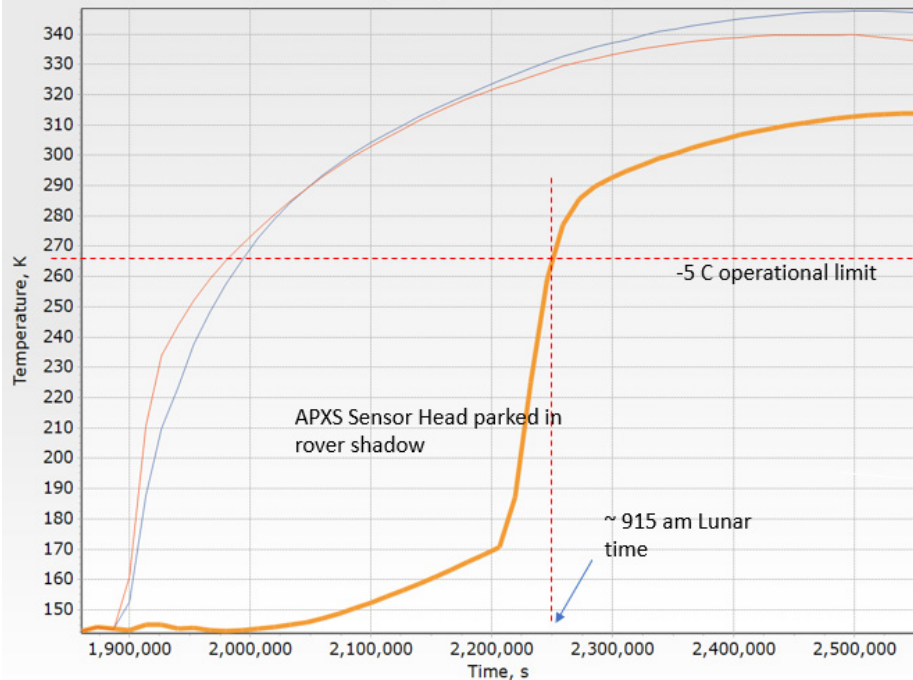


Figure C-16. APXS thermal response.

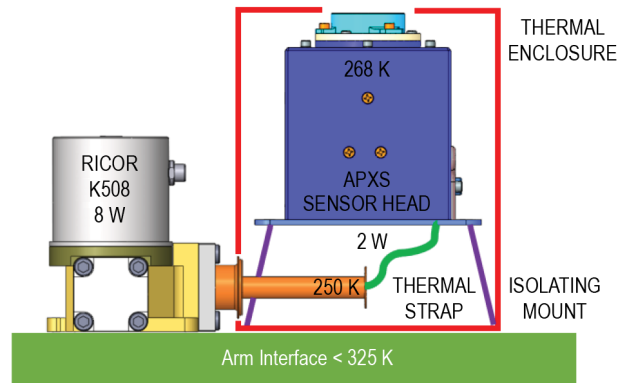


Figure C-17. APXS cryocooler configuration.

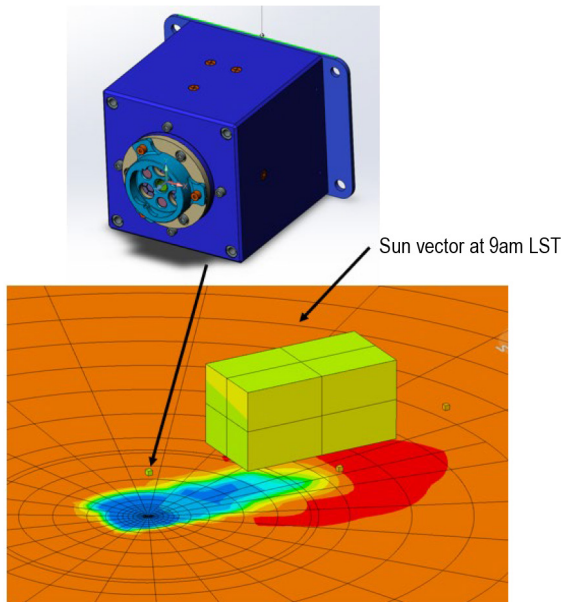


Figure C-15. APXS sensor thermal model.

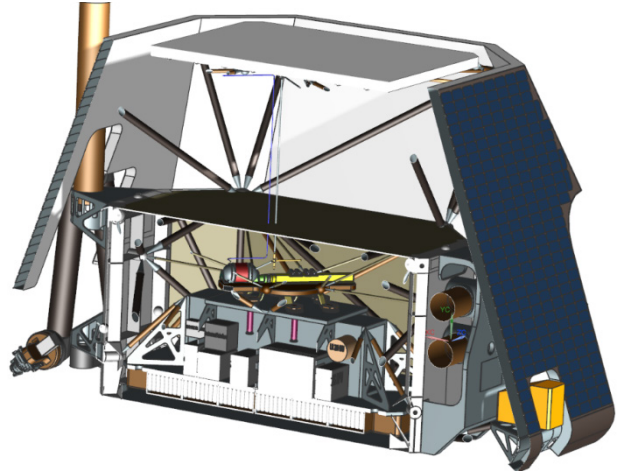
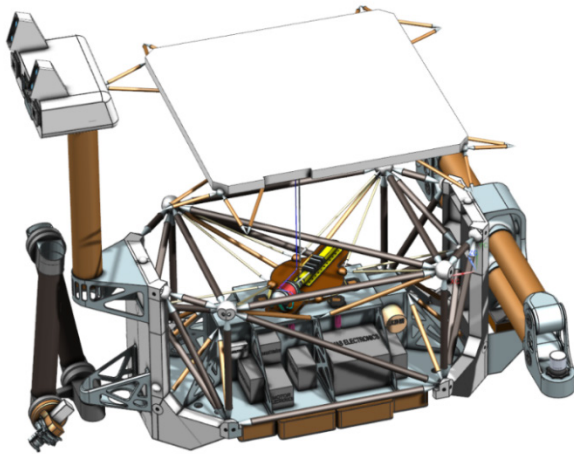


Figure C-18. Solar rover thermal system design overview (left) and cut-away including solar array (right).

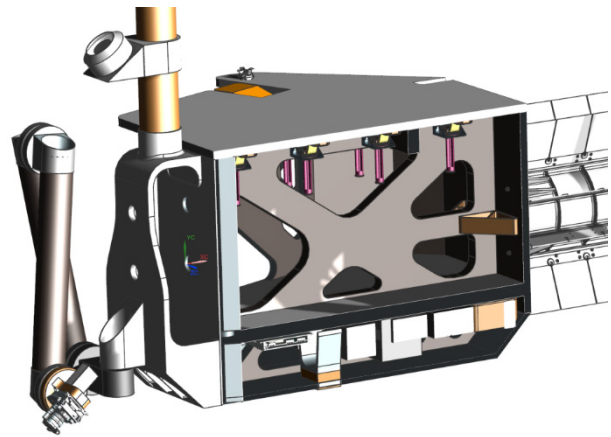
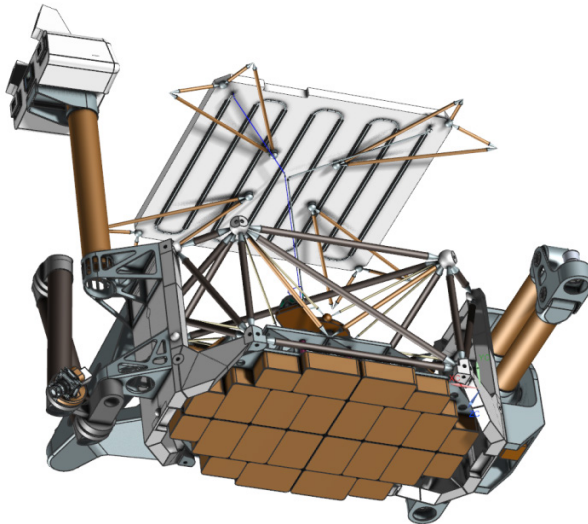


Figure C-20. Cut-away view showing RPS rover thermal design.

Figure C-19. Solar rover thermal design bottom view showing battery layout.

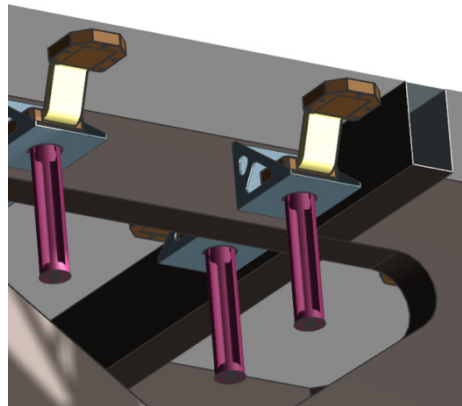


Figure C-21. Thermal switch mounting detail.



C.4 ARCHITECTURE

Both versions of the rover (Figure C-22) have an architecture based around a central warm electronics box (WEB) chassis which carries most of the avionics and payload electronics and which is connected to the wheels via a rocker and two stationary outriggers. In the RTG version, the rocker is on the front of the rover (where the camera head and robotic arm are), and the outriggers connect to the rear wheels; on the solar version, it is the reverse.

The rover is supported on four 80-cm compliant mesh wheels, and each is connected via a C-shaped structure to a steering actuator as well as a drive actuator. The rover belly has 63 cm of clearance on flat terrain, and the rocker provides stability over uneven terrain.

Solar Version

The solar-powered rover is covered by a fixed solar array with views 360 degrees around the rover, such that at least 1.3 m² of array surface is illuminated independent of rover orientation or local solar time.

Aside from this array, the solar-powered rover architecture is distinct from the RTG version largely due to thermal requirements and the large mass of batteries needed. The WEB chassis carries the payload on a central honeycomb structure with embedded heat pipes to carry waste heat from the payload to the thermal switches. This structure is supported by composite struts (each greater than 6" long) in order to thermally isolate it. Long composite struts also support the thermal collection plate to the evaporator. The evaporator is then connected to the radiator via a loop heat pipe, which allows for further thermal isolation due to the distance between the evaporator and the radiator. The solar-panel shell and radiator are also supported by composite struts.

The batteries constitute most of the mass inside the WEB, so they are located on the underside of the thermal structure that also carries avionics and payload. There is a lightweight bottom cover to shield the batteries from thermal radiation from the surface and from debris.

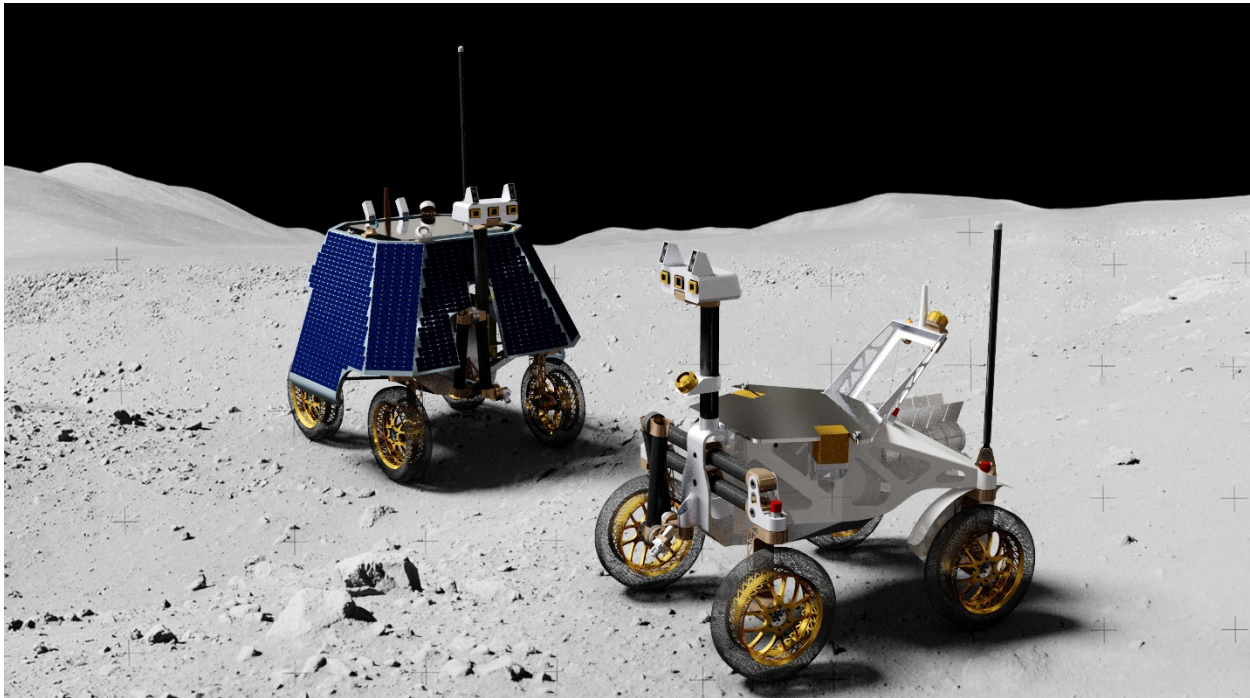


Figure C-22. Intrepid configurations for solar- (left) and RTG- (right) powered rovers.

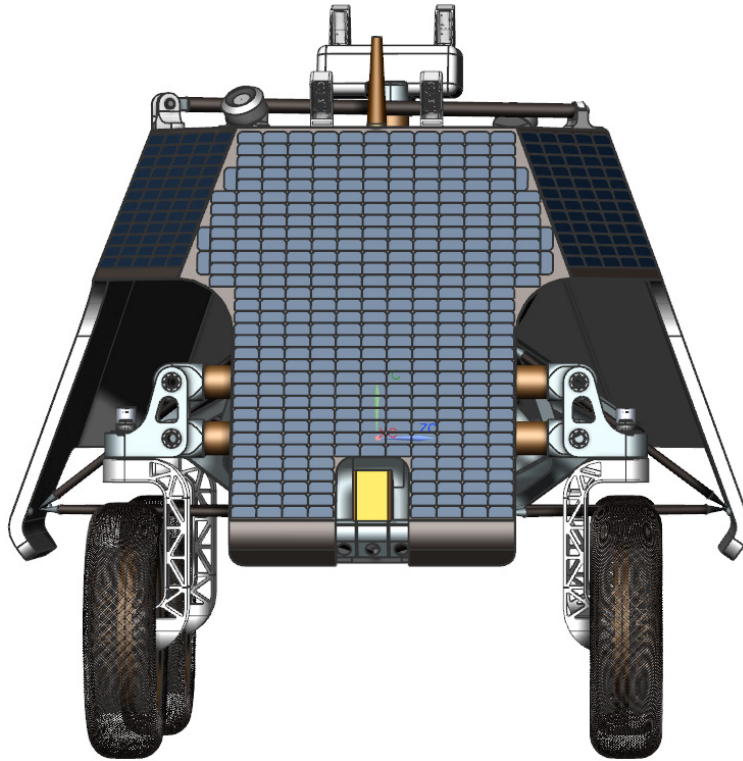


Figure C-23. Rear view of the rover showing ARMAS, LGAs, and rear navigation cameras.

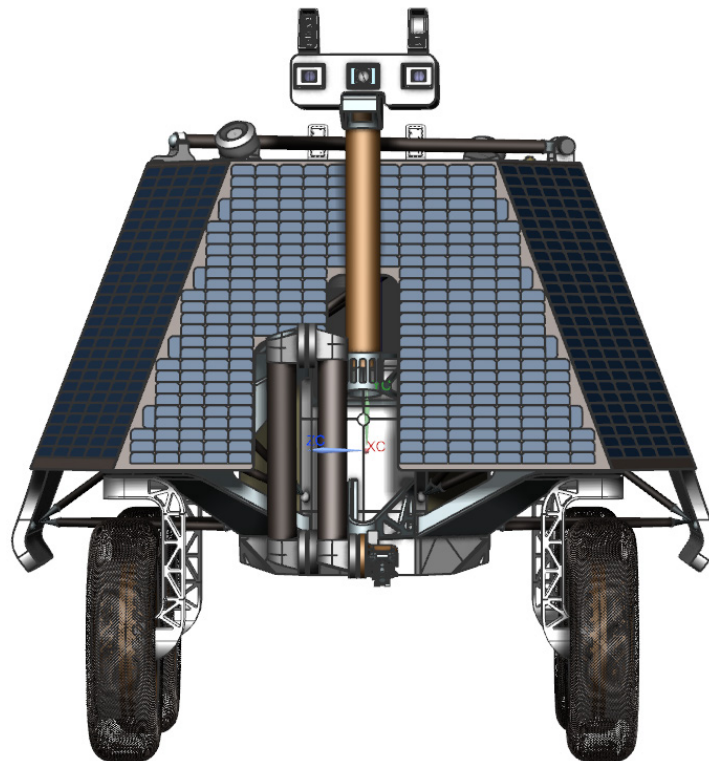


Figure C-24. Front view of the rover with the camera head and robotic arm.

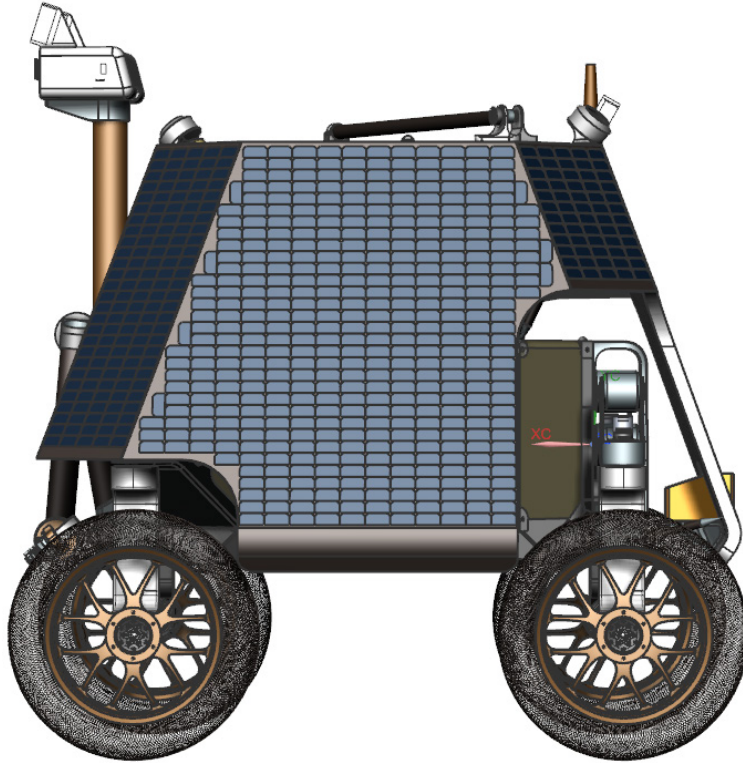


Figure C-25. Left side view of the rover.

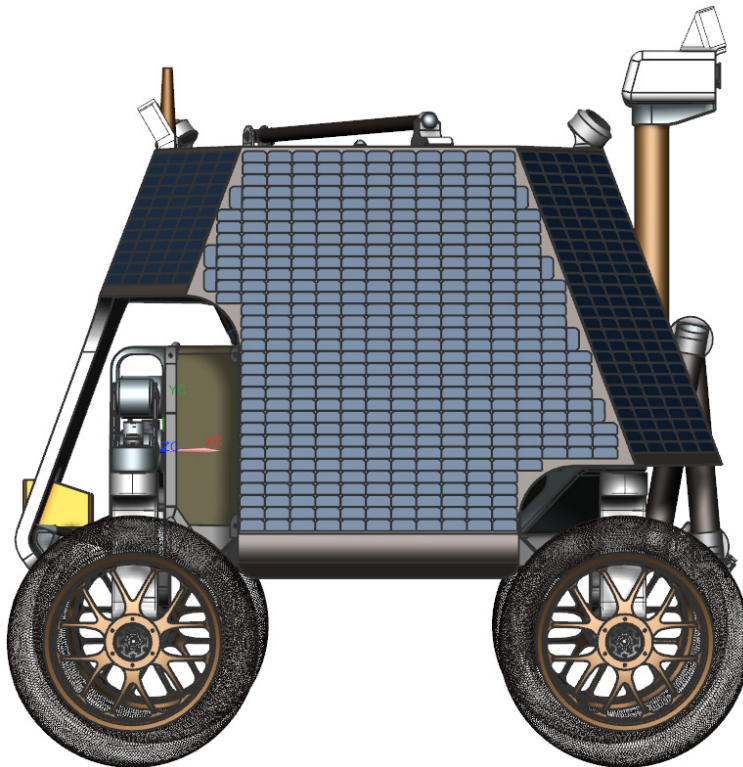


Figure C-26. Right side view of the rover.

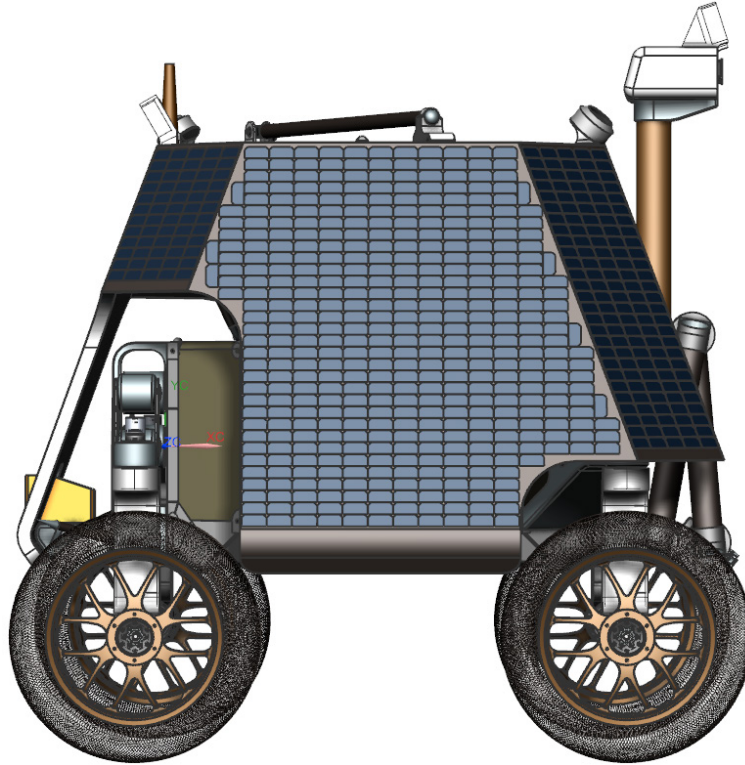


Figure C-27. Isometric view of the rover with the magnetometer boom deployed.

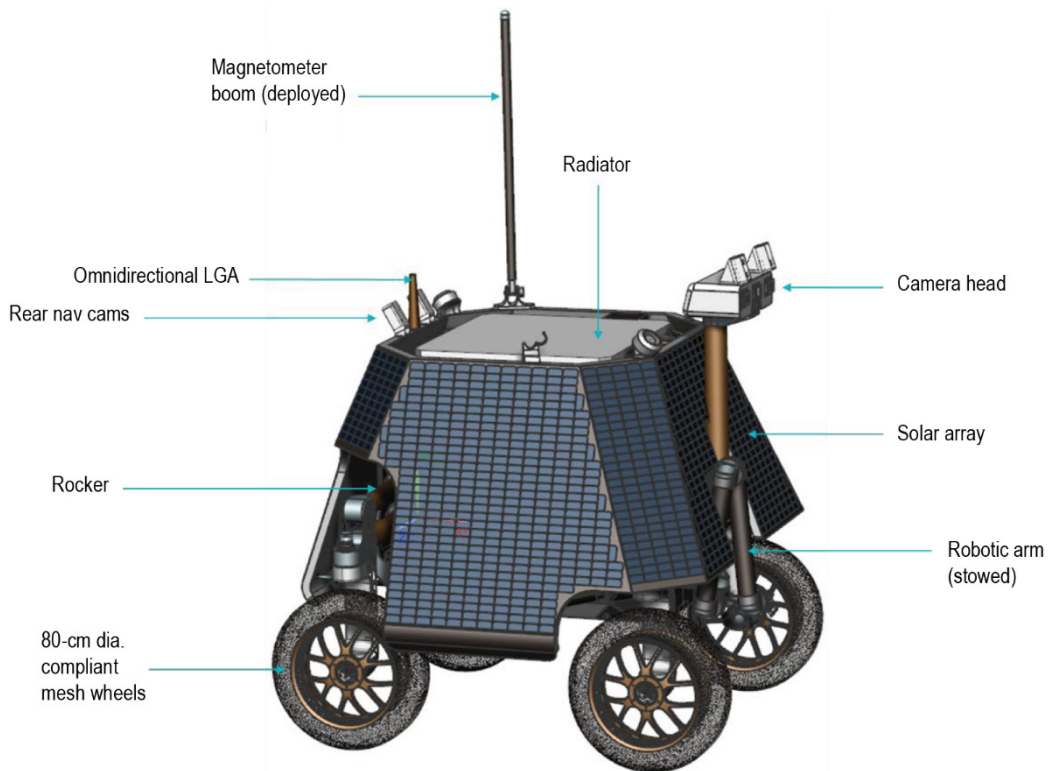


Figure C-28. Isometric view of the rover.

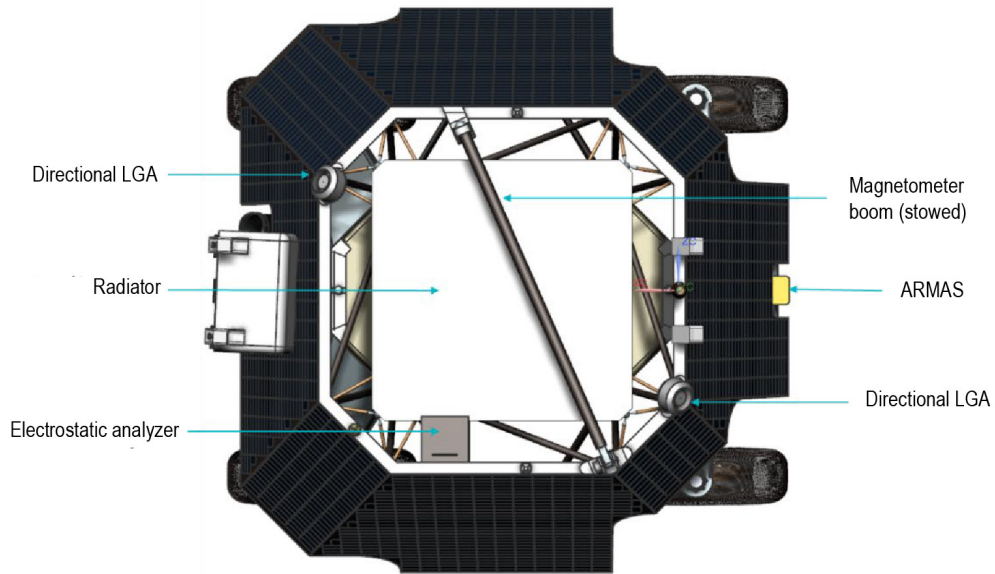


Figure C-29. Top view of the rover.

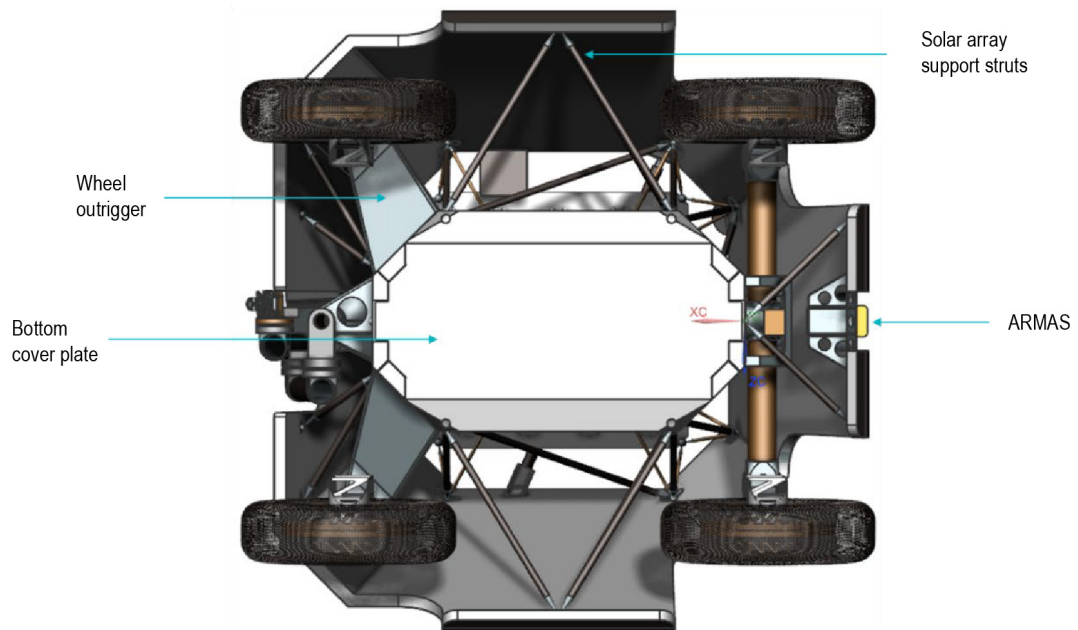


Figure C-30. Bottom view of the rover.

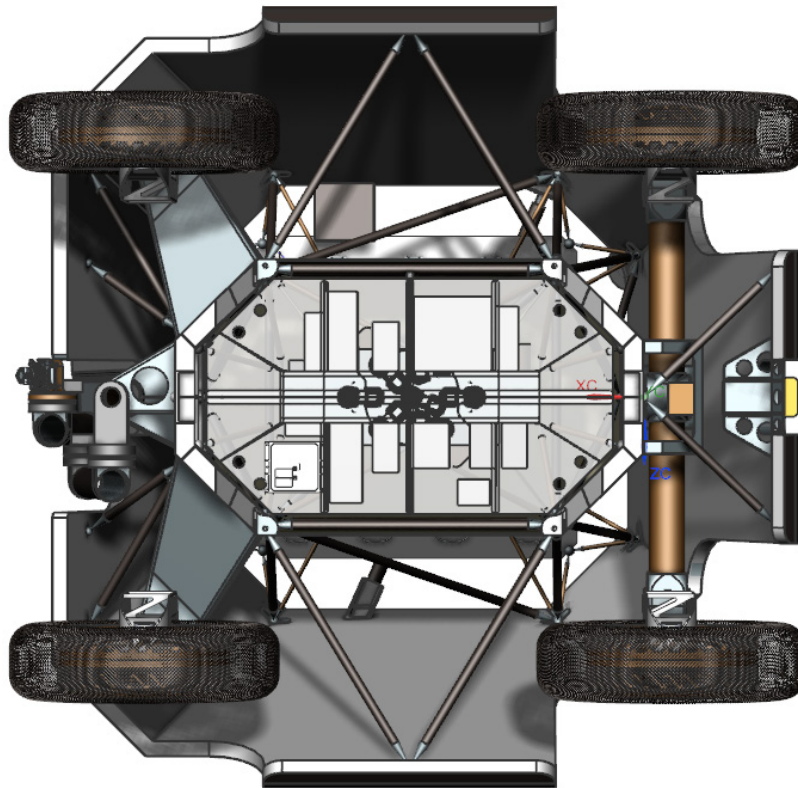


Figure C-31. Bottom view of the rover with the avionics shown.

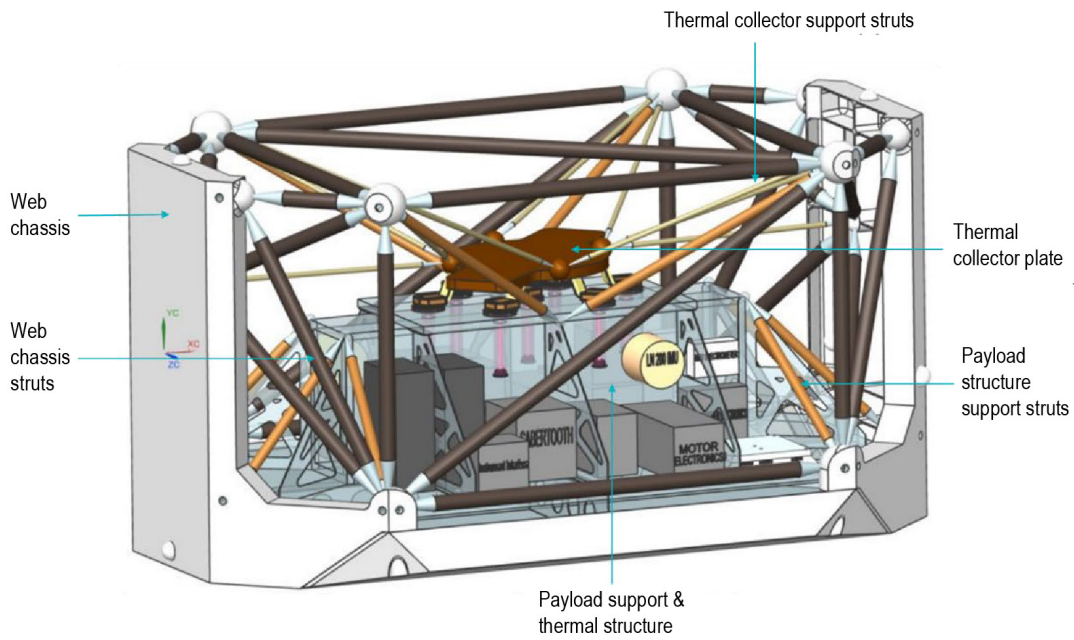


Figure C-32. Isometric view of the WEB structure.

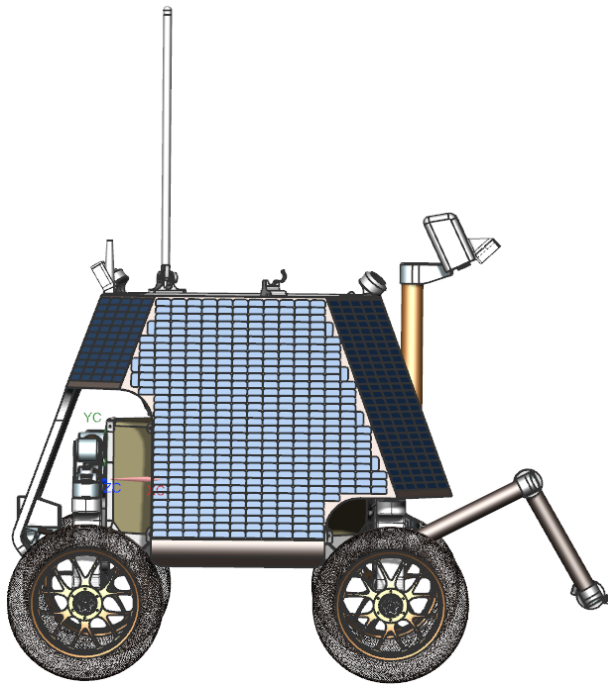


Figure C-33. Right side view of the rover with the arm extended and the camera head pointed down.

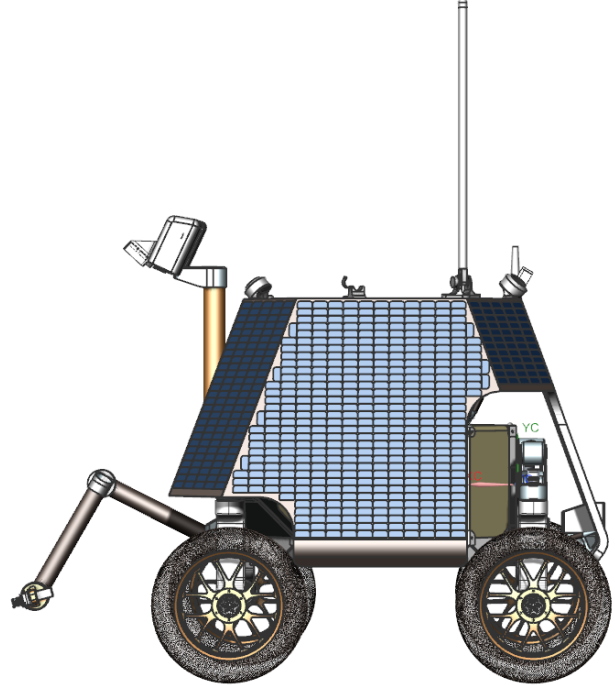


Figure C-34. Left side view of the rover with the arm extended and the camera head pointed down.

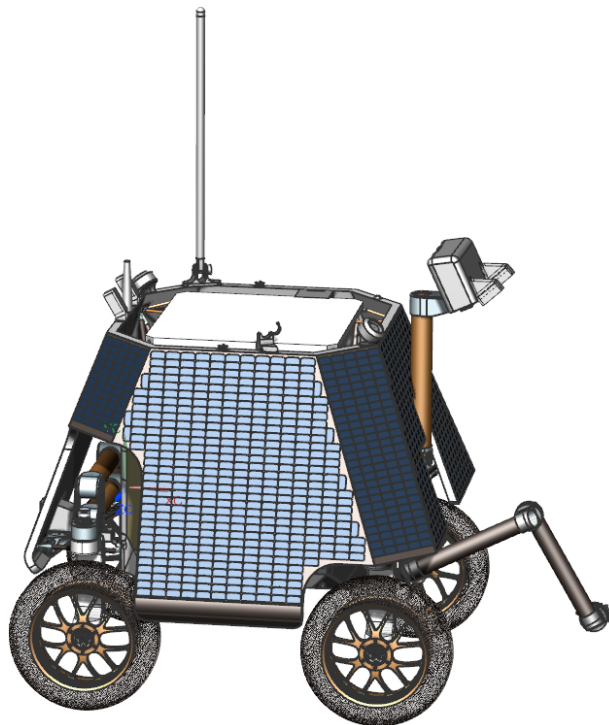


Figure C-35. Isometric view of the rover with the arm extended and the camera head pointed down.

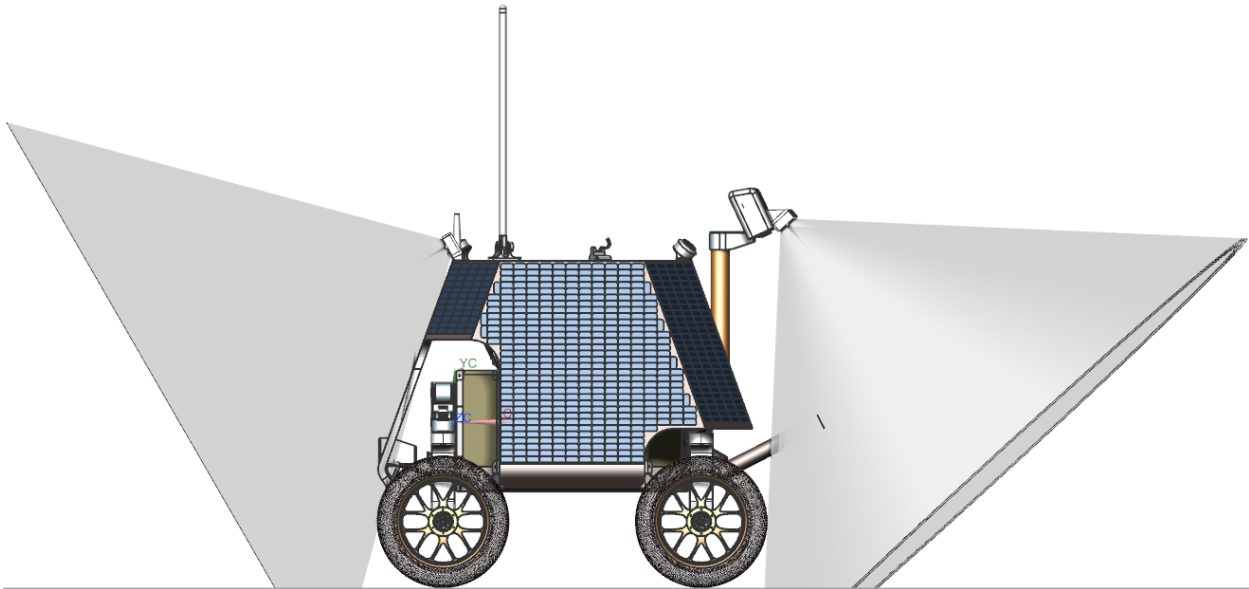


Figure C-36. Right side view of the rover with the navigation camera FOVs shown (front and rear).

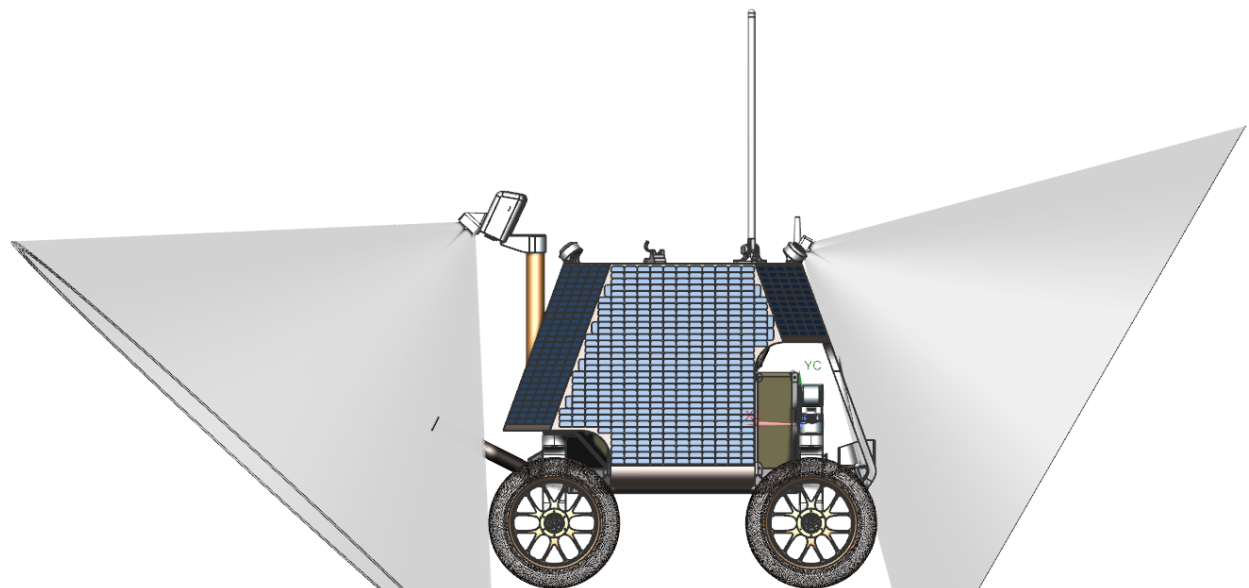


Figure C-37. Left side view of the rover with the navigation camera FOVs shown (front and rear).

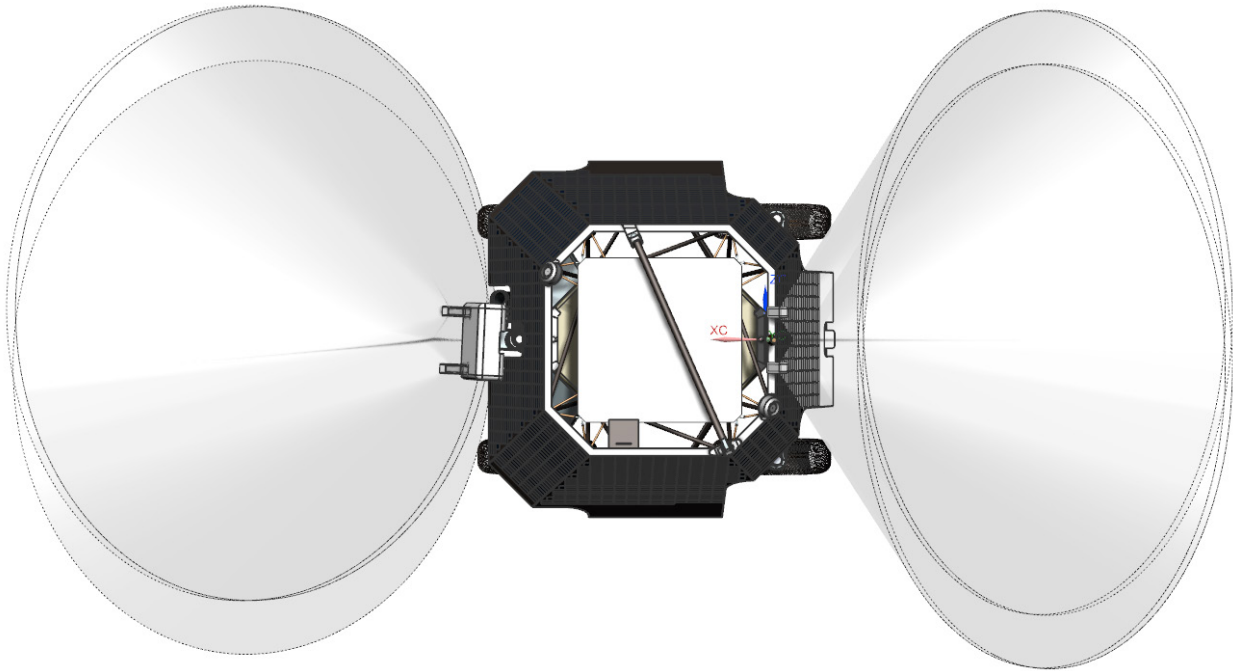


Figure C-38. Top view of the rover with the navigation camera FOVs shown (front and rear).

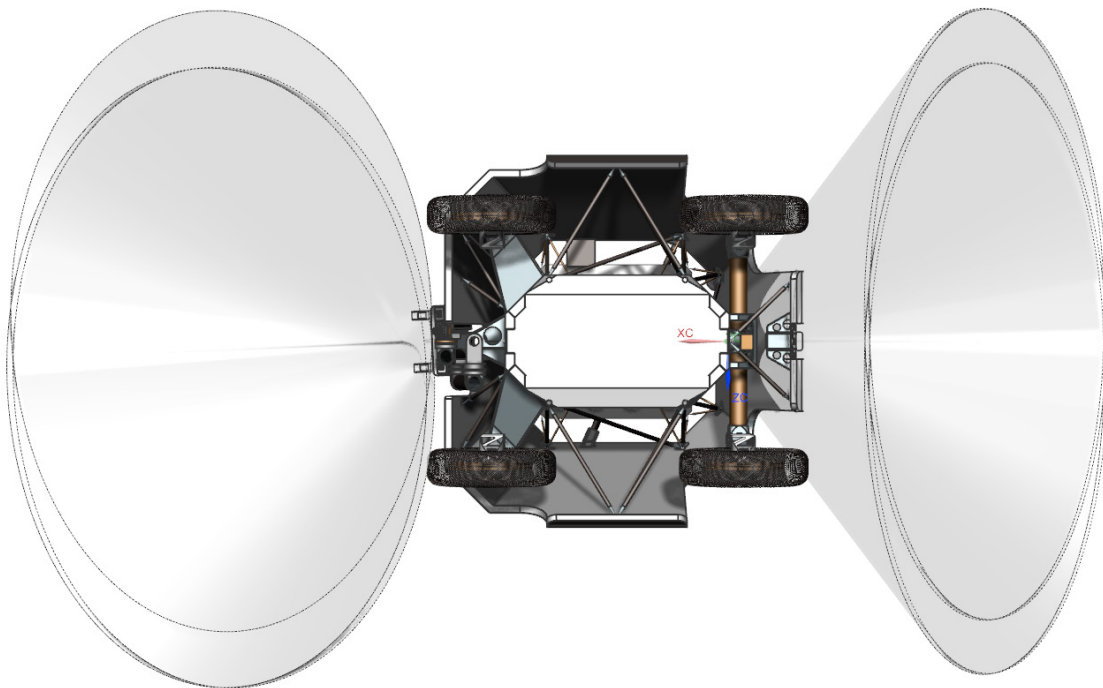


Figure C-39. Bottom view of the rover with the navigation camera FOVs shown (front and rear).

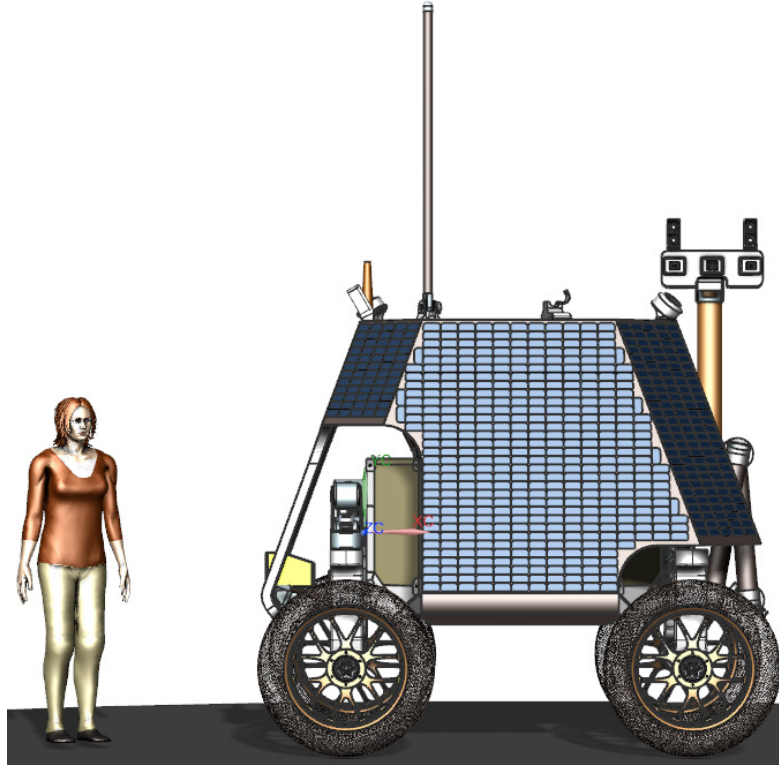


Figure C-40. Right side view of the rover with a human shown for scale.

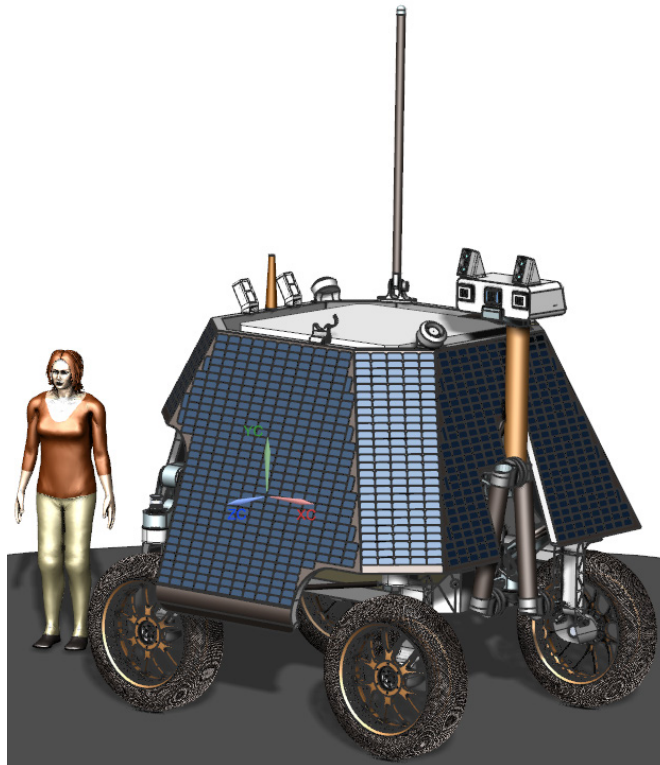


Figure C-41. Isometric view of the rover with a human shown for scale.

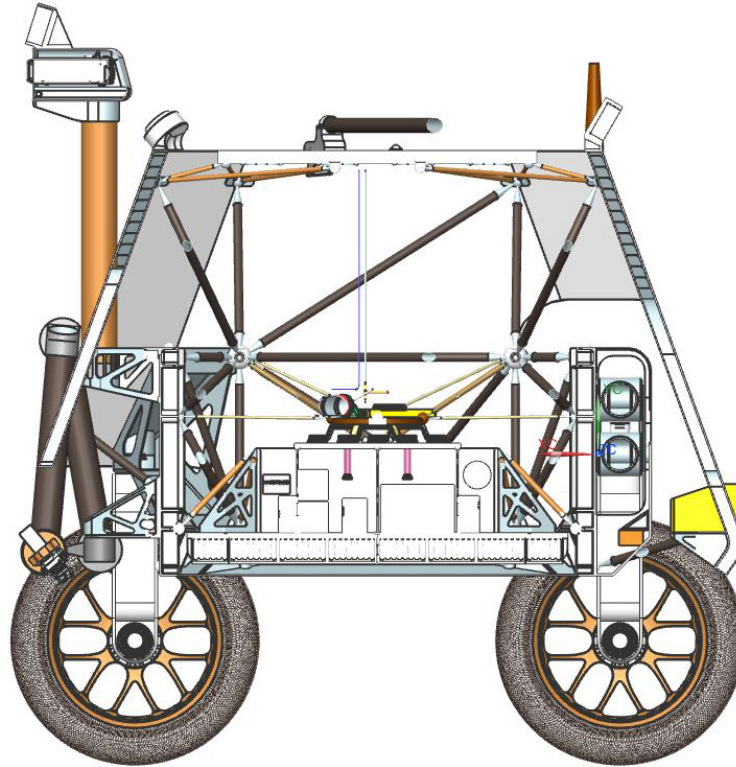


Figure C-42. Left cross-sectional side view of the rover with the payload and thermal system shown.

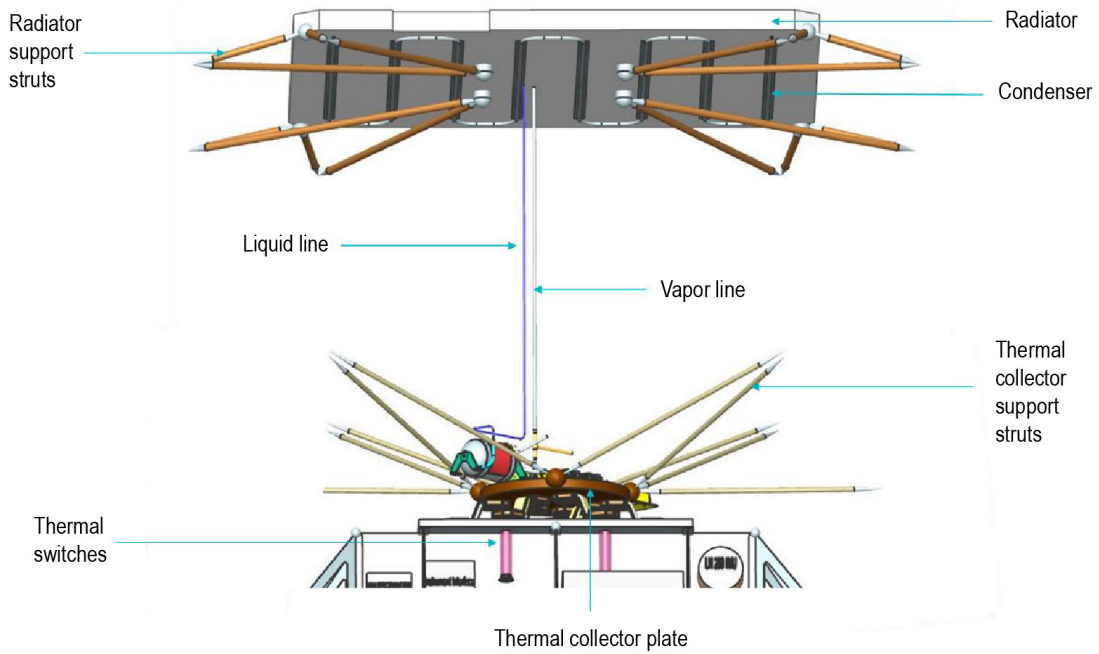


Figure C-43. View of the thermal system.

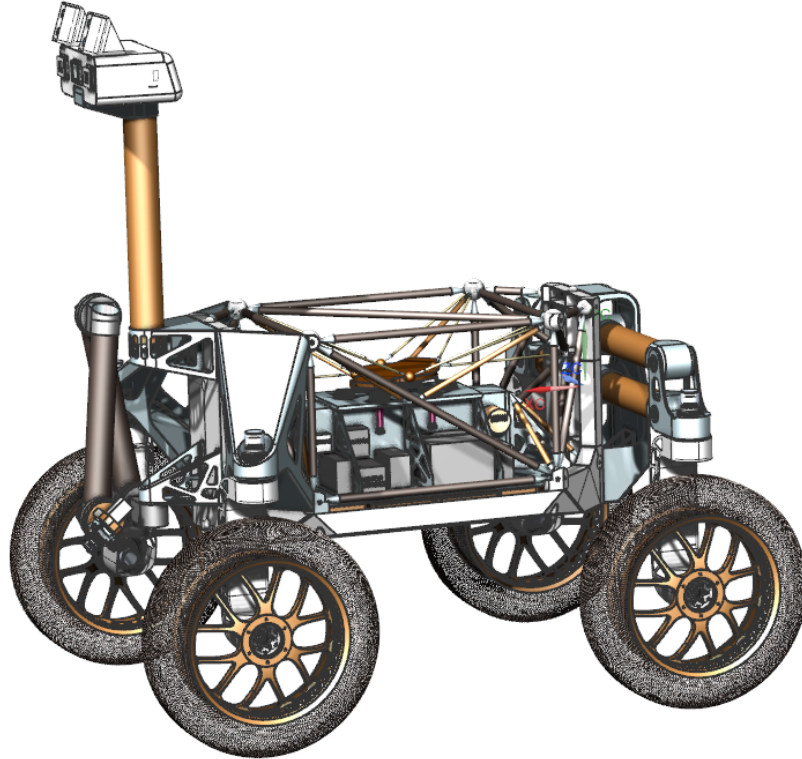


Figure C-44. Isometric view of the rover without the array or MLI.

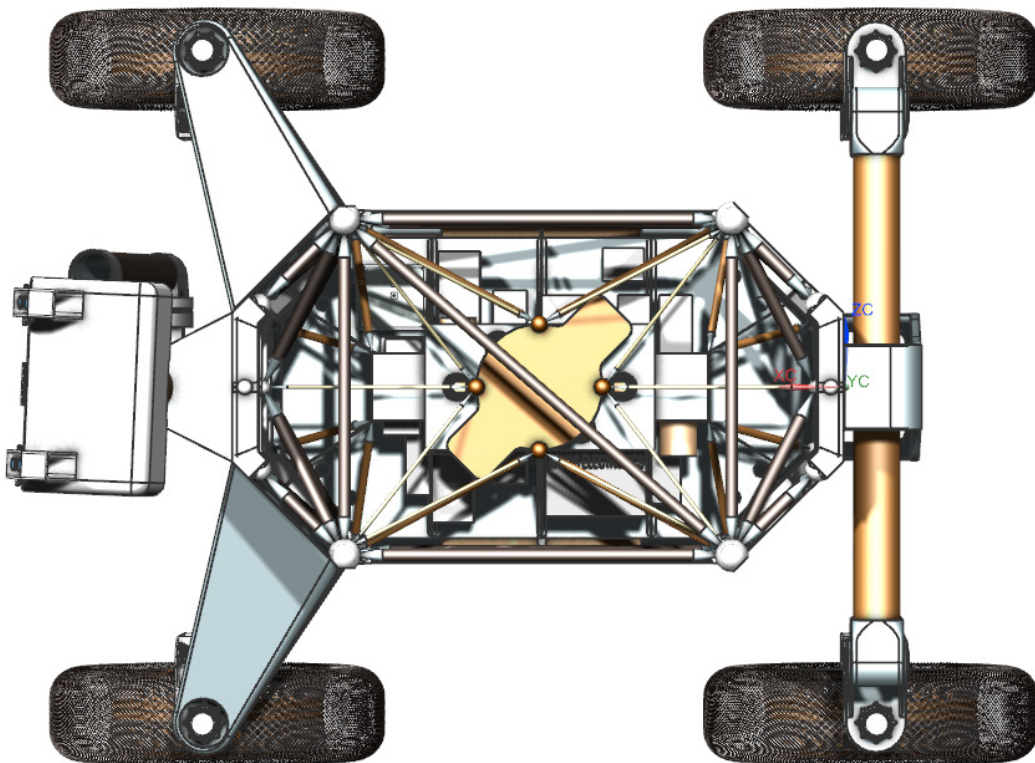


Figure C-45. Top view of the rover with the thermal collector plate and payload shown.

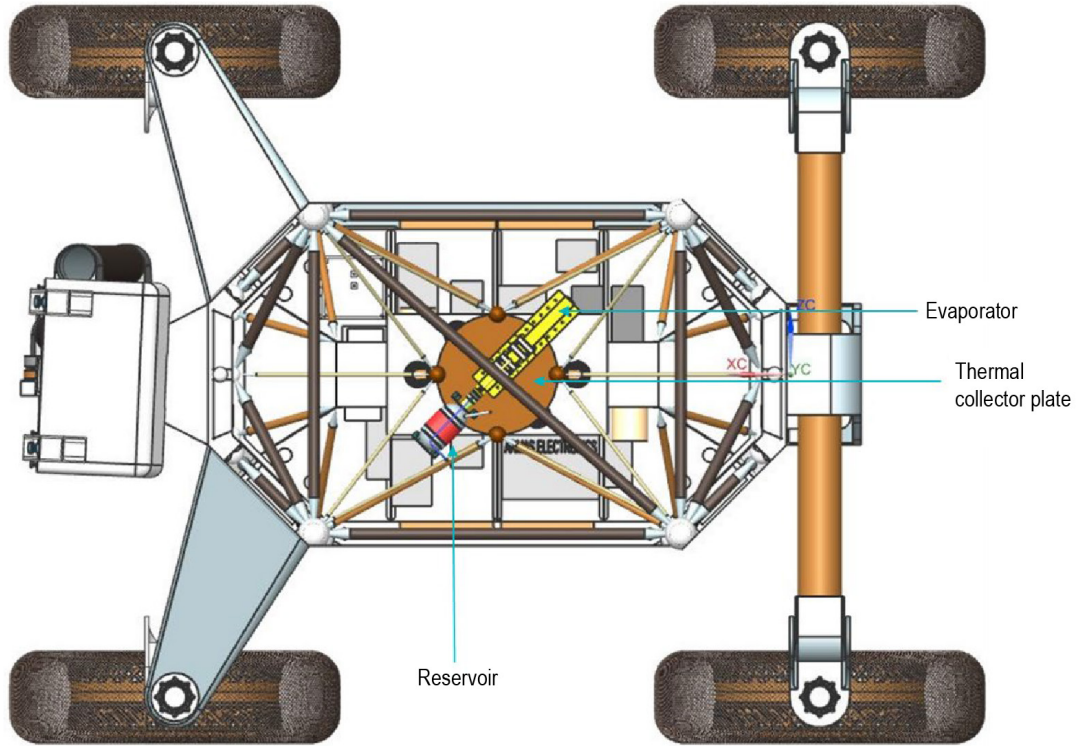


Figure C-46. Top view of the rover with the payload, evaporator, reservoir, and thermal collector plate.

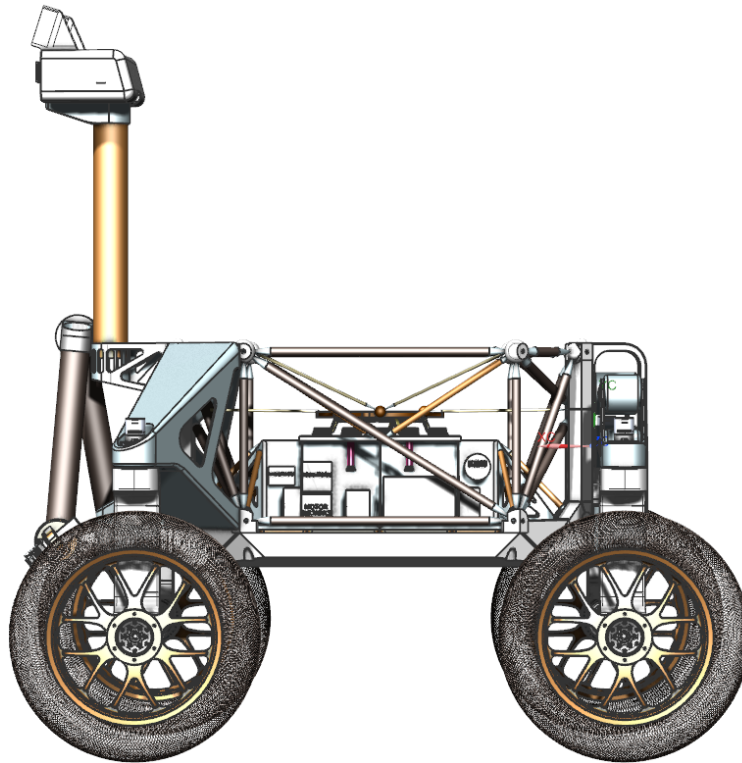


Figure C-47. Left side view of the rover with the payload, thermal collector plate, and heat switches.

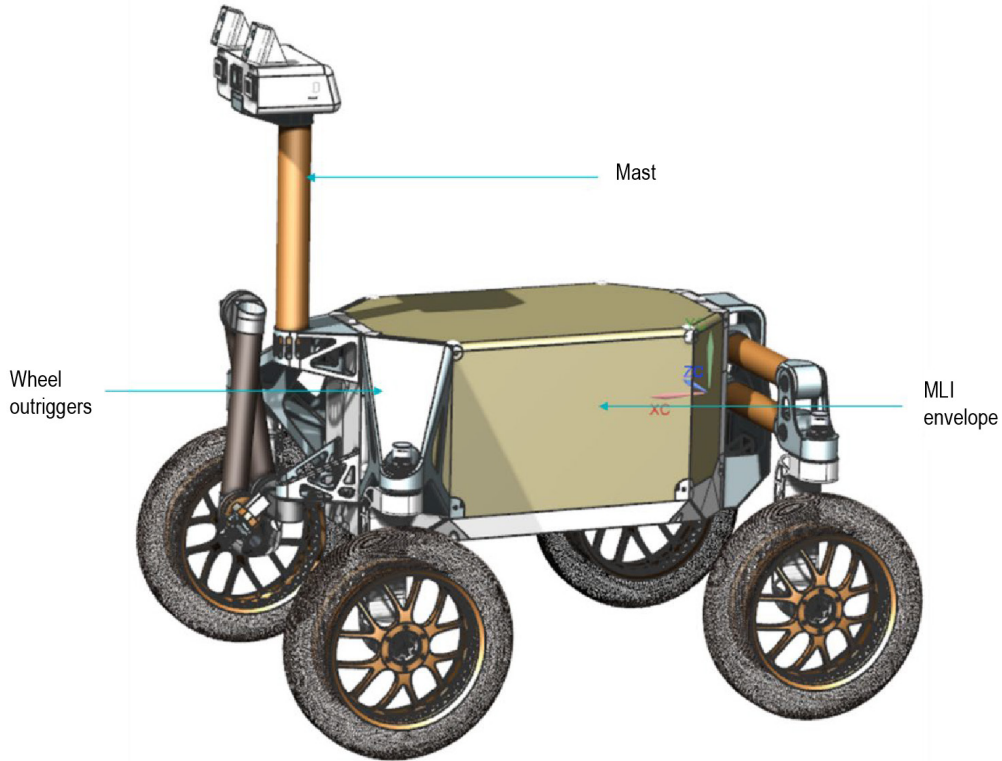


Figure C-48. Isometric view of the rover without the solar array but with MLI.

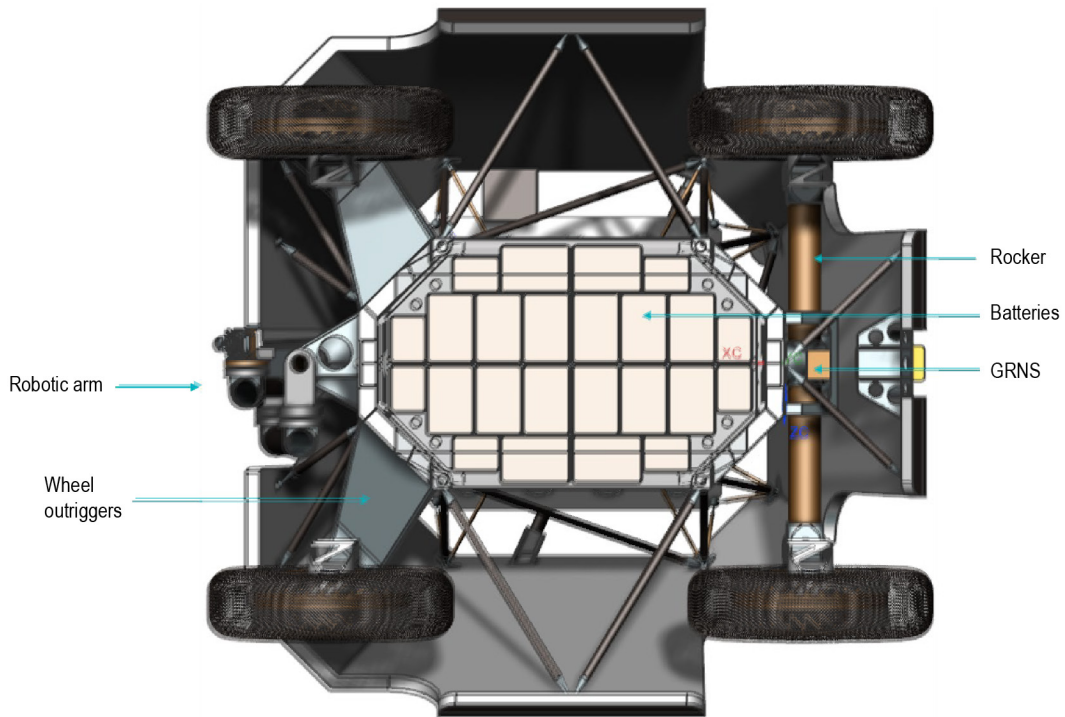


Figure C-49. Bottom view of the rover showing the batteries.

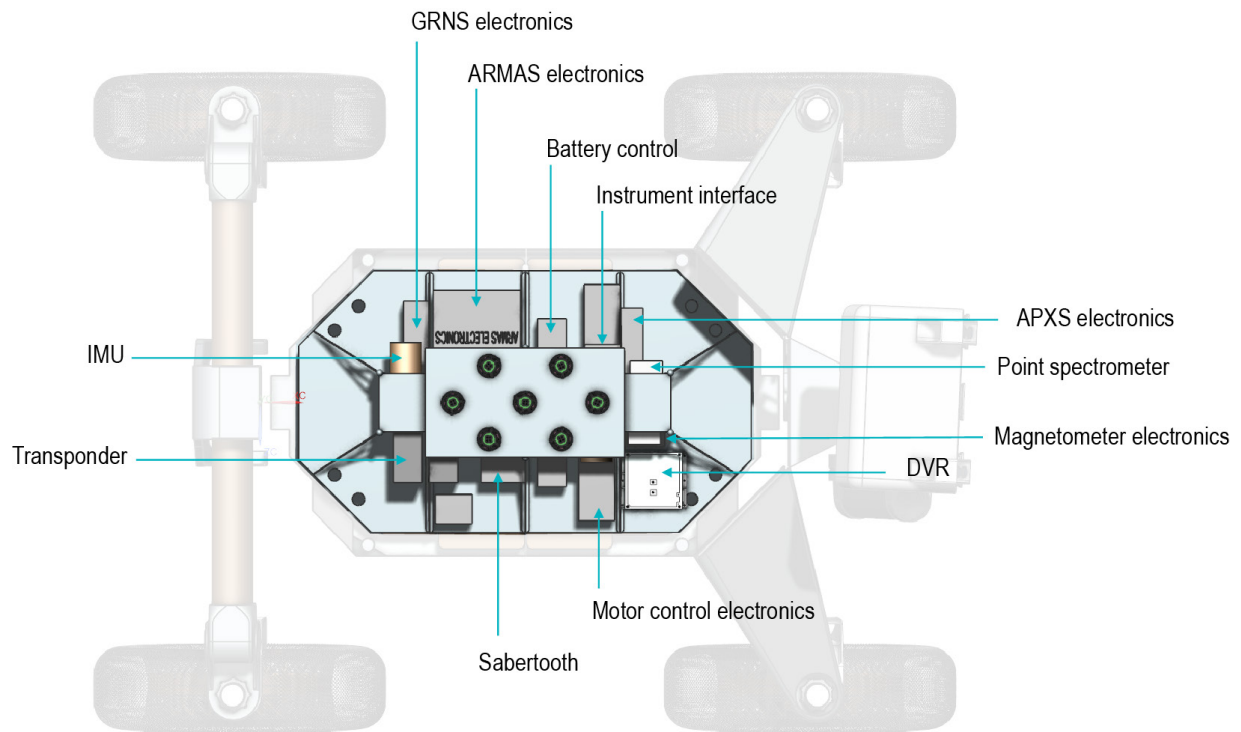


Figure C-50. Top view of the payload.



RTG Version

The RTG-powered rover has a simpler structural design than the solar-powered version. The WEB is a composite structure that is mostly hollow and has the internal payload and avionics on the underside. The RTG is attached to the back, and there is a central structural “spine” from the RTG to the front of the rover to provide additional support.

Because the RTG can provide power at all times, there is no need for a large number of batteries, and thermal isolation is less of a concern because systems remain powered and heaters can be used during the night. As in the solar version, the rover avionics deck is connected via heat pipes to the thermal switches, but these thermal

switches are connected directly (via thermal straps) to the radiator, rather than going through a loop heat pipe as in the solar version. The internal avionics on the bottom of the WEB is shielded with a lightweight bottom cover in the same manner as the solar version.

The back wheels of the RTG rover also are shielded from RTG radiant heat by thermal shields.

Because the RTG rover is not as tall as the solar-powered version (since there is no solar panel structure and the radiator does not need to be as high to remain thermally isolated from the WEB), some of the instruments that require the height, such as the rear LGAs and navigation cameras, are mounted on a lightweight aluminum structure on the back of the rover.

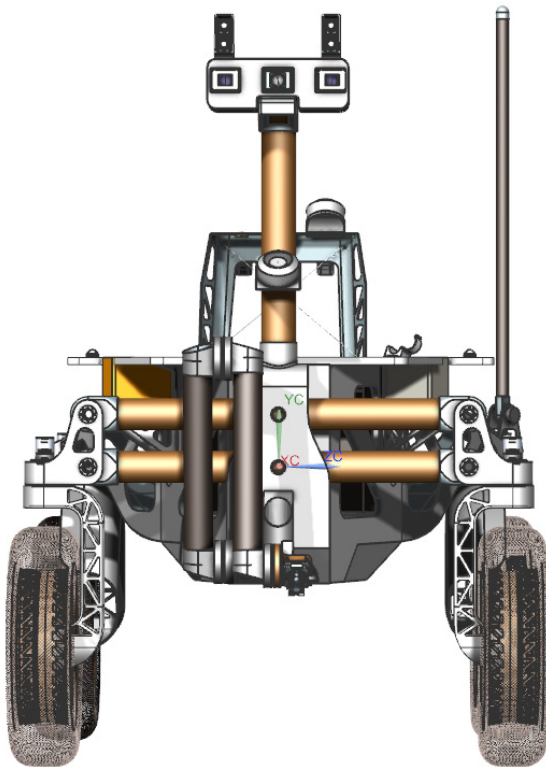


Figure C-51. Front view of the rover showing the camera head and robotic arm.

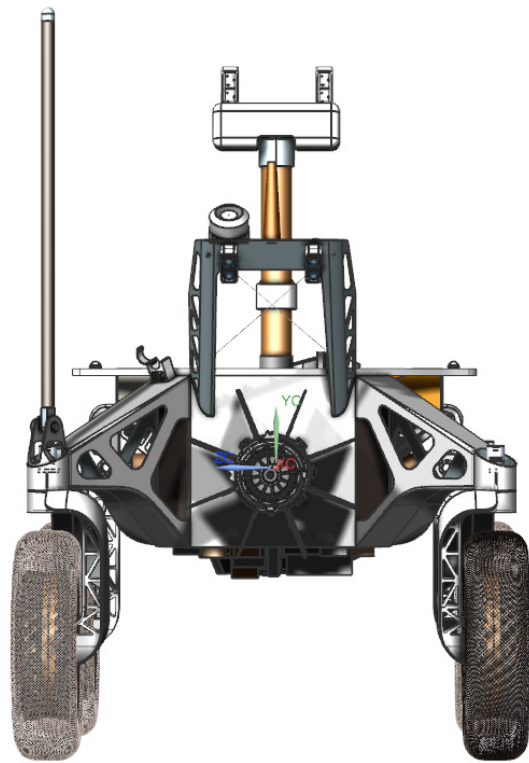


Figure C-52. Rear view of rover showing LGAs and navigation cameras.

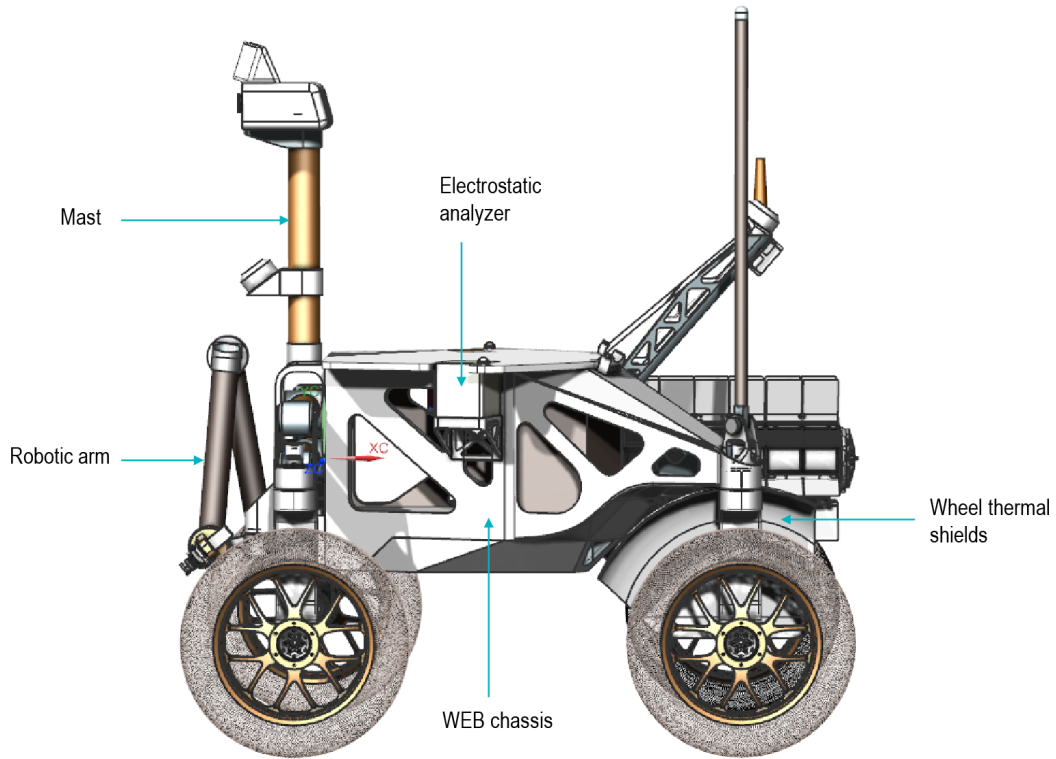


Figure C-53. Left side view of the rover.

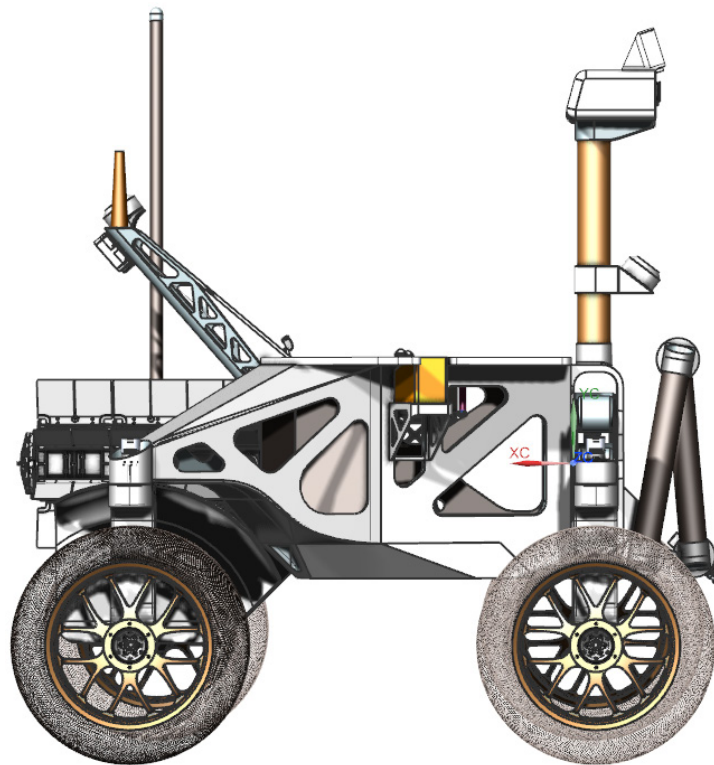


Figure C-54. Right side view of the rover.

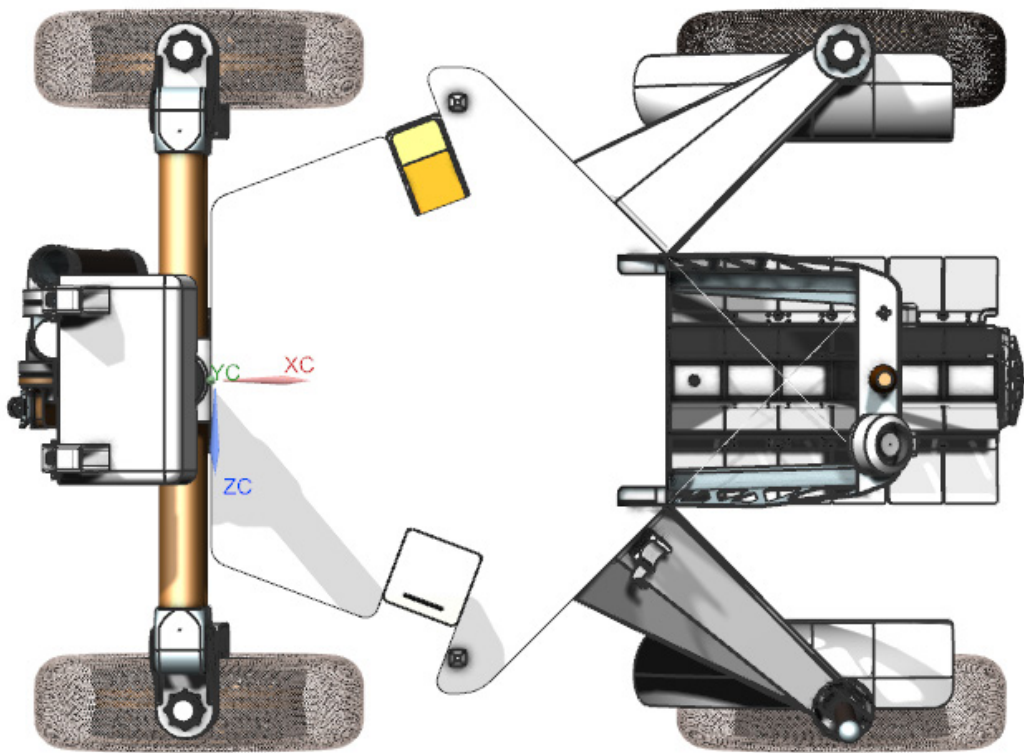


Figure C-55. Top view of the rover showing the radiator.

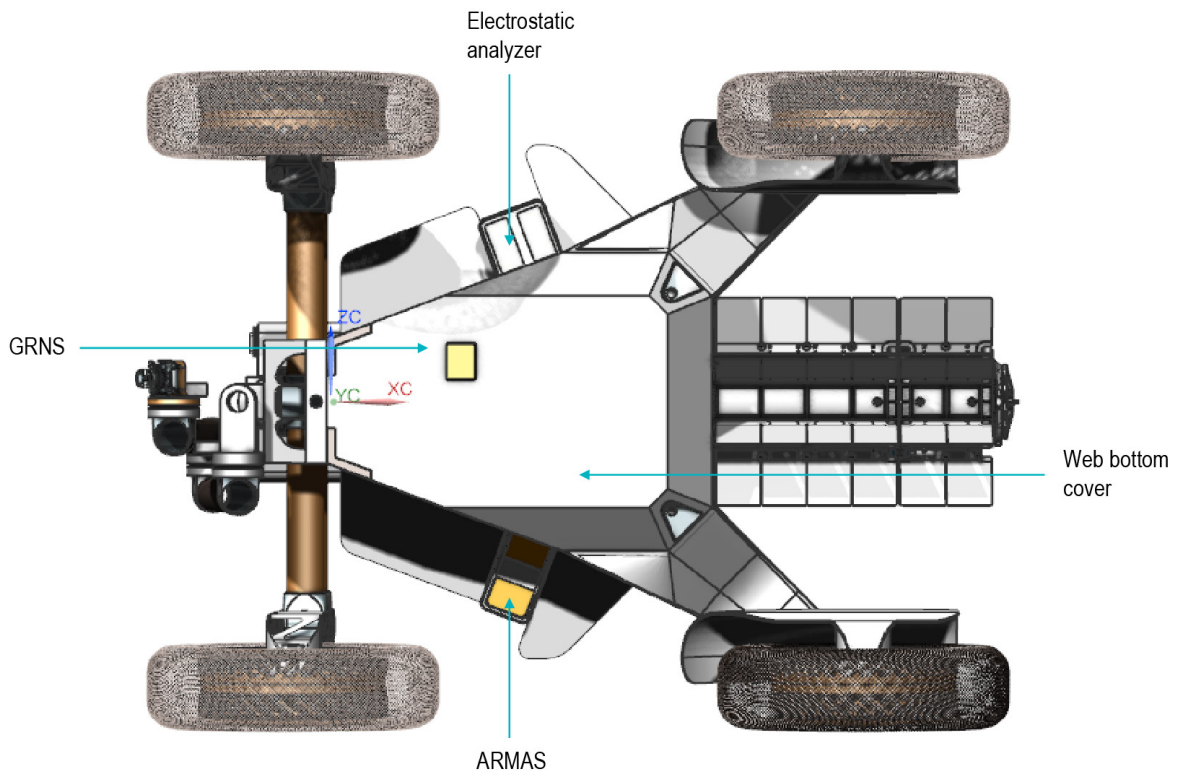


Figure C-56. Bottom view of the rover.

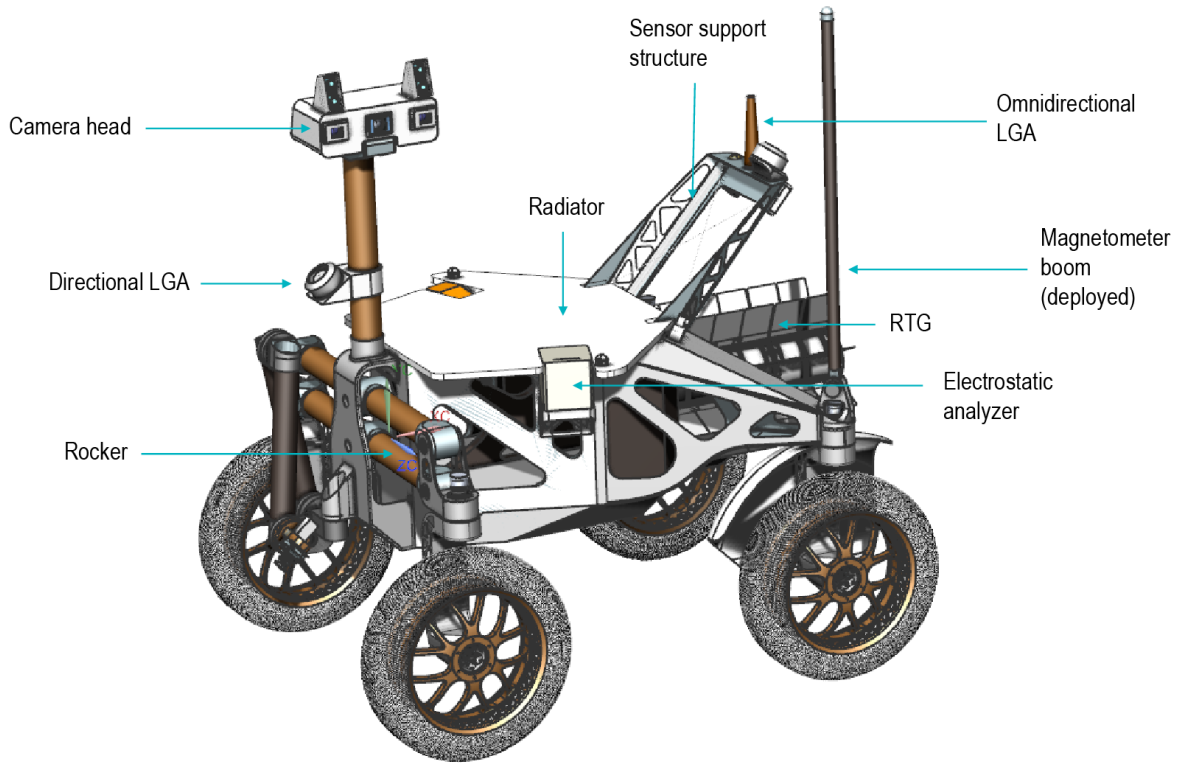


Figure C-57. Isometric view of the rover.

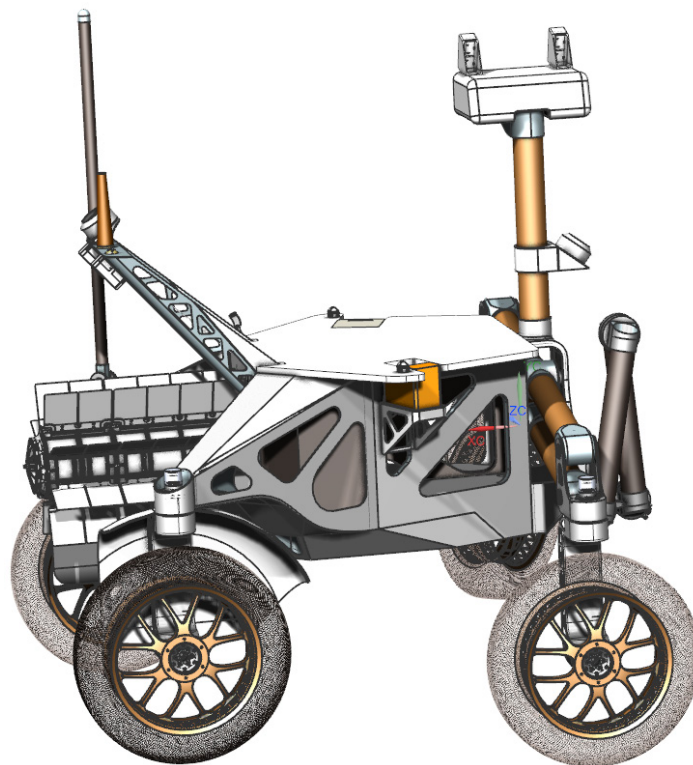


Figure C-58. Isometric view of the rover.

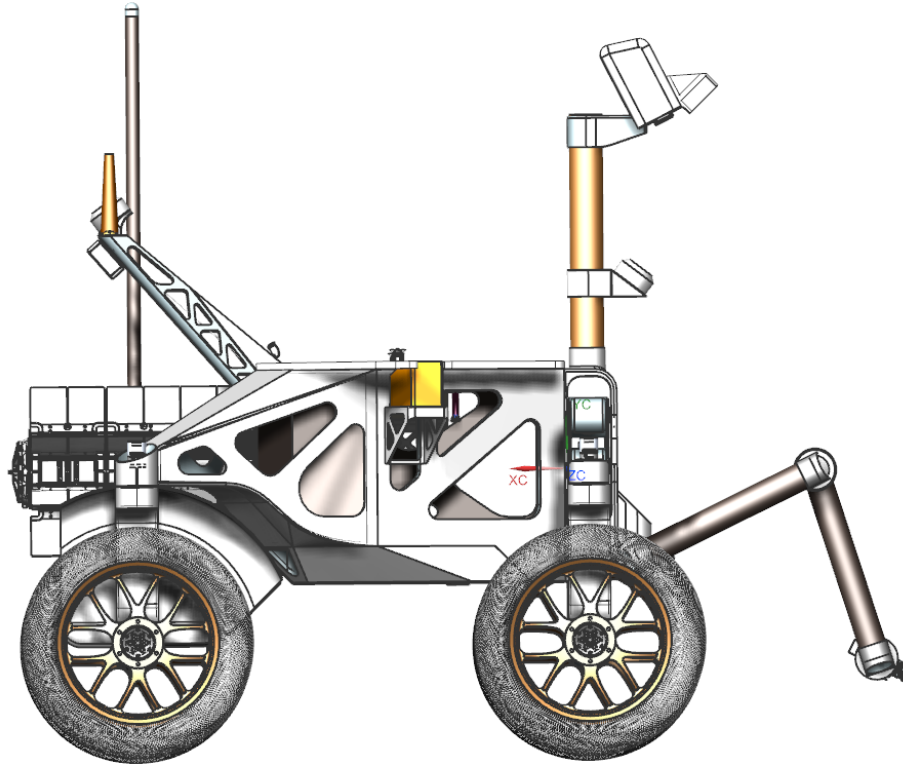


Figure C-59. Right side view of the rover with the arm extended and the camera head pointed down.

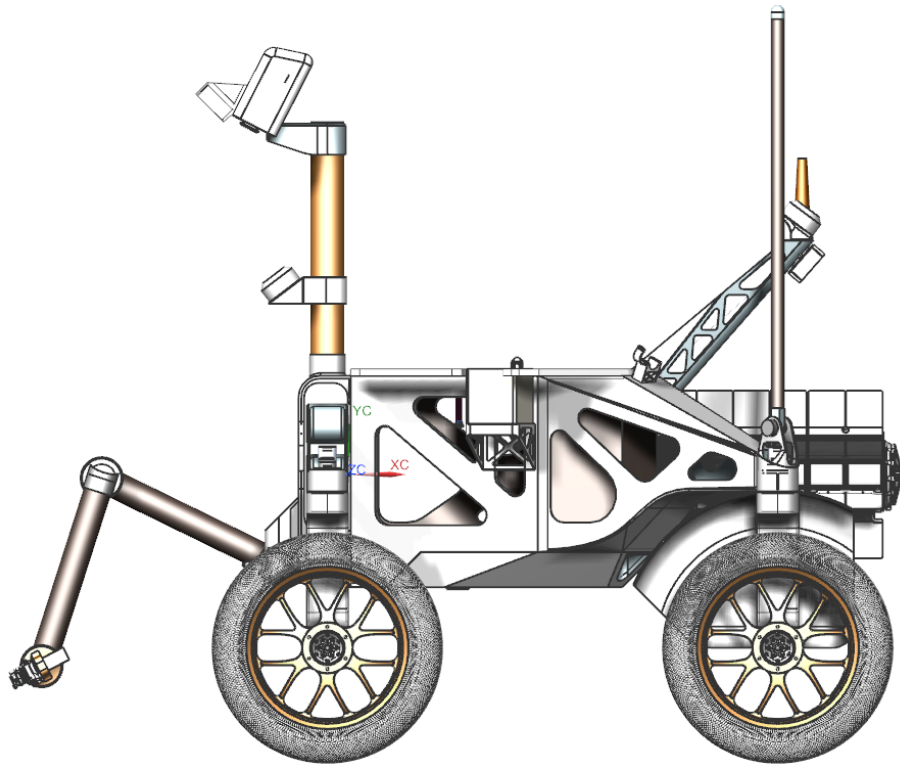


Figure C-60. Left side view of the rover with the arm extended and the camera head pointed down.

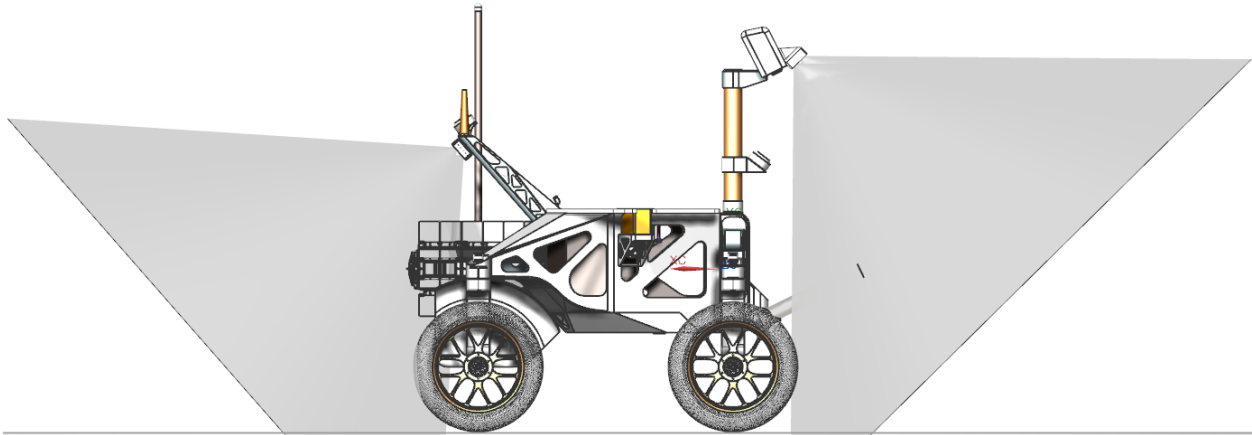


Figure C-61. Right side view of the rover with the navigation camera FOVs shown (front and rear).

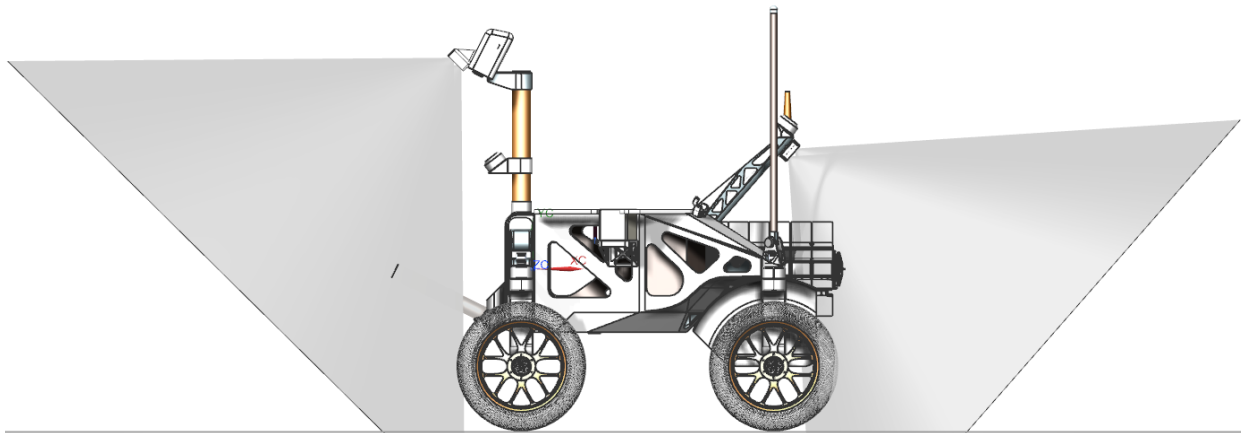


Figure C-62. Left side view of the rover with the navigation camera FOVs shown (front and rear).

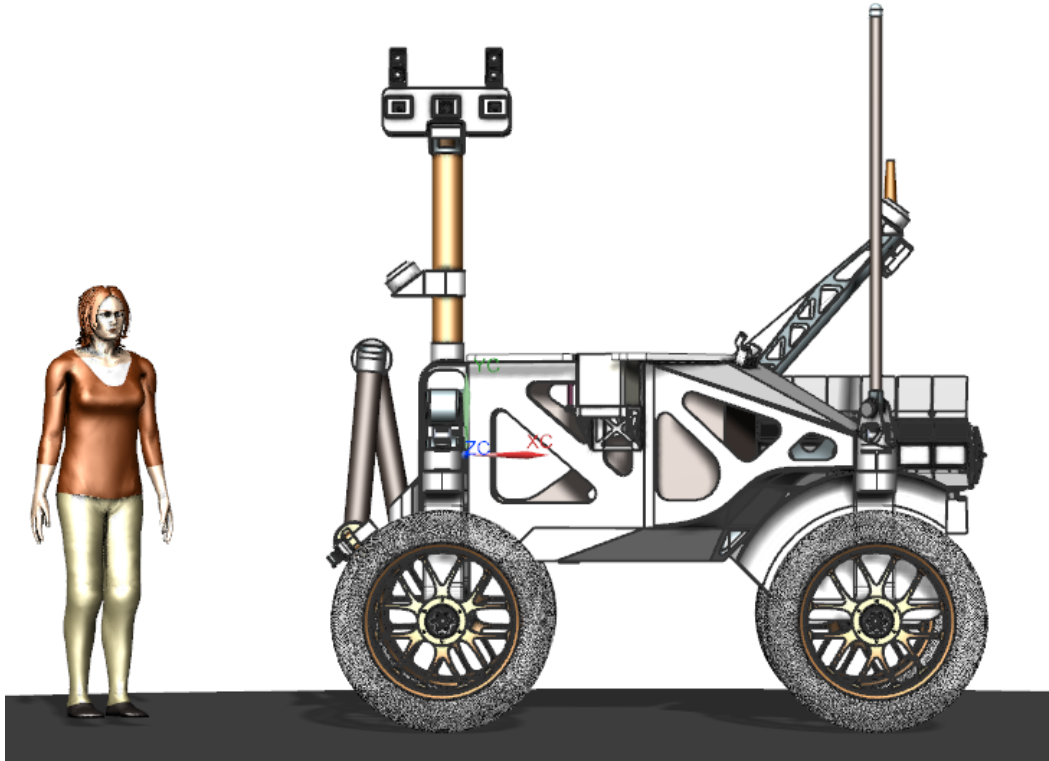


Figure C-63. Left side view of the rover with a human shown for scale.

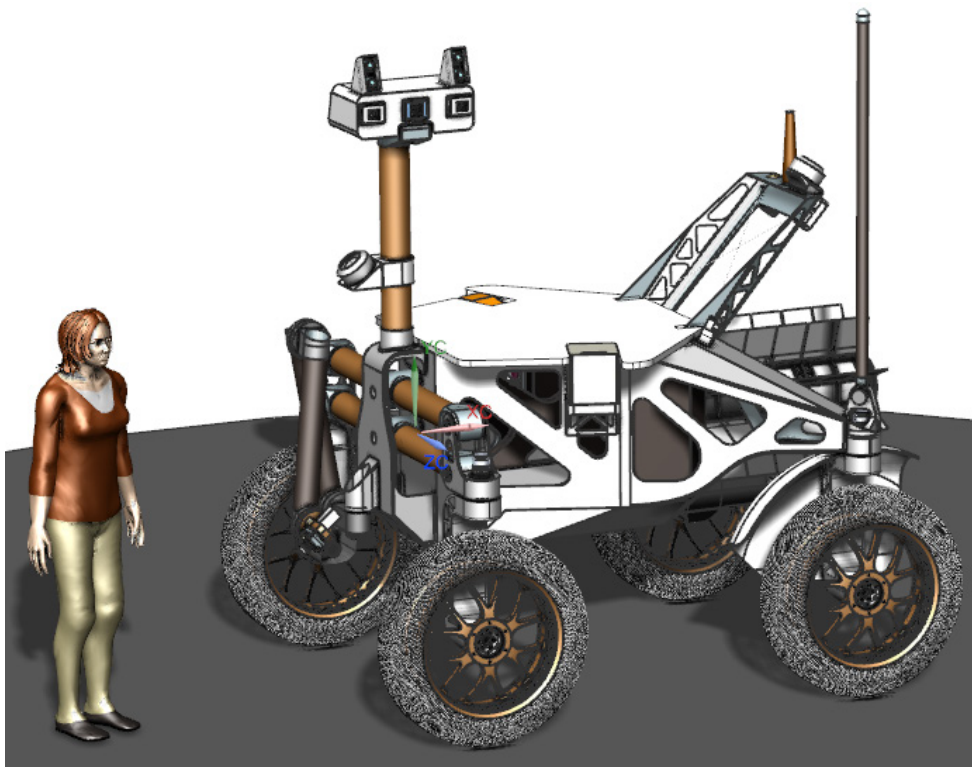


Figure C-64. Isometric view of the rover with a human shown for scale.



RTG Version Thermal Architecture

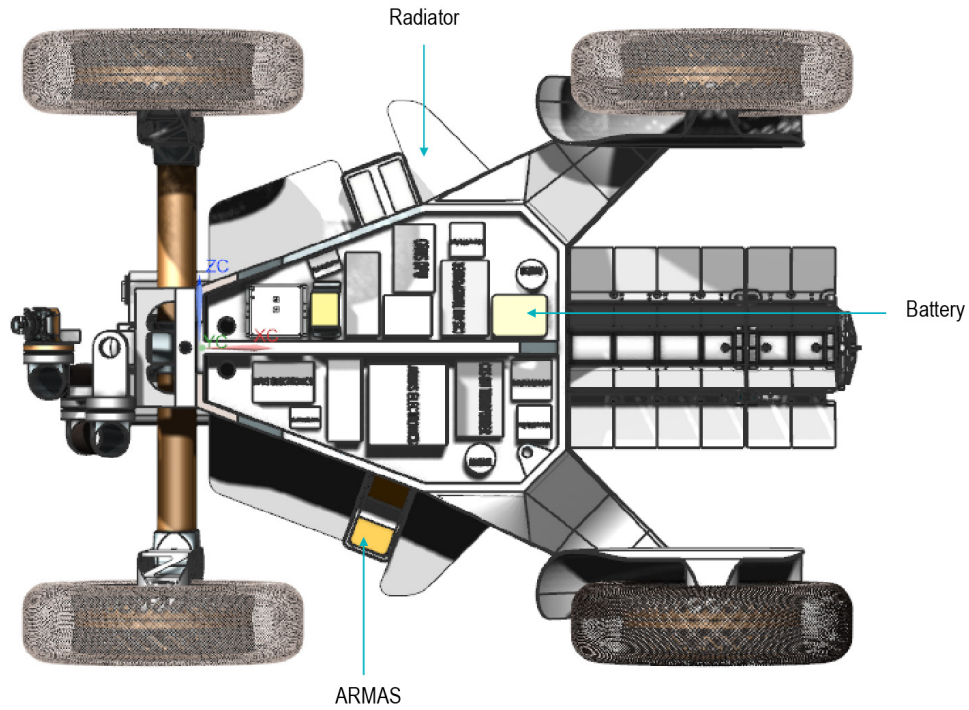


Figure C-65. Bottom view of the rover with the payload shown.

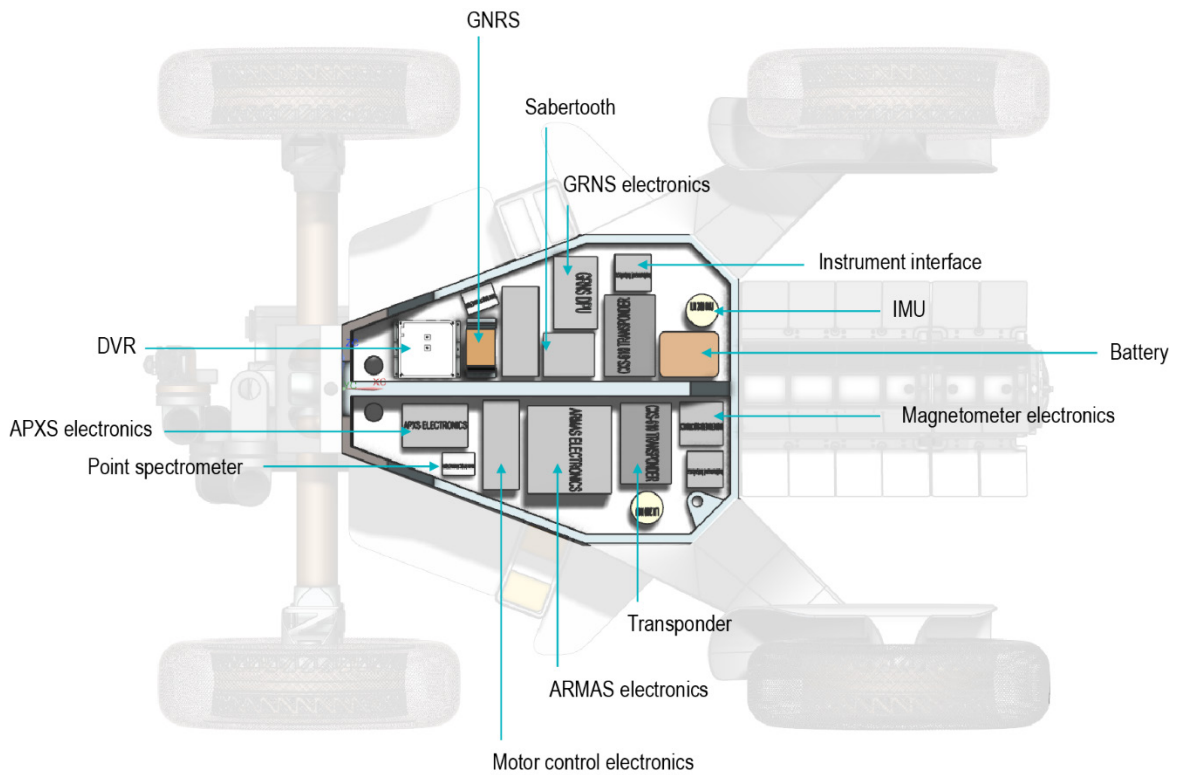


Figure C-66. Bottom view of the payload.

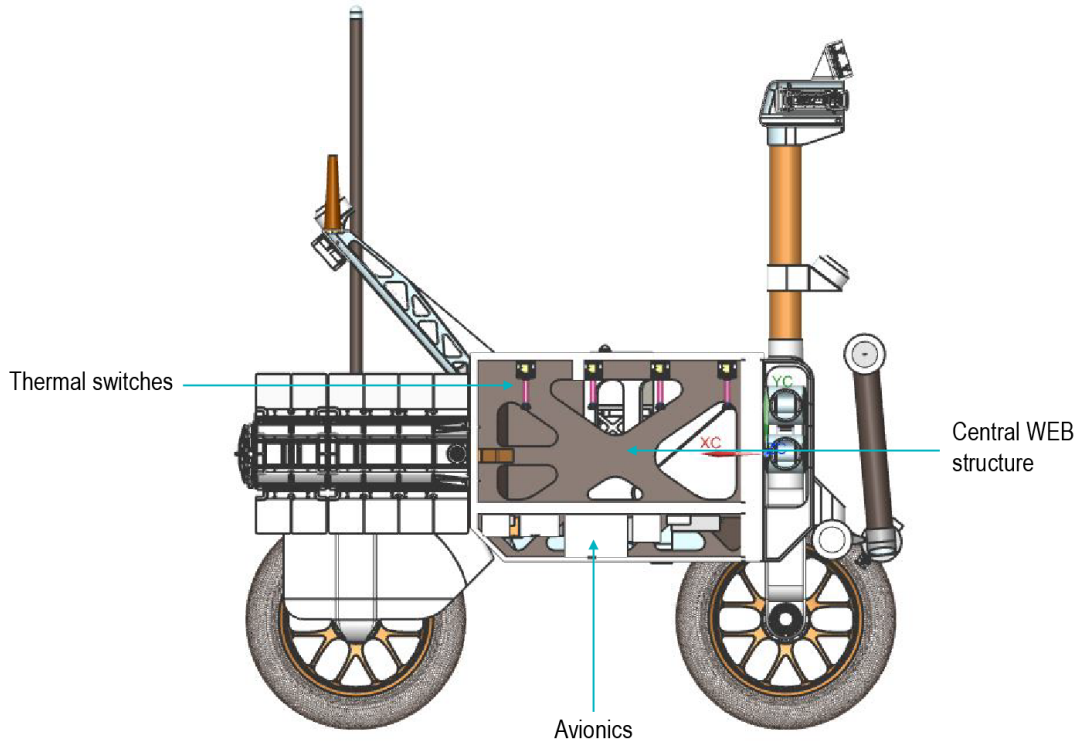


Figure C-67. Right side cross-sectional view of the rover.

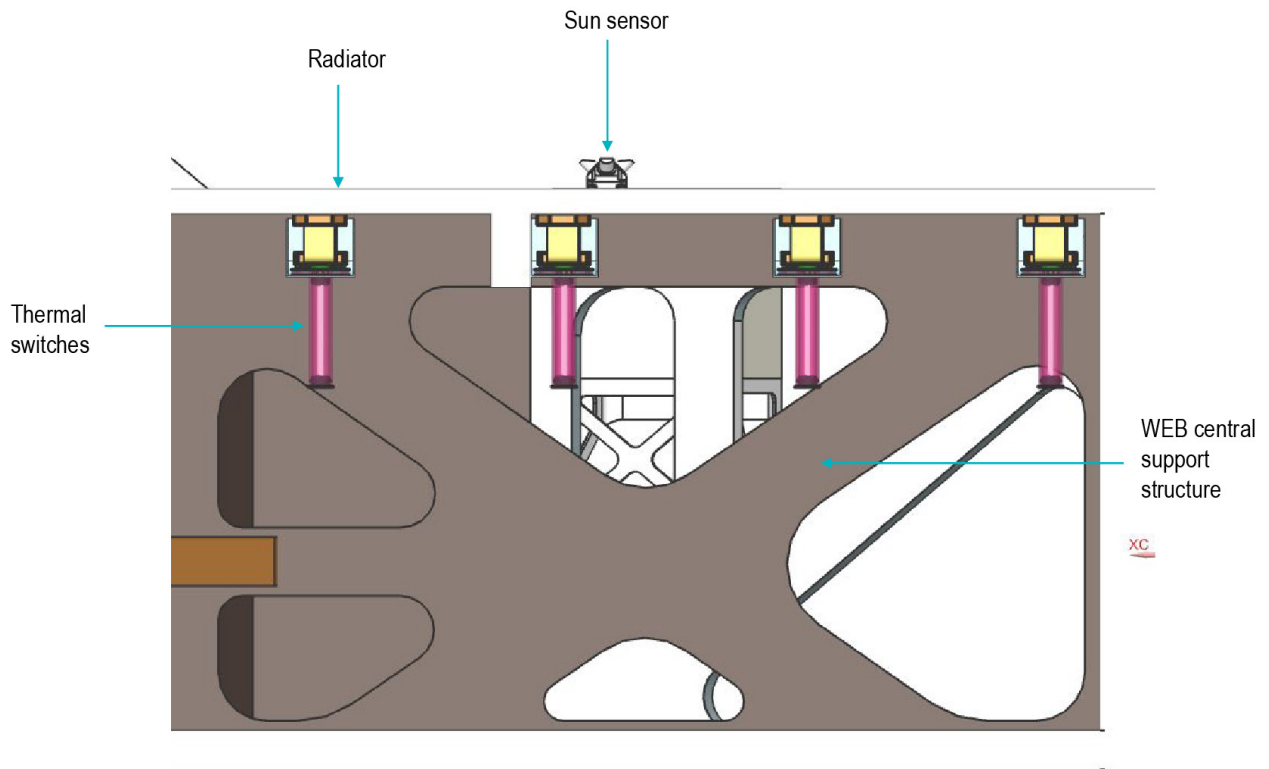


Figure C-68. Right side cross-sectional close-up view showing the thermal switches.

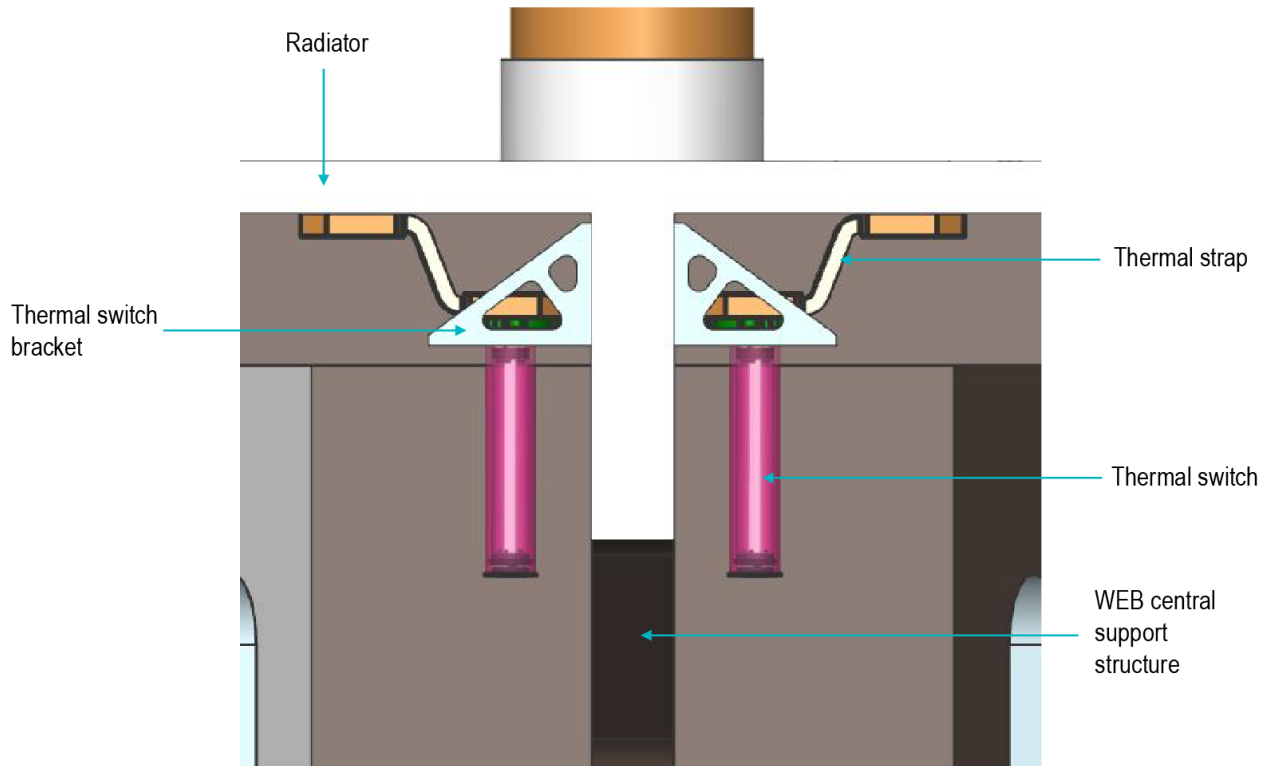


Figure C-69. Rear cross-sectional close-up view showing the thermal switches.

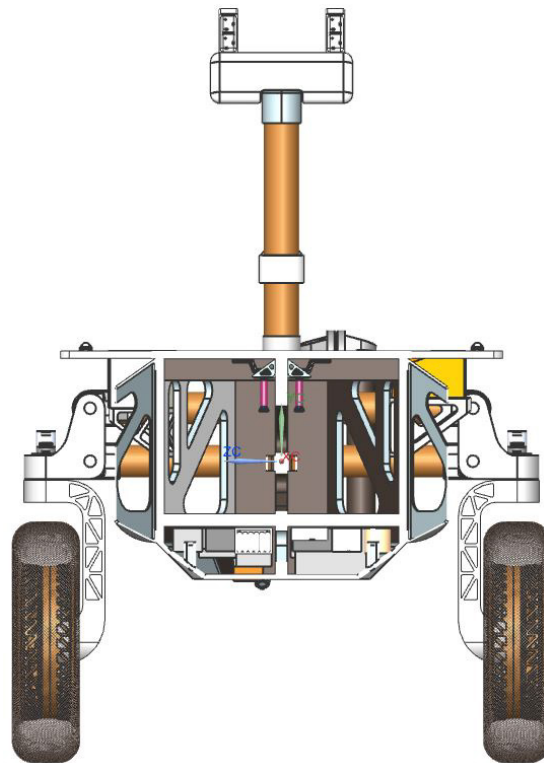


Figure C-70. Rear cross-sectional view of the rover.



Intrepid Rover (RTG and Solar Versions) Masthead

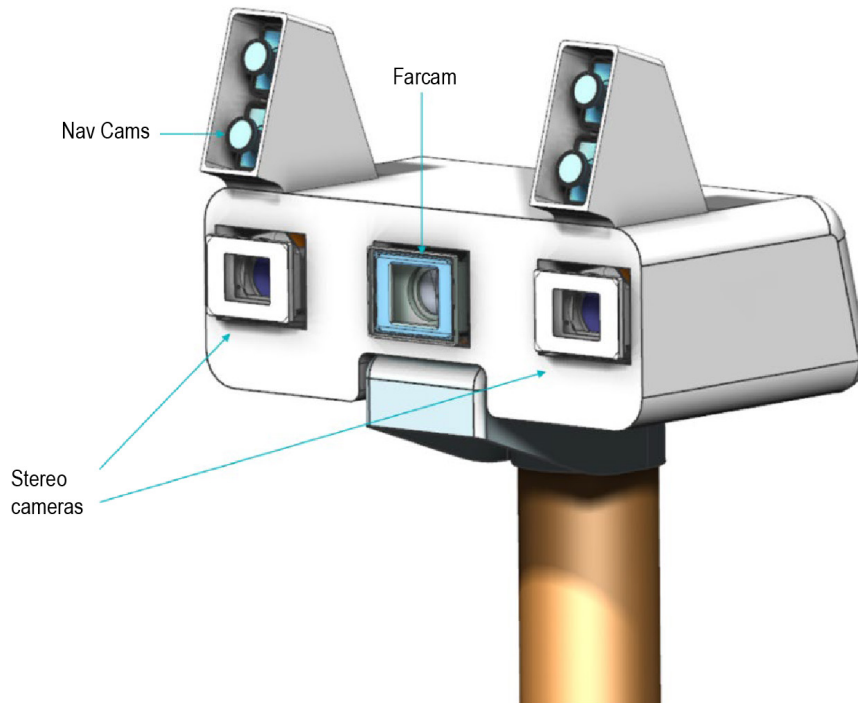


Figure C-71. Isometric view of the camera head, including the front navigation cameras and science cameras.

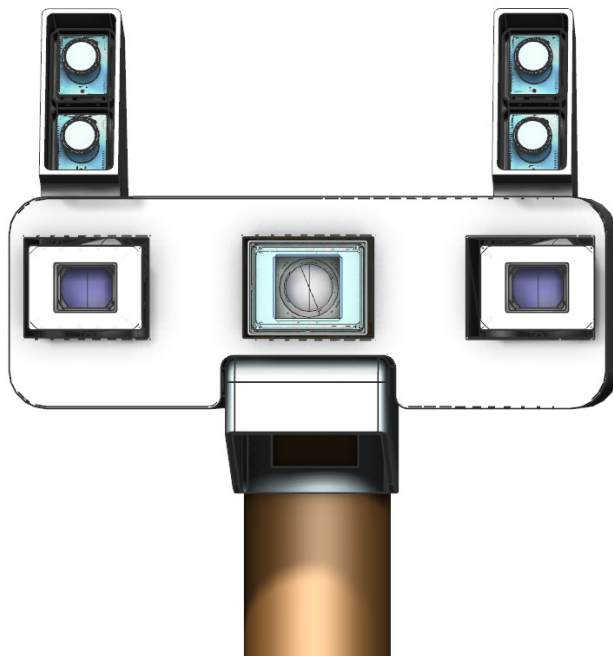


Figure C-72. Front view of the rover camera head, including the front navigation cameras and science cameras.

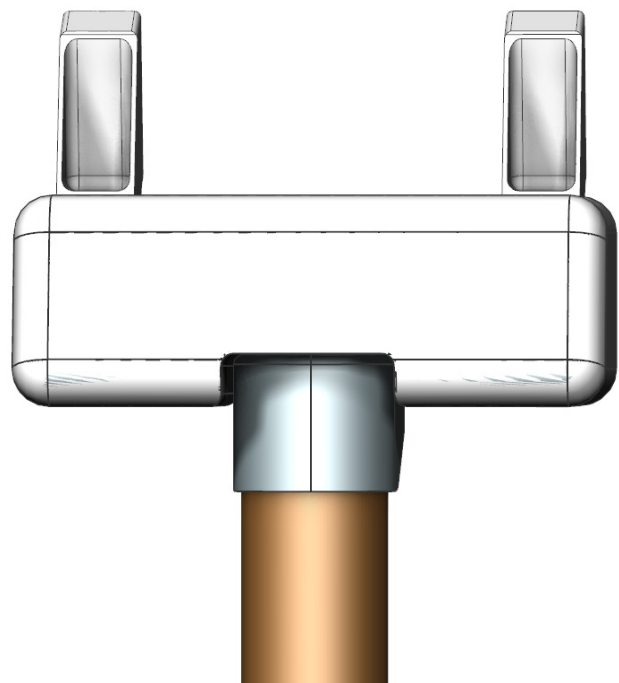


Figure C-73. Rear view of the rover camera head.



D ADDITIONAL INFORMATION ON TECHNOLOGIES AND TECHNIQUES

D.1 ADDITIONAL COST MODELING INFORMATION

JPL’s business organization performed an additional assessment of the Intrepid costs using the following methodologies.

- Historical wrap factors for science, mission operations system, and ground data system that are level-of-effort.
- SEER and TruePlanning for the payload and lander systems.
- Space Operations Cost Model (SOCM) for Phases E-F mission operations and data analysis costs

The cost results from these parametric estimates are summarized in Table D-1 for the RTG options and Table D-2 for the solar option.

In addition to the parametric model validations, a top-level crosscheck of the lunar rover (WBS 06) plus system I&T (WBS 10) was performed by looking at cost versus mass. Figure D-1 plots \$/kg for the Mars rover missions (Pathfinder, MEL, and MSL) and the two Intrepid options. A trendline

through the Mars missions show the solar option is almost right on the trendline and the RTG option is above. This indicates that the estimates for both lunar rover options are reasonable.

Phase A costs were added to the cost model estimates. As a gauge for the amount to apply, the previous New Frontiers 4 AO from 2016 was used as the basis. New Frontiers had a value of \$4M RY for Phase A with a start date in FY2018. Taking this same value of \$4M and inflating it to FY2025 dollars using the NASA New Start Inflation Index, the cost rounds up to \$5M.

D.2 WRAP FACTORS

Wrap factors were developed from historical costs of selected JPL missions. The mission set includes:

- Mars Pathfinder, MER, and MSL – Rover missions developed in-house at JPL
- Stardust, Genesis, Deep Impact, Dawn, GRAIL, Phoenix, Insight – Discovery class missions managed by JPL
- Juno – New Frontiers class mission managed by JPL

Historical cost data comes from the NASA Cost Analysis Data Requirement (CADRe) for

Table D-1. Cost model results for Intrepid RTG option (FY25\$M). Highlighted cells represent Wraps and SOCM

WBS Element	Team X	SEER	TruePlanning (MSL Calibrated)	TruePlanning (Space Msn Catalog)	Model Average	Model Avg – Team X Delta (\$)	Delta (%)
Phase A Concept Study	Incl. below	5.0	5.0	5.0	5.0	-	-
01 Project Management	24.1	41.1	21.7	44.7	86.7	3.7	4%
02 Project System Engineering	26.9	56.5	15.5	29.6			
03 Safety & Msn Assurance	32.1	Incl. above	19.6	31.6			
04 Science	37.3	18.9	20.7	11.7	17.1	-20.2	-54%
05 Payload	73.4	67.1	95.8	95.3	86.1	12.7	17%
06 Flight System	426.1	384.9	353.8	293.5	344.1	-82.0	-19%
07 Mission Ops	33.3	23.9	26.1	15.9	21.9	-11.4	-34%
09 Ground Data System	36.1	22.2	24.3	20.7	22.4	-13.9	-38%
10 Project System I&T	33.2	30.6	78.0	60.7	56.4	23.2	70%
Total Dev. w/o Reserves	722.5	650.1	660.4	608.7	639.7	-82.7	-11%
Development Reserves	326.2	325.1	330.2	304.3	319.9	-6.4	-2%
Total A-D Development Cost	1,048.7	975.2	990.7	913.0	959.6	-89.1	-8%
01 Project Management	6.7	2.5	2.5	2.5	2.5	-4.2	-63%
04 Science	71.7	90.0	90.0	90.0	90.0	18.3	26%
07 Mission Operations System	104.9	107.7	107.7	107.7	107.7	2.8	3%
09 Ground Data System	32.9	30.9	30.9	30.9	30.9	-2.0	-6%
Total Ops w/o Reserves	216.2	231.0	231.0	231.0	231.0	14.8	7%
Operations Reserves	26.2	28.4	28.4	28.4	28.4	2.2	8%
Total E-F Operations Cost	242.4	259.4	259.4	259.4	259.4	17.0	7%
08 Launch System	220.0	220.0	220.0	220.0	220.0	0.0	0%
Total Cost	1,511.1	1,454.5	1,470.0	1,392.4	1,439.0	-72.1	-5%



Table D-2. Cost model results for Intrepid solar option (FY25\$M). Highlighted cells represent Wraps and SOCM.

WBS Element	Team X	SEER	TruePlanning (MSL Calibrated)	TruePlanning (Space Msn Catalog)	Model Average	Model Avg – Team X Delta (\$)	Delta (%)
Phase A Concept Study	Incl. below	5.0	5.0	5.0	5.0	-	-
01 Project Management	24.1	29.4	23.0	48.3	82.0	1.6	2%
02 Project System Engineering	26.9	41.5	16.5	32.2			
03 Safety & Msn Assurance	29.4	Incl. above	20.7	34.5			
04 Science	37.3	14.6	22.3	11.7	16.2	-21.1	-57%
05 Payload	80.4	67.1	95.8	95.3	86.1	5.7	7%
06 Flight System	361.6	276.9	390.2	235.5	300.9	-60.7	-17%
07 Mission Ops	33.3	18.5	28.1	17.4	21.3	-12.0	-36%
09 Ground Data System	36.5	17.2	26.1	18.3	20.5	-16.0	-44%
10 Project System I&T	35.4	29.4	82.5	66.4	59.5	24.1	68%
Total Dev. w/o Reserves	664.8	499.7	710.3	564.6	591.5	-73.3	-11%
Development Reserves	332.4	249.8	355.2	282.3	295.8	-36.6	-11%
Total A-D Development Cost	997.2	749.5	1,065.5	846.9	887.3	-109.9	-11%
01 Project Management	11.1	4.2	4.2	4.2	4.2	-6.9	-62%
04 Science	119.4	147.9	147.9	147.9	147.9	28.5	24%
07 Mission Operations System	122.2	151.7	151.7	151.7	151.7	29.5	24%
09 Ground Data System	56.4	52.5	52.5	52.5	52.5	-3.9	-7%
Total Ops w/o Reserves	309.1	356.4	356.4	356.4	356.4	47.3	15%
Operations Reserves	40.6	47.7	47.7	47.7	47.7	7.1	17%
Total E-F Operations Cost	349.7	404.1	404.1	404.1	404.1	54.3	16%
08 Launch System	200.0	200.0	200.0	200.0	200.0	0.0	0%
Total Cost	1,546.9	1,353.5	1,669.5	1,451.0	1,491.4	-55.6	-4%

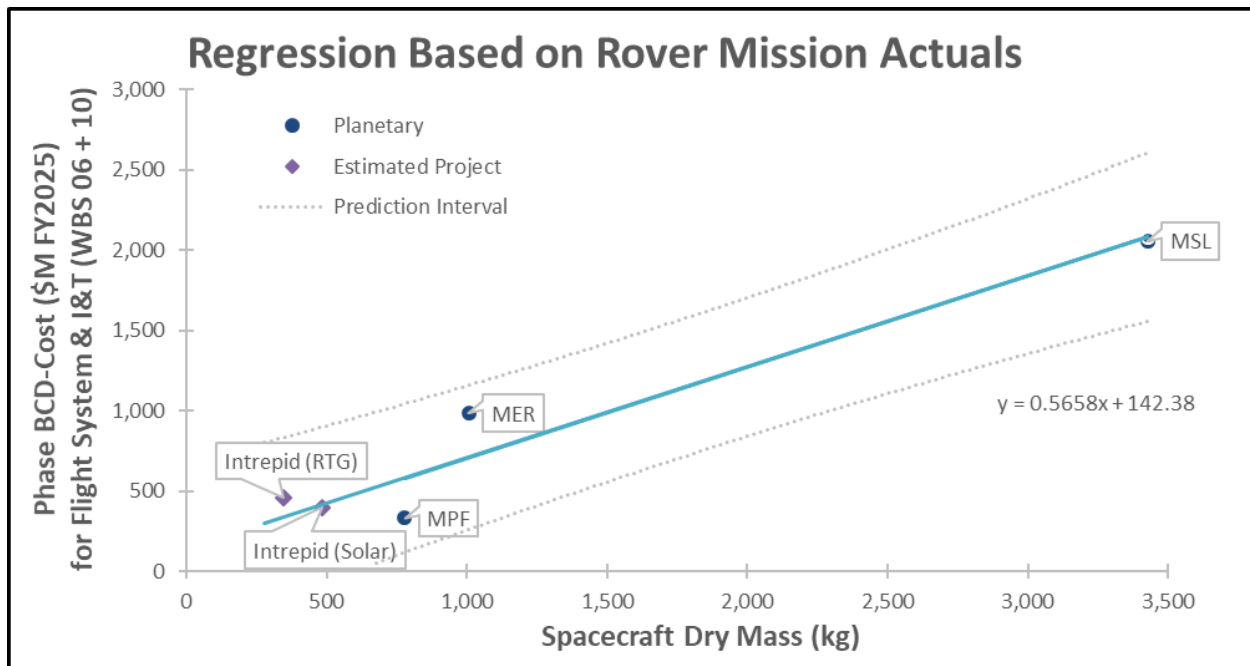


Figure D-1. \$/Kg Comparison of Intrepid to Mars Rover Missions for WBS 06 and 10.



Launch or End of Mission. Wrap factors for WBS 04, 07, and 09 are computed as a percentage of total Phase B/C/D cost without LV or Reserves. Figure D-2 shows the calculated historical wrap factor for each WBS that was applied to the SEER and TruePlanning models which do not estimate these costs.

D.3 SEER

SEER (version 7.4.13) is a component level cost tool that is recognized for its built-in Knowledge Bases (KBases) that pre-populate most inputs with appropriate industry values and optional calibration adjustments. In particular, the Application and Acquisition Category KBases are important for defining the hardware component, the level of maturity, and how it will be acquired. As an additional aid for using the tool, a companion document, SEER-H Space Guidance (Rev 3.1), is available to the user. It presents a standardize approach for setting up an estimate and provides recommended setting for important inputs.

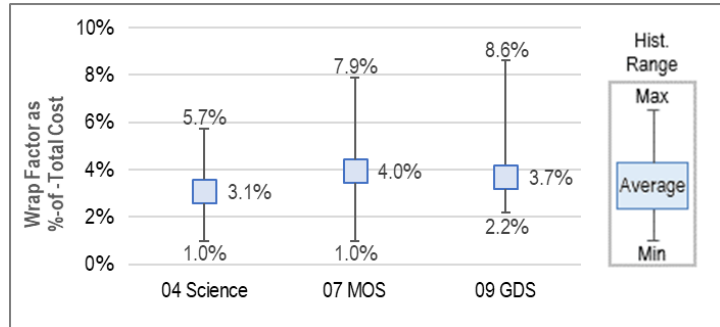


Figure D-2. Historical wrap factors for WBS 04, 07, and 09.

Table D-3 lists the Application and Acquisition Category KBase selections for each hardware component in the MEL. Table D-4 lists user-entered data that overrode the KBase default values. Software costs were added using a wrap factor of 10% on the hardware cost, which is based on historical data.

An additional 10% was added to account for the autonomous software development. In comparison to the Team X estimate, the software cost was 15% and 20% of the hardware cost for the RTG and Solar options, respectively.

Table D-3. Application and Acquisition Category KBase Settings for RTG and Solar Option.

Hardware Element	Application	Acquisition Category
Science Payload	Space System - Payload/Instrument, Science	System Eng and Program Mgmt Only
ARMAS	Photon Detector - Space	Buy and Integrate
Magnetometer	Field Sensor - Space	Buy and Integrate
TriCam	Electro-Optical Sensor	Buy and Integrate
GRNS	Field Sensor - Space	Buy and Integrate
Point Spectrometer	Electro-Optical Sensor	Buy and Integrate
HLI	Electro-Optical Sensor	Buy and Integrate
APXS	Photon Detector - Space	Buy and Integrate
Electrostatic Analyzer	Field Sensor - Space	Buy and Integrate
Laser Corner Reflector	Laser - Space	Buy and Integrate
Flight System	Spacecraft Bus	System Eng and Program Mgmt Only
Lunar Rover	Spacecraft Bus	System Eng and Program Mgmt Only
C&DH Subsystem		
Sabertooth based Compute Element	Processor - Central Processing Unit	Make
Instrument Interface	Interconnect - Data Bus	Make
Motor Controller	Controller - Electro-Mechanical Control	Modification - Major
Telecom Subsystem		
CXS-610 STDN/DSN Space Transponder	Transponder - S-Band, Deep Space	Modification - Average
Coax Transfer Switches	RF Components - Space	Make
S-band Diplexer	RF Components - Space	Make
S-band Omnidirectional LGA	Antenna - Conical/Horn, Space	Modification - Major
S-band Directional LGA	Antenna - Conical/Horn, Space	Modification - Major
Coax Cabling	Cabling	Make
GNC Subsystem		
LN 200 IMU	Inertial Measurement Unit - Space	Space Procure To Print



Hardware Element	Application	Acquisition Category
Sun Sensor	Sun Sensor - Space	Space Procure To Print
Front Nav Cameras (EECAM)		
Detector	Area Si CCD	Modification - Minor
Optics	!~Optical General	Modification - Minor
Back Nav Cameras (EECAM)		
Detector	Area Si CCD	Modification - Minor
Optics	!~Optical General	Modification - Minor
Power Subsystem		
RTG (for RTG option only)	Auxiliary Power Unit	Buy and Integrate
Solar Array (for Solar option only)		
Battery	Battery - Lithium, Space	Modification - Average
Placeholder SBIS/ PBC - Shunt & Battery I/F / Power Bus Control	Power Supply	Modification - Average
Load and Heater Switching	Power Supply	Modification - Average
Placeholder Pyro Drivers	Controller - Electro-Mechanical Control	Modification - Average
Thermal Control Subsystem		
Avionics radiator	Radiator/Heat Pipe - Space	Make
Thermal switch	Thermal Control - Active	Make
MLI	Thermal Control - MLI/Paint/Coating	Make
Loop heat pipe	Radiator/Heat Pipe - Space	Make
PRT temperature sensors	Thermal Control - Active	Make
Mechanical thermostats	Thermal Control - Active	Make
Structures & Mechanisms Subsystem		
Structures		
Web Chassis	Spacecraft Structure	Make
Back Wheels Outrigger	Spacecraft Structure	Make
Front Chassis	Spacecraft Structure	Make
Ins. Boom	Spacecraft Structure	Make
Wheel Chassis	Spacecraft Structure	Make
Rocker Booms	Spacecraft Structure	Make
Rocker Articulation Wheel	Spacecraft Structure	Make
Rocker Articulation Boom Fitting	Spacecraft Structure	Make
Rocker Articulation Boom Middle	Spacecraft Structure	Make
Back Camera Structure	Spacecraft Structure	Make
Ins. Bracket	Spacecraft Structure	Make
Magnetometer Boom	Spacecraft Structure	Make
Mag. Bracket	Spacecraft Structure	Make
Harnessing (5%) (for Solar option only)	Harness - Space	Make
Bolts (1%)	!~Structural General	Make
Mobility		
Drive Actuators	Precision Mechanism	Make
Steer Actuators	Precision Mechanism	Make
Drive Actuator housing	Spacecraft Structure	Make
Steer Actuators Housing	Spacecraft Structure	Make
Wheels	Spacecraft Structure	Make
Launch Locks / wheel-steer restraints / rocker restraints	Separation Mechanism	Make
Arm		
Yaw Actuator	Precision Mechanism	Make
Pitch Actuator	Precision Mechanism	Make
Actuator housing assembly	Spacecraft Structure	Make



Hardware Element	Application	Acquisition Category
Links	Spacecraft Structure	Make
Launch Lock	Separation Mechanism	Make
Strain Gauges	Precision Mechanism	Make
End Effector	Precision Mechanism	Make
Contact sensor	Field Sensor - Space	Make
Mast		
Pan Tilt Actuators	Precision Mechanism	Make
Pan Tilt Housing	Spacecraft Structure	Make
Scan Platform	Spacecraft Structure	Make
Mast Boom	Spacecraft Structure	Make
Engineering Camera Housing	Spacecraft Structure	Make
Science Camera Housing	Spacecraft Structure	Make
Total System Harness	Harness - Space	Make

Table D-4. User-specified inputs for SEER.

Input Parameter	Least	Likely	Most	Notes
Weight (kg)	CBE	CBE + contingency	1.3 * (CBE + Contingency)	SEER-H Space Guidance applied to all Mechanical elements.
Sabertooth based Compute Element - Total PCBs	5	6	7	Assume ~1 kg per board
Camera Detectors - Array Size Rows	5,120	5,120	5,120	Based on EECAM for Mars2020.
Camera Detectors - Array Size Columns	3,840	3,840	3,840	Based on EECAM for Mars2020.
Camera Detectors - Pitch	6	6	6	Based on EECAM for Mars2020.
Complexity of Form	VHi	VHi+	VHi+	SEER-H Space Guidance for 9 instruments which is applied to mechanical elements using the Application KBase “Spacecraft Structure”
Prototype Quantity		0.65 per unit		SEER Rule of Thumb for an EM. It was assumed all subsystems would build an EM.
Certification Level	Hi	Hi	Hi+	SEER-H Space Guidance for a Class B mission applied to all elements.
Reliability Standard	Hi+	VHi-	VHi-	SEER-H Space Guidance for a Class B mission applied to all EOS elements.

D.4 TRUEPLANNING

TruePlanning (version 16.1 SR1) was used two ways to develop an estimate. One method was at the subsystem level using MSL as an analogy to calibrate the model and the other was at the component level using the Space Missions catalog.

For the calibrated estimate., the MSL Launch CADRe was the source for the cost and mass data. A subsystem level estimate is developed with the mass information. Then the built-in calibration tool is used to solve for the value of Manufacturing Complexity for Structure and Manufacturing Complexity for Electronics with the known cost as the target. With the calibrated complexity factors in hand, these settings can now be applied

to Intrepid by simply replacing and entering the mission’s subsystem mass.

For the second estimate, Intrepid was modeled using the Space Missions Model with the Component Type Calculator. Inputs for the Component Type Calculator include Subsystem Type, Component Type, Platform, Parts Class, Unit Mass, Quantities, Heritage for Structure and Electronics, Advanced Technology Development, and a few other element unique parameters. The calculator uses these inputs to define values for Operating Specification, Weight of Structure, Weight of Electronics, Volume, Manufacturing Complexity for Structure, Manufacturing Complexity for Electronics, Percent New for Structure and Electronics, and Engineering Complexity. Software

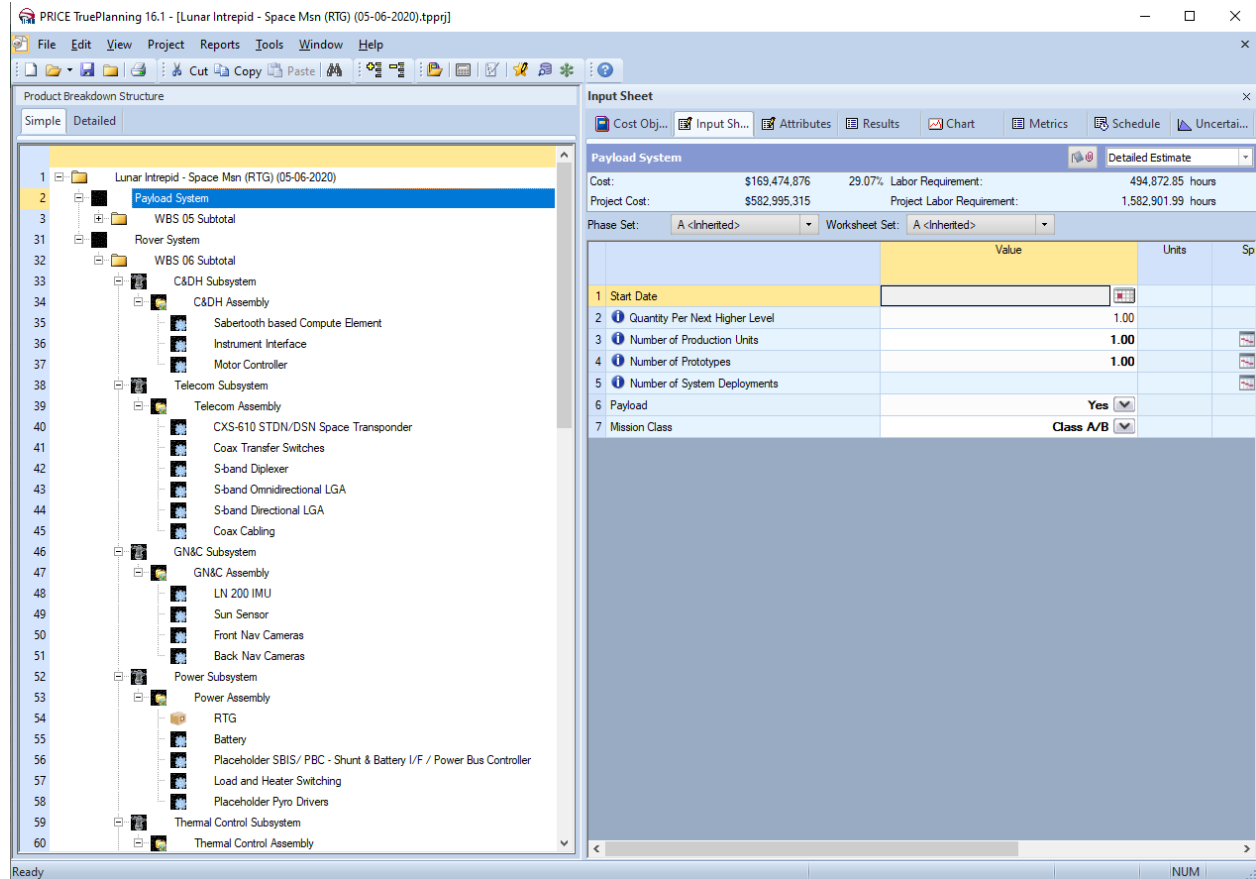


Figure D-3. TruePlanning Structure for Space Missions Model.

costs are included as part of the hardware estimate, so it does not need to be modeled. The model inputs used for each component in the MEL is provided in Table D-5. For Platform, Parts Type, and Advanced Technology Development, the same setting of “Planetary”, “S1”, and “No” was used for all elements.

For the Payload System cost object, data was entered for the following inputs.

- Number of Production Units – set to 1
- Number of Prototypes – set to 1 for the assumption that there will at least one EM or prototype built for every instrument.
- Payload – set to Yes
- Mission Class – set to Class A/B
- Likewise for the Rover System cost object, the data entered was:
- Number of Production Units – set to 1
- Number of Prototypes – set to 1 for the assumption that there will at least one EM or prototype built for every instrument.
- Payload – set to No
- Mission Class – set to Class A/B



Table D-5. TruePlanning model inputs using the Space Missions Model's Component Type Calculator.

Hardware Element	Subsystem Type	Component Type	Unit Mass (kg)	Heritage	Additional Input
Science Payload					Payload set to Yes; Mission Class set to A/B
ARMAS	Sensor Systems	Sensors/Detectors	1.1	Minimal Mod	Type set to Nominal
Magnetometer	Sensor Systems	Magnetometer	0.55	Minimal Mod	Type set to Advanced
TriCam	Sensor Systems	Charge Coupled Device Detectors	6.49	Minimal Mod	Type set to Advanced Visible Detector or UV/IR Detector
GRNS	Sensor Systems	Gamma Sensor	3.278	Minimal Mod	Type set to Simple
Point Spectrometer	Sensor Systems	Sensors/Detectors	0.26	Major Mod	Type set to Complex
HLI	Sensor Systems	Charge Coupled Device Detectors	0.638	Minimal Mod	Type set to Advanced Visible Detector or UV/IR Detector
APXS	Sensor Systems	Neutron Sensor	1.804	Minimal Mod	Type set to Standard
Electrostatic Analyzer	Sensor Systems	Electro-Static Analyzer Sensor	4.6530	Minimal Mod	Type set to Simple
Laser Corner Reflector	N/A	N/A	0.23	Minimal Mod	Used the Space Laser cost object
Lunar Rover					Payload set to No; Mission Class set to A/B
C&DH Subsystem	Command and Data Handling				
Sabertooth based Compute Element	Command and Data Handling	Command/Data Processing	7.8	Major Mod	Type set to Most Microprocessors, RAD6000
Instrument Interface	Command and Data Handling	Command/Data Processing	2.5	Major Mod	Type set to Simple or non-Programmable
Motor Controller	Command and Data Handling	Command/Data Processing	3.9	Major Mod	Type set to Advanced Devices
Telecom Subsystem	Communications				
CXS-610 STDN/DSN Space Transponder	Communications	Transponder	2.75	Minimal Mod	Frequency Band set to S - band
Coax Transfer Switches	Communications	Miscellaneous RF Electronics	0.1365	Minimal Mod	Frequency Band set to S - band
S-band Diplexer	Communications	Miscellaneous RF Electronics	0.165	Minimal Mod	Frequency Band set to S - band
S-band Omnidirectional LGA	Communications	Medium Gain Antenna/Low Gain Antenna	0.275	Minimal Mod	Frequency Band set to S – band; Antenna set to Array
S-band Directional LGA	Communications	Medium Gain Antenna/Low Gain Antenna	0.275	Minimal Mod	Frequency Band set to S – band; Antenna set to Array
Coax Cabling	Communications	Waveguides - Comm Cabling	0.975	Minimal Mod	Frequency Band set to S - band
GNC Subsystem	Guidance, Navigation and Control				
LN 200 IMU	Guidance, Navigation and Control	IMU-Gyro	0.814	Minimal Mod	
Sun Sensor	Guidance, Navigation and Control	Sun Sensor	0.1463	Minimal Mod	Type set to Standard
Front Nav Cameras (EECAM)	Guidance, Navigation and Control	Charge Coupled Device Detectors	0.6325	Minimal Mod	Type set to Advanced Visible Detector or UV/IR Detector
Back Nav Cameras (EECAM)	Guidance, Navigation and Control	Charge Coupled Device Detectors	0.6325	Minimal Mod	Type set to Advanced Visible Detector or UV/IR Detector
Power Subsystem	Power				



Hardware Element	Subsystem Type	Component Type	Unit Mass (kg)	Heritage	Additional Input
RTG (for RTG option only)	Power		66.131		Used the Purchased Good cost object; Unit Cost set to \$70,000,000; Component Type set to Hardware; Component Integration Size set to Midsize Components or Assemblies; Component Complexity set to High; External Integration Complexity set to 4.00
Solar Array (for Solar option only)	Power	Solar Cells/Electrical	10.01	New	Type set to Multi- Junction and High Efficiency
Battery	Power	Batteries	5.07 for RTG option; 29.601 for Solar option	Minimal Mod	Chemistry set to Li-ion
Placeholder SBIS/ PBC - Shunt & Battery I/F / Power Bus Control	Power	Power Management and Distribution	1.43	Major Mod	Type set to Nominal Space based Device
Load and Heater Switching	Power	Power Management and Distribution	2.7885	Major Mod	Type set to Complex Device with Advanced Switching
Placeholder Pyro Drivers	Power	Pyrotechnics	1.43		Type set to Simple
Thermal Control Subsystem	Thermal Control				
Avionics radiator	Thermal Control	Radiators/Louvers	4.875	New	Material set to Aluminum
Thermal switch	Thermal Control	Heaters, RHUs, Thermostats	0.18	New	Material set to Composite
MLI	Thermal Control	MLI, Paints, Coatings	5.85	New	
Loop heat pipe	Thermal Control	Heat Pipes	1.3	New	Material set to Aluminum
PRT temperature sensors	Thermal Control	Heaters, RHUs, Thermostats	0.0013	New	Material set to Stainless Steel
Mechanical thermostats	Thermal Control	Heaters, RHUs, Thermostats	0.0325	New	Material set to Stainless Steel
Structures & Mechanisms Subsystem	Structure and Mechanisms				
Structures					
Web Chassis	Structure and Mechanisms	Primary Structure	18.0	New	Material set to Aluminum
Back Wheels Outrigger	Structure and Mechanisms	Primary Structure	11.4	New	Material set to Aluminum
Front Chassis	Structure and Mechanisms	Primary Structure	7.2	New	Material set to Aluminum
Ins. Boom	Structure and Mechanisms	Primary Structure	0.36	New	Material set to Aluminum
Wheel Chassis	Structure and Mechanisms	Primary Structure	1.8	New	Material set to Aluminum
Rocker Booms	Structure and Mechanisms	Primary Structure	0.6	New	Material set to Aluminum
Rocker Articulation Wheel	Structure and Mechanisms	Primary Structure	1.8	New	Material set to Aluminum
Rocker Articulation Boom Fitting	Structure and Mechanisms	Secondary Structure	0.96	New	Material set to Aluminum
Rocker Articulation Boom Middle	Structure and Mechanisms	Primary Structure	0.6	New	Material set to Aluminum



Hardware Element	Subsystem Type	Component Type	Unit Mass (kg)	Heritage	Additional Input
Back Camera Structure	Structure and Mechanisms	Secondary Structure	1.44	New	Material set to Aluminum
Ins. Bracket	Structure and Mechanisms	Secondary Structure	0.36	New	Material set to Aluminum
Magnetometer Boom	Structure and Mechanisms	Primary Structure	0.36	New	Material set to Aluminum
Mag. Bracket	Structure and Mechanisms	Secondary Structure	0.6	New	Material set to Aluminum
Harnessing (5%) (for Solar option only)	Power	Harness	3.408	New	
Bolts (1%)	Structure and Mechanisms	Secondary Structure	0.6816	New	Material set to Aluminum
Mobility					
Drive Actuators	Structure and Mechanisms	Motor-Actuator	3.445	New	Type set to Advanced
Steer Actuators	Structure and Mechanisms	Motor-Actuator	3.445	New	Type set to Advanced
Drive Actuator housing	Structure and Mechanisms	Primary Structure	1.95	New	Material set to Aluminum
Steer Actuators Housing	Structure and Mechanisms	Primary Structure	1.95	New	Material set to Aluminum
Wheels	Structure and Mechanisms	Mechanisms	7.41	New	Type set to Very Advanced
Launch Locks / wheel-steer restraints / rocker restraints	Structure and Mechanisms	Mechanisms	2.6	New	Type set to Standard
Arm					
Yaw Actuator	Structure and Mechanisms	Motor-Actuator	3.9	New	Type set to Advanced
Pitch Actuator	Structure and Mechanisms	Motor-Actuator	2.6	New	Type set to Advanced
Actuator housing assembly	Structure and Mechanisms	Primary Structure	1.3	New	Material set to Aluminum
Links	Structure and Mechanisms	Primary Structure	1.3	New	Material set to Aluminum
Launch Lock	Structure and Mechanisms	Mechanisms	2.6	New	Type set to Standard
Strain Gauges	Structure and Mechanisms	Mechanisms	0.0001	New	Type set to Advanced
End Effector	Structure and Mechanisms	Mechanisms	2.6	New	Type set to Very Advanced
Contact sensor	Sensor Systems	Sensors/Detectors	0.0001	New	Type set to Complex
Mast					
Pan Tilt Actuators	Structure and Mechanisms	Motor-Actuator	3.25	New	Type set to Advanced
Pan Tilt Housing	Structure and Mechanisms	Primary Structure	1.95	New	Material set to Aluminum
Scan Platform	Structure and Mechanisms	Primary Structure	2.6	New	Material set to Aluminum
Mast Boom	Structure and Mechanisms	Primary Structure	3.9	New	Material set to Aluminum
Engineering Camera Housing	Structure and Mechanisms	Primary Structure	0.65	New	Material set to Aluminum
Science Camera Housing	Structure and Mechanisms	Primary Structure	0.8667	New	Material set to Aluminum



Hardware Element	Subsystem Type	Component Type	Unit Mass (kg)	Heritage	Additional Input
Total System Harness	Power	Power Harness/Cabling	22.62 for RTG option; 41.08 for Solar option	New	

D.5 SOCM

The Space Operations Cost Model (SOCM) was used for the validation of Phase E/F. SOCM estimates the costs and staffing for space operations projects using high-level project characteristics that are typically known at the early stages of a project’s lifecycle. Running the cost model at Level 1 generates an estimate with an accuracy of ± 30%. The Level 1 Earth Orbiting inputs selected to reflect the Intrepid mission are identified in Figure D-4 and Figure D-5. The only difference is nominal mission duration which is 4 years for the RTG and 5 years for the Solar option.

The Level 2 Earth Orbiting inputs may also be adjusted to refine the estimate and improve the accuracy. Figure D-6 provides the Level 2 settings that was the same for both options.

The Space Operations Cost Model (SOCM) estimates all Phase E/F costs, with the exception of ground station tracking (WBS 07.03). Therefore, the Team X estimates for tracking (\$42.8M for the RTG and \$27.2M for the Solar option) were used as pass-throughs and added to the SOCM results. The final outputs from SOCM are provided in Figure D-7 and Figure D-8.

EARTH ORBITING - LEVEL 1 INPUTS							
	Value ->	1	2	3	4	5	6
MISSION CHARACTERIZATION							
Mission Type	4	Survey - Earth Science	Survey - Space Science	Targeted - Earth Science	Targeted - Space Science		
Tracking Network	3	Ground	TDRSS	DSN			
Orbit	4	LEO, circular	L1, halo	Highly Elliptical	Non-		
# of Identical Flight Systems	1	1	2	3	4	5	6
Nominal Mission Duration (mo)	50						
Extended Mission Duration (mo)	0						
Post-Flight Data Analysis Duration	6						
PROGRAMMATICS CHARACTERIZATION							
Mission Risk Class	4	Technology Demo	SMEX	MIDEX/ESSP	Explorers	Great Observatories	
Development Schedule	3	Fast (< 2.5 yrs)	Moderate (2.5-4 yrs)	Long (> 4 yrs)			
Management Mode	1	PI	NASA				
Contract Type	2	In-House	Augmented Hybrid	Hybrid	Out-of-House		
GDS/MOS CHARACTERIZATION							
Operations Approach	2	Dedicated MOC	Multimission MOC	Remote MOC/SOC	Contracted		
Architecture Design	2	COTS	Heritage/GOTS	New/Custom			
Science Team Role	3	Data Processing	Instrument Health	Sequence Planning			
PAYLOAD CHARACTERIZATION							
# of Non-Imaging Instruments	7					# of Instr Scoring	
# of Imaging Instruments	2					Score	11
Pointing Requirements	2	Low	Medium	High		Max Score	20
Conflicts Among Instruments	2	Low	Medium	High			
Scope of Guest Investigator Program	3	Small	Medium	Large			
# of Separate Science Investigations	4	Less than 2	From 2-5	2-5	5-10	> 10	
Science Team Size (not all FT)	3	Less than 10	10-20	more than 20	more than 50		
Science Team Location/Distribution	4	Colocated at 1 facility	Central SOC w/1-2 remote	Central SOC w/ 2+ remotes	Central SOC w/ wide distr	2 - 3 SOC locations	Multiple SOCs w/ wide distr
S/C DESIGN CHARACTERIZATION							
S/C Design Implementation	2	High Heritage	Cost-Capped	Requirements-Driven			
Design Complexity	3	Low (minimal # of flight rules)	Medium	High (several unique engmg reqs)			

Figure D-4. SOCM Level 1 Cost Inputs for the RTG option.



EARTH ORBITING - LEVEL 1 INPUTS							
	Value ->	1	2	3	4	5	6
MISSION CHARACTERIZATION							
Mission Type	4	Survey - Earth Science	Survey - Space Science	Targeted - Earth Science	Targeted - Space Science		
Tracking Network	3	Ground	TDRSS	DSN			
Orbit	4	LEO, circular	L1, halo	Highly Elliptical	Non-		
# of Identical Flight Systems	1	1	2	3	4	5	6
Nominal Mission Duration (mo)	86						
Extended Mission Duration (mo)	0						
Post-Flight Data Analysis Duration	6						
PROGRAMMATICS CHARACTERIZATION							
Mission Risk Class	4	Technology Demo	SMEEX	MIDEX/ESSP	Explorers	Great Observatories	
Development Schedule	3	Fast (< 2.5 yrs)	Moderate (2.5-4 yrs)	Long (> 4 yrs)			
Management Mode	1	PI	NASA				
Contract Type	2	In-House	Augmented Hybrid	Hybrid	Out-of-House		
GDS/MOS CHARACTERIZATION							
Operations Approach	2	Dedicated MOC	Multimission MOC	Remote MOC/SOC	Contracted		
Architecture Design	2	COTS	Heritage/GOTS	New/Custom			
Science Team Role	3	Data Processing	Instrument Health	Sequence Planning			
PAYLOAD CHARACTERIZATION							
# of Non-Imaging Instruments	7					# of Instr Scoring	
# of Imaging Instruments	2					Score	11
Pointing Requirements	2	Low	Medium	High		Max Score	20
Conflicts Among Instruments	2	Low	Medium	High			
Scope of Guest Investigator Program	3	Small	Medium	Large			
# of Separate Science Investigations	4	Less than 2	From 2-5	2-5	5-10	> 10	
Science Team Size (not all FT)	3	Less than 10	10-20	more than 20	more than 50		
Science Team Location/Distribution	4	Colocated at 1 facility	Central SOC w/1-2 remote	Central SOC w/ 2+ remotes	Central SOC w/ wide distr	2 - 3 SOC locations	Multiple SOC's w/ wide distr
S/C DESIGN CHARACTERIZATION							
S/C Design Implementation	2	High Heritage	Cost-Capped	Requirements-Driven			
Design Complexity	3	Low (minimal # of flight rules)	Medium	High (several unique engng reqs)			

Figure D-5. SOCM Level 1 Cost Inputs for the Solar option.



EARTH ORBITING - LEVEL 2 INPUTS					
LEVEL 2 ESTIMATE					
<i>Intrepid</i>					
LEVEL 2 INPUTS					
Selected Cost Drivers:	Ops\$ Range	Ops\$ Range	Ops\$ Range	units	Definitions
Mission Implementation					
	Low	Medium	High		
Engineering Event Complexity	<input checked="" type="radio"/> Routine, Non-hazardous events	<input type="radio"/> Repetitive/No Hazardous Events	<input type="radio"/> Risky events/Significant Real-Time Contact		Number of unique engrng cmd sequences
Targeted Observations	<input checked="" type="radio"/> targeted observations implemented in > 24 hours, or No targeted observations observed	<input type="radio"/> Targeted observations implemented in 6-24 hours	<input type="radio"/> Targeted observations implemented in less than 6 hours		High level characterization of operation concept
Science Event Complexity	<input type="radio"/> Survey	<input type="radio"/> Few constraints	<input checked="" type="radio"/> Constrained/Multiple observation modes		Number of unique science instrument command sequences
Programmatic Implementation					
	Low	Medium	High		
Staff Experience	<input type="radio"/> More than 2 similar missions	<input checked="" type="radio"/> 1 or 2 similar missions	<input type="radio"/> New OPS team		Experience of ops staff with similar systems
Risk Plan - S/C	<input type="radio"/> Small S/C, No redundancy, Tech demo mission	<input type="radio"/> Class C, \$100M fit system development	<input checked="" type="radio"/> Redundant S/C, several \$100M development		Measure of the S/C operational risk based on design implementation
Risk Plan - Instruments/Payload	<input type="radio"/> Simple payload, No redundancy	<input checked="" type="radio"/> Few hazardous OPS, Limited redundancy	<input type="radio"/> Complex, redundant S/C		Measure of the instrument/payload operational risk based on design implementation
Risk Plan - GDS/MOS	<input type="radio"/> Accept min risk to msn safety, and mod data loss	<input checked="" type="radio"/> Accept mod risk to efficiency and data loss < 5%	<input type="radio"/> Accept min risk to efficiency and data loss < 1%		Measure of the GDS/MOS operational risk based on design implementation
Crosstraining/Staffing Overlaps	<input type="radio"/> Fully crosstrained	<input checked="" type="radio"/> Crosstrained within functions	<input type="radio"/> Limited crosstraining		Number of staff assigned/trained to perform same function
H/W Redundancy	<input type="radio"/> Limited or no redundancy	<input checked="" type="radio"/> Selected redundancy	<input type="radio"/> Full redundancy with rapid switchover		GDS/MOS system redundancy
Spacecraft Design Implementation					
	Low	Medium	High		
S/C Autonomy	<input type="radio"/> Proven sophisticated autonomy	<input checked="" type="radio"/> Simple robust safe mode; Onboard telem monitor	<input type="radio"/> Several complex safe modes or exper approach		Ability of the s/c to operate without ground control
Maneuver Frequency	<input type="radio"/> Once per year or less	<input type="radio"/> Couple of times per year	<input checked="" type="radio"/> Once a month or more		Frequency of S/C maneuvers over nominal operations period
Data Return Margin	<input checked="" type="radio"/> > 2	<input type="radio"/> 1.1 - 2	<input type="radio"/> < 1.1		Ratio of max amount of data that can be downlinked to the average amount required per downlink
Power Margin	<input type="radio"/> > 1.2	<input checked="" type="radio"/> 1 - 1.2	<input type="radio"/> < 1		Ratio of max avail power to peak power demand
Memory Margin	<input checked="" type="radio"/> > 2	<input type="radio"/> 1.5 - 2	<input type="radio"/> < 1.2		Ratio of on-board storage capacity to max quantity of data to be downlinked in a single pass

Figure D-6. SOCM Level 2 Cost Inputs for both options.



GDS/MOS Implementation			Low	Medium	High		
Command Frequency - Sequences	<input checked="" type="radio"/>	Loaded less than once per day	<input type="radio"/>	Daily	<input type="radio"/>	Loaded more than once per day	Frequency of developing sequences for uplink
Data Processing - Data Completeness	<input type="radio"/>	< 95%	<input checked="" type="radio"/>	95-98%	<input type="radio"/>	> 98%	% Measure of data return requirement vs. minimal acceptable data return
Data Processing - Data Delivery Time	<input type="radio"/>	More than 24 hours	<input checked="" type="radio"/>	6 to 24 hours	<input type="radio"/>	Less than 6 hours	hrs Time allowed to deliver data products after raw data is downlinked
Data Processing - Autonomy	<input type="radio"/>	Extensive	<input checked="" type="radio"/>	Nominal	<input type="radio"/>	Minimal	Measure of the degree of autonomy in ground data handling system
Data Processing - Heritage/Reuse	<input type="radio"/>	More than 85%	<input checked="" type="radio"/>	75%	<input type="radio"/>	Less than 60%	% % of ground data processing system based on existing designs
Command Frequency - Generation Time	<input checked="" type="radio"/>	More than one day before upload	<input type="radio"/>	One day before upload	<input type="radio"/>	Less than one day before upload	Time allowed to generate commands to modify/affect mission ops
Command Frequency - Real-Time Commands	<input type="radio"/>	No commands on some passes	<input checked="" type="radio"/>	Routine commands on most passes	<input type="radio"/>	Special commands on some passes	Frequency of real-time commands for uplink
Data Processing - Max. Downlink Rate	<input type="radio"/>	less than 1	<input checked="" type="radio"/>	1 to 2	<input type="radio"/>	10s to 100s	Mbps Maximum downlink data rate accommodated
Data Processing - Max. Bits/Day	<input type="radio"/>	< 10	<input checked="" type="radio"/>	10-100	<input type="radio"/>	> 100	Gb Maximum # of bits downlinked per day
Data Processing - On-Line Storage	<input type="radio"/>	> 20	<input checked="" type="radio"/>	2 - 20	<input type="radio"/>	< 2	GB Size/capacity of onboard data storage system
Data Processing - Storage/Playback Frequency	<input type="radio"/>	Once per day or less	<input checked="" type="radio"/>	Several times per day	<input type="radio"/>	Once per orbit	Number of days that data can be stored without downlink
Payload Implementation			Low	Medium	High		
Instrument Support Complexity	<input type="radio"/>	Simple instrument with few operations	<input checked="" type="radio"/>	Routine calibrations, few sched constraints	<input type="radio"/>	Constrained operation, Complex instr interactions	Relates to # of instruments, conflicts, flight rules for instr operation
Payload Flight Heritage	<input type="radio"/>	Most instruments have flown together; No advanced technology	<input checked="" type="radio"/>	Most instruments have flight heritage	<input type="radio"/>	New instruments; Payload includes advanced technology	Measure of individual instruments and total payload package flight experience
Instrument/Payload Operating Modes	<input checked="" type="radio"/>	2-3 operating modes per instrument; Single observing mode for all instruments	<input type="radio"/>	Less than 3 operating modes per instrument; 2-3 observing modes	<input type="radio"/>	Several instruments with multiple operating modes; 3+ observing modes	Identifies number of operating modes for each instrument and observing modes for total payload; Modes include calibration

Figure D-6. SOCM Level 2 Cost Inputs for both options.



JPL WBS V5	SOCM Activity Descriptors	Cruise	Encounter	Post-Flight DA	Total
01	Proj Management	4231.05	0.00	0.00	4231.05
04	Science				
	<i>Science Data Procesing</i>	80635.44	0.00	5625.73	86261.17
	<i>Long Term Archives</i>	39185.44	0.00	2733.87	41919.31
	<i>Investigations</i>	18403.52	0.00	1283.97	19687.48
07	MOS				
	<i>Mission Planning & Integration (NAV)</i>	7930.95	0.00	0.00	7930.95
	<i>Command/Uplink Management</i>	18724.90	0.00	0.00	18724.90
	<i>Mission Control & OPS</i>	21628.17	0.00	0.00	21628.17
	<i>Pos/Loc Planning & Analysis (NAV)</i>	1083.24	0.00	0.00	1083.24
	<i>S/C Planning & Analysis</i>	3445.53	0.00	0.00	3445.53
	<i>Science Planning & Analysis</i>	60501.01	0.00	0.00	60501.01
09	GDS				
	<i>Data Capture</i>	19264.94	0.00	0.00	19264.94
	<i>System Engineering Integ & Test</i>	22222.04	0.00	0.00	22222.04
	<i>Computer & Com Support</i>	10338.73	0.00	721.31	11060.04
	Project Direct Total	307594.96	0.00	10364.87	317959.83
				Tracking costs from Team X	38400

Figure D-8. SOCM Level 2 Cost Results for the Solar option.



E REFERENCES

- Asnani, V., D. Delap, and C. Creager (2009), The development of wheels for the Lunar Roving Vehicle, *Journal of Terramechanics*, 46(3), 89–103.
- Backes, P., A. Diaz-Calderon, M. Robinson, M. Bajracharya, and D. Helmick (2005), Automated rover positioning and instrument placement, paper presented at 2005 IEEE Aerospace Conference, IEEE.
- Bandfield, J. L., M. J. Poston, R. L. Klima, and C. S. Edwards (2018), Widespread distribution of OH/H₂O on the lunar surface inferred from spectral data, *Nature geoscience*, 11(3), 173–177, doi:10.1038/s41561-018-0065-0.
- Banks, M. E., T. R. Watters, M. S. Robinson, L. L. Tornabene, T. Tran, L. Ojha, and N. Williams (2012), Morphometric analysis of small-scale lobate scarps on the Moon using data from the Lunar Reconnaissance Orbiter, *Journal of Geophysical Research: Planets*, 117(E12), doi:10.1029/2011je003907.
- Bekker, M. G. (1985), The Development of a Moon Rover, *Journal of the British Interplanetary Society*, 38, 537.
- Bell, J. F., and B. R. Hawke (1982), The Reiner Gamma Formation-Composition and origin as derived from remote sensing observations, paper presented at Lunar and Planetary Science Conference Proceedings.
- Benzing II, J. A., J. C. Kish, and V. Asnani, "Tire." US 8,141,606 B2, issued on March 27, 2012.
- Besse, S., J. Sunshine, M. Staid, N. Petro, J. Boardman, R. Green, J. Head, P. Isaacson, J. Mustard, and C. Pieters (2011), Compositional variability of the Marius Hills volcanic complex from the Moon Mineralogy Mapper (M3), *Journal of Geophysical Research: Planets*, 116(E6), doi:10.1029/2010JE003725.
- Blewett, D. T., E. I. Coman, B. R. Hawke, J. J. Gillis-Davis, M. E. Purucker, and C. G. Hughes (2011), Lunar swirls: Examining crustal magnetic anomalies and space weathering trends, *Journal of Geophysical Research: Planets*, 116(E2), doi:10.1029/2010JE003656.
- Blewett, D. T., et al. (2016), Optical space weathering on Vesta: Radiative-transfer models and Dawn observations, *Icarus*, 265, 161–174, doi:10.1016/j.icarus.2015.10.012.
- Blewett, D. T., G. C. Ho, H. Korth, L. L. Hood, and J. Halekas (2010), A Landed Experiment Package for Investigation of Lunar Magnetic and Albedo Anomalies, paper presented at Ground-Based Geophysics on the Moon, Tempe, AZ.
- Boyce, J. M. (1976), Ages of flow units in the lunar nearside maria based on Lunar Orbiter IV photographs, paper presented at Lunar and Planetary Science Conference Proceedings.
- Braden, S. E., J. D. Stopar, M. S. Robinson, S. J. Lawrence, C. H. Van Der Bogert, and H. Hiesinger (2014), Evidence for basaltic volcanism on the Moon within the past 100 million years, *Nature Geoscience*, 7(11), 787–791, doi:10.1038/ngeo2252.
- Buehler, M., K. Iagnemma, and S. Singh (2009), *The DARPA urban challenge: autonomous vehicles in city traffic*, Springer, Springer Tracts in Advanced Robotics.
- Byrne, P. K., C. Klimczak, D. A. Williams, D. M. Hurwitz, S. C. Solomon, J. W. Head, F. Preusker, and J. Oberst (2013), An assemblage of lava flow features on Mercury, *Journal of Geophysical Research: Planets*, 118(6), 1303–1322, doi:10.1002/jgre.20052.
- Byrne, P. K., J. Whitten, C. Klimczak, F. McCubbin, and L. Ostrach (2018), The Volcanic Character of Mercury, in *Mercury: The View after MESSENGER*, edited by S. C. Solomon, L. R. Nittler and B. J. Anderson, pp. 287–323, Cambridge University Press.
- Campbell, B. A., B. Hawke, and D. B. Campbell (2009), Surface morphology of domes in the Marius Hills and Mons Rümker regions of the Moon from Earth-based radar data, *Journal of Geophysical Research: Planets*, 114(E1), doi:10.1029/2008je003253.
- Chapman, C. R., D. M. H. Baker, O. S. Barnouin, C. I. Fassett, S. Marchi, W. J. Merline, L. R. Ostrach, L. M. Prockter, and R. G. Strom (2018), Impact Cratering of Mercury, in *Mercury: The View after MESSENGER*, edited by S. C. Solomon, L. R. Nittler and B. J. Anderson, pp. 217–248, Cambridge University Press.



- Chien, S., R. Sherwood, D. Tran, B. Cichy, G. Rabideau, R. Castano, A. Davies, R. Lee, D. Mandl, and S. Frye (2004), The EO-1 autonomous science agent, paper presented at Proceedings of the Third International Joint Conference on Autonomous Agents and Multiagent Systems—Volume 1.
- Colwell, J. E., S. R. Robertson, M. Horányi, X. Wang, A. Poppe, and P. Wheeler (2009), Lunar dust levitation, *Journal of Aerospace Engineering*, 22(1), 2–9.
- Creager, C., K. Johnson, and S. Moreland (2016), The Development of High Performance Compliant Tires for Mars Rovers, paper presented at International Society of Terrain-Vehicle Systems (ISTVS) Conference.
- Creager, C., S. Padula, C. Young, M. Kennedy, K. Johnson, and D. Gaydosh (2018), Optimization of the Non-pneumatic Spring Tire for Traction in Soft Soil, paper presented at American Society of Civil Engineers (ASCE) Earth and Space Conference.
- Denevi, B. W., C. Ernst, L. Prockter, and M. Robinson (2018), The Geologic History of Mercury, in *Mercury: The View after MESSENGER*, edited by S. C. Solomon, L. R. Nittler and B. J. Anderson, pp. 144–175, Cambridge University Press.
- Denevi, B. W., et al. (2013), The distribution and origin of smooth plains on Mercury, *Journal of Geophysical Research: Planets*, 118(5), 891–907, doi:10.1002/jgre.20075.
- Denevi, B. W., M. S. Robinson, A. K. Boyd, D. T. Blewett, and R. L. Klima (2016), The distribution and extent of lunar swirls, *Icarus*, 273, 53–67, doi:10.1016/j.icarus.2016.01.017.
- Denevi, B. W., M. S. Robinson, A. K. Boyd, H. Sato, B. W. Hapke, and B. R. Hawke (2014), Characterization of space weathering from Lunar Reconnaissance Orbiter Camera ultraviolet observations of the Moon, *Journal of Geophysical Research: Planets*, 119(5), 976–997, doi:10.1002/2013JE004527.
- Denevi, B. W., et al. (2009), The Evolution of Mercury's Crust: A Global Perspective from MESSENGER, *Science*, 324(5927), 613–618.
- Domingue, D. L., et al. (2014), Mercury's weather-beaten surface: Understanding Mercury in the context of lunar and asteroidal space weathering studies, *Space Science Reviews*, 181(1-4), 121–214, doi:10.1007/s11214-014-0039-5.
- Elder, C. M., P. O. Hayne, J. Bandfield, R. Ghent, J.-P. Williams, K. D. Hanna, and D. A. Paige (2017), Young lunar volcanic features: Thermophysical properties and formation, *Icarus*, 290, 224–237, doi:10.1016/j.icarus.2017.03.004.
- Elkins-Tanton, L. T., P. C. Hess, and E. Parmentier (2005), Possible formation of ancient crust on Mars through magma ocean processes, *Journal of Geophysical Research: Planets*, 110(E12), doi:10.1029/2005JE002480.
- Fleder, M., I. A. Nesnas, M. Pivtoraiko, A. Kelly, and R. Volpe (2011), Autonomous rover traverse and precise arm placement on remotely designated targets, paper presented at 2011 IEEE International Conference on Robotics and Automation, IEEE, Shanghai, China.
- Freitag, D. R., A. J. Green, and K.-J. Melzer (1970), Performance evaluation of wheels for lunar vehicles *Rep.*, Army Engineer Waterways Experiment Station, Vicksburg.
- Fu, R. R., B. P. Weiss, D. L. Shuster, J. Gattacceca, T. L. Grove, C. Suavet, E. A. Lima, L. Li, and A. T. Kuan (2012), An ancient core dynamo in asteroid Vesta, *Science*, 338(6104), 238–241, doi:10.1126/science.1225648.
- Gaddis, L. R., M. I. Staid, J. A. Tyburczy, B. R. Hawke, and N. E. Petro (2003), Compositional analyses of lunar pyroclastic deposits, *Icarus*, 161(2), 262–280, doi:10.1016/S0019-1035(02)00036-2.
- Gaier, J. R., M. C. Hicks, and R. M. Misconin (2013), Studies of Simulated Lunar Dust on the Properties of Thermal-Control Surfaces, *Journal of Spacecraft and Rockets*, 50(4), 848–852, doi:10.2514/1.A32135.
- Garrick-Bethell, I., J. W. Head III, and C. M. Pieters (2011), Spectral properties, magnetic fields, and dust transport at lunar swirls, *Icarus*, 212(2), 480–492, doi:10.1016/j.icarus.2010.11.036.



- Garrick-Bethell, I., and M. R. Kelley (2019), Reiner Gamma: A Magnetized Elliptical Disk on the Moon, *Geophysical Research Letters*, 46(10), 5065–5074, doi:10.1029/2019GL082427.
- Ghent, R. R., L. M. Carter, J. Bandfield, C. T. Udovicic, and B. A. Campbell (2016), Lunar crater ejecta: Physical properties revealed by radar and thermal infrared observations, *Icarus*, 273, 182–195, doi:10.1016/j.icarus.2015.12.014.
- Glotch, T. D., J. L. Bandfield, P. G. Lucey, P. O. Hayne, B. T. Greenhagen, J. A. Arnold, R. R. Ghent, and D. A. Paige (2015), Formation of lunar swirls by magnetic field standoff of the solar wind, *Nature Communications*, 6(1), 1–8, doi:10.1038/ncomms7189.
- Glotch, T. D., et al. (2010), Highly Silicic Compositions on the Moon, *Science*, 329(5998), 1510–1513, doi:10.1126/science.1192148.
- Gouge, T. A., et al. (2014), Global inventory and characterization of pyroclastic deposits on Mercury: New insights into pyroclastic activity from MESSENGER orbital data, *Journal of Geophysical Research: Planets*, 119(3), 635–658, doi:10.1002/2013JE004480.
- Grieve, R. A. (1975), Petrology and chemistry of the impact melt at Mistastin Lake crater, Labrador, *Geological Society of America Bulletin*, 86(12), 1617–1629, doi:10.1130/0016-7606(1975)86<1617:PACOTI>2.0.CO;2.
- Grove, T. L., and M. J. Krawczynski (2009), Lunar Mare Volcanism: Where Did the Magmas Come From?, *Elements*, 5(1), 29–34, doi:10.2113/gselements.5.1.29.
- Hapke, B., and H. Sato (2016), The porosity of the upper lunar regolith, *Icarus*, 273, 75–83, doi:10.1016/j.icarus.2015.10.031.
- Haruyama, J., et al. (2009), Long-lived volcanism on the lunar farside revealed by SELENE Terrain Camera, *Science*, 323(5916), 905–908, doi:10.1126/science.1163382.
- Hauck II, S. A., M. Grott, P. K. Byrne, B. W. Denevi, S. Stanley, and T. J. McCoy (2018), Mercury's Global Evolution, in *Mercury: The View after MESSENGER*, edited by S. C. Solomon, L. R. Nittler and B. J. Anderson, pp. 516–543, Cambridge University Press.
- Hawke, B., C. Coombs, B. Campbell, P. Lucey, C. Peterson, and S. Zisk (1991), Remote sensing of regional pyroclastic deposits on the north central portion of the lunar nearside, paper presented at Lunar and Planetary Science Conference Proceedings, Lunar and Planetary Institute, Houston, TX.
- Hayne, P. O., et al. (2017), Global Regolith Thermophysical Properties of the Moon From the Diviner Lunar Radiometer Experiment, *Journal of Geophysical Research: Planets*, 122(12), 2371–2400, doi:10.1002/2017JE005387.
- He, C., X. Zeng, and A. Wilkinson (2013), Geotechnical properties of GRC-3 lunar simulant, *Journal of Aerospace Engineering*, 26(3), 528–534.
- Head, J. W., et al. (2011), Flood volcanism in the northern high latitudes of Mercury revealed by MESSENGER, *Science*, 333(6051), 1853–1856, doi:10.1126/science.1211997.
- Head, J. W., and A. Gifford (1980), Lunar mare domes: Classification and modes of origin, *The Moon and the Planets*, 22(2), 235–258, doi:10.1007/BF00898434.
- Heather, D. J., S. K. Dunkin, and L. Wilson (2003), Volcanism on the Marius Hills plateau: Observational analyses using Clementine multispectral data, *Journal of Geophysical Research: Planets*, 108(E3), doi:10.1029/2002je001938.
- Heiken, G. H., D. T. Vaniman, and B. M. French (1991), *Lunar Sourcebook, A User's Guide to the Moon*, Cambridge University Press.
- Hemingway, D., and I. Garrick-Bethell (2012), Magnetic field direction and lunar swirl morphology: Insights from Airy and Reiner Gamma, *Journal of Geophysical Research: Planets*, 117(E10), doi:10.1029/2012JE004165.
- Hendrix, A. R., et al. (2016), Lunar swirls: Far-UV characteristics, *Icarus*, 273, 68–74, doi:10.1016/j.icarus.2016.01.003.
- Hendrix, A. R., D. M. Hurley, W. M. Farrell, B. T. Greenhagen, P. O. Hayne, K. D. Retherford, F. Vilas, J. T. Cahill, M. J. Poston, and Y. Liu (2019), Diurnally Migrating Lunar Water: Evidence From Ultraviolet Data, *Geophysical Research Letters*, 46(5), 2417–2424, doi:10.1029/2018GL081821.



- Hess, P. C. (1989), *Origins of Igneous Rocks*, Harvard University Press.
- Hiesinger, H., J. Head III, U. Wolf, R. Jaumann, and G. Neukum (2003), Ages and stratigraphy of mare basalts in Oceanus Procellarum, Mare Nubium, Mare Cognitum, and Mare Insularum, *Journal of Geophysical Research: Planets*, 108(E7), doi:10.1029/2002JE001985.
- Hiesinger, H., J. Head, U. Wolf, R. Jaumann, and G. Neukum (2011), Ages and stratigraphy of lunar mare basalts: A synthesis, in *Recent Advances and Current Research Issues in Lunar Stratigraphy*, edited by W. A. Ambrose and D. A. Williams, pp. 1–51, The Geological Society of America.
- Hood, L., and G. Schubert (1980), Lunar magnetic anomalies and surface optical properties, *Science*, 208(4439), 49–51.
- Hood, L., and C. Williams (1989), The Lunar Swirls: Distribution and Possible Origins, paper presented at Proceedings of the 19th Lunar and Planetary Science Conference, Cambridge University Press/Lunar and Planetary Institute.
- Hood, L., A. Zakharian, J. Halekas, D. Mitchell, R. Lin, M. Acuña, and A. Binder (2001), Initial mapping and interpretation of lunar crustal magnetic anomalies using Lunar Prospector magnetometer data, *Journal of Geophysical Research: Planets*, 106(E11), 27825–27839, doi:10.1029/2000JE001366.
- Hurwitz, D. M., J. W. Head, P. K. Byrne, Z. Xiao, S. C. Solomon, M. T. Zuber, D. E. Smith, and G. A. Neumann (2013a), Investigating the origin of candidate lava channels on Mercury with MESSENGER data: Theory and observations, *Journal of Geophysical Research: Planets*, 118(3), 471–486, doi:10.1029/2012JE004103.
- Hurwitz, D. M., J. W. Head, and H. Hiesinger (2013b), Lunar sinuous rilles: distribution, characteristics, and implications for their origin, *Planetary and Space Science*, 79, 1–38, doi:10.1016/J.PSS.2012.10.019.
- Iagnemma, K., and M. Buehler (2006), Editorial for Journal of Field Robotics—Special Issue on the DARPA Grand Challenge, *Journal of Field Robotics*, 23(9), 655–656.
- International Space Exploration Coordination Group (ISECG) (2018), *The Global Exploration Roadmap*, 3rd ed., NASA, Washington, DC.
- Jarvinen, R., M. Alho, E. Kallio, P. Wurz, S. Barabash, and Y. Futaana (2014), On vertical electric fields at lunar magnetic anomalies, *Geophysical Research Letters*, 41(7), 2243–2249, doi:10.1002/2014GL059788.
- Jolliff, B. L., J. J. Gillis, L. A. Haskin, R. L. Korotev, and M. A. Wieczorek (2000), Major lunar crustal terranes: Surface expressions and crust-mantle origins, *Journal of Geophysical Research: Planets*, 105(E2), 4197–4216, doi:10.1029/1999JE001103.
- Keller, L. P., and D. S. McKay (1997), The nature and origin of rims on lunar soil grains, *Geochimica et Cosmochimica Acta*, 61(11), 2331–2341.
- Kilkenny, N. S. (2017), NASA Glenn Research Center: Reinventing the Wheel, www.nasa.gov/specials/wheels/
- Kim, W. S., I. A. Nesnas, M. Bajracharya, R. Madison, A. I. Ansar, R. D. Steele, J. J. Biesiadecki, and K. S. Ali (2009), Targeted Driving Using Visual Tracking on Mars: From Research to Flight, *Journal of Field Robotics*, 26(3), 243–263.
- Kramer, G. Y., et al. (2011a), M3 spectral analysis of lunar swirls and the link between optical maturation and surface hydroxyl formation at magnetic anomalies, *Journal of Geophysical Research: Planets*, 116(E9), doi:10.1029/2010JE003729.
- Kramer, G. Y., J. P. Combe, E. M. Harnett, B. R. Hawke, S. K. Noble, D. T. Blewett, T. B. McCord, and T. A. Giguere (2011b), Characterization of lunar swirls at Mare Ingenii: A model for space weathering at magnetic anomalies, *Journal of Geophysical Research: Planets*, 116(E4), doi:10.1029/2010JE003669.
- Kurata, M., H. Tsunakawa, Y. Saito, H. Shibuya, M. Matsushima, and H. Shimizu (2005), Mini-magnetosphere over the Reiner Gamma magnetic anomaly region on the Moon, *Geophysical Research Letters*, 32(24), doi:10.1029/2005GL024097.
- Lawrence, D., W. Feldman, R. Elphic, R. Little, T. Prettyman, S. Maurice, P. Lucey, and A.



- Binder (2002), Iron abundances on the lunar surface as measured by the Lunar Prospector gamma-ray and neutron spectrometers, *Journal of Geophysical Research: Planets*, 107(E12), 13-11-13-26, doi:10.1029/2001je001530.
- Lawrence, D., R. Puetter, R. Elphic, W. Feldman, J. J. Hagerty, T. H. Prettyman, and P. Spudis (2007), Global spatial deconvolution of Lunar Prospector Th abundances, *Geophysical Research Letters*, 34(3), doi:10.1029/2006gl028530.
- Lawrence, S. J., et al. (2013), LRO observations of morphology and surface roughness of volcanic cones and lobate lava flows in the Marius Hills, *Journal of Geophysical Research: Planets*, 118(4), 615–634, doi:10.1002/jgre.20060.
- Lewis, K. W., S. Peters, K. Gonter, S. Morrison, N. Schmerr, A. R. Vasavada, and T. Gabriel (2019), A surface gravity traverse on Mars indicates low bedrock density at Gale crater, *Science*, 363(6426), 535–537, doi:10.1126/science.aat0738.
- Livengood, T., et al. (2015), Moonshine: Diurnally varying hydration through natural distillation on the Moon, detected by the Lunar Exploration Neutron Detector (LEND), *Icarus*, 255, 100–115, doi:10.1016/j.icarus.2015.04.004.
- Longhi, J. (2006), Petrogenesis of picritic mare magmas: constraints on the extent of early lunar differentiation, *Geochimica et Cosmochimica Acta*, 70(24), 5919–5934, doi:10.1016/j.gca.2006.09.023.
- Lunar Exploration Analysis Group (LEAG) (2016), The Lunar Exploration Roadmap: Exploring the Moon in the 21st Century: Themes, Goals Objectives, Investigations, and Priorities, 2016, edited, LEAG, LEAG Annual Meeting.
- Maimone, M., J. Biesiadecki, E. Tunstel, Y. Cheng, and C. Leger (2006), Surface navigation and mobility intelligence on the Mars Exploration Rovers, *Intelligence for Space Robotics*, 45–69.
- Matsunaga, T., et al. (2008), Discoveries on the lithology of lunar crater central peaks by SELENE Spectral Profiler, *Geophysical Research Letters*, 35(23), doi:10.1029/2008gl035868.
- McCauley, J. F. (1967a), Geologic map of the Hevelius region of the Moon.
- McCauley, J. F. (1967b), The nature of the lunar surface as determined by systematic geologic mapping, in *Mantles of the Earth and Terrestrial Planets*, edited, p. 431.
- McCauley, J. F. (1968), Geologic results from the lunar precursor probes, *ALAA Journal*, 6(10), 1991–1996, doi:10.2514/3.4912.
- McEwen, A. S., M. C. Malin, M. H. Carr, and W. K. Hartmann (1999), Voluminous volcanism on early Mars revealed in Valles Marineris, *Nature*, 397(6720), 584–586, doi:10.1038/17539.
- McEwen, A. S., M. S. Robinson, E. M. Eliason, P. G. Lucey, T. C. Duxbury, and P. D. Spudis (1994), Clementine observations of the Aristarchus region of the Moon, *Science*, 266(5192), 1858–1862, doi:10.1126/science.266.5192.1858.
- McGill, G. E., and S. W. Squyres (1991), Origin of the Martian crustal dichotomy: Evaluating hypotheses, *Icarus*, 93(2), 386–393, doi:10.1016/0019-1035(91)90221-E.
- McKenzie, D., P. G. Ford, C. Johnson, B. Parsons, D. Sandwell, S. Saunders, and S. C. Solomon (1992), Features on Venus generated by plate boundary processes, *Journal of Geophysical Research: Planets*, 97(E8), 13533–13544, doi:10.1029/92JE01350.
- McSween, H. Y., G. J. Taylor, and M. B. Wyatt (2009), Elemental Composition of the Martian Crust, *Science*, 324(5928), 736–739, doi:10.1126/science.1165871.
- Melosh, H. J. (1989), *Impact Cratering: A Geologic Process*, Oxford University Press, New York.
- Mighani, S., H. Wang, D. L. Shuster, C. S. Borlina, C. I. Nichols, and B. P. Weiss (2020), The end of the lunar dynamo, *Science Advances*, 6(1), doi:10.1126/sciadv.aax0883.
- Milliken, R. E., and S. Li (2017), Remote detection of widespread indigenous water in lunar pyroclastic deposits, *Nature Geoscience*, 10(8), 561–565, doi:10.1038/ngeo2993.
- Nakamura, R., et al. (2009), Ultramafic impact melt sheet beneath the South Pole–Aitken



- basin on the Moon, *Geophysical Research Letters*, 36(22), doi:10.1029/2009gl040765.
- NASA (2014), NASA 2014 Science PlanRep., NASA, Washington, DC.
- NASA Advisory Council (NAC) (2007), NASA Advisory Council Workshop on Science Associated with the Lunar Exploration Architecture, February 27–March 2, 2007, edited, Tempe, AZ.
- National Academies of Sciences, Engineering, and Medicine (NASEM), (2020), *Report Series: Committee on Astrobiology and Planetary Science: Options for the Fifth New Frontiers Announcement of Opportunity*, 30 pp., The National Academies Press, Washington, DC, doi:10.17226/25868.
- National Research Council (NRC) (2007), *The Scientific Context for Exploration of the Moon*, 120 pp., The National Academies Press, Washington, DC, doi:10.17226/11954.
- National Research Council (NRC) (2011), *Vision and Voyages for Planetary Science in the Decade 2013-2022*, 398 pp., The National Academies Press, Washington, DC, doi:10.17226/13117.
- Neish, C., D. Blewett, D. Bussey, S. Lawrence, M. Mechtley, B. Thomson, and The Mini-RF Team (2011), The surficial nature of lunar swirls as revealed by the Mini-RF instrument, *Icarus*, 215(1), 186–196, doi:10.1016/j.icarus.2011.06.037.
- Nesnas, I. A., M. W. Maimone, and H. Das (2000), Rover Maneuvering for Autonomous Vision-Based Dexterous Manipulation, paper presented at Proceedings 2000 ICRA. IEEE International Conference on Robotics and Automation, IEEE, San Francisco, CA.
- Nuttall Jr., C. (1965), A dimensionless consolidation of WES data on the performance of sand under tire loadsRep., US Army Engineer Waterways Experiment Station.
- Ohtake, M., et al. (2009), The global distribution of pure anorthosite on the Moon, *Nature*, 461(7261), 236–240, doi:10.1038/nature08317.
- Pedersen, L., M. Deans, D. Lees, S. Rajagoplan, and D. E. Smith (2005), Multiple-target single cycle instrument placement, paper presented at Proceedings of the 8th International Symposium on Artificial Intelligence, Robotics and Automation in Space, Munich, Germany.
- Pieters, C., D. Moriarty, and I. Garrick-Bethell (2014), Atypical regolith processes hold the key to enigmatic lunar swirls, in *45th Lunar and Planetary Science Conference*, edited, p. 1408.
- Pinet, P. C., V. V. Shevchenko, S. D. Chevrel, Y. Daydou, and C. Rosemberg (2000), Local and regional lunar regolith characteristics at Reiner Gamma Formation: Optical and spectroscopic properties from Clementine and Earth-based data, *Journal of Geophysical Research: Planets*, 105(E4), 9457–9475, doi:10.1029/1999JE001086.
- Povilaitis, R., M. Robinson, C. Van der Bogert, H. Hiesinger, H. Meyer, and L. Ostrach (2018), Crater density differences: Exploring regional resurfacing, secondary crater populations, and crater saturation equilibrium on the moon, *Planetary and Space Science*, 162, 41–51, doi:10.1016/j.pss.2017.05.006.
- Qiao, L., J. W. Head, L. Xiao, L. Wilson, and J. D. Dufek (2018), The role of substrate characteristics in producing anomalously young crater retention ages in volcanic deposits on the Moon: Morphology, topography, subresolution roughness, and mode of emplacement of the Sosigenes lunar irregular mare patch, *Meteoritics & Planetary Science*, 53(4), 778–812, doi:10.1111/maps.13003.
- Rennilson, J., and D. R. Criswell (1974), Surveyor observations of lunar horizon-glow, *The Moon*, 10(2), 121–142, doi:10.1007/BF00655715.
- Richmond, N., L. Hood, J. Halekas, D. Mitchell, R. Lin, M. Acuña, and A. Binder (2003), Correlation of a strong lunar magnetic anomaly with a high-albedo region of the Descartes mountains, *Geophysical research letters*, 30(7), doi:10.1029/2003GL016938.
- Robinson, M. S., et al. (2010), Lunar Reconnaissance Orbiter Camera (LROC) Instrument Overview, *Space Science Reviews*, 150(1-4), 81-124, doi:10.1007/s11214-010-9634-2.



- Robinson, M. S., and M. Ravine (2012), Telephoto Reconnaissance Imaging for Lunar Rover Applications, paper presented at International Workshop on Instrumentation for Planetary Missions.
- Robinson, M. S., J. Thangavelautham, B. J. Anderson, A. Deran, S. J. Lawrence, R. Wagner, R. Ridenoure, B. Williams, D. Dunham, and A. Babuscia (2018), Swirl mission concept: Unraveling the enigma, *Planetary and Space Science*, 162, 73–88.
- Saito, Y., M. N. Nishino, M. Fujimoto, T. Yamamoto, S. Yokota, H. Tsunakawa, H. Shibuya, M. Matsushima, H. Shimizu, and F. Takahashi (2012), Simultaneous observation of the electron acceleration and ion deceleration over lunar magnetic anomalies, *Earth, Planets and Space*, 64(2), 83–92, doi:10.5047/eps.2011.07.011.
- Schultz, P. H., M. I. Staid, and C. M. Pieters (2006), Lunar activity from recent gas release, *Nature*, 444(7116), 184–186, doi:10.1038/nature05303.
- Shoemaker, E. (1959), Impact mechanics at Meteor Crater, Arizona, 55 pp, Princeton University, Princeton, NJ.
- Shoemaker, E., R. Batson, H. Holt, E. Morris, J. Rennilson, and E. Whitaker (1967), Television Observations from Surveyor III Rep. JPL Technical Report 21-1177, 9–67 pp.
- Shoemaker, E., R. Batson, H. Holt, E. Morris, J. Rennilson, and E. Whitaker (1968), Television Observations from Surveyor VII Rep. NASA Special Paper #173, 13–81 pp.
- Shoemaker, E., R. Batson, H. Holt, E. Morris, J. Rennilson, and E. Whitaker (1969), Observations of the lunar regolith and the Earth from the television camera on Surveyor 7, *Journal of Geophysical Research*, 74(25), 6081–6119, doi:10.1029/JB074i025p06081.
- Speyerer, E. J., R. Z. Povilaitis, M. S. Robinson, P. C. Thomas, and R. V. Wagner (2016), Quantifying crater production and regolith overturn on the Moon with temporal imaging, *Nature*, 538(7624), 215–218, doi:10.1038/nature19829.
- Stadermann, A. C., M. R. Zanetti, B. L. Jolliff, H. Hiesinger, C. H. van der Bogert, and C. W. Hamilton (2018), The age of lunar mare basalts south of the Aristarchus Plateau and effects of secondary craters formed by the Aristarchus event, *Icarus*, 309, 45–60, doi:10.1016/J.ICARUS.2018.02.030.
- Staid, M. I., et al. (2011), The mineralogy of late stage lunar volcanism as observed by the Moon Mineralogy Mapper on Chandrayaan-1, *Journal of Geophysical Research: Planets*, 116(E6), doi:10.1029/2010je003735.
- Strom, R. G., N. J. Trask, and J. E. Guest (1975), Tectonism and volcanism on Mercury, *Journal of Geophysical Research*, 80(17), 2478–2507, doi:10.1029/JB080i017p02478.
- Stubbs, T. J., R. R. Vondrak, and W. M. Farrell (2007), Impact of dust on lunar exploration, paper presented at Workshop on Dust in Planetary Systems, Kauai, Hawaii, 2007.
- Sunshine, J. M., T. L. Farnham, L. M. Feaga, O. Groussin, F. Merlin, R. E. Milliken, and M. F. A'Hearn (2009), Temporal and Spatial Variability of Lunar Hydration As Observed by the Deep Impact Spacecraft, *Science*, 326(5952), 565–568, doi:10.1126/science.1179788.
- Sutoh, M., J. Yusa, T. Ito, K. Nagatani, and K. Yoshida (2012), Traveling performance evaluation of planetary rovers on loose soil, *Journal of Field Robotics*, 29(4), 648–662.
- Swann, G. A., et al. (1977), Geology of the Apollo 14 Landing Site in the Fra Mauro Highlands Rep., Washington, DC.
- Tikoo, S. M., B. P. Weiss, W. S. Cassata, D. L. Shuster, J. Gattacceca, E. A. Lima, C. Suavet, F. Nimmo, and M. D. Fuller (2014), Decline of the lunar core dynamo, *Earth and Planetary Science Letters*, 404, 89–97, doi:10.1016/j.epsl.2014.07.010.
- Tikoo, S. M., B. P. Weiss, D. L. Shuster, C. Suavet, H. Wang, and T. L. Grove (2017), A two-billion-year history for the lunar dynamo, *Science Advances*, 3(8), doi:10.1126/sciadv.1700207.
- VanBommel, S. J., R. Gellert, J. A. Berger, L. M. Thompson, K. S. Edgett, M. J. McBride, M. E. Minitti, N. I. Boyd, and J. L. Campbell (2017), Modeling and mitigation of sample relief effects applied to chemistry measurements by the Mars Science Laboratory Alpha Particle X-ray



- Spectrometer, *X-Ray Spectrometry*, 46(4), 229–236, doi:10.1002/xrs.2755.
- Watters, T. R., M. S. Robinson, M. E. Banks, T. Tran, and B. W. Denevi (2012), Recent extensional tectonics on the Moon revealed by the Lunar Reconnaissance Orbiter Camera, *Nature Geoscience*, 5(3), 181–185, doi:10.1038/ngeo1387.
- Watters, T. R., R. C. Weber, G. C. Collins, I. J. Howley, N. C. Schmerr, and C. L. Johnson (2019), Shallow seismic activity and young thrust faults on the Moon, *Nature Geoscience*, 12(6), 411–417, doi:10.1038/s41561-019-0362-2.
- Wdowiak, T. J., G. Klingelhöfer, M. L. Wade, and J. I. Nuñez (2003), Extracting science from Mössbauer spectroscopy on Mars, *Journal of Geophysical Research: Planets*, 108(E12), doi:10.1029/2003JE002071.
- Weitz, C. M., and J. W. Head III (1999), Spectral properties of the Marius Hills volcanic complex and implications for the formation of lunar domes and cones, *Journal of Geophysical Research: Planets*, 104(E8), 18933–18956, doi:10.1029/1998JE000630.
- Wettergreen, D. (2008), Long-distance autonomous survey and mapping in robotic investigation of life in the Atacama, paper presented at International Symposium on Artificial Intelligence, Robotics and Automation in Space (i-SAIRAS), Los Angeles, CA.
- Whitaker, E. A. (1999), *Mapping and Naming the Moon: A History of Lunar Cartography and Nomenclature*, Cambridge University Press.
- Whitford-Stark, J. L., and J. W. Head (1977), The Procellarum volcanic complexes—contrasting styles of volcanism, paper presented at Lunar and Planetary Science Conference Proceedings, Pergamon Press, Inc., Houston, TX.
- Whitten, J. L., J. W. Head, B. W. Denevi, and S. C. Solomon (2014), Intercrater plains on Mercury: Insights into unit definition, characterization, and origin from MESSENGER datasets, *Icarus*, 241, 97–113, doi:10.1016/j.icarus.2014.06.013.
- Wieczorek, M. A., et al. (2013), The Crust of the Moon as Seen by GRAIL, *Science*, 339(6120), 671–675, doi:10.1126/science.1231530.
- Wilhelms, D. E., and J. F. McCauley (1971), Geologic map of the near side of the Moon, US Geological Survey.
- Wilson, L., and J. W. Head (2017), Generation, ascent and eruption of magma on the Moon: New insights into source depths, magma supply, intrusions and effusive/explosive eruptions (Part 1: Theory), *Icarus*, 283, 146–175, doi:10.1016/j.icarus.2015.12.039.
- Yoshida, J. (2020), Full AV Stacks: Who, What, Where, etc., EE|Times, www.eetimes.com/full-av-stacks-who-what-where-etc/
- Zanetti, M., A. Stadermann, B. Jolliff, H. Hiesinger, C. Van der Bogert, and J. Plescia (2017), Evidence for self-secondary cratering of Copernican-age continuous ejecta deposits on the Moon, *Icarus*, 298, 64–77, doi:10.1016/j.icarus.2017.01.030.
- Zisk, S., C. Hodges, H. Moore, R. Shorthill, T. Thompson, E. Whitaker, and D. Wilhelms (1977), The Aristarchus-Harbinger region of the Moon: Surface geology and history from recent remote-sensing observations, *The Moon*, 17(1), 59–99, doi:10.1007/bf00566853.